Politecnico di Torino

MASTER'S Degree in ARCHITECTURE FOR THE SUSTAINABILITY DESIGN
AY. 2021/2022
Graduation Session July 2022

Ultralightweight foamed concrete reinforced with natural fibers compatible with 3D printing

Energy-efficient building materials

Supervisor:
Luciana Restuccia
DISEG, Politecnico di Torino
Co-supervisor:
Devid Falliano

Candidate:
Adriana Carolina Bravo Celi
Student ID: 277064

Index

Index I

Abstract 1

Chapter 1 Concrete's sustainability strategies 3

1.1. Introduction 3
1.2. Sustainability of concrete 4
1.2.1. Materials Manufacturing 4
1.2.1.1. Cement production 5
1.2.1.2. Aggregates production 6
1.2.1.3. Reinforcement production 6
1.2.2. Mix Design 7
1.2.2.1. Reduce the total amount of binder 7
1.2.2.2. Reduce the environmental impact and resource use of binders 8
1.2.2.3. Reduce the environmental impact and resource use of water 9
1.2.2.4. Reduce the environmental impact of aggregates 10
1.2.2.5. Reduce the environmental impact of reinforcement 11
1.2.3. Concrete Mixing 11
1.2.4. Optimization of construction methods 11
1.2.5. Efficiency underuse 12
1.2.5.1. Increase the durability of reinforced concrete 12
1.2.5.2. CO_2 mineralization and utilization 13
1.2.5.3. Thermal conductivity improvement and energy saving 13
1.2.6. End of life 14

Chapter 2 Fiber addition in concrete 15

2.1. Effects of fiber addition in concrete 15
2.1.1. Increased mechanical properties 16
2.1.2. Increased ductility 16

2.1.3. Delay crack propagation 16
2.2. Types of fiber compatible with concrete 17
2.2.1. Artificial fibers 17
2.2.2. Natural fibers 18
2.3. Animal fibers in concrete: Sheep wool fibers 19

Chapter 3 Foamed concrete 23

3.1. Foamed concrete properties and advantages 23
3.2. Mix design of foamed concrete 25
3.3. Density, mechanical resistance, and instability 27

Chapter 4 Additive manufacturing with concrete 32

4.1. Additive manufacturing processes compatible with concrete 32
4.1.1. Contour crafting 35
4.1.2. 3D concrete printing 36
4.2. Properties of extrudable concrete 37
4.2.1. Fresh state properties 37
4.2.1.1. Pumpability 38
4.2.1.2. Extrudability 38
4.2.1.3. Printability 38
4.2.1.4. Open-time, layer cycle-time, and green-strength 39
4.2.2. Dry state properties 40
4.2.2.1. Adhesion between layers 41
4.2.2.2. Constant filament density 42
4.2.2.3. Shrinkage cracks and durability 43
4.2.2.4. Geometric accordance 43
4.2.2.5. Mechanical properties 46
4.3. Potential for construction 49
4.4. Properties of extrudable foamed concrete 52
4.4.1. Mix design and fresh state properties 52
4.4.1.1. Consistency and green strength 52
4.4.2. Dry state characteristics of the material 54

4.4.2.1. Dimension and distribution of the pores 54
4.4.2.2. Compressive strength 56
4.4.2.3. Flexural strength 56
4.4.2.4. Thermal conductivity 57

Chapter 5 Experimentation: Mechanical and thermal tests of innovative foamed concretes 58

5.1. Materials and methods 58
5.2. Results and discussions 65
5.2.1. Rheological characterization of the fresh state 65
5.2.2. Density variation 70
5.2.3. Microstructural characterization 73
5.2.4. Mechanical properties after 28 days of maturation 92
5.2.4.1. Flexural strength 92
5.2.4.2. Compressive strength 124
5.2.5. Thermal conductivity 154

Chapter 6 Conclusions and possible scenarios from experimentation 158

6.1. Considerations and conclusions 158
6.2. Research and possible future scenarios 160

List of figures 162

List of tables 182

Bibliography 184

Abstract

Concrete is one of the world's most produced and widely applied materials. Its versatility has drawn the attention of the construction industry, making it the number one material for building houses, buildings, facilities, and even civil works worldwide. Unfortunately, due to its fabrication processes, energy consumption, and elevated expenditure on raw materials, concrete has become one of the most pollutant materials. Taking into consideration the environmental impact of the material, this research focuses on four well-known strategies to improve concrete's sustainability, the reduction of the amount of binder, the implementation of secondary materials to the cementitious matrix, the diminution of energy consumption during the material's lifetime, and the efficiency improvement of the construction process.

The reduction of the amount of binder occurs due to the presence of the foaming agent that creates a microporous matrix reducing the amount of cement in terms of volume of the material considerably. This characteristic contributes to reducing the energy consumption in buildings as well because the air bubbles found in the matrix reduce the thermal conductivity. The implementation of sheep wool fiber reinforcement not only contributes to the material's mechanical properties but also gives a second life to a widespread and pollutant secondary-material that would otherwise be disposed of. The studied material possesses the ability to develop green strength; therefore, it can be applied to automated construction processes that lead to material, time, and cost savings in construction.

The present research studied the effects of the incorporation of sheep wool fiber reinforcement into extrudable foamed concrete and performed several laboratory experiments to determine the most suitable fiber characteristics for this type of concrete. The research divides into two parts. The first aims to determine the most performant fiber-treatments (non-treated, salt-treated, lime-treated, NaOH-treated, and surfactant-treated fibers), fiber-length (6, 12, and 20mm), and fiber/cement ratio (2,5, 5, and 10%) for ultralightweight extrudable foamed concrete in terms of mechanical strength. The second part consisted of applying the fiber characteristics outlined in the first experimental campaign to ultralightweight cement pastes with 100, 300, and 500 kg/m³ target densities to evaluate the influence of fiber-addition in diverse lightweight conditions. In this part, each admixture was analyzed in terms of its rheology, density variation, microstructure, compressive and flexural strength, and thermal conductivity.

The studied material can be applied to both traditional and automated construction. In addition, its application can occur onsite and as part of a prefabrication process. Its main application is thermal insulation, leading to the improvement of the energy efficiency of a building. Finally, in a 3D concrete printing context, its application can occur by inserting the insulating material inside a 3D printed structural shell acting as formwork or extruding it with a multi-material process. For this last option to be possible, further experimental research should lead to determine the effective extrudability and printability capabilities of extrudable ultralightweight foamed concrete reinforced with sheep wool fibers, as expressed in the last chapter of this thesis in addition to the final experimental considerations.

Chapter 1

Concrete's sustainability strategies

1.1. Introduction

Cement has become an essential material for the construction sector. Its wide use happens because the raw materials needed to produce it are available worldwide and also because it is a versatile material that gives architectural freedom [1]. When cement blends with water, aggregates, and sometimes additives, it results in mortars and concrete. These are paste-based materials compatible with every type of construction like houses, buildings, facilities, and civil works.

Concrete is a widely diffused material due to its competitiveness and durability; unfortunately, it is also one of the most pollutant materials in the world. It is responsible for approximately 8% of global anthropogenic greenhouse gas emissions and 3% of global energy demand [2]. With global warming and greenhouse gas emissions growing at high-speed rates, it is crucial to ensure that concrete becomes sustainable.

Concrete is the second most-consumed material globally, only below water; it approaches an estimated demand of 30 billion tons per year [2]. Cement, water, aggregates, and sometimes admixtures combine to produce it. Of these materials, cement is by far the most pollutant. The production of clinker of Portland cement requires approximate temperatures of 1450°C; during this process, fuel combustion and limestone calcination release approximately one ton of CO_2 for every ton of cement produced [2].

In addition to the global warming impacts caused during the production process, we must also consider the rest of the material's life cycle. For example, before the manufacturing process of cement, the mining of raw materials such as limestone, clay, and gypsum provokes severe effects on the environment due to deforestation and loss of surface soil. Furthermore, the building's use and demolition stages also contribute to air pollution, especially if the design phase does not consider sustainability, quality, recycling, and demolition.

Given the latest increase in natural disasters worldwide and the recent UN Secretary-General calling the latest global warming report a "code red for humanity," the construction industry must reduce its ecological footprint. Increasing concrete's sustainability will contribute to accomplishing this target.

1.2. Sustainability of concrete

Reducing the carbon footprint to zero is impossible because of the carbon dioxide inherent in Portland cement manufacturing. Instead, we can reduce the carbon footprint to an acceptable level.

Knowing the impact on the environment that concrete generates during its whole life cycle, the construction sector has been doing some research to individuate the different areas of action and strategies to follow to make concrete a feasible option for the future. Figure 1.1 shows a schematic of the strategies to follow in every part of the life cycle of concrete to reduce its carbon footprint.

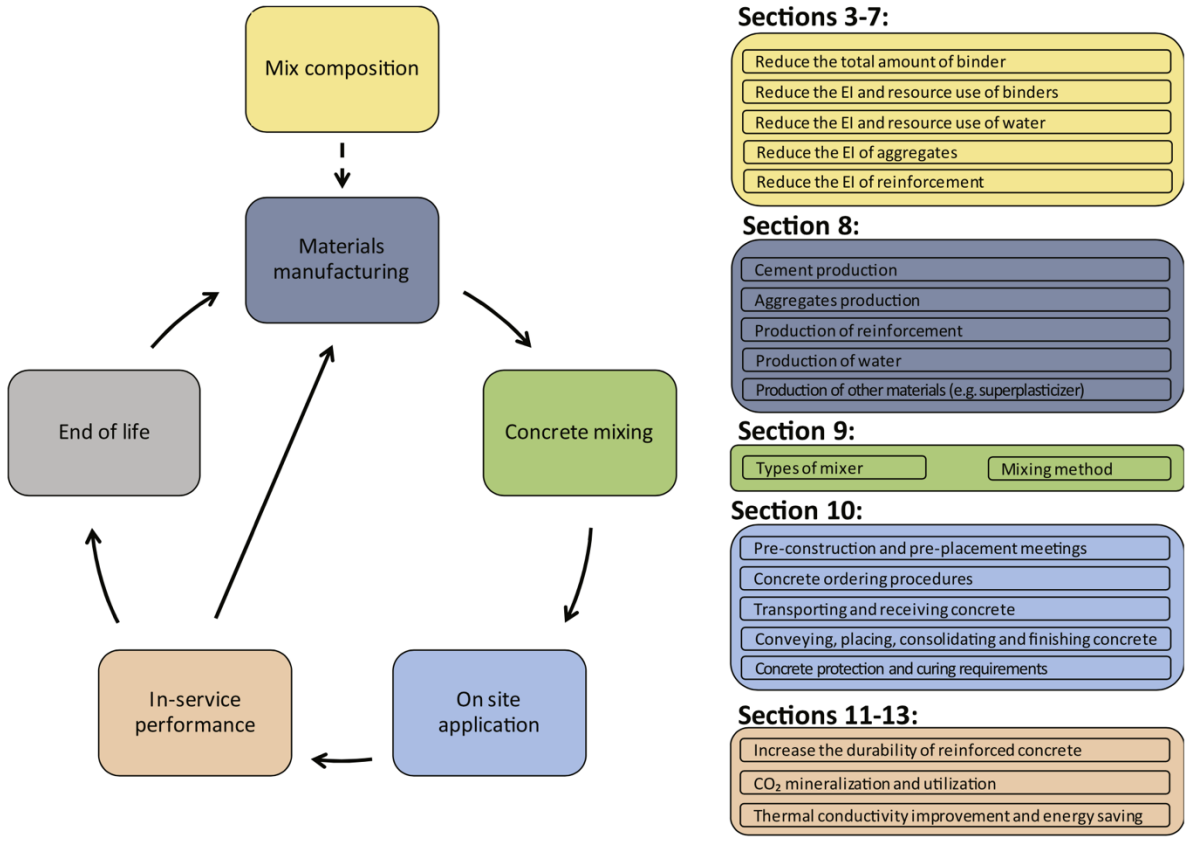

Figure 1. Life cycle stages of concrete and its respective strategies for sustainability [3].

1.2.1. Materials Manufacturing

The elevated carbon emissions and energy consumption associated with each material required in concrete production demand finding alternative manufacturing processes beneficial for the environment. This path acts upstream of the problem and aims to improve the environmental performance of the raw materials that make up the concrete. However, studies on this sustainability path are still very scarce to date.

1.2.1.1. Cement production

Cement production classifies into five stages: raw materials extraction, transport, fuel and energy consumption, calcination, and grinding. Each one of these processes can improve to reduce its associated pollution [4].

Mining with alternative fuels or renewable energies [5] and minimizing environmental damage during the extraction of raw materials [6] reduces the atmospheric impact of the raw materials extraction process. In addition, the transportation and the energy consumption in every stage of the cement production process can be replaced by more energy-efficient methods like the use of an oxy-fuel kiln [7].

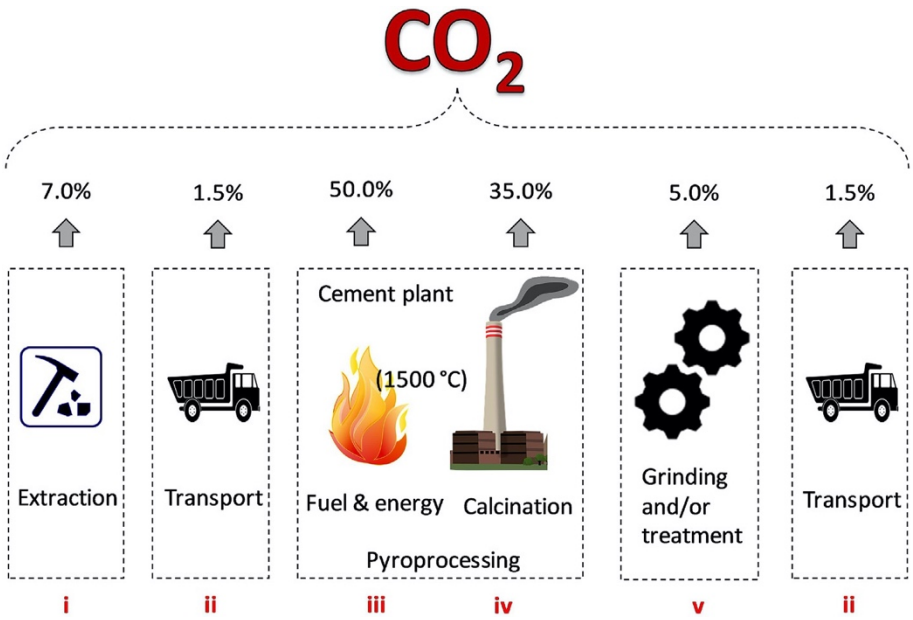

Figure 2. Distribution of CO2 emissions released during the different phases of the cement production process [3].

- In the extraction and crushing phases, it is possible to improve mining practices by minimizing the use of equipment, using alternative fuels, increasing the efficiency of machinery, using specific lubricants to reduce wear on machinery, using recycled aggregates, and using mills powered by renewable energy.
- For the transport phase from the quarry to the production plant, it is possible to envisage the use of underground and more efficient conveyor belts.
- For the combustion phase, it is possible to foresee the use of alternative fuels.
- It is possible to envisage using alternatives to carbonization with limestone for the carbonization phase.

- Using renewable energy sources for the crushing, grinding, and size reduction phases is possible.
- For the process in general, it is possible to pursue the goal of producing cement with almost zero carbon footprint and improving the technologies used to make the cement plant greener. In this context, it is possible to foresee the presence of a chamber at controlled pressure and humidity, filled with aggregates recycled from concretes rich in magnesium and calcium; which, crossed by the gases emitted by the industry, allow the sequestration of CO_2 and other greenhouse gases generated during production.

1.2.1.2. Aggregates production

Fine and coarse aggregates are essential materials for concrete production. Therefore, the extraction and production processes should become energy efficient by optimizing tools, production processes, equipment, and transportation [8]. Another strategy is to replace aggregates in concrete with others recycled from construction and demolition waste [9].

1.2.1.3. Reinforcement production

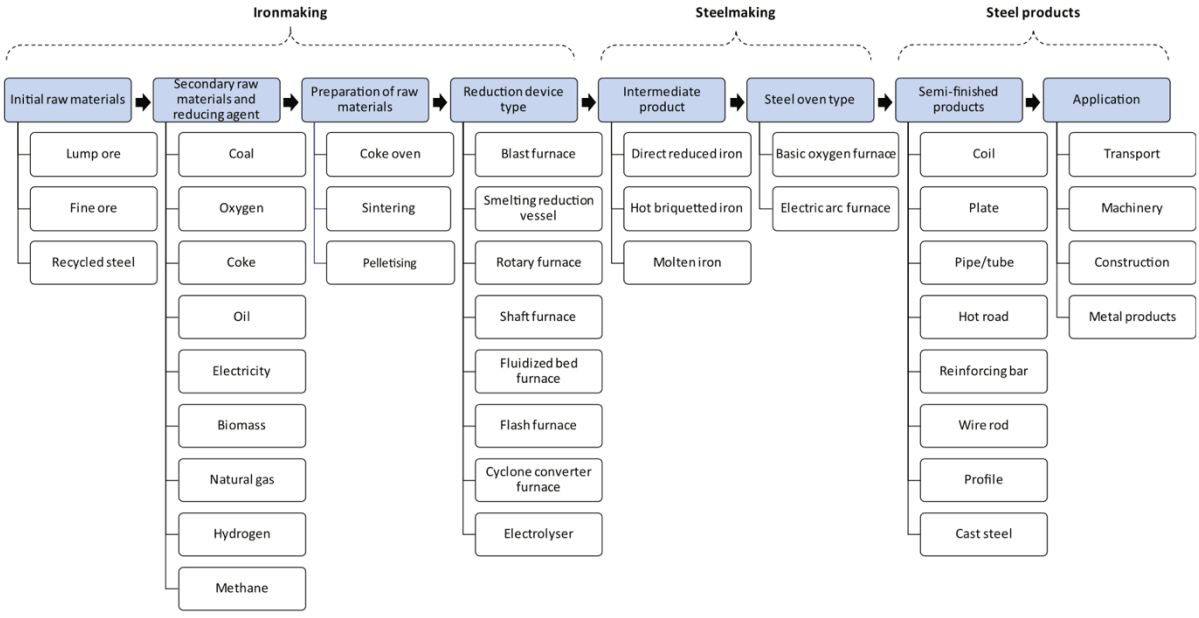

Figure 3. Iron and steel production [3].

As shown in figure 2, the production of steel products that work as reinforcements for concrete follows a broad series of steps. Modifications are possible in every step of steel production; for example, recycling steel structures from construction waste and substituting the extraction of raw materials reduces the environmental impact of concrete. In addition, the temperatures required to complete these processes result in high energy consumption; therefore, steel production companies are

implementing alternative manufacturing processes that can cut CO_2 emissions and energy consumption.

1.2.2. Mix Design

1.2.2.1. Reduce the total amount of binder

Reducing the cement content would help obtain environmentally friendly, economical, and durable concrete. Although this strategy is not easy to practice because it requires thorough research, it would offer an excellent contribution. Its feasibility derives from a series of studies that prove the possibility of employing a lower cement quantity than 260kg/m^3, the minimum allowed by the normative [10], without any performance reductions [3].

Within this scope, some of the specific actions to reduce the amount of binder are the following:

- Employ pozzolanic or hydraulic powders as supplementary cement materials:

Supplementary cementitious materials, when employed, replace part of the required binder content. These materials generally increase the durability properties of concrete. [11] However, the implementation of pozzolanic or hydraulic powders leads to a decrease in resistance to carbonation. Therefore, it is essential to consider their use only in certain situations, such as structures not directly exposed to high CO_2 contents like foundation or underwater structures, structures with unconventional reinforcements, or massive structures that require minimizing hydration heat [12].

- Employ filler powders:

A small quantity of cement can compromise some essential properties of the mixture, such as workability and cohesion, and consequently lead to poor compaction with repercussions in terms of strength, porosity, and durability [13]. Studies show that the implementation of fillers such as limestone powder, marble waste, quartz, and granite solves this issue; however, it is necessary to deepen how employing fillers affects the workability, mechanical resistance, and durability of the work concrete.

- Reduce the water to binder ratio and add dispersants:

Some researchers affirm that reducing the water to binder ratio and adding dispersants is the most promising strategy to reduce the cement employed in concrete production, obtaining economic and environmental benefits. [3] The water/binder ratio reduction results in a higher quality mixture due to the proximity

between cement particles; reduced pore diameter because most of the water is absorbed by hydration products, improving carbonation and penetration resistance. There is a significant reduction in costs and environmental impact even when chemical additives are needed to improve workability because the quantity of additives employed is much lower than the spared cement. Also, in some cases, the presence of fillers contributes to increasing compressive strength because these materials remain encapsulated in between the cement particles [14].

Previous research shows that it is possible to obtain concrete with a low binder content and high technical and environmental performance, thus reducing the environmental impact linked to cement. However, it is essential to take the hardening phase into consideration to avoid cracking and increase durability.

- Indirect reduction of the binder content:

The implementation of nanomaterials, binary/quaternary mixes, stainless rebars, and barriers against the penetration of aggressive agents allow the enhancement of concrete characteristics, compensating for the reduced amount of binder. By applying one or more of these strategies, concrete with low cement quantities can become durable and increase resistance performance.

1.2.2.2. Reduce the environmental impact and resource use of binders

Another possible strategy to increase concrete sustainability is substituting part of the cement with supplementary cementitious materials but without reducing the total binder content. Multiple studies show promising results concerning the mechanical properties and the durability of concrete when adding these materials, especially the ones regarding carbonation.

It is crucial to consider that the sole application of supplementary cementitious materials does not mean that concrete automatically becomes sustainable and economically feasible. To achieve this objective, a proper life cycle assessment (LCA) analysis should be performed, considering how these new materials affect every step of the life cycle of concrete.

Within this scope, some of the specific actions to reduce the environmental impact of the binder are the following:

- Agricultural and aquacultural wastes:

The agricultural and aquacultural wastes need prior treatment to be suitable for construction. This treatment consists of burning the waste products at a temperature of 1000ºC; once these residues turn into ashes, they can partially substitute the cement as a binder.

Some studies show that when applying this type of waste as supplementary cementitious materials, the workability and drying shrinkage of concrete decrease while the setting time increases. However, this type of waste varies from region to region. A varied chemical composition translates into the need for profound studies on different types of residue to determine their performance advantages and the correct combustion technique to be applied.

The research developed until now applies secondary materials like rice husk ashes, palm oil, corn cob, cane bagasse, straw, leaves, wood, forest biomass bottom ashes, and various plants. In addition, ashes from animal residues like oysters, mussels, clams, or eggshells have been applied as supplementary cementitious materials. However, further research is necessary to confirm the effectiveness of these materials on the performance and sustainability of concrete.

- Industrial wastes:

The industrial residue is one of the most studied substitution materials for cement in concrete production. Even though many studies have been made on technical, economic, and environmental performance, more profound research is required to cover the different chemical variations each type of industrial byproduct may present. The most common industrial wastes applied as secondary cementitious materials are coal fly ashes, coal bottom ashes, industrial slags, silica fumes, and natural and artificial pozzolans.

- Urban wastes:

The most suitable urban wastes that can be used as secondary cementitious materials are glass powder, sludge ashes, and municipal solid waste incineration ashes. This category, in particular, needs more profound research to become applicable in the construction sector.

1.2.2.3. Reduce the environmental impact and resource use of water

The construction industry is responsible for 12% of freshwater consumption worldwide. The concrete industry is responsible for a considerable amount of that consumption because every cubic meter of the material requires about 150 liters of water for its production; when considering the washing phase and the losses during production and transportation, this number can rise to 500 liters [15]. Taking this into consideration, some literature proposes strategies to reduce the wastage of hydric resources.

The use of seawater is possible for construction with concrete in situations where steel reinforcements are not required. Another option is to use recycled water recovered from the preparation of ready-mixed concrete, treated water from

sewers, and industrial and domestic wastewater. Currently, these hypothetical options must be studied profoundly before being applicable; for now, the normative only recommends using freshwater to develop high-performance, durable concretes. These alternatives require technical research to make water use from unconventional origins possible.

1.2.2.4. Reduce the environmental impact of aggregates

Although aggregates are, after water, the second most consumed material in concrete production, and they are present 12 times more than cement in the admixture, the environmental impact of aggregates is not significant when compared to the binder. However, the elevated use of concrete and its increasing application rates make the quantity of raw materials extracted as aggregates considerable.

Using aggregates coming from waste in concrete manufacturing hardly reduces the environmental impact of the material by up to 10% [16]. Several studies in this field define the characteristics recycled aggregates must possess in terms of components, water absorbance, humidity content, dimensions, shape, density, maximum quantity employable, and quality of the original material to be suitable for concrete manufacturing. It is ascertained, on a technical level, that in most cases, the content and the characteristics of the aggregates do not affect the durability of concrete, but the applicability of non-traditional aggregates depends on the mechanical resistance of concrete; therefore, it is only recommended on low performant concretes.

To reduce the environmental impact of aggregates, it is possible to employ aggregates with several origins and characteristics:

- Aggregates from construction and demolition waste, recycled from concrete, masonry, a mix of both, or even residues contaminated with other materials like wood, glass, asphalt, or plastic.
- Aggregates from agricultural and aquacultural waste like sugar cane bagasse ash, peanut shells, sawdust, wheat straw, wood ash, rice husk, cork, and fruit kernels. Due to the abundance of agricultural residues and the elevated demand for aggregates worldwide, these waste materials can partially replace conventional fine aggregates. In particular, they are beneficial in the production of lightweight concrete with low thermal conductivity.
- Aggregates from industrial waste like siliceous and volcanic ashes, iron and steel slags, silica fumes, and rubber and plastic wastes can replace part of the fine aggregates in a concrete admixture.
- Urban waste aggregates like glass, solid urban residues, wastewater sludge ashes, paper sludge, and granite waste sludge.

- Insulating aggregates like plastic, rubber, foamed glass, expanded clay, pumice, and sludge ash reduce the consumption of virgin raw materials. In addition, these materials reduce the density of concrete elements and their thermal conductivity, contributing to avoiding thermal bridges in buildings.
- Other types of aggregates include alkali-activated aggregates, mine tailings, and biochar.

1.2.2.5. Reduce the environmental impact of reinforcement

The last strategy, which consists of modifying the composition of concrete for structural applications, concerns the replacement of traditional steel bars with more sustainable materials. This strategy also refers to finding solutions that reduce the damage or increase the performance during the use phase of the building's life cycle to reduce maintenance and substitutions. Some approaches consider unconventional alternatives like using bamboo, basalt, fiberglass-reinforced polymers, carbon-reinforced polymers, or stainless steel to replace traditional steel rebars in structural concrete [3].

1.2.3. Concrete Mixing

The mixing phase of concrete is particularly energy-consuming in the production of concrete, and therefore, another phase to focus on to reduce the environmental impact of this process. This phase can be carried out in a production plant for premixed concretes or directly onsite using concrete mixers. In both cases, mixing strongly influences the quality and final homogeneity of the mixed compound and, consequently, the properties of the final element and its performance.

Given the importance of this influence, to date, research has focused on the evaluation of a long series of alternative mixing methods and tools to guarantee the quality and technical performance of the final admixture; taking into consideration the importance of reducing the environmental impact of this phase, especially as regards energy consumption. Therefore, it is necessary to carry out new studies capable of simultaneously considering the effect that alternative mixing methods and tools have on the final quality of the dough and the environment.

1.2.4. Optimization of construction methods

The onsite application of different construction methods affects the sustainability of the final concrete obtained. In recent years, various research studies have paid particular attention to developments in the digitalization of production processes in the construction sector. In the case of concrete, in particular, two methods based on

Additive Manufacturing extrusion processes have been identified, 3D Concrete Printing and Contour Crafting. In the construction sector, using automated production methods can bring significant benefits in terms of saving resources, energy, costs, and time in producing concrete structures and elements, both in the prefabrication field and, above all, onsite. Furthermore, some fascinating aspects from an environmental point of view concern the possibility of no longer using formwork, a costly element with a significant environmental impact eliminating the production of waste; and predicting, through an intelligent design based on the principles of topological optimization and hybridization functional, the presence of material only where it is structurally or functionally necessary, leading overall to a high saving in terms of resources. In this context, many research studies and experiments are in progress to evaluate all the aspects that introducing this innovation would involve in the concrete production field. Further studies are still to evaluate the overall environmental performance offered by buildings constructed using this technology during the entire life cycle.

1.2.5. Efficiency underuse

The fifth path aims to reduce the environmental impacts of concrete production during the use phase, which plays a central role within the life cycle due to the high temporal extension. In this context, three possible strategies intervene to obtain potential benefits at the environmental level: increase the durability of concrete structures, sequester CO2 from the environment through the material, and improve the performance of the final elements through the reduction of thermal conductivity resulting in energy savings.

1.2.5.1. Increase the durability of reinforced concrete

A particularly well-known strategy to reduce the environmental impact of concrete consists of increasing its durability to extend its useful life and reduce the maintenance/replacement cycles performed during the use phase of the life cycle. In this context, there are primarily two types of methods that can be adopted: the intrinsic and extrinsic methods. The first involves action on the concrete at the mixture level: mix design, additions, replacements, coverage of the mixture, and the use of more resistant steel reinforcements. The second provides various possible solutions, such as using hydrophobic paints or coatings. Although these actions often involve an initial increase in the cost and environmental impact of the structure due to increased required performance, they are winners in the long term, both economically and environmentally, due to the reduction in the number of maintenance interventions necessary during the use phase of the elements in the case of using high-performance concrete. In general, any action taken in this area has the purpose of slowing or stopping the corrosion of the reinforcement. For

example, using reinforcements in stainless steel, chromium steel with low carbon content, basalt, reinforced polymers with glass or carbon fibers, epoxy coating, anti-corrosion additives, or galvanized can reduce the damage caused by corrosion. In addition, preventing the penetration of aggressive agents into the material by controlling shrinkage, using self-healing concretes, or surface protections made with coating or treatments of various kinds prevent corrosive agents from reaching the rebars. Reducing the degradation rate of the material by paying attention to issues such as the alkali-aggregate reaction, the resistance to freeze-thaw cycles, and other physical and chemical attacks helps to prevent not only the degradation of concrete but also of steel reinforcements. The durability design refers to the many aspects that must already be considered at the design level and can be considered the key element for improving the sustainability of concrete.

1.2.5.2. CO_2 mineralization and utilization

It is possible to adopt some strategies to sequester this gas from the environment to reduce the greenhouse gas emissions, mainly CO_2, that characterize the production of cement-based materials and produce low-carbon concrete. Consequently, reducing the environmental footprint that is typically linked to such materials. At the material level, it is possible to foresee the sequestration of CO_2 through mineral carbonation. This procedure can be carried out by various types of elements such as metals like zinc, copper, nickel, and iron; or rocks containing magnesium, calcium, and basalt, which are more suitable for CO_2 sequestration due to their high diffusion in nature and their reduced cost compared to the former. The possibility of carrying out carbonation to sequester CO_2 from the environment is influenced by the conditions of exposure to this greenhouse gas and by the properties of cement-based materials like water content, chemical composition, size and surface area of particles, porosity, and permeability.

1.2.5.3. Thermal conductivity improvement and energy saving

One of the most effective strategies to reduce the environmental impact is the reduction of the building's energy expenditure during its useful life, a much longer life cycle phase, and consequently a more significant impact on the environment than the construction phase. In order to save energy by reducing the energy requirements for heating and cooling systems, the best solution is to reduce the thermal transmittance of the envelope and, in this specific area, the thermal conductivity of the concrete.

Several factors influence the last physical parameter in concrete, such as:

- Density and microstructure: The density, in particular, is influenced by the water/binder ratio, size and proportion of the aggregates, and porosity and nature of the pores. Therefore, acting on the density of materials

represents the best strategy, and the most studied in the literature, to modify the thermal transmittance value of any type of cement-based materials.

- Type, size, and proportion of aggregates and other additional materials like natural aggregates, lightened materials, aggregates recycled from waste from various sources, and any content of phase change materials. Since the aggregates make up most of the volume of the concrete, this factor dramatically influences the thermal transmittance value of the final elements.
- Moisture content and temperature.
- The binder type and content, although not among the most significant factors.
- The possible presence of natural fibers: vegetable, mineral, or animal).

1.2.6. End of life

The end of life path aims to reduce concrete's environmental impacts after demolition. This includes all the strategies aimed at reintroducing concrete into a new life cycle through reusing the elements as they are and, as more often happens, through recycling and subsequent use as aggregates for producing new concrete. In this context, it is possible to predict, in the design phase, what the end of life scenarios of concrete elements will be. Consequently, making strategic design choices to facilitate the disposal procedures, such as creating dry joints, which allow the disassembling of joints with other concrete elements and materials of different nature. Another viable strategy is the realization of elements with a standard cement matrix but characterized by portions with different densities in such a way as to satisfy a plurality of performance requirements without the need to use materials of different nature that can irreversibly contaminate future waste recycled.

Chapter 2

Fiber addition in concrete

2.1. Effects of fiber addition in concrete

As seen in chapter 1, the sustainability of concrete can improve with the modification of the mix design. There are several ways to accomplish improvements when modifying the admixture. One of these methodologies is the addition of fiber reinforcements to the admixture in a fresh state.

Fiber-reinforced concrete is, as its name suggests, concrete containing fibers. Generally, these fibers tend to be distributed uniformly and oriented randomly [17]. Therefore, including fibers generates a series of advantages to the material's properties.

On a concrete admixture, fibers can be added either manually or with a dosing device [18]. The former method must take into account that the fibers should be evenly distributed; however, this distribution cannot be guaranteed due to human error. On the other side, the latter method automatizes the process and leads to even results in fiber distribution.

Another important aspect of fiber inclusion is the dosage. Table 1 shows the standard dosages for fiber-reinforced concrete.

Table 1. Standard dosages for fiber-reinforced concrete [18].

fiber material	min. dosage	usual dosage	
	[kg/m^3]	von [kg/m^3]	bis [kg/m^3]
plastic PP	2,5	3	7
steel	30	30	70
glass	1	1,5	3

Concrete is a construction material characterized by a higher brittleness and a lower tensile strength than other materials like metals and polymers [19]. As a result, it can quickly develop cracks that let harmful agents inside the construction element leading to "early saturation, freeze-thaw damage, scaling, discoloration, and steel corrosion" [19]. The inclusion of fiber reinforcement in concrete can help overcome these challenges by improving various characteristics further explained in this chapter.

2.1.1. Increased mechanical properties

The mechanical properties of concrete characterize by an elevated compressive strength and a low flexural strength. This is why, for structural applications, concrete needs to collaborate with steel rebars that provide the required flexural strength. Fiber-reinforcements can be included in concrete for many reasons. However, if the goal is to improve its mechanical properties, the mix design should contemplate several parameters such as "fiber type, content, aspect ratio, and length" [20].

As it can be inferred, the flexural and tensile strength are more affected by the presence of fiber-reinforcements than the compressive strength [20]. This phenomenon occurs because fibers are able to support tensile stresses and, therefore, carry the applied loads after the concrete has cracked. On the other hand, although the compressive strength is less affected by the presence of fibers in the cement mix, it presents some improvement; however, some studies have shown a decline in the compressive strength of fiber-reinforced concrete when compared to traditional concrete. Therefore, to properly understand how each type of fiber and its characteristics on the admixture affect the mechanical properties of a building component, further research needs to be held.

2.1.2. Increased ductility

A material is considered ductile when it can withstand plastic deformations when submitted to tensile stress. Concrete characterizes by a brittle behavior; it cannot withstand elastic deformations by itself. However, with the addition of fiber-reinforcements, it acquires a more flexible behavior. Moreover, the ductile properties of the fibers can resist the tensile loads after the cementitious material has failed and, therefore, render the deformation capabilities of said material higher.

2.1.3. Delay crack propagation

In fiber-reinforced concrete, the strands create a matrix that is held together by the cement paste. This particular conformation reduces the crack formation and propagation caused by plastic and drying shrinkage. The property of reducing cracks leads to increased durability of concrete components, given that many degradation processes occur when they are present. The durability is fundamental for sustainability because if a construction component lasts longer, the replacement or maintenance rate decreases, and therefore the CO_2 emissions corresponding to the material become less frequent.

2.2. Types of fiber compatible with concrete

Fiber reinforcements vary in numerous characteristics like shape and size; this variety allows them to fulfill a wide range of purposes. They classify into artificial and natural fibers.

2.2.1. Artificial fibers

Artificial fibers applicable as concrete reinforcement can be metallic (steel); synthetic such as acrylic, aramid, carbon, polypropylene, polystyrene, nylon, and polyester; glass of aramid fibers; and carbon fibers. Figure 4 shows the mentioned types of artificial fibers.

Figure 4. Various types of artificial fibers [21].

Steel fibers are one of the most resistant types of fiber; however, they are susceptive to corrosion. They vary in the range of 0,7-1,2 mm in diameter and 25-60 mm in length [22]. These fibers can have different section shapes circular or polygonal, and

also they can be wavy or straight. However, these types of fiber are not fully compatible with lightweight concrete because of their increased mass.

Polymeric fibers are broadly researched, they come in many shapes and sizes depending on the purpose of application and have shown results leading to increased mechanical properties of both, traditional and foamed concrete. However, some researchers have found a marginal reduction of compressive strength, limited to a few cases, when adding synthetic fibers to a concrete mix [23], [24]. In addition, improvements of a 2-5% in compressive strength and 13-70% in flexural strength have been achieved in foamed concrete depending on the curing conditions and the development of the hydration process [25].

Glass fibers, in general, are applied on the reinforcement of thin-sheet cement or mortar matrices. This type of fibers cannot withstand the alkalinity of Portland cement; therefore, alkali-resistant fibers must be applied in these cases. Alkali-resistant fibers improve the compressive strength, flexural strength, and elastic modulus performance of concrete in a higher rate than polymeric ones [26].

Carbon fibers have a higher elasticity modulus and flexural strength than steel fibers. They show good adhesion to the cement paste and have shown favorable results when applied as concrete reinforcement. However, because of their brittleness, a resin coating is recommended.

2.2.2. Natural fibers

To reduce carbon emissions, the latest focus of research in fiber-reinforcement of concrete has focused on finding less pollutant alternatives than the ones already in use. This is where natural fibers come to the picture. Generally, these fibers come from secondary products which increases the sustainability of the applied reinforcement because it is not obtained from raw materials, but from recycling or waste recovery processes. For instance, in the case of foamed concrete, polymeric or glass fibers can be replaced by natural fibers.

Overall, concrete reinforcement natural fibers are plant-derived and consist of hemicellulose, lignin, and pectin [27]. Bamboo, banana, coconut, cotton, hemp, jute, and palm are a few fiber species that have given promising results as a concrete aggregate. Henequen fibers, for example, have the potential to be widely introduced as a construction material since they have proven to increase the mechanical properties of concrete, mainly when submitted to an alkaline treatment which encourages an improved fiber-matrix interaction [28].

Figure 5. Various types of natural fibers [21].

Although there is a vast database on plant-based fibers, scientists started to drive their interest toward animal fibers. Pig hair, for example, applied to regular mortar, shows higher tensile strengths than other natural fibers and proves to be an effective crack control mechanism, particularly for plastic shrinkage cracking. [29]

2.3. Animal fibers in concrete: Sheep wool fibers

To keep sheep healthy and clean, they should be sheared at least once a year which means that sheep wool is able to renew at rapid rates and therefore, should be considered as a renewable resource. In Europe, sheep wool is widely produced; lamentably, not all the produced material is suitable for the textile industry, nearly 75% of this raw material becomes waste and requires a high energy consumption to sterilize it at 130°C and then needs to be thrown away as special waste [30].

Due to its high production rate and its large impact in the world's contamination, sheep wool has caught the attention of the construction industry to be employed as a sustainable and economical building material. Its primary application is as thermal insulation inside walls or partitions to improve the energy efficiency of buildings [31].

In the last decade, studies on the application of sheep wool as a fiber reinforcement for concrete have revealed encouraging results. The performed tests have used several techniques to treat the fibers and improve their characteristics, including non-treated, water-rinsed, neutral detergent-washed, salt water-dipped, and plasma-treated fibers. In general, adding sheep wool fibers to mortar or concrete increases flexural strength, fracture toughness, and tensile strength, but compressive strength decreases in some cases [32], [33].

Figure 6. Ordinary sheep wool fibers used in concrete reinforcement [34].

Regarding the treatments found in previous works, washing the fibers improves adhesion with concrete and, therefore, improves mechanical performance [35]. Dipping sheep wool fibers in saltwater increases their surface tension, and therefore, improves adhesion to the cement matrix, causing the concrete to withstand more compressive and flexural strength [36]. The addition of plasma-treated wool fibers increases flexural strength by a 5% more than the addition of non-treated fibers; however, fracture toughness has a 300% increment in both cases [37].

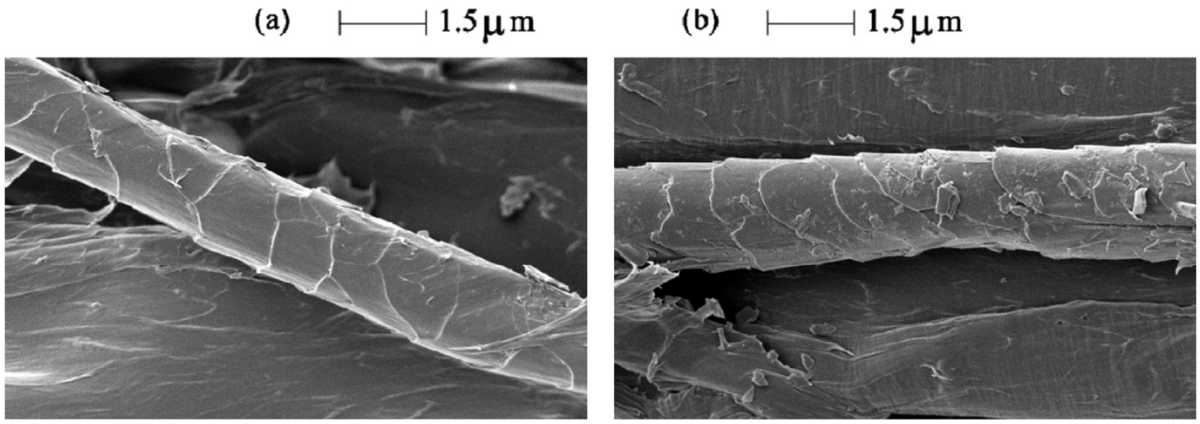

Figure 7. Non-treated sheep wool filament on the left and plasma treated sheep wool fiber on the right [38].

The fiber content rate and the fiber length affect the mechanical properties. For example, some researchers show that a fiber content between 2-3% is optimal, but when applying treated fibers, this trend is reduced to 0,5-1% to achieve a similar resistance capacity [39], [40]. Furthermore, other experimental works show better performances when varying fiber length. Short 1mm fibers act only as a filler, and longer fibers of about 20mm, create agglomeration; more desirable results were conceivable using a mid-length value of 6mm with up to a 13% fiber content [35].

Figure 8. Sheep wool fibers with 20 (a), 6 (b), and 1 (c) mm length [35].

In addition, some researchers have analyzed the internal curing process of concrete and mortar reinforced with sheep wool fibers. It has been proven that long curing periods translate in a reduction of compressive strength because the strength gaining capacity of concrete reinforced with sheep wool fibers is lower than usual when referred to the curing period [32].

The crystallization phenomenon in concrete curing is proof of good hydration; in concrete reinforced with sheep wool fibers the presence of C-S-H gel is higher, therefore, the microporosity is reduced; however, when a higher content than 4% of sheep wool fibers is added, agglomerations of C-S-H gel are registered [40]. The layers of silica and C-S-H gels present good adhesion properties within the cement matrix but the formation of crystals translates in a higher stiffness [40].

During the curing process, sheep wool fibers degrade because of the high alkalinity present in Portland cement influencing negatively on their resistance; therefore, the application of low alkaline concrete types should be considered [41]. In this terms, it can be established that if the alkalinity an curing time in water increases, the quality of the fibers decreases [42]. The curing conditions of the concrete admixtures affects the durability of sheep wool fibers. Fantilli et al. compared sheep wool fiber reinforced mortars cured in dry conditions (20°C and 50% R.H.) and cured in water both for 28 days; the former presented an improved performance while the latter did not because the presence of water led to an alkaline reaction that corroded the fibers completely leaving open pores where the fibers were and leaving the cement matrix without support [34].

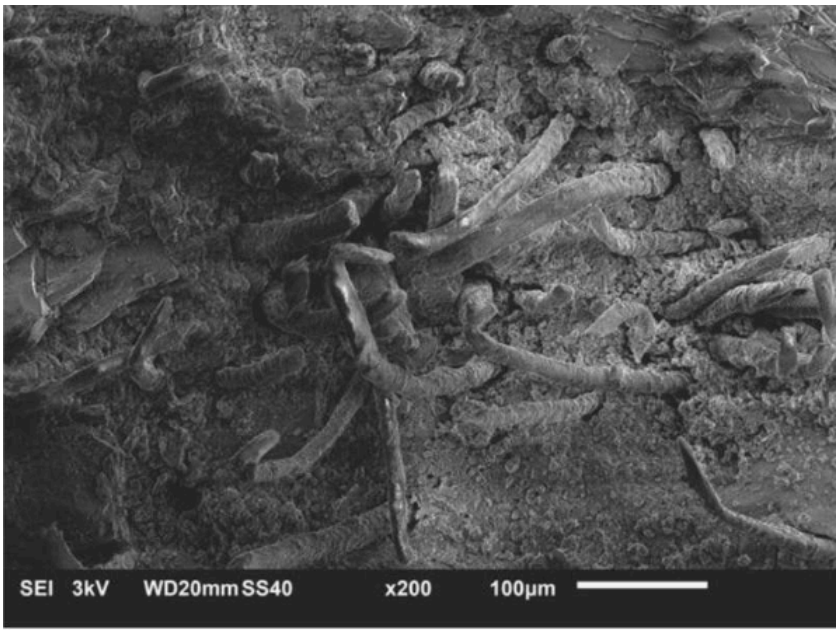

Figure 9. SWF reinforced mortar stored on air with visible wool filaments [34].

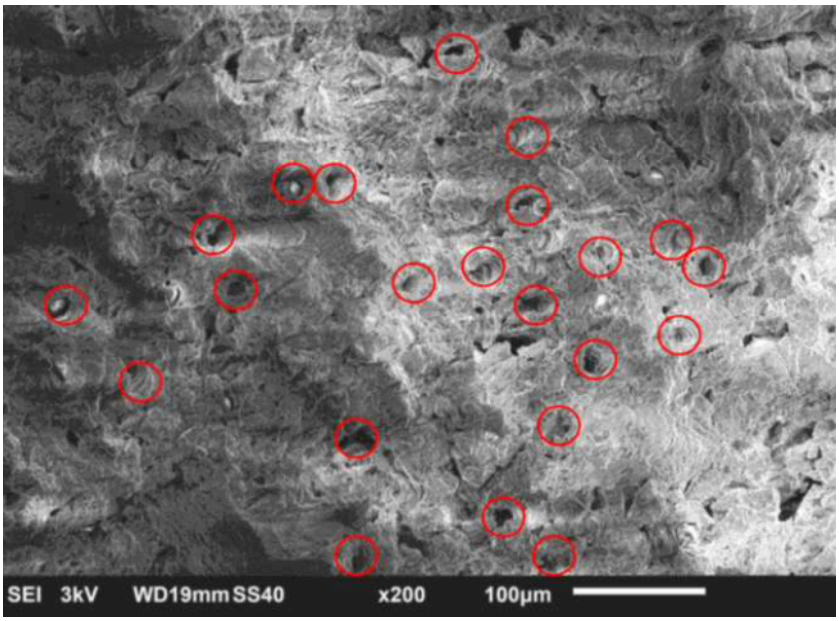

Figure 10. SWF reinforced mortar stored in water with visible empty holes where the wool filaments used to be [34].

As shown on the previous analysis, sheep wool fiber concrete reinforcements have shown promising results, however, they have not yet been applied to foamed concrete.

Chapter 3

Foamed concrete

3.1. Foamed concrete properties and advantages

Within the large family of concretes, lightened concretes differ from the standard version mainly due to their lower density. Lightweight concretes' density varies in a range of approximately 200 to 2000 kg/m³, while traditional concretes fluctuate around 2000 and 2500 kg/m³. The lightness of foamed concrete relies on a series of voids produced by the addition of foaming surfactants into the cement mix [43]. Two primary strategies have the ability to allow concrete to obtain this characteristic; these are the addition of foaming agents and the Autoclaved Aerated Concrete method. These methods introduce air bubbles to the cement paste generating cavities in the conglomerate.

From the above-mentioned strategies, the first one, also known as dry foam method, consist of adding a pre-formed foam into the cement mix that is made by mixing a surfactant agent with water at high speeds forcing pressurized air into the solution and creating bubbles generally of an even size of less than 1mm [44]. It can also be obtained by adding a mix-forming agent (wet foam method) directly into the cement mix, which consists of spraying a water/foaming agent solution over a fine mesh which causes pressure to drop across the mix and allows suctioning air from the environment; this creates a 2-5mm bubble size, which is unsuitable for densities below 1100 kg/m^3 [45]. On the other hand, the Autoclaved Aerated Concrete method consists of mixing traditional mortar ingredients such as cement, water, sand, and lime with aluminum powder. This last ingredient acts as an expansion agent due to its reaction with cement and forms microscopic hydrogen bubbles, making concrete grow up to five times its original volume leaving empty voids after evaporation. Autoclaved Aerated Concrete receives its name because it is steam-cured in a pressurized chamber or autoclave [23].

In recent years, the use of lightweight concrete has expanded thanks to several reasons considerably: the increase in the strength/weight ratio; the development of new cementitious materials, foaming agents, and fillers for specific applications; the implementation of production methods; and the increased ability to control the final properties of concrete.

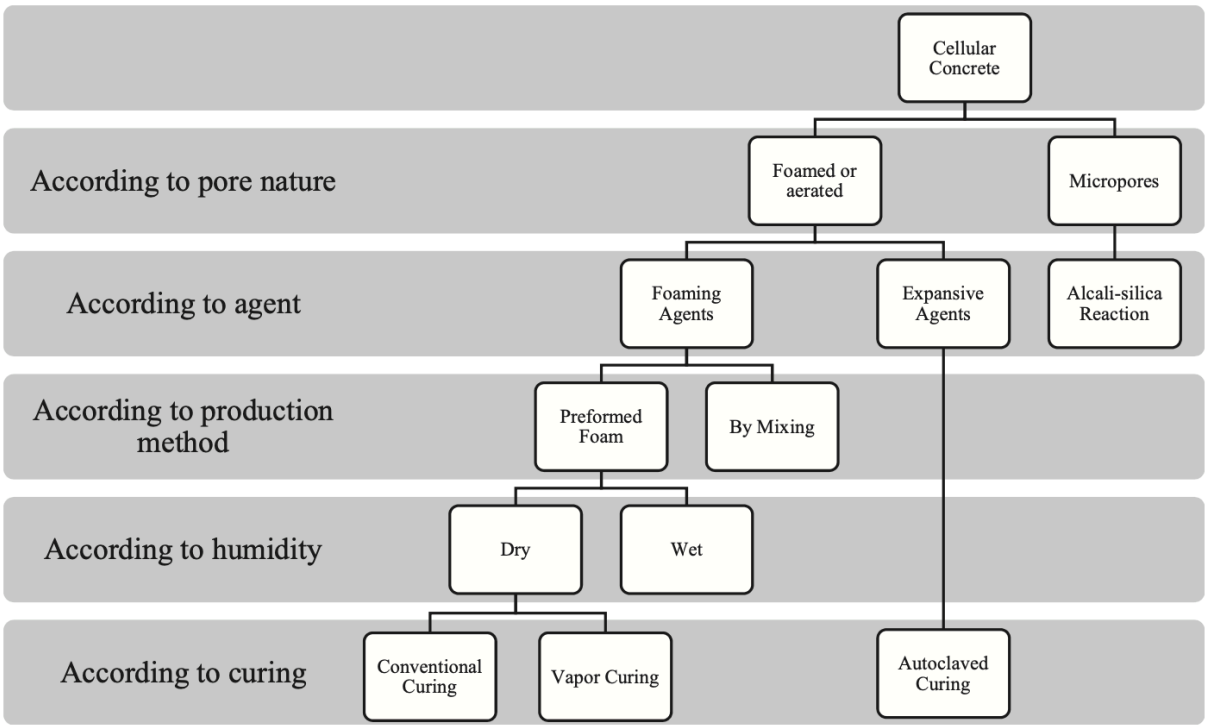

Figure 11. Classification of light-weight cellular concrete [46].

According to its density, cellular concrete can permit various applications. Ultralightweight concrete, with a density of 300-600 kg/m^3, is mainly used as thermal and acoustic insulation or fire protection due to its low mechanical performance. A density of 700-1100 kg/m^3 typically produces bricks, blocks, fillers, floor leveling mortars, and non-structural elements. Higher densities such as 1200-1800 kg/m^3 support higher loads and, therefore, can be applied to create precast or onsite structural elements and reduce the weight of components that require high strengths [46].

Lately, foamed concrete has aroused growing interest in the construction industry thanks to some characteristics that make it more performing and multi-functional than ordinary concrete, such as:

- Lightness: It can be up to 80% lighter than ordinary concrete [46]. Its lower specific weight allows for reducing the size of the resistant supporting structures. As a result, it can be helpful not to place excessive loads on existing structures in the event of seismic renovations and retrofitting in vulnerable areas.
- Excellent thermal and acoustic insulation, thanks to the presence of air bubbles, and especially for low-density mixtures, the thermal conductivity can be reduced between 5% and 30% compared to ordinary concrete [47].
- Good fire resistance.
- Greater workability.

- Economic convenience, thanks to the use of simple, inexpensive, and easily available building blocks locally. For these reasons, foamed concretes represent the most economical solution in thermal, acoustic insulation, and cavity filling.
- Material saving thanks to cavities that reduce the element's density and the minimum consumption of aggregate.
- Potential use with a large scale of by-products deriving from other processes such as fly ash and blast furnace slag.
- Increased sustainability in environmental terms and economic terms.

3.2. Mix design of foamed concrete

Foamed concrete is obtained from the same essential elements used for conventional concrete. However, it differs from it by the addition of surfactants which, through chemical reactions, produce air bubbles that remain incorporated in the cement conglomerate. The mixture consists of the following components: a binder (Portland cement or other types of cement and substitutes), water, surfactant foaming agent, any aggregates, fillers, fibers, and additives.

Cement can be partially replaced by by-products deriving from other processes such as fly ash (30-70% in mass), ground blast furnace slag (10-50% in mass), silica fumes (up to 10% in mass), or construction and demolition waste, to reduce costs, improve the consistency of the mix, reduce the heat of hydration and increase the compressive and flexural strength of the final product [47].

The water requirement of the admixture depends on many factors such as the composition of the mix (water/cement ratio, the proportion between ingredients in the mix, and the presence of additives), the characteristics to be obtained in the fresh mixture (consistency, stability, and workability), and in the hardened state (density, mechanical resistance, and thermal performance). For example, in the event of insufficient water, the admixture would be rigid, causing the bubbles to break. In contrast, in the event of excessive moisture, the mixture would separate from the air, causing instability. The water/cement ratio can vary from 0.4 to 1.25, but it is possible to reduce water consumption through a careful combination of superplasticizers and mineral mixes [47].

The surfactant foaming agents, determining the ability to include air bubbles in the cement mixture, are necessary to control the density and porosity of the final element and, consequently, its performance. The agents mainly used for producing foamed concrete can be of two origins: natural (protein-based) and synthetic. The former generates bubbles due to degradation of the agent itself; they greatly depend on the temperature and pH of the mixture and develop a more resistant and tight porous structure which determines better mechanical performance. On

the other hand, the latter works by reducing the surface tension of liquids allowing to reach lower densities, are cheaper, create more stable foams, and generate a complex chemical environment for which it is essential to pay attention to the compatibility between surfactant and type of concrete. Two different methods can be used to generate the foam mixture: the use of pre-formed foam or the mixed foam method. The first consists of separately producing the base mixture (cement, water, additives, and aggregates) and the stable foam (foaming agent and water). Everything will be further mixed for a few minutes until obtaining a homogeneous, lightened mixture. On the other hand, the second method requires the surfactant foaming agent to be incorporated directly with all the other ingredients that make up the admixture for which the foam will form during the mixing process. It is usually preferable to use pre-formed foam to reduce the amount of foaming agents, to have a direct and close relationship between the quantity of foaming agent and the air content of the mixture, and to obtain a higher quality foam. In any case, the foam must be added to the mix as soon as possible from the moment of mixing. It must be stable to withstand the pressure of the mortar until the cement reaches its initial setting and begins to build around the air bubbles. Given a specific final density, the foam requirement essentially depends on the materials making up the mixture, for example, the type of cement used, the water/cement ratio, and the mixing speed. In general, it is necessary to pay particular attention to the characteristics of the foam since they mainly influence the mechanical resistance of the final product.

The aggregates are usually made up of fine sand. Aggregates must be applied exclusively on higher densities than 500 kg/m^3 since otherwise, there would be segregation of the compound due to the sedimentation of the aggregates under the force of gravity. However, they too can be partially replaced with alternative fine aggregates such as fly ash, lime, gypsum, crushed concrete from construction and demolition waste, ashes from incinerators, recycled glass, foundry or quarry sand, expanded polystyrene, and PVC to reduce the density of foamed concrete and to reduce the consumption of raw materials [47].

The addition of synthetic or natural fibers in specific sizes and dosages can improve the shear behavior of foamed concrete up to reaching the levels of ordinary concrete, mitigate brittleness, reduce the problem of shrinkage cracks, and reduce the weight and cost of the final product. However, an adverse effect of using fibers is represented by the possibility of decreasing the porosity of the element, so it is essential to pay attention to the choice of the type, size, and quantity of fibers.

The addition of additives must be weighted, paying particular attention to compatibility with the foaming agent used and the system of chemical reactions that allow the air to be successfully trapped inside the product.

To produce a stable mixture, it is necessary to consider the mix design at the level of both ingredients (substitutions or additions) and proportions, the foaming agent used, the method of preparation of the foam, and the tools and procedures used for mixing. These aspects affect the generation of adequate porosity with uniform distribution of the air gaps and allow to control the properties of the mixture in the fresh state and, consequently, the properties and performance of the product once hardened. To design and proportionate the admixture, there is no standard dosage method. However, one usually starts from the final product's density and mechanical resistance requirements. Based on these data, the quantities and proportions between the ingredients and the foam amount vary to obtain different final densities. In general, the optimal combination of strength, density, workability, and cost can be obtained by changing the foam content, the water/cement ratio of the mixture, and, if present, the type of fibers used.

3.3. Density, mechanical resistance, and instability

The air that can be included in the mix can vary between 30 and 60% by volume in the case of structural uses and between 70 and 85% by volume in concrete with thermal insulation or secondary element function [5]. However, the lightness that intrinsically distinguishes this type of material, in addition to determining a series of advantageous characteristics, also leads to two main problems, lower mechanical strength and a possible phenomenon of instability of the admixture, especially for densities lower than 500 kg/m³.

The mechanical characteristics essentially depend on factors such as final density, surfactant foaming agent, hardening conditions, type of cement, water/cement ratio, air/cement ratio, and any presence of fibers or other reinforcements. In this regard, various studies aimed at improving mechanical strength through, for example, the addition of fly ash or silica fumes to enhance compressive and flexural strength, the addition of biochar to improve fracture strength or the incorporation of short fibers or the use of reinforcements made by bidirectional fiber grids to increase the flexural strength. Other studies also propose and experiment with nanofiber reinforcement. As for the hardening conditions, their influence on the hydration process affects the final resistance of the element.

A fundamental phenomenon that characterizes foamed concrete, and in particular ultra-low density concrete, is the compound's instability, which consists of the segregation of the fresh mix with separation between solids and air, which causes the complete dispersion of the latter in the environment, making the mixture inadequate.

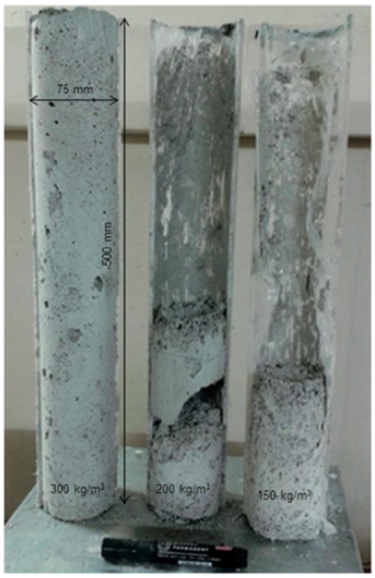

Figure 12. Example of instability in ultralightweight foamed concrete. From left to right, density is equal to 300, 200, and 150 kg/m³ [48].

This phenomenon can occur almost immediately or, more often, after a specific time from the beginning of mixing as the final formation of bubbles in the admixture does not occur instantaneously when the foam is incorporated but takes place over time through a dynamic process based on the search for a balance within the system of forces to which each bubble is subject.

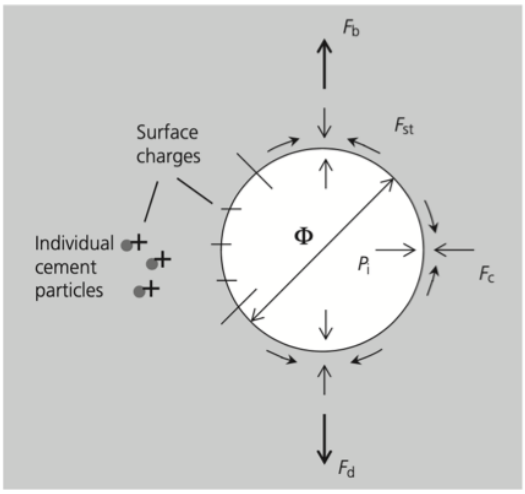

Figure 13. Graphical representation of the forces acting on a single air bubble inside a foamed concrete fresh admixture [48].

The dimensional expansion of the bubbles inside the admixture depends on two factors, the confinement force to which they are subject, which can generate a pressure difference between the outside and inside of the air bubble with consequent growth to seek equilibrium; and the natural dimensional variability that characterizes the bubbles which facilitate the gas diffusion phenomenon from the

smallest to the largest bubbles. The confinement strength depends on the density of the fresh mix, the aggregates used, the type of cement, and the rheological characteristics of cohesion and viscosity of the mixture. The size of the bubbles, on the other hand, depends on density, water/cement ratio, type of cement, and type of fillers used.

The phenomenon of instability is an irreversible process that potentially occurs in all foamed concretes but is particularly problematic in ultra-low density because the reduced density, the lack of aggregates or fillers, and the decrease in the water and cement content lead to a considerable reduction of the confinement force, to larger and closer bubbles, and the formation of micro-bubbles in the dividing walls between the bubbles themselves. These factors increase the probability of the occurrence of the instability phenomenon since the process diffusion of the gas in the fresh state is facilitated. It continues rapidly without encountering opposition until the bubbles become so large that they undergo a buoyancy force more significant than the force of confinement and consequently rise to the surface and disperse the air in the environment. Since the phenomenon of instability stops only when the mix hardens, to prevent it from occurring, it is necessary that hardening takes place before the bubbles become large enough to float. In higher density concretes, this is easily achieved during the typical hardening process of Portland cement, while in ultra-low density concretes, one of the methods studied at the research level consists in replacing part of the Portland cement with a quantity of calcium sulfoaluminate cement (CSA) intended to accelerate the hardening process. In this experimental study published in 2015 [48], it emerged that the addition of CSA in partial replacement of Portland cement (up to a maximum of 10% by mass) allows to obtain products with a final density of up to 150 kg/m^3 without incurring in instability. On the other hand, it is not possible to use higher percentages of CSA as the time before the hardening would be insufficient to incorporate the foam and deposit the foamed concrete. In fact, with a replacement equal to 15% of the mass, there would be only 2 minutes before the start of hardening, while with 10%, there are about 20 minutes. In addition, some studies have shown that the presence of fly ash in the mix makes the bubbles smaller with the same density as it increases the confinement force thanks to creating a sort of barrier around the bubbles themselves.

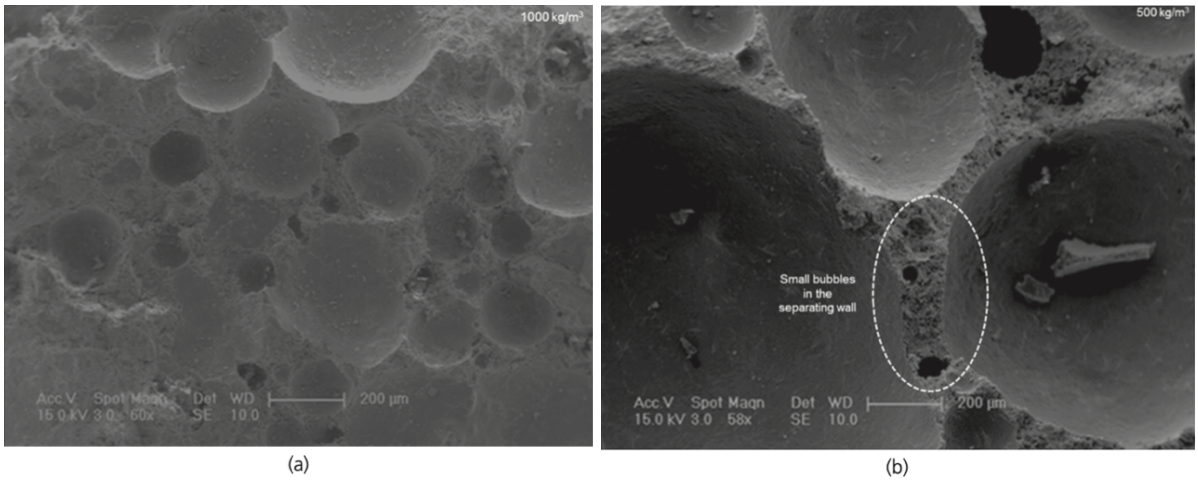

Figure 14. High density foamed concrete on the left and low density on the right. The second presents macro-bubbles [48].

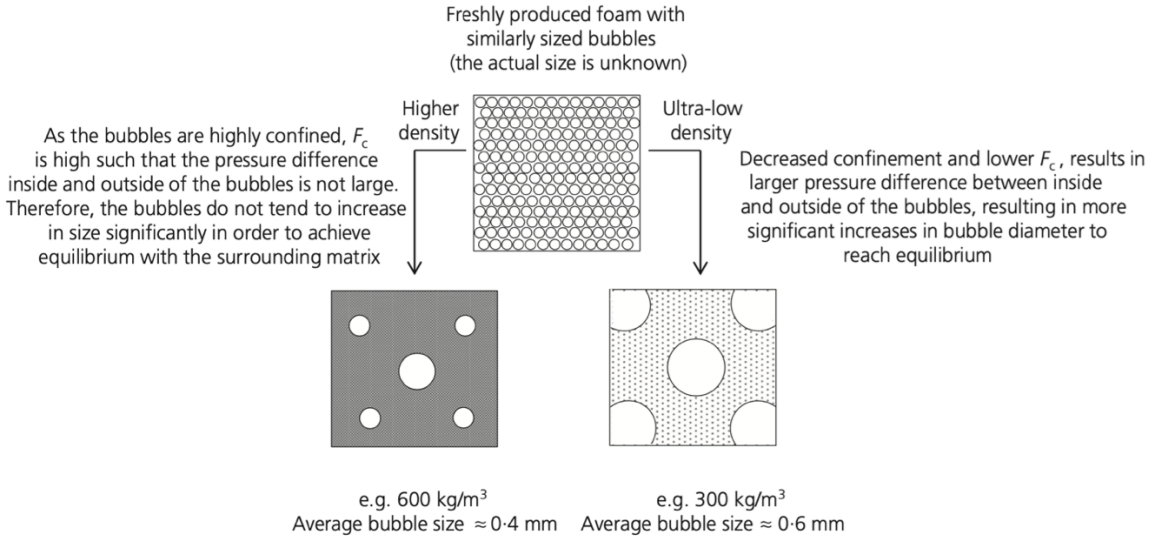

Figure 15. Schematic comparison between the bubbles in 300 and 600 kg/m³ foamed concrete [48].

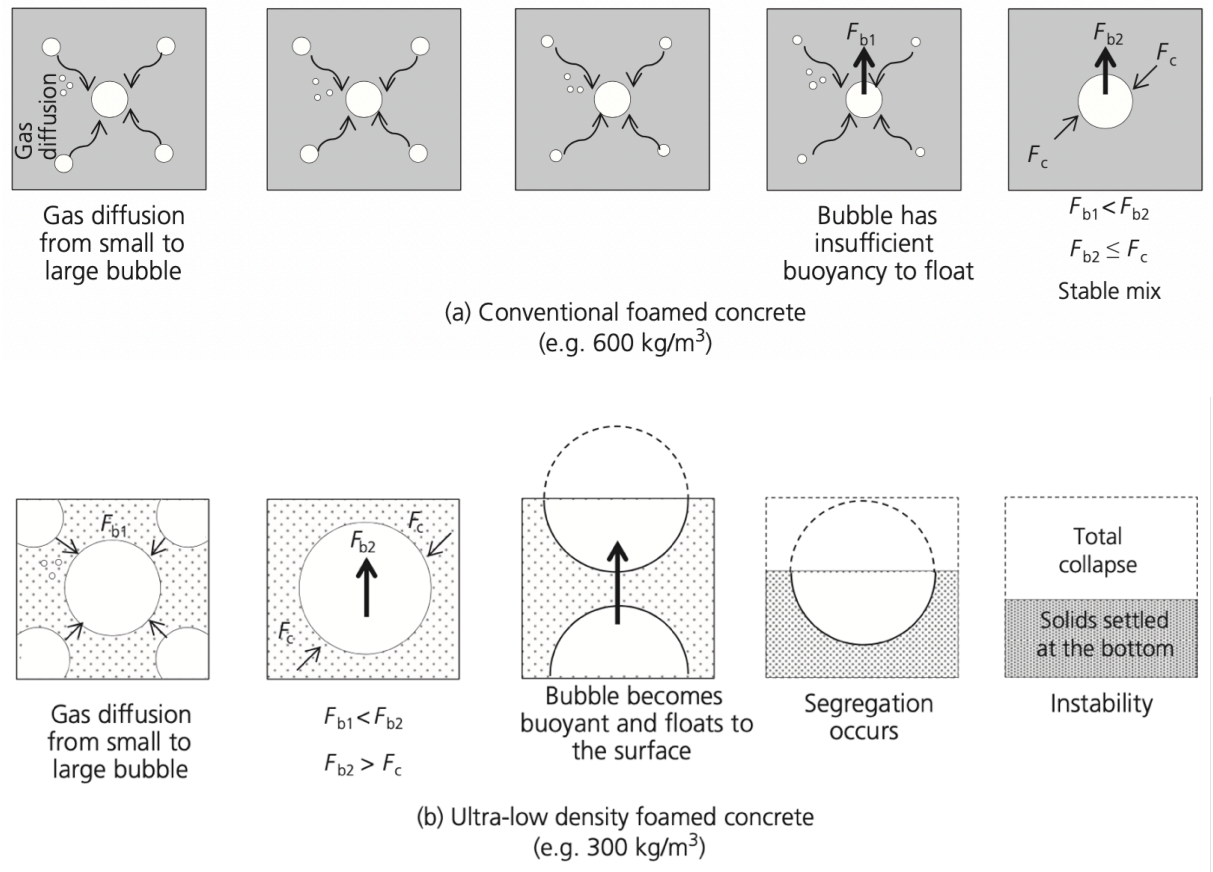

Figure 16. Graphic representation of the gas diffusion process in 600 kg/m³ foamed concrete above and 300 kg/m³ below. On the second, the instability phenomenon leads to the composite's segregation [48].

Chapter 4

Additive manufacturing with concrete

4.1. Additive manufacturing processes compatible with concrete

Additive manufacturing (AM) is a production methodology that originated from the first 3D printing process conceived by Ciraud in 1972, which consisted of making objects layer by layer from a 3D model [49]. AM differs from traditional manufacturing processes because it puts together an object from the raw materials instead of subtracting portions of the material to achieve the desired shape. AM has developed considerably in the last years and is becoming more and more common in production processes. Joseph Pegna was one of the first to suggest its use in construction to build large structures without formworks in 1997. He created a process called Selective Aggregation (SA) which, although it has not been vastly applied, has become a source of inspiration for the development of similar AM methods, which have led over the years to the realization of many projects and advances in this area of innovation.

The additive manufacturing methods developed in the last decades that appear to have potential in the construction sector are in all 15. However, they can be divided into seven categories based on the type of process used.

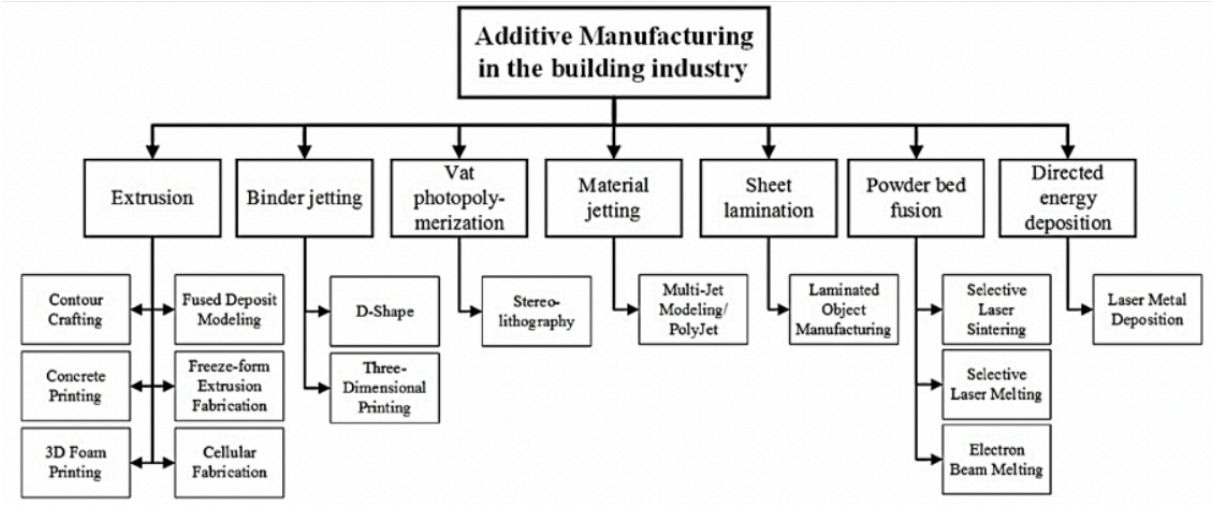

Figure 17. Outline of AM processes and methods used in the construction sector [50].

Each method characterizes by the type of process and material used. However, the choice of a specific method is also conditioned by the desired final product in terms

of dimensional scale, location of production, possible load-bearing function, formal complexity, and surface finish.

Table 2. Characteristics of the process and materials for each method of AM applicable in the construction sector.

Method		*Process Properties*	*Manufactured Materials*	*State of Starting Material*
CC	*Contour Crafting*	Extrusion, Requires Support Structure	Concrete, Ceramics	Paste
CP	*Concrete Printing*	Extrusion, Re-usable Support Structure	Concrete	Paste
C-Fab	*Cellular Fabrication*	Extrusion, No Support Structure	Polymers	Paste
3DFP	*3D Foam Printing*	Extrusion, Support Structure Not Always Necessary	Polyurethane Foam (PUR)	Liquid
FDM	*Fused Deposit Modeling*	Extrusion, Requires Support Structure	Ceramics, Glass, Polymers	Paste
FEF	*Freeze-form Extrusion Fabrication*	Extrusion, Solidification by Freezing, No Support Structure	Ceramics, Metals, FGMs	Paste
DS	*D-Shape*	Binder Jetting, No Support Structure	Sandstone	Powder
3DP	*Three-Dimensional Printing*	Binder Jetting, No Support Structure	Sandstone, Ceramics, Polymers, Metals	Powder
SLA	*Stereolithography*	Vat Photopolymerization, Requires Support Structure	Ceramics, Polymers, Metals	Liquid
MJM	*Multi-Jet Modeling (and PolyJet)*	Material Jetting, Requires Support Structure	Polymers, Metals, FGMs	Liquid
LOM	*Laminated Object Manufacturing*	Sheet Lamination, Requires Support Structure	Ceramics, Polymers, Metals, Wood, FGMs	Solid Sheets
SLS	*Selective Laser Sintering*	Powder Bed Fusion, No Support Structure	Ceramics, Glass, Polymers, Metals	Powder
SLM	*Selective Laser Melting*	Powder Bed Fusion, No Support Structure	Ceramics, Glass, Metals	Powder
EBM	*Electron Beam Melting*	Powder Bed Fusion, No Support Structure	Metals	Powder
LMD	*Laser Metal Deposition*	Directed Energy Deposition, Support Structure Not Always Necessary	Metals, FGMs	Powder, Solid Wire

Of the 15 AM methods suitable for use in the construction sector, only two are compatible with using concrete as a material: Contour Crafting (CC) and 3D Concrete Printing (CP).

To build the final elements, both use the extrusion process, the most extensively used and the most promising of the processes based on AM. This type of process consists of the creation of physical objects through the creation of overlapping self-supporting layers. In this instance, the material gets released as a continuous filament through a pumping method that pushes it through a nozzle mounted on a gantry arm or a digitally controlled robot. By respecting a specific timing for the overlapping of the layers (layer cycle-time), a high-strength bond is created between them, generating a solid structure capable of maintaining its shape under the increasing hydrostatic pressure caused by the deposition of the subsequent layers and avoiding the formation of cold joints which represent localized weaknesses in the final element.

The material typically used in concrete extrusion processes consists of a mortar with a high cement content and a maximum particle size of 2-3 mm to avoid problems during the extrusion process. The shape of the extrusion can vary based on the nozzle head, which can be circular, oval, or rectangular. The linear extrusion speed usually varies from 50 to 500 mm/s. The print orientation is usually vertical but can also be horizontal.

The layer properties and, therefore, the printing orientation significantly influence the ultimate product. Thanks to its layered nature, it is anisotropic and thus has variable mechanical strength within the three directions (x, y, and z). In addition, the ribbed surface finish is affected by the thickness of the layer as the layers remain visible in the final product. Generally, the thicker the layer, the more post-processing will be required to achieve a smooth surface finish. As for the geometric characteristics, the printed elements can be planar or volumetric, and it is possible to create cantilevered elements and empty spaces within the volume.

In the construction sector, AM's technology using concrete applies to three product families [51]:

- Components such as blocks and panels made in a factory
- Walls and columns printed onsite
- Permanent shell with possible filling made onsite by conventional casting

In the literature, there is also a distinction between large, medium, and small-scale AM methods. The first involves entire walls/buildings built onsite and large structural elements. The second concerns building components that can be assembled in construction. Finally, the third concerns detailed and complex objects such as facade elements and joints. Depending on the scale, a different type of printer or

robot is used. For example, gantry systems and robotic arms are often used for large and medium-scale methods.

4.1.1. Contour crafting

The CC method aims to automatize onsite construction, particularly for structures prioritizing reduced construction times and economy, such as social housing projects and buildings in devastated areas. According to the Contour Crafting Corporation (www.contourcrafting.com), a 185 m^2 house can be built in less than 24 hours with this method. Also, CC reduces construction costs by up to 70%.

The CC system operates with a portal-like structure, similar to a crane controlled by a computer. The double nozzle version of this system can print internal and external layers of a wall simultaneously. The internal layer is typically sinusoidal to ensure stability and material saving, generating articulated shapes that already envisage the integration of reinforcement, water, electrical, and ventilation systems at the design level. However, CC must be combined with traditional construction techniques for constructing and installing elements such as foundations, windows, and horizontal elements. Furthermore, it does not allow for achieving particularly complex shapes such as double curved walls.

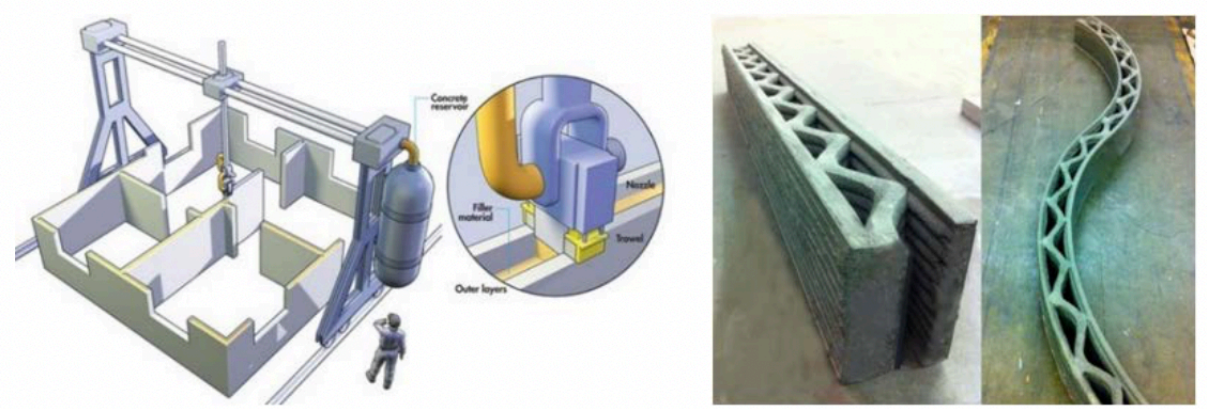

Figure 18. CC operating model on the left, rectilinear and curvilinear CC built walls on the right [50].

At the beginning of 2020 in Dubai, Apis Cor (www.apis-cor.com) built the largest CC building in the world. It is a two-story building, with an area of 640 square meters, built using only three onsite workers, without any extra assembly work, with minimal waste materials production, minimal environmental impact, and rapid execution times.

Figure 19. Construction and result of the Apis Corp Dubai project (www.apis-cor.com/dubai-project)

4.1.2. 3D concrete printing

CP differs from CC because it offers unlimited formal freedom for the printed object's external and internal geometries, allowing the construction of double-curved elements. The research team of Freeform Construction at Loughborough University conceived it for the prefabrication of concrete elements in a factory. However, thanks to its evolution, it allows onsite construction and the possibility of adding different types of materials to the concrete mix to obtain a high-performance material.

Figure 20. CP construction process (left), CP built wall-bench (center), and façade element projected parametrically by Bruil (2019) (right) [50].

CP is employable in constructing objects of every scale, from buildings constructed onsite to single prefabricated elements such as walls, façade panels, and infill blocks. As CC, 3D concrete printing can foresee the presence of multiple nozzles that allow printing several parts of the element simultaneously, even with materials of different characteristics like density or function. CP can also foresee the presence of empty spaces that can host reinforcing elements, insulating materials, pipes, electrical systems, and ventilation systems. In addition, it offers significant contributions in terms of thermal and acoustic insulation and the weight reduction of the finished element.

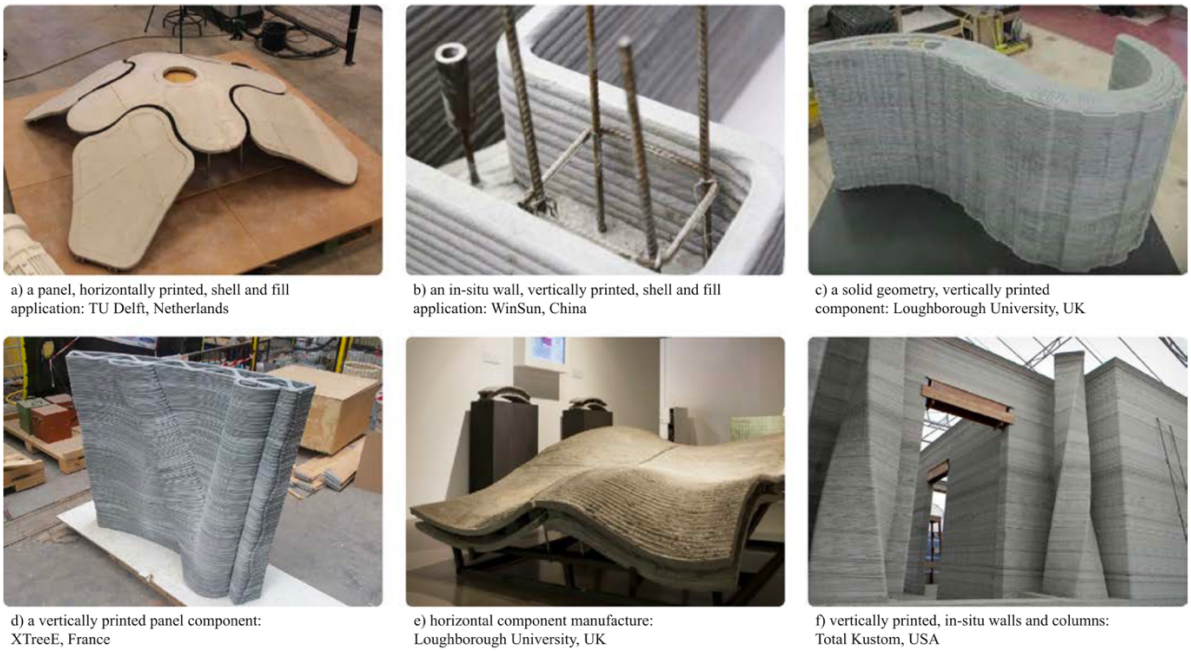

Figure 21. Examples of 3D Concrete Printing with different printing typologies and orientations [51].

4.2. Properties of extrudable concrete

4.2.1. Fresh state properties

Traditional cement-based materials cannot be employed for additive manufacturing processes regardless of their release date, quality, or properties. Concrete must have specific characteristics to become suitable for its application in an extrusion process; hence the fresh state properties of the material must follow some rules to create high-performance elements. The material used in AM processes compatible with concrete must have specific rheological and stiffening properties. It should have enough fluidity to be able to reach the print head during the pumping process. In addition, it should possess the ability to promptly develop a specific stiffness right after the filament detaches from the extrusion nozzle to support itself and the subsequently deposited layers maintaining their shape and undergoing minimal or no deformation after extrusion.

The rheological properties of an admixture depend on the chemical-physical composition of the mix design, the mixing procedure, the environmental conditions, and the duration of the extrusion process. T. T. Le et al. identified the essential characteristics that the mixture must possess in the fresh state, "pumpability, extrudability, and buildability" [52]. In addition, other correlated qualities such as “Open time, layer cycle-time, and green strength” have mutual relationships with the previously mentioned main characteristics.

4.2.1.1. Pumpability

Pumpability defines as “the ease with which the fresh mix is transported from the pump to the extrusion nozzle” [51]. Fundamentally, it represents the need for a fluidity that allows the material to circulate inside the pipe to reach the print head. A phenomenon that can affect this transfer is the possible segregation of the particles in the tube with the consequent formation of blocks caused by the incorrect design of the mixture or insufficient mixing of the compound before pumping. The blocks, and in general, the interruptions during the extrusion process, are particularly problematic in AM processes because they can derive into the formation of cold joints between the layers due to the lack of bond between them. A proper layer-bond is essential for the realization of homogeneous and high-quality components.

4.2.1.2. Extrudability

Extrudability is "the ability to extrude the mix through a nozzle without considerable cross-sectional deformation and with an acceptable degree of splitting/tearing of filament" [51]. The shape and size of the nozzle influence this feature; these characteristics must be compatible and consistent with the material to be extruded and the final product to be made. Furthermore, it is crucial to carefully evaluate the type of aggregates used and the possible fiber content in the dough. Currently, extrudability is assessed by visual inspection.

4.2.1.3. Printability

To evaluate the printability of a material, researchers or material developers should print a series of overlapping layers with a single-filament print path. The mix design, the mixing time, and the time between the mixing process and the extrusion of each layer impact the printability and the printing quality. Regarding the mix design, the presence of superplasticizer and accelerant additives and the content of fine aggregates or other stabilizer materials improve the stability of printable concrete.

It is essential to consider the time between the mixing process and the extrusion of each layer. If it is insufficient, the compound will not yet have developed the cohesion and viscosity to allow the layer to support the weight of the subsequently deposited material. On the other hand, if too much time has passed, the viscosity could be too elevated and complicate the pumping; if the setting time is exceeded, it could generate defects and cold joints in the final element, compromising its performance.

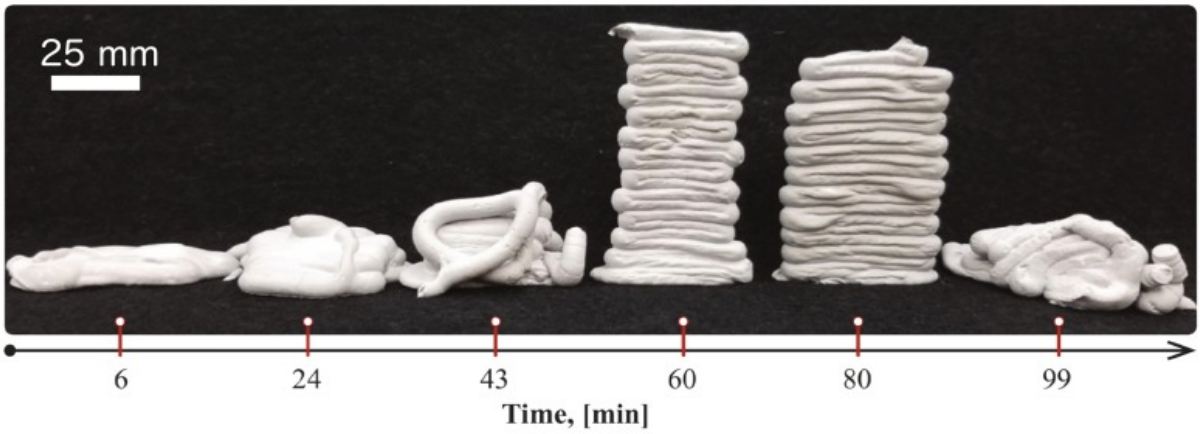

Figure 22. Example of a printability test to identify the time window when the material can create a self-sustaining structure. Being 0, the time when the cement first came in contact with water [51].

4.2.1.4. Open-time, layer cycle-time, and green-strength

Open-time represents a time window in which a specific material volume must be extruded to maintain the suitable viscosity and cohesion to carry out the process. Research is still working on the inclusion of additives that can help stabilize the mixture to extend the open time. The printability test determines the open time of the admixture. Consequently, it leads to the optimization of the tool path and the machine's operating parameters like the printing speed to minimize or eliminate the formation of cold joints during the production of the elements.

Layer cycle-time represents the time that elapses between the deposition of two successive layers. It affects the bond strength between the layers, which, if insufficient, can lead to the formation of cold joints. The extrusion path's length and the speed rate at which the material can be deposited are critical factors that influence the component's production time and layer cycle-time. A limiting factor that affects the printing speed set at the machine level is the amount of material that can be deposited when there is a change of direction in the path followed by the nozzle. Consequently, the design and creation of the printing path must consider this factor, the material properties, the characteristics of the process, and the size, shape, and final properties of the component to be produced.

Compiling without formworks, the extrusion process must consider the employment of a material with minimal or no post extrusion deformation. An important aspect to consider is the layer deformation due to its own weight, but most importantly, under the weight of the successive layers that will be added with the vertical development of the printed element. Therefore, the material should have a high yield strength and an adequate and constant thixotropy. The former keeps the stability of each single extruded layer, and the latter supports the subsequent layers keeping a stable shape. Furthermore, as the number of layers increases, the material needs to promptly develop a high resistance and rigidity to guarantee the shape and stability

of the printed element. For this purpose, the hydration process must proceed rapidly to provide a load-bearing internal skeleton. This characteristic, typical of materials subjected to extrusion, is called green-strength. The minimal deformation that derivates from the addition of a new layer favors the adhesion between layers because it increases the contact surface. However, if this deformation is excessive, it risks affecting the final object's geometry and, above all, compromises the stability of the element in the printing phase, bringing it to collapse. This aspect is primarily relevant in high elements printed in a vertical orientation. It is possible to foresee the dynamic adjustment of the nozzle's height during printing and to control the buildup rate with the possibility of injecting, just before the extrusion, some additives capable of accelerating the hardening process of the lower layers to carry the subsequent ones without problems and avoid deformation. The use of specific additives or other additions such as fly ashes can help achieve adequate cohesion and thixotropic behavior without compromising the fluidity in the fresh state.

In conclusion, achieving adequate, repeatable, and constant rheological properties is essential to guarantee the extrusion process's feasibility and the realization of a high-quality final element. Currently, research focuses on the rheology of extrudable concrete, particularly the fundamental aspects, such as viscosity and yield stress, and more complex behaviors, such as thixotropy, green-strength, and shape stability. In this context, a fascinating new approach is represented by the active control of rheology and stiffening carried out in real-time during production. Furthermore, new measurement techniques are being adopted to quantify the significant quantities that characterize each admixture in the fresh state, which have proved reliable, such as those carried out by portable rotating rheometers.

4.2.2. Dry state properties

The use of 3D Concrete Printing, and therefore the fact that to make objects extruded filaments of cement conglomerate superimpose, has a significant influence on the characteristics and performance of the final object. Furthermore, there is a close correlation between properties in the fresh state and the hardened state, so they should not be considered separately. At this juncture, research is still trying to understand the effects of process and mix design on final properties so that they can be controlled and minimized.

Up to now, the case studies carried out using 3D Concrete Printing are characterized by low final performance, especially considering that future applications will have to be carried out in real contexts and under environmental conditions. Research has focused on creating a series of overlapping layers without incurring the element's collapse. At the current development level, little attention is paid to the final performance of the product, such as the mechanical performance and durability of

the element. However, they are essential for achieving the marketing of high-quality quality products. To date, the reproduction of final "as-good-as-cast" properties has not yet been achieved, and, at the research level, work is also underway in this area.

Some aspects and characteristics that the element must have in the hardened state determine the overall performance of the printed objects:

- Adhesion between layers and the consequent absence of cold-joints.
- Constant filament density, avoiding areas with low material filling.
- Absence of shrinkage cracks and consequent durability of the final product.
- Geometric conformity with the project's previsions and the 3D model.
- Mechanical performance required in terms of compressive and tensile strength.

While some of these characteristics can be assessed through visual observations, for others, such as mechanical performance, it is necessary to proceed through precise measurements capable of quantifying the products' properties and performance. In this regard, for extruded materials, there are still no standardized methods to test such performances for two main reasons: the fact that the components made through the extrusion process have anisotropic nature and also very variable characteristics within the same element, and the fact that currently there is no coherent format for the realization of the specimens to be tested and for describing the process parameters like the size of the nozzle, the height of the layer, the size of the filament, the printing speed, the size of the component, and the cycle-time layer that allow the comparability between the data from different studies. Especially, given the near-future use of 3D Concrete Printing, it is necessary to identify new methods of analysis and standardized testing since those currently used for concrete elements made traditionally are inadequate due to the difference in process, material, and product. Furthermore, even at the structural design level, current software and 3D models are not yet able to predict the final mechanical properties of extruded elements, so further studies and developments are necessary on this front as well.

4.2.2.1. Adhesion between layers

An important aspect, already mentioned several times, is the adhesion between layers to form a solid bond and avoid the formation of cold joints, which represent points and areas of weakness in the final element and influence the mechanical performance. Cold joints are generally caused by an excessive layer cycle-time and other factors such as the printing speed and the size of the sand particles when present. They can also be temporary as the strength of adhesion between the layers increases as the hydration of the cement progresses. In the case of components with structural uses, it is essential to try to minimize the influences that the production

process can generate on the final product, considering them already in the design phase to guarantee the achievement of the required performance.

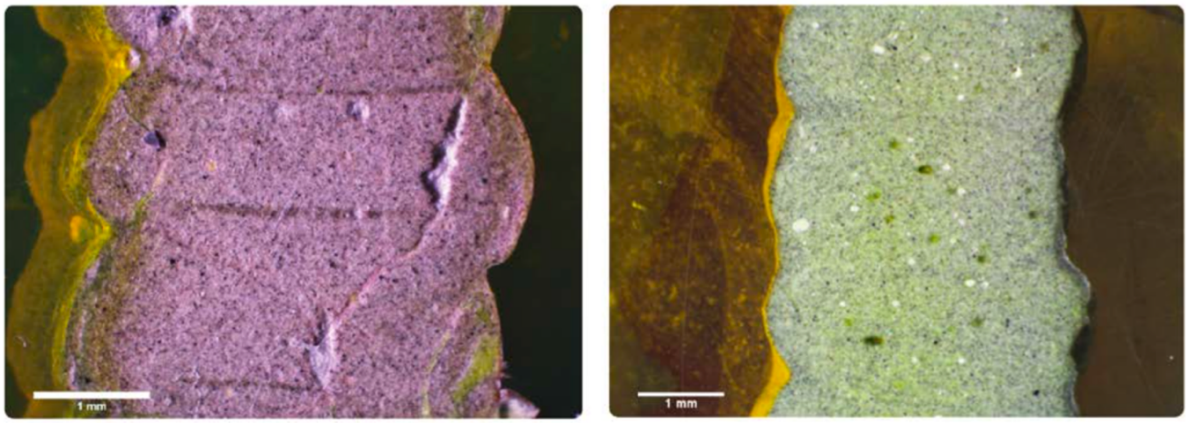

Figure 23. Example of an element characterized by cold-joints on the left and another without cold-joints on the right [51].

4.2.2.2. Constant filament density

Another essential aspect is the achievement of the design density in every part of the element, avoiding, through the mix design and the stability of the rheological properties during printing, voids generation inside the extruded filaments since they would affect the element's effective density, its performance, and its durability. In addition to the mix design and the admixture's stability, the printed material's deformation also plays an essential role because it can push the material into these voids, minimizing its occurrence. Other factors leading to this phenomenon are the nozzle's path and the direction changes. According to the properties in the fresh state, the size and geometry of the nozzle, and the deposition speed, specific bending radios are used to avoid fractures or defects in the component.

Figure 24. Elements characterized by variable filament density on the left and constant filament density on the right. In the first case, the various layers and voids of various sizes are recognized, while in the second, the element is homogeneous [51].

4.2.2.3. Shrinkage cracks and durability

Unlike the traditional concrete construction process, the absence of formworks, the larger exposed surface, and the low water/cement ratio that characterize printable concrete increase the appearance of cracks due to the spontaneous shrinkage of the material during the maturation phase. The mix design and the hardening phase play a fundamental role in minimizing the occurrence of this type of problem, which can cause a reduction in the durability of the final element, as well as an aesthetic defect. In the field of prefabrication, it is easier to take specific measures to control the hardening conditions, which can significantly influence the extruded element. However, at a research level, work is still being done as it is essential for an actual future use of the extrusion process and to improve the environmental performance of the product's life cycle, acting on the durability of the extruded components and consequently on the reduction of the maintenance and replacement rate.

Figure 25. Example of shrinkage cracks in an element made using 3D Concrete Printing [53].

4.2.2.4. Geometric accordance

A fundamental manufacturing process requirement is the geometric accordance between the final element, the project, and the 3D model since it can strongly determine its value. Very often, geometries have both an aesthetic and functional value. However, in the 3D Concrete Printing process, they are bound by some intrinsic limitations to the process, so, in terms of geometric accordance, there are some essential aspects to consider, such as:

- Dimensions and minimal tolerances.
- Creation of fully dense components.
- Creation of overhangs

As part of the 3D Concrete Printing extrusion process, some factors influence and limit the geometric dimensions and the minimum achievable tolerances. The print

resolution mainly depends on the material's rheological properties, the nozzle's path, and the process parameters (nozzle size, layer size, extrusion times), which, at the same time, depend on the element to be created and the construction strategy adopted. Furthermore, print resolution has a significant role in the case of component assembly because it impacts the surface finish of the finished elements. Therefore, various strategies can be adopted to overcome the limitations imposed by the extrusion process:

- Use automatic spatulas to smooth the vertical surface of the printed elements.
- Use a machine that allows the nozzle to move in 3 axes (x, y, and z) to build with variable inclinations between the nozzle and the work surface.
- Create an element with similar geometry to the desired one, to which additional material is applied or subtracted to obtain the required precision.
- Contemplate the print path to be continuous on the outer edges of the component.

Two different strategies can be adopted to obtain a solid element. First, a sort of hatch can be created by an internal path of extruded material which will inevitably leave small gaps that can affect the element's expected density, performance, and durability due to insufficient print resolution. In addition, it is possible to fill the extruded perimeter with a filling casted material that can have a different density to increase the element's performance, making it multi-functional, thanks to which no void will remain inside the finished component.

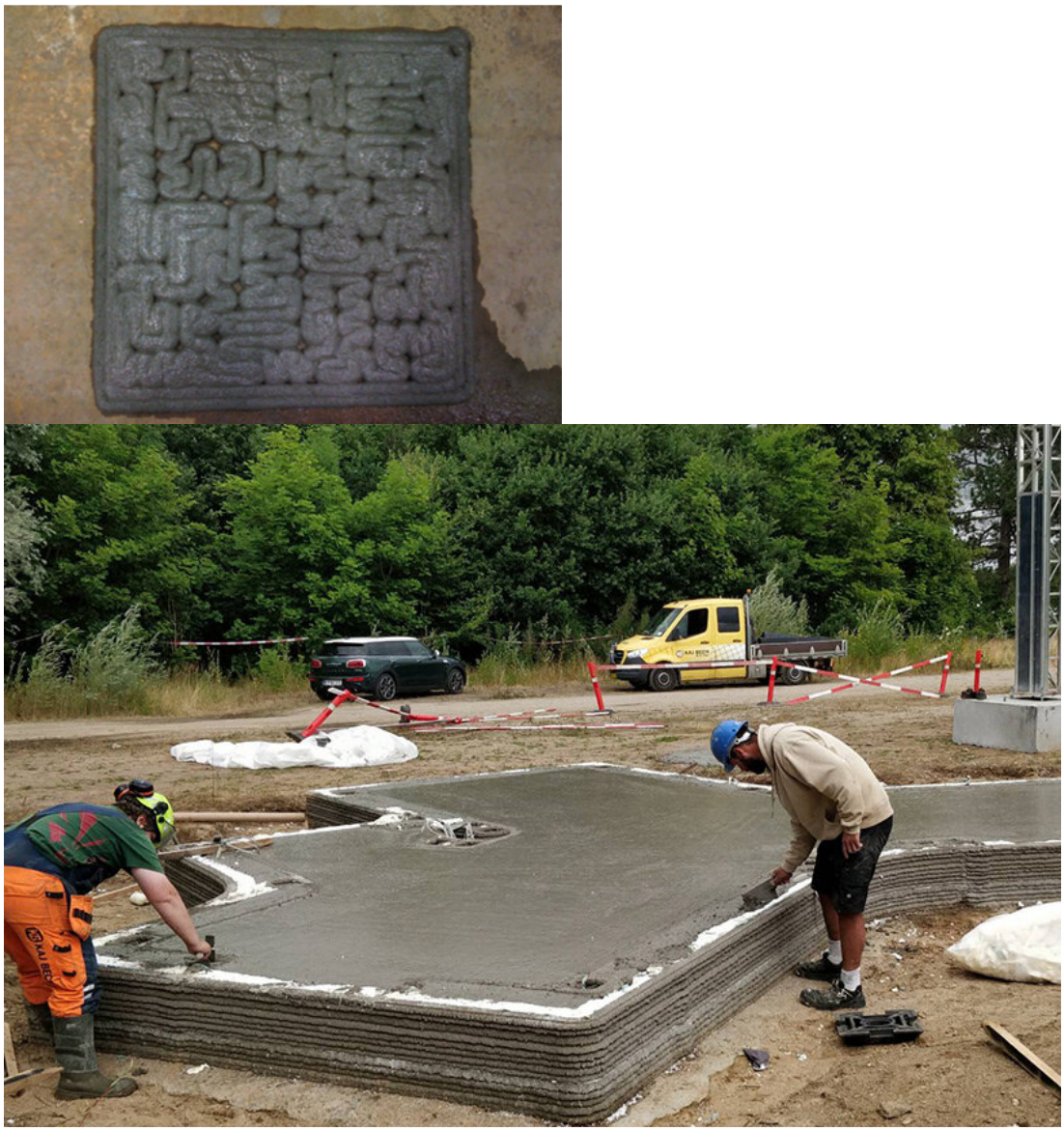

Figure 26. Example of a hatch created by an internal path on the left [51] *and a perimeter filled with casted material on the right (3dcp.dk).*

The last aspect to consider at the level of geometric accordance concerns the creation of overhangs and projections that, in the context of 3D Concrete Printing, can be created in two different ways: with some temporary external support that will be removed after the hardening or through “corbeling,” the creation of overlaps between layers set with displacements at the level of the printing path. However, the latter solution is currently only possible up to a certain degree of overhang because it can lead to instability and collapse of the element, especially when printing a single-stranded structure. The instability, in this case, is essentially due to the material’s properties and how the machine can move the nozzle. In this regard, instead of the classic "2D slicing" method used primarily in 3D Printing, it is appropriate to use the "tangential continuity method," which, thanks to the use of a nozzle with rotation capabilities, allows to exploit the maximum contact surface between the layers thus stabilizing the overall structure. With this method, it is

possible to obtain greater design freedom. However, at a practical level, it is necessary to carry out further tests to ensure the stability of various types and degrees of overhang, avoiding a weakening or even a collapse of the stratification.

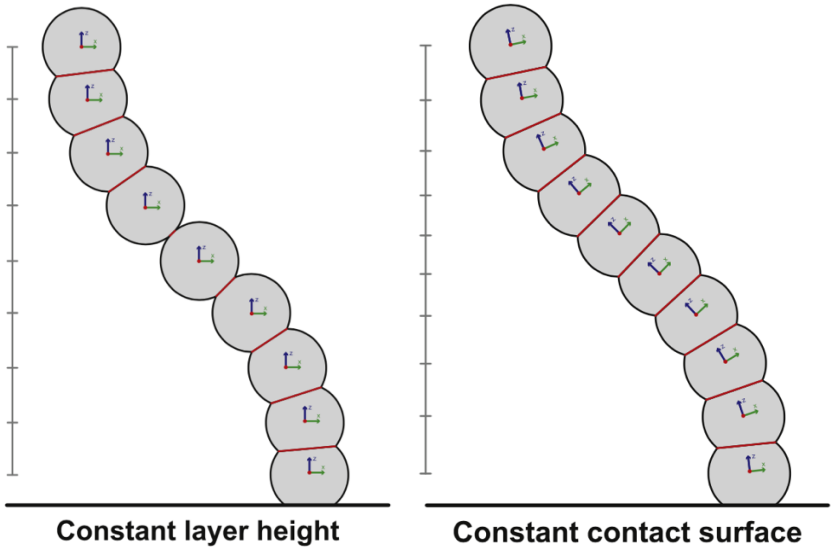

Figure 27. 2D slicing method on the left and tangential continuity method on the right. The latter has a constant contact surface between layers which reduces the risk of collapse [51].

4.2.2.5. Mechanical properties

The previously treated characteristics significantly influence the mechanical performance of the final product, which represents essential requirements that it must possess to perform the role for which it was designed. Consequently, with an appropriate resistance, the prefabrication of building components and the onsite construction of 3D printed concrete become possible.

An essential but currently unsolved aspect from a mechanical point of view concerns the insertion of reinforcing elements to obtain the mechanical performance suitable for structural applications comparable to casted reinforced concrete. In this regard, various approaches have been proposed on research, but an adequate solution has not yet been reached. Therefore, in addition to understanding which can be the best method from the construction point of view, it is necessary to identify which solution allows to obtain the best mechanical performance according to a series of significant parameters: mechanical strength, yield, deformation, and adhesion to printed concrete.

The possible solutions currently hypothesized and only partially tested are the following:

1. Create only the permanent formwork with 3D printed cementitious material. Then, place the reinforcements inside, wrapped in a conventional concrete filling to make an entire solid element.

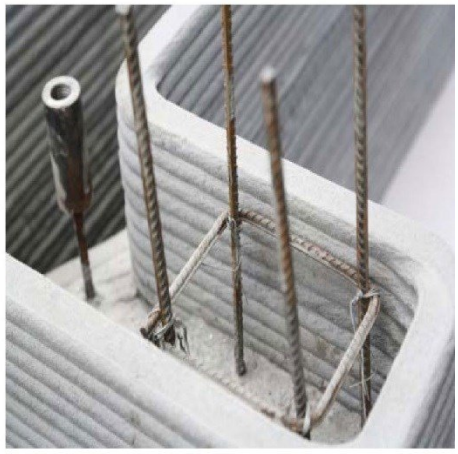

Figure 28. Example of the integration of classic reinforcements to a 3D printed formwork.

2. A reinforcement mesh is made with automation strategies, filled with concrete, and then a concrete layer is sprayed on the outer sides of the mesh. This method is Mesh Mould Metal by ETH Zurich.

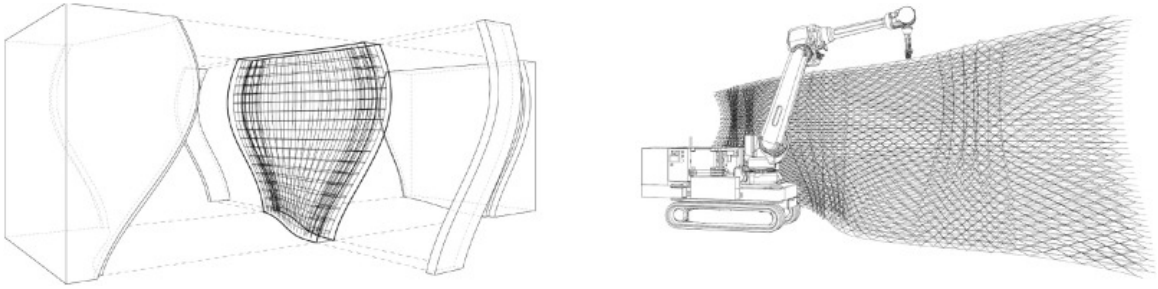

Figure 29. Comparison between the traditional curved reinforced wall on the left and the Mesh Model Metal case study of ETH Zurich on the right [54].

3. Insert steel fibers and short polymer fibers into the cement mix to extrude. In this case, the fibers have a dispersed reinforcement function but are also helpful for increasing the initial strength and reducing shrinkage phenomena during hardening. However, they can create problems regarding the pumpability and extrudability of the fresh mixture.
4. Insert fabric reinforcements or bidirectional fiber grids in the areas where the element is most stressed by traction to improve the mechanical performance in flexural strength [55].

Figure 30. Specimens with bi-directional reinforcement in fiberglass and dispersed fibers after the flexural strength test [55].

5. Print the concrete elements, also as separate elements to be assembled, providing special cavities to attach the post-tensioned reinforcements at a later time, ensuring their contact with the concrete by using a low viscosity cement mortar or a structural adhesive [49].

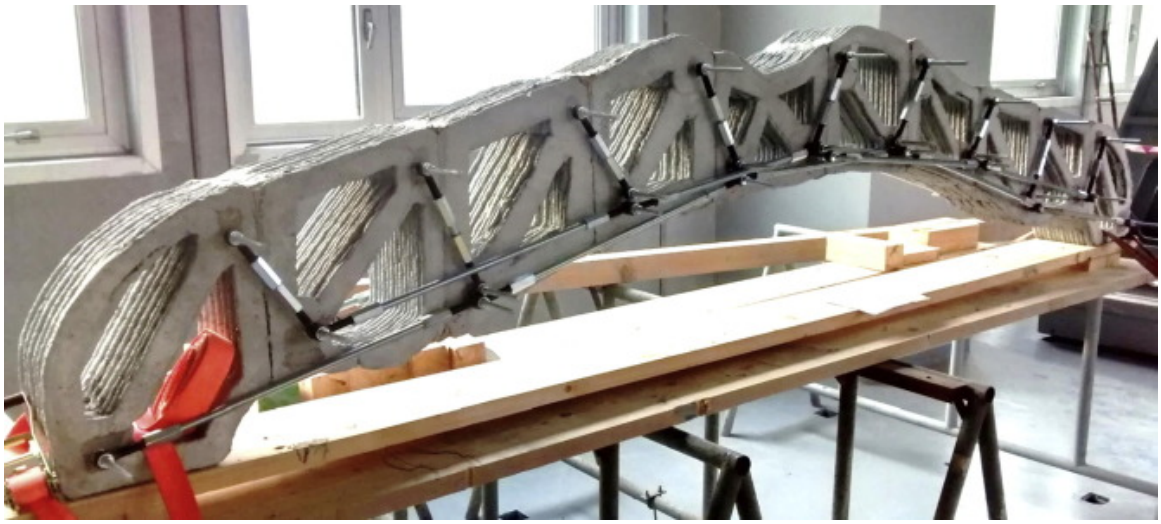

Figure 31. Example of a 3D printed beam with steel reinforcements integrated after the printing process [49].

6. Position reinforcement elements and simultaneously print the concrete with a multi-arm or multi-nozzle system.

3D Concrete Printing can integrate the reinforcements in a parallel orientation to the printed layers or perpendicular to them. For example, the former includes experiments with fabric reinforcements or fiber grids parallel to the extruded layers. However, it is not convenient to insert steel reinforcing bars in this direction since the diameter of the reinforcing element will influence the thickness of the layer and consequently the extrusion diameter, the discretization of the volume according to the size of the filament, the tool path, the rheological characteristics in the fresh state, the layer cycle-time, and the dimensional tolerances. These variables affect the geometric conformity of the final product. Therefore, reinforcements in steel bars should be inserted perpendicular to the print layers.

A satisfactory reinforcement solution has not been identified yet. Therefore, it is crucial to experiment with specific solutions for this new type of construction process instead of adapting traditional solutions that have been designed for an altogether different process from the extrusive one.

4.3. Potential for construction

The search for new processes capable of innovating the current production in-plant and on-site practice of the construction sector stems from the desire to identify more efficient, economical, and sustainable processes. Traditional construction techniques are slow, expensive, unsustainable, risky for workers' health, and based on subtractive production techniques; the material is removed or cut from a larger piece resulting in tool wear and generation of large amounts of waste. Therefore, the growing interest in 3D Concrete Printing in the construction sector derives from the potential and benefits it could bring, both from the point of view of the production process and the final products.

1. Concrete 3D printing offers unlimited formal and expressive freedom that allows total customization without additional costs as the geometric complexity increases.

   This aspect offers the possibility of creating a new and varied architectural landscape as opposed to the formal standardization that usually characterizes the concrete structures built up to now. In fact, in conventional processes, the shape has always been limited by traditional construction techniques and the use of formwork which, for formally complex elements, has high environmental impacts, considerable delays, and elevated costs in terms of material, labor, and machining. Hence, creating geometrically simple and standardized elements is convenient for reusing the formworks. Thanks to the introduction of 3D Concrete Printing, it is possible to create double curvature elements, structural elements designed through topological optimization, elements with hollow sections designed through functional hybridization, and different materials to ensure a multi-functionality of the element itself without any additional costs.

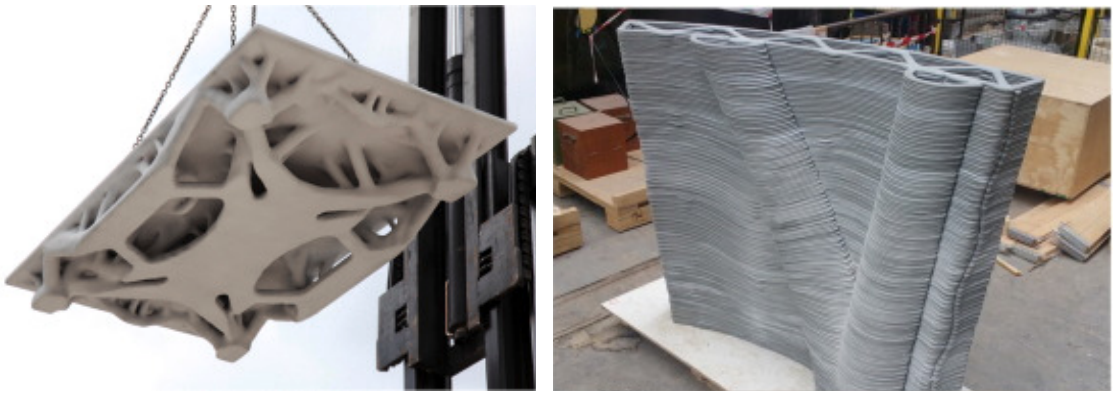

Figure 32. Structural element designed through topological optimization on the left [56] *and element with hollow sections designed through functional hybridization on the right* [57].

2. Greater efficiency of the construction process and the product in terms of quality, production times, and costs.

3. Possibility of managing fast, accurate, and low costs urgent design changes during construction.

4. Heightened precision and control over the characteristics and performance of the final element due to the lower occurrence of human error and better management of the construction process thanks to its digitization.

5. Outstanding worker safety in the case of on-site construction thanks to the drastic reduction of the work to be carried out manually, which allows enhanced security and protection in the construction sector, one of the categories subject to the most significant number of accidents.

6. Birth of new professional figures specialized in the digitalization of construction processes. Automating operations do not reduce jobs; in reality, low-skilled workers are replaced by highly skilled workers such as experts in robotics, programming, and concrete technology. Furthermore, the demographic range of workers in the construction sector will be enlarged thanks to the minor importance of factors such as age, sex, and physical capacity.

7. Lower environmental impact of the construction processes in terms of reductions in energy and material consumption, CO2 emissions, elimination of waste products, and a good choice of materials to reduce the impact during the entire life cycle of the building. From an environmental point of view, the distinction between the formal complexity used as a design strategy to optimize the use of material or only as an aesthetic virtuosity would lead to an increase in the material and a more significant environmental impact. In this context, some scholars have shown that it is possible to reduce the environmental impact by up to about 50% in digitally produced concrete structures compared to conventional processes [53].

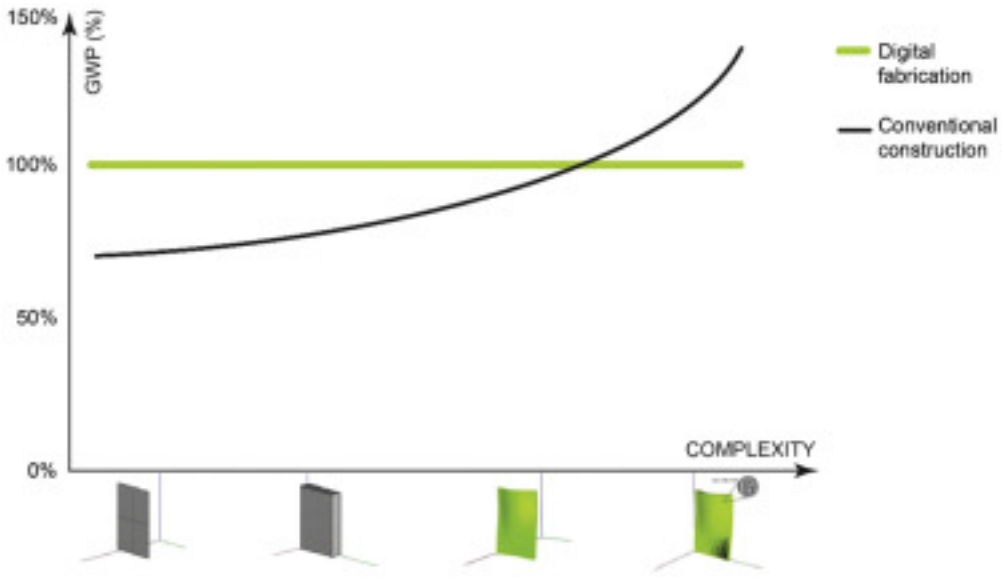

Figure 33. Global warming potential compared to complexity. Advantage of digital fabrication against conventional construction [53].

8. Possibility of designing according to the topological or structural optimization principle to lighten the printed elements and save up to 50% of the material [53].

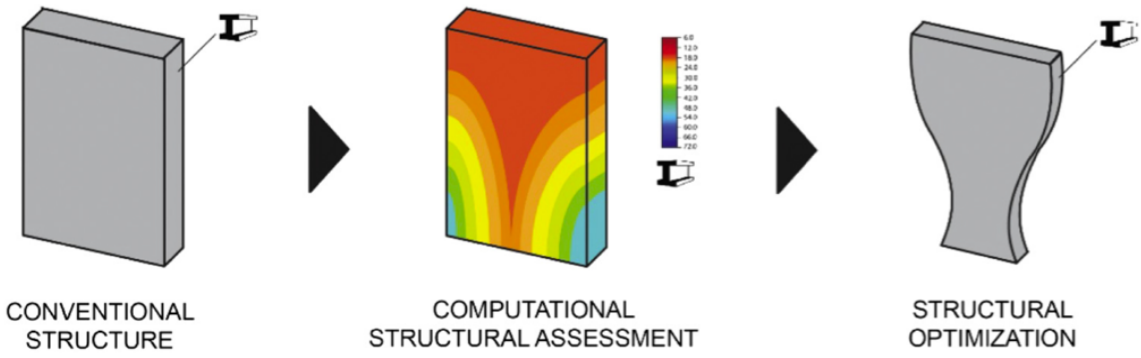

Figure 34. Schematic of the topological or structural optimization system [53].

9. Possibility to integrate multifunctionality in building elements through functional integration and functional hybridization. The former contemplates incorporating services such as pipes or systems through a complex structure geometry that includes shafts suitable for hosting these elements. The latter optimizes construction through the shape or materials used for making the components, which can provide one or more secondary functions that add value to the printed product. Functional hybridization allows a single element to perform multiple tasks through the shape, material or by combining the shape with the use of one or more materials within the same element. In this regard, if hybridization can reduce the environmental impacts in the digital production phase, it can also make the maintenance and replacement of the parts more problematic and frequent or affect the recyclability of the final product due to the combination of materials of different nature. To avoid this, in addition to a

careful choice of materials, it is necessary to prevent the coupling of functions that have very different life cycles in time that would lead to remarkably high replacement cycles for the entire element or provide flexibility to allow the maintenance of only some components.

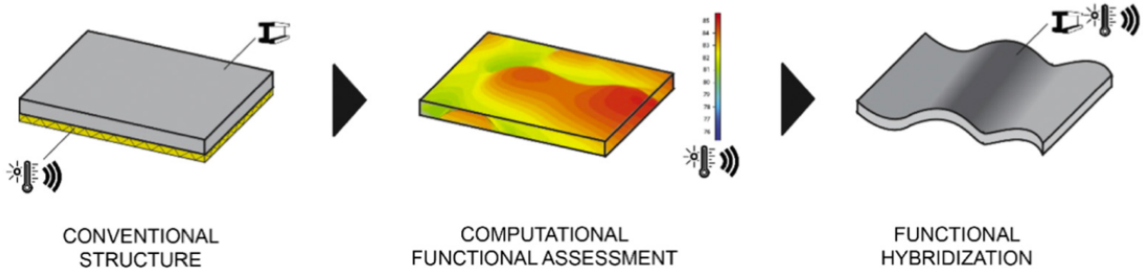

Figure 35. Schematics of the functional hybridization system [53].

4.4. Properties of extrudable foamed concrete

4.4.1. Mix design and fresh state properties

Compared to the classic foamed concrete, the extrudable version characterizes by a different mix design which involves the addition of a specific additive capable of offering green-strength to the mix. This property is indispensable for concrete to maintain its shape when submitted to its own weight and that of the subsequently deposited layers during an automated construction process. Incorporating a viscosity enhancer agent (VEA) or viscosity modifier guarantees the extrudability and printability requirements of the material, increasing its cohesion and viscosity without affecting its workability and pumpability. At the same time, it helps stabilize the bubbles inside the cement matrix. The VEA used for extrudable foamed concrete differs from that used for the extrusion of non-foamed concrete as the latter would cause instability and the consequent loss of air from the mix. The increased viscosity produced by VEA in extrudable foamed concrete reduces the amount of air the mix can retain. However, at the same time, it helps prevent the bubble loss as they are subject to higher confinement forces and more consistent admixtures. The difficulty of retaining the air inside the cement matrix solves by using a more significant amount of foam; the need for foam with the same final density in the case of extrudable foamed concrete is higher than for classic foamed concrete.

4.4.1.1. Consistency and green strength

Adding an element to the mix design has consequences on the characteristics of the material, both in the fresh and hardened state. In the former, the most evident characteristics that differentiate extrudable foamed concrete from the classic foamed version concern the consistency of the mixture and the ability to develop

timely green strength following extrusion. Both aspects derive from the original process and require other requisites to be carried out successfully. In particular, green-strength is obtained thanks to a high thixotropy of the material that derives from the presence of the VEA and necessarily characterizes all extrudable materials. This is an essential property since it allows the material to build an internal structure that increases the admixture's strength and guarantees its dimensional stability over time. In fact, following extrusion, the VEA is predominantly absorbed by the concrete particles and acts as a connection bridge between adjacent particles, thus improving stability. The ability of a foamed material to generate green-strength also depends on the size of the bubbles present in the mix; the reduced size of the bubbles that characterize the extrudable foamed concrete, which derives from the high cohesion that characterizes the mix due to the presence of VEA, promotes and further accelerates the internal structure. To evaluate the green-strength of extrudable foamed concrete, it is necessary to carry out an extrusion test since the slump test used for the classic foamed concrete could be unreliable, especially at low densities, due to the lightness of the mixture and the high cohesion, the material may not slip off the cone.

Figure 36. Quality comparison in terms of consistency, cohesion and viscosity in the fresh state between an extrudable foamed concrete mix (above) and a classic foamed concrete mix (below) both made to obtain a final density of 600 kg/m³ [55].

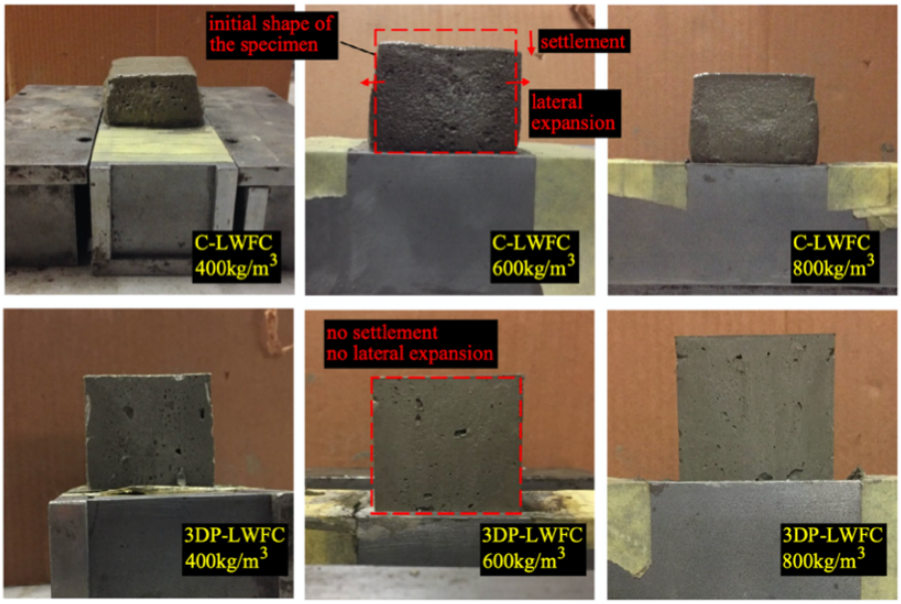

Figure 37. Comparison of the final configuration following extrusion tests and after a rest time of 5 minutes between mixtures of different densities made with classic foamed concrete (above) and with extrudable foamed concrete (below). In the second case we are with the consequent maintenance of the shape following extrusion [58].

4.4.2. Dry state characteristics of the material

Each change made at the level of mix design, such as the addition of the VEA additive, affects the material's properties in the fresh state and those in the hardened condition. The latter depends on many factors such as the mix design, the mixing procedures like the type of mixer and mixing speed, the properties in the fresh state, and the hardening conditions. In this context, from the comparison with the classic foamed concrete, some differences emerge concerning the pores' structure, the mechanical resistance, and the thermal conductivity.

4.4.2.1. Dimension and distribution of the pores

Through the use of digital systems, which involve special software for the analysis of images carried out under the microscope and depicting cross-sections of foamed concrete elements, it is possible to analyze in detail various parameters relating to the air cavities present in the porous material, such as volume, size, size distribution, shape, and spacing between air voids. These aspects are highly significant for several reasons: to understand the effectiveness of the mixing and extrusion process and, consequently, to confirm the validity of products made with this material due to the close dependence between the characteristics of the pores and the final performance of the extruded elements in terms of weight, mechanical resistance, thermal and acoustic properties, and durability; to understand any changes to be made at the mix design or process level; to identify the limits of a material like the minimum density achievable with the same material and process.

Through the analysis of images carried out under the microscope on some specimens made during an experimental comparison study between classic and extrudable foam concrete [58], it was shown that in the latter, with the same mixing process, final density, and hardening conditions, the air bubbles are smaller and more homogeneously distributed inside the cement matrix compared to the classic foamed concrete. The same result also emerged during another study comparing autoclaved aerated concrete and extrudable foamed concrete [59]. The reduced size of the bubbles and the homogeneous distribution have positive effects on performance, mechanical strength, and reducing the thermal conductivity of the final elements [47]. Furthermore, the diameter of the bubbles can be further reduced, consequently obtaining additional performance benefits by increasing the mixing speed [58].

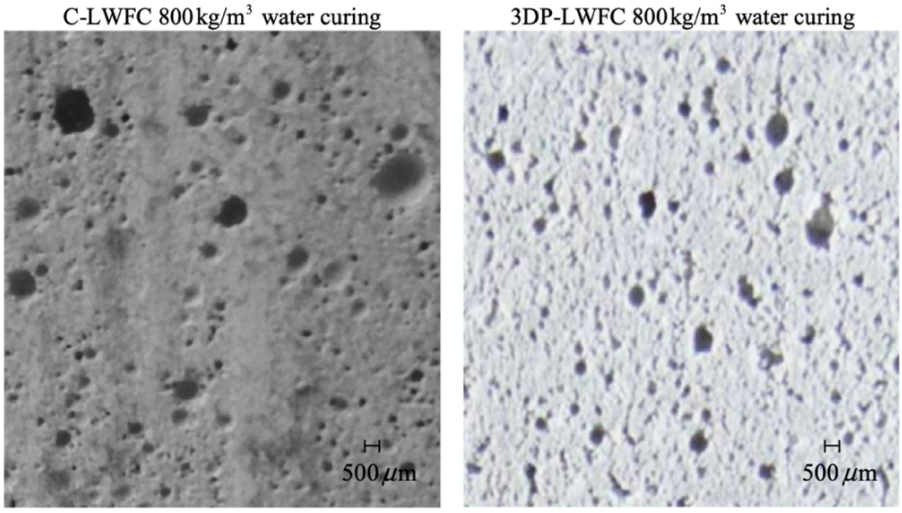

Figure 38. Comparison in size and distribution of pores between cross-sections made on a classic foamed concrete element on the left and an extrudable foamed concrete one with the same final density, mixing speed, and hardening conditions on the right. Pore size diminished, and the distribution is more homogeneous on the latter [58].

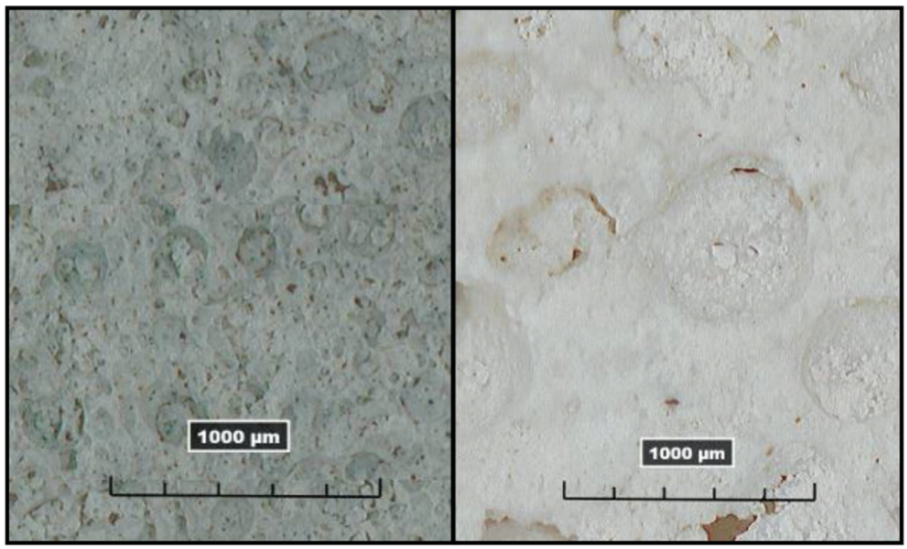

Figure 39. Comparison in terms of size and distribution of pores between cross-sections made on an extrudable foamed concrete element on the left and one in autoclaved aerated concrete with the same final density on the right. The first image shows that the pore size reduced, and the distribution became more homogeneous [59].

4.4.2.2. Compressive strength

With the same final density, foaming agent, hardening conditions, type of cement, and water/cement ratio, the compressive strength is slightly higher in extrudable foam concrete than in its classic version. This increase can be attributed to the more homogeneous distribution and the smaller size of the pores.

Furthermore, in an experimental study [59] carried out on three samples with a final density equal to 400, 600, and 800 kg/m³, made with CEM II A-L 42.5 R cement and a water/cement ratio equal to 0.3, some interesting observations valid for the density range considered emerged:

- The increase in compressive strength with the increase in density presents an almost linear trend.
- The hardening conditions of the specimen greatly influence the compressive strength. For all the densities analyzed, the highest values are found in the case of hardening in cellophane; the worst ones refer to air hardening, and the intermediate ones concern the hardening in water.

4.4.2.3. Flexural strength

As regards the tensile strength, in the same experimental study [8], it emerged that:

- The increase in tensile strength with the increase in density does not show a linear trend as it is much more pronounced in the transition from 400 to 600 kg/m³ than that between 600 and 800 kg/m³.

- Unlike compressive strength, the tensile strength is not affected by the hardening condition. However, at the same time, an aspect that significantly impacts the organization of the microstructure in the collapse zone.

4.4.2.4. Thermal conductivity

The thermal conductivity values decrease significantly as the density of the material decreases because there is a higher presence of air. Furthermore, at the same density, extrudable foamed concrete is characterized by considerably lower thermal conductivity values compared to classic foamed concrete and autoclaved aerated concrete. This reduction is essentially due to the smaller size and more homogeneous distribution of the bubbles that characterize extrudable foamed concrete compared to the other two types of concrete.

Chapter 5

Experimentation: Mechanical and thermal tests of innovative foamed concretes

5.1. Materials and methods

The experimental part of this research took place at the Department of Structural, Geotechnical, and Building engineering (DISEG) laboratory. The research tested ultralightweight foamed concrete in its fresh and hardened states.

Each concrete mix follows the same ratios to be comparable when performing the experiments. The studied concrete mixes contain type CEM I 52,5 R cement, with a 33% water/cement (W/C) content. In addition, a viscosity modifier/cement (VM/C) content of 15-20% and a superplasticizer/cement (S/C) content of 0,25-1% contribute to the mix design. The pre-formed foam employed was made with a surfactant/water ratio of 5%, and its quantities vary according to the expected density. Furthermore, the inclusion of natural fibers improves the mechanical characteristics of ultralight foamed concrete like compressive and flexural strength while increasing its sustainability by utilizing residuary sheep wool fibers (SWF).

Various aspects influence the final characterization of the cement mix:

- Fiber treatment: salt, lime, sodium hydroxide, or surfactant-treated fibers
- Fiber length: 6, 12, or 20 mm
- Fiber content ratio: 2,5%, 5%, or 10%
- Target cement paste density (dry): 100, 300, 500 kg/m^3

The experimental study consisted of two parts: the first selected the most performant fiber treatment, length, and content ratio, and the second applied them to analyze cement mixes with the chosen fiber characteristics and the three different target densities.

The selection process of the fiber treatment consisted of formulating six cement paste mixes. The first did not contain any fibers (NF), the second had non-treated fibers (NTF), and the remaining four incorporated each alternative of treated fibers: salt-treated fibers (NaClTF), lime-treated fibers (LTF), sodium hydroxide-treated fibers (NaOHTF), and surfactant-treated fibers (STF). Given that the research had not yet identified the fiber length, the fiber content ratio, and the cement paste density, the mix design assessed the values: 12mm, 2,5%, and 300 kg/m^3, respectively.

Table 3. Characteristics of the mixes dedicated to selecting the fiber treatment.

MIX ID		01-NF	01-NTF	01-NaClTF	01-LTF	01-NaOHTF	01-STF
Cement							
Cem I 52.5 R		450 g	450 g	450 g	450 g	450 g	450 g
Viscosity modifier	15 %	67.5 g	67.5 g	67.5 g	67.5 g	67.5 g	67.5 g
Water	33 %	148.5 g	148.5 g	148.5 g	148.5 g	148.5 g	148.5 g
Superplasticizer	1 %	4.5 g	4.5 g	4.5 g	4.5 g	4.5 g	4.5 g
Fibers added							
Sheep wool fibers	2.5 %	0 g No fibers	12 mm - 11.25 g Non treated fibers Machine washed in tap water at 30°C and air-dried for one week	12 mm - 11.25 g Salt treated fibers Immersed for 72h in a 35g/L salt-water solution, rinsed with tap water, and oven-dried at 30°C for 72h	12 mm - 11.25 g Lime treated fibers Immersed in a 1% lime-water solution for 2h and oven-dried at 30°C for 72h	12 mm - 11.25 g NaOH treated fibers Immersed for 1h in a 2% NaOH-water solution, rinsed with tap water, and oven-dried at 30°C for 72h	12 mm - 11.25 g Surfactant treated fibers Immersed for 72h in a 3% surfactant-water solution and oven-dried at 30°C for 72h
Foam Mixed							
Water	95 %	285 g	285 g	285 g	285 g	285 g	285 g
Surfacatant	5 %	15 g	15 g	15 g	15 g	15 g	15 g
Final Characteristics							
Foam added		251.97 g	250.94 g	251.4 g	250 g	250.96 g	225 g
Fresh state density		398.5 kg/m^3	425 kg/m^3	420.6 kg/m^3	405 kg/m^3	403 kg/m^3	425 kg/m^3

Table 3 shows the characteristics of each cement mix dedicated to selecting the fiber treatment. As mentioned before, every one of them follows the same proportions for each component.

The manufacturing process of the admixtures for this first analysis consisted of:

1. Weight the components.
2. Stir the cement and viscosity modifier to homogenize the powder mixture.
3. Pre-form the foam by mixing the surfactant agent with water at 1500rpm.
4. Add the water and superplasticizer to the powder mixture, mix keeping the same speed, and add the correspondent fibers when needed.
5. Re-mix the foam to recover its consistency.
6. Add the amount of foam required to reach the target density to the cement paste while mixing at 1500rpm until reaching the desired density. The reached density is evaluated by measuring the weight of the mix on a glass with a known volume.

The fiber length and fiber content selection process consisted of formulating five cement paste admixtures with non-treated fibers and a target density of 300 kg/m^3. The admixtures formulated for this analysis had 6, 12, and 20mm length fibers and fiber/cement (F/C) ratios of 2,5, 5, and 10%. For practical purposes, the fiber content considered to analyze the most performant fiber length was a 2,5% F/C ratio. On the contrary, the evaluation of the fiber content ratio considered a 12mm fiber length. Therefore, the admixture containing 12mm fibers and an F/C ratio of 2,5% is equivalent for both analyses.

Table 4. Characteristics of the mixes dedicated to selecting the fiber length and the fiber content.

MIX ID		01-6mm-2.5	01-12mm-2.5 ✳	01-20mm-2.5	01-12mm-5	01-12mm-10
Cement						
Cem I 52.5 R		450 g	450 g	450 g	450 g	450 g
Viscosity modifier	15 %	67.5 g	67.5 g	67.5 g	67.5 g	67.5 g
Water	33 %	148.5 g	148.5 g	148.5 g	148.5 g	148.5 g
Superplasticizer	1 %	4.5 g	4.5 g	4.5 g	4.5 g	4.5 g
Fibers added						
Sheep wool fibers	2.5 % 5 % 10 %	12 mm - 11.25 g Non treated fibers Machine washed in tap water at 30°C and air-dried for one week	12 mm - 11.25 g Non treated fibers Machine washed in tap water at 30°C and air-dried for one week	12 mm - 11.25 g Non treated fibers Machine washed in tap water at 30°C and air-dried for one week	12 mm - 22.5 g Non treated fibers Machine washed in tap water at 30°C and air-dried for one week	12 mm - 45 g Non treated fibers Machine washed in tap water at 30°C and air-dried for one week
Foam Mixed						
Water	95 %	285 g	285 g	285 g	285 g	285 g
Surfacatant	5 %	15 g	15 g	15 g	15 g	15 g
Final Characteristics						
Foam added		249.27 g	250.94 g	251.72 g	249.66 g	250 g
Fresh state density		392.4 kg/m³	422.2 kg/m³	408.5 kg/m³	392.8 kg/m³	382.1 kg/m³

✳ Mix ID containing an asterisk represents one admixture employed in both fiber length and fiber content studies.

Table 2 shows the characteristics of each cement mix dedicated to selecting the fiber length and the fiber content.

The fibers tangled up on the mixing handle during the fiber treatment experimentation; as a result, the mixing method was updated in this manufacturing process:

1. Weight the components.
2. Stir the cement and viscosity modifier to homogenize the powder mixture.
3. Pre-form the foam by mixing the surfactant agent with water at 1500rpm.
4. Add the water and superplasticizer to the powder mixture, and mix, keeping the same speed.
5. Re-mix the foam to recover its consistency.
6. Add the amount of foam required to reach the target density to the cement paste while mixing at 1500rpm until reaching the desired density. The reached density is evaluated by measuring the weight of the mix on a glass with a known volume.
7. Add the correspondent fibers to the admixture by folding them in manually to keep the foam.
8. Mix at 1500 rpm for a couple of seconds for better integration.

This first experimental campaign identified the most performant fiber treatments, length, and content ratio. For fiber treatment, the chosen options for further analysis

were LTF and STF; in addition, the research considered a mixture with NTF for each combination as a reference as well as a mixture without fibers. For fiber length, the chosen characteristic was 12mm. Lastly, the chosen F/C ratios for fiber content were 2,5 and 5%; however, for the 500 Kg/m^3 density, these ratios decreased to 1,25 and 2,5% due to volumetric inconsistencies.

The admixtures formulated for the second part of the experimentation aim to analyze how the mentioned fiber characteristics perform on three densities: 100, 300, and 500 Kg/m^3.

The densities obtained for similar cement pastes in the previous experimental campaign vary; this might be due to a difference in the foam quality. The reason for this issue might be that laboratory does not have a foam generator; therefore, the foam is generated manually. The mixing methodology changed subsequently to ensure similar foam densities:

1. Timing the mixing process of pre-forming the foam for three minutes and re-mixing it to recover the foam for one minute to produce approximately 300 grams of foam to reach the cement paste densities of 100 and 300 Kg/m^3.
2. Timing the mixing process of pre-forming the foam for four minutes and re-mixing it to recover the foam for one minute and thirty seconds to produce approximately 400 grams of foam to reach a cement paste density of 500 Kg/m^3.

Table 5. Characteristics of the mixes with a target density of 100 Kg/m^3 containing 12mm fibers with three treatment options and two fiber content ratios.

MIX ID		02-NF-100	02-NTF-100-2.5	02-NTF-100-5	02-LTF-100-2.5	02-LTF-100-5	02-STF-100-2.5	02-STF-100-5
Cement								
Cem I 52.5 R		225 g	225 g	225 g	225 g	225 g	225 g	225 g
Viscosity modifier	20 %	45 g	45 g	45 g	45 g	45 g	45 g	45 g
Water	33 %	74.25 g	74.25 g	74.25 g	74.25 g	74.25 g	74.25 g	74.25 g
Superplasticizer	1 %	2.25 g	2.25 g	2.25 g	2.25 g	2.25 g	2.25 g	2.25 g
Fibers added								
Sheep wool fibers	2.5 % 5 %	- - -	12 mm - 5.63 g Non treated fibers Machine washed in tap water at 30ºC and air-dried for one week	12 mm - 11.25 g Non treated fibers Machine washed in tap water at 30ºC and air-dried for one week	12 mm - 5.63 g Lime treated fibers Immersed in a 1% lime-water solution for 2h and oven-dried at 30ºC for 72h	12 mm - 11.25 g Lime treated fibers Immersed in a 1% lime-water solution for 2h and oven-dried at 30ºC for 72h	12 mm - 5.63 g Surfactant treated fibers Immersed for 72h in a 3% surfactant-water solution and oven-dried at 30ºC for 72h	12 mm - 11.25 g Surfactant treated fibers Immersed for 72h in a 3% surfactant-water solution and oven-dried at 30ºC for 72h
Foam Mixed								
Water	95 %	300 g	300 g	300 g	300 g	300 g	300 g	300 g
Surfacatant	5 %	15.8 g	15.8 g	15.8 g	15.8 g	15.8 g	15.8 g	15.8 g
Final Characteristics								
Foam added		289.96 g	290.73 g	290 g	291.83 g	291.16 g	281.23 g	291.05 g
Fresh state density		210.81 kg/m^3	199.9 kg/m^3	195.75 kg/m^3	200.4 kg/m^3	217.73 kg/m^3	215 kg/m^3	209.43 kg/m^3

Table 6. Characteristics of the mixes with a target density of 300 Kg/m³ containing 12mm fibers with three treatment options and two fiber content ratios.

MIX ID		02-NF-300	02-NTF-300-2.5	02-NTF-300-5	02-LTF-300-2.5	02-LTF-300-5	02-STF-300-2.5	02-STF-300-5
Cement								
Cem I 52.5 R		450 g	450 g	450 g	450 g	450 g	450 g	450 g
Viscosity modifier	15 %	67.5 g	67.5 g	67.5 g	67.5 g	67.5 g	67.5 g	67.5 g
Water	33 %	148.5 g	148.5 g	148.5 g	148.5 g	148.5 g	148.5 g	148.5 g
Superplasticizer	1 %	4.5 g	4.5 g	4.5 g	4.5 g	4.5 g	4.5 g	4.5 g
Fibers added								
Sheep wool fibers	2.5 % 5 %	- - -	12 mm - 11.25 g Non treated fibers Machine washed in tap water at 30°C and air-dried for one week	12 mm - 22.5 g Non treated fibers Machine washed in tap water at 30°C and air-dried for one week	12 mm - 11.25 g Non treated fibers Machine washed in tap water at 30°C and air-dried for one week	12 mm - 22.5 g Non treated fibers Machine washed in tap water at 30°C and air-dried for one week	12 mm - 11.25 g Non treated fibers Machine washed in tap water at 30°C and air-dried for one week	12 mm - 22.5 g Non treated fibers Machine washed in tap water at 30°C and air-dried for one week
Foam Mixed								
Water	95 %	285 g	285 g	285 g	285 g	285 g	285 g	285 g
Surfacatant	5 %	15 g	15 g	15 g	15 g	15 g	15 g	15 g
Final Characteristics								
Foam added		250.3 g	249.94 g	250.39 g	250.78 g	251.48 g	252.32 g	250.16 g
Fresh state density		384.97 kg/m³	396.8 kg/m³	420 kg/m³	403.7 kg/m³	397.65 kg/m³	427.5 kg/m³	423.5 kg/m³

Table 7. Characteristics of the mixes with a target density of 500 Kg/m³ containing 12mm fibers with three treatment options and two fiber content ratios

MIX ID		02-NF-500	02-NTF-500-1.25	02-NTF-500-2.5	02-LTF-500-1.25	02-STF-500-1.25
Cement						
Cem I 52.5 R		900 g	900 g	900 g	900 g	900 g
Viscosity modifier	15 %	135 g	135 g	135 g	135 g	135 g
Water	33 %	297 g	297 g	297 g	297 g	297 g
Superplasticizer	0.25 %	2.25 g	2.25 g	✳ 9 g	2.25 g	2.25 g
Fibers added						
Sheep wool fibers	1.25 % 2.5 %	- - -	12 mm - 11.25 g Non treated fibers Machine washed in tap water at 30°C and air-dried for one week	12 mm - 22.5 g Non treated fibers Machine washed in tap water at 30°C and air-dried for one week	12 mm - 11.25 g Lime treated fibers Immersed in a 1% lime-water solution for 2h and oven-dried at 30°C for 72h	12 mm - 11.25 g Surfactant treated fibers Immersed for 72h in a 3% surfactant-water solution and oven-dried at 30°C for 72h
Foam Mixed						
Water	95 %	395 g	395 g	395 g	395 g	395 g
Surfacatant	5 %	20.8 g	20.8 g	20.8 g	20.8 g	20.8 g
Final Characteristics						
Foam added		389.2 g	388.18 g	350.01 g	388.99 g	388.90 g
Fresh state density		567.57 kg/m³	735.57 kg/m³	574.6 kg/m³	739.35 kg/m³	657.41 kg/m³

✳ Superplasticizer/cement content amounts to 1%.

Tables 3, 4, and 5 show the mix design characteristics of each admixture. For example, as seen in table 5, the fiber content is lower for a target density of 500Kg/m³ because a higher F/C rate was not compatible with the produced volume of concrete. Likewise, the S/C rate of 1% generated increased fluidity issues for this density, so it was reduced in the admixtures with a 1,25% F/C ratio.

Figure 40. Images of the base ingredients of every admixture: cement and viscosity modifier on the left, water and superplasticizer in the center, and pre-formed foam made with water and a surfactant agent on the right

Figure 41. mages of final mixture with fibers: 100Kg/m^3 on the left, 300Kg/m^3 in the center, and 500Kg/m^3 on the right

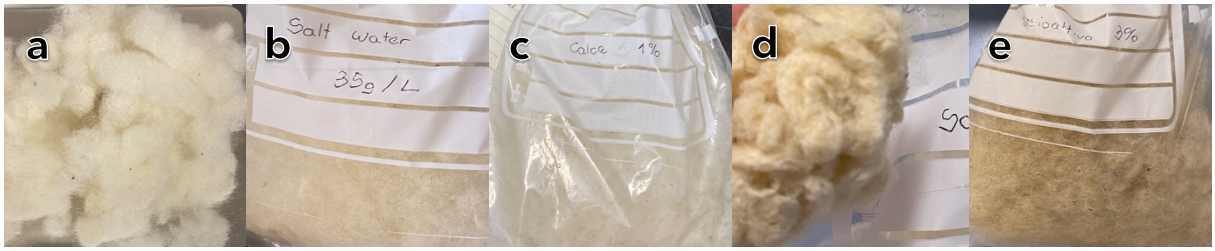

Figure 42. Images of the employed SWF with different treatments: a=NTF, b=NaClTF, c=LTF, d=NaOHTF, and e=STF

As shown in Figure 42, the NaOH treatment modified the fibers. As a result, these fibers attached to each other and became brittle, which made their separation challenging and caused the rupture of the fibers during the process. On the other hand, the visual analysis of the other fiber treatments does not present significant alterations to the fiber structure other than a different coloration.

After completing each admixture, the samples destined to develop each test were confectioned. Formworks used for admixtures with a target density of 100kg/m^3 were covered in cellophane film because, at such low densities, there is a reaction

with the oil. On the other hand, natural corn oil was used on the formworks for admixtures of a 300-500 kg/m^3 target density. To perform the density evaluation and the 28-day mechanical tests, each admixture considered three prismatic samples of 40x40x160 mm. The realization of three samples allows to compare various tests and leads to more realistic results. In addition, the admixtures in the second part of the experimental campaign confectioned three cubic samples of 70x70x70 mm destined for the microstructural analysis of the porosity. The 28-day maturation occurred on-air at room temperature (20±3°C) and natural humidity.

Figure 43. Images of the confectioning process of the prismatic samples above and confectioned cubic samples bellow

The experimental campaign carried out the tests listed below regarding the analyses of the properties of the mixtures.

On the admixtures 01-NF, 01-NTF, 01-NaClTF, 01-LTF, 01-NaOHTF, 01-STF, 01-6mm-2,5, 01-12mm-2,5, 01-20mm-2,5, 01-12mm-5, and 01-12mm-10:

1. Evaluation of mechanical properties (compressive and flexural strength) developed after 28 days of maturation of the samples.
2. A slump test performed after the mixing phase carried out the rheological characterization of the fresh state.

On the admixtures from the second part of the experimental campaign 02-NF-100, 02-NTF-100-2,5, 02-NTF-100-5, 02-LTF-100-2,5, 02-LTF-100-5, 02-STF-100-2,5, 02-STF-100-5, 02-NF-300, 02-NTF-300-2,5, 02-NTF-300-5, 02-LTF-300-2,5, 02-LTF-300-5, 02-STF-300-2,5, 02-STF-300-5, 02-NF-500, 02-NTF-500-1,25, 02-NTF-100-2,5, 02-LTF-100-1,25, and 02-STF-100-1,25:

10. Evaluation of mechanical properties (compressive and flexural strength) developed after 28 days of maturation of the samples.
11. A slump test performed after the mixing phase carried out the rheological characterization of the fresh state.
12. Evaluation of density variation between fresh state, maturation until the remotion of the samples from the formworks, maturation up to 28 days, and dry state density after drying the samples at 100°C for at least 72 hours up to reaching a constant weight.
13. Microstructural characterization of porosity and pore dimensions was evaluated through image analyses executed after oven drying the samples for at least 72h at 60°C until a constant weight was reached.

5.2. Results and discussions

5.2.1. Rheological characterization of the fresh state

A slump test performed at the end of the mixing process evaluated the rheological characterization of the fresh state. To begin with, the fresh material was introduced into a hollow cylinder with 8cm height and internal diameter. Next, the cylinder was removed. Once the material had stabilized, the deformation produced in the material along with two perpendicular horizontal directions and three vertical ones was measured. Lastly, an average of these quantities was calculated to obtain the final results.

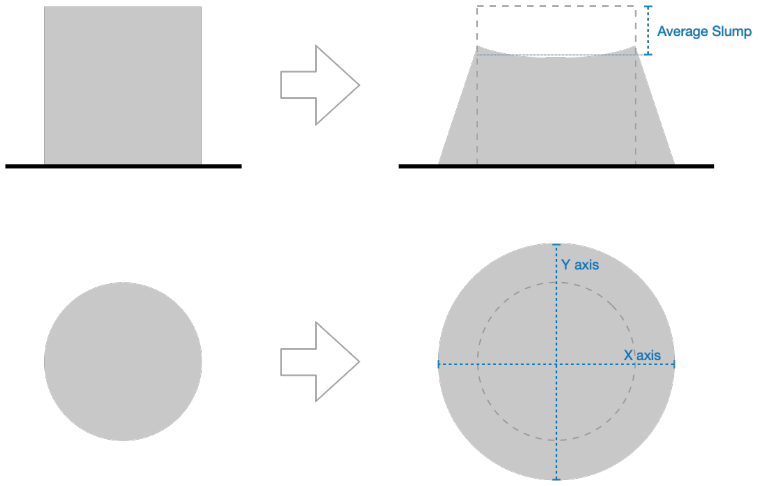

Figure 44. Image indicating how the slump test was measured to obtain the vertical and horizontal slump results.

Table 8. Results of the slump test for the first part of the experimental campaign dedicated to fiber treatment, length, and content choice

MIX ID	SLUMP			
	Lowest	Medium	Highest	Avg. [mm]
Fiber treatment choice				
01-NF	49.0	52.0	55.0	**52.0**
01-NTF	39.0	41.0	48.0	**42.7**
01-NaClTF	36.0	46.0	48.0	**43.3**
01-LTF	39.0	46.0	51.0	**45.3**
01-NaOHTF	45.0	50.0	54.0	**49.7**
01-STF	40.0	44.0	47.0	**43.7**
Fiber length and fiber content choice				
01-6mm-2.5	48.0	50.0	53.0	**50.3**
01-12mm-2.5	39.0	41.0	48.0	**42.7**
01-20mm-2.5	35.0	41.0	45.0	**40.3**
01-12mm-5	23.0	35.0	41.0	**33.0**
01-12mm-10	7.0	16.0	25.0	**16.0**

Table 9. Results of the slump test for the second part of the experimental campaign dedicated to the analysis of different target densities.

MIX ID	SLUMP				HORIZONTAL SLUMP		
	Lowest	Medium	Highest	Avg. [mm]	X axis	Y axis	Avg. [mm]
100 kg/m³							
02-NF-100	27.0	36.0	39.0	**34.0**	122.0	127.0	**124.5**
02-NTF-100-2.5	11.5	11.5	11.5	**11.5**	86.0	88.5	**87.3**
02-NTF-100-5	10.0	10.0	10.0	**10.0**	87.0	89.0	**88.0**
02-LTF-100-2.5	11.5	11.5	11.5	**11.5**	89.0	90.0	**89.5**
02-LTF-100-5	10.0	10.0	10.0	**10.0**	84.0	85.0	**84.5**
02-STF-100-2.5	10.0	14.0	17.0	**13.7**	91.0	94.0	**92.5**
02-STF-100-5	10.5	10.5	10.5	**10.5**	83.0	84.0	**83.5**
300 kg/m³							
02-NF-300	45.0	48.0	52.0	**48.3**	160.0	161.0	**160.5**
02-NTF-300-2.5	19.0	28.0	31.0	**26.0**	117.0	110.0	**113.5**
02-NTF-300-5	11.0	16.0	20.0	**15.7**	89.0	91.0	**90.0**
02-LTF-300-2.5	23.0	33.0	35.0	**30.3**	114.0	118.0	**116.0**
02-LTF-300-5	11.0	20.0	25.0	**18.7**	94.0	95.0	**94.5**
02-STF-300-2.5	31.0	32.0	34.0	**32.3**	113.0	127.0	**120.0**
02-STF-300-5	19.0	20.0	22.0	**20.3**	110.0	112.0	**111.0**
500 kg/m³							
02-NF-500	38.0	40.0	43.0	**40.3**	151.0	151.0	**151.0**
02-NTF-500-1.25	14.0	22.0	25.0	**20.3**	92.0	95.0	**93.5**
02-NTF-500-2.5	44.0	54.0	59.0	**52.3**	144.0	160.0	**152.0**
02-LTF-500-1.25	14.0	22.0	29.0	**21.7**	97.0	98.0	**97.5**
02-STF-500-1.25	14.0	20.0	25.0	**19.7**	93.0	97.0	**95.0**

Table 8 and Table 9 show the results of the rheological tests for each admixture developed in both experimental campaigns.

- Fiber content:

As a general rule, the addition of fibers reduces the slump. For example, in Table 8, it is noticeable that the admixtures with fibers have, on average, a 14% lower slump value when compared to the admixture without fibers.

Figure 45. Image showing the influence of fiber addition on the slump for the first experimental campaign on the fiber treatment choice. On the left, mix 01-NF represents the slump without fibers; on the right, mix 01-NTF shows the slump of an admixture containing fibers.

On the other hand, for the second part of the experimental campaign, the results are divided according to the densities analyzed. For 100 kg/m^3, the slump decreased on average a 64% for admixtures with a 2,5% F/C ratio and a 70% for admixtures with a 5% F/C ratio.

Figure 46. Image showing the influence of fiber addition on the slump for the second experimental campaign on the 100kg/m^3 density. On the left, mix 02-NF-100 represents the slump without fibers; in the middle, mix 02-NTF-100-2,5% shows an admixture with a 2,5% F/C ratio; on the right, mix 02-NTF-100-5% shows the slump of an admixture with a 5% F/C ratio.

On a density of 100kg/m^3, the addition of fibers makes the slump decrease significantly. However, the admixtures with the two different F/C ratios are similar. Therefore, the cement paste tends to maintain its shape at this density when SWFs are added to the admixture.

For 300 kg/m^3, the slump decreased on average a 40% for admixtures with a 2,5% F/C ratio and a 60% for admixtures with a 5% F/C ratio.

Figure 47. Image showing the influence of fiber addition on the slump for the second experimental campaign on the 300kg/m^3 density. On the left, mix 02-NF-300 represents the slump without fibers; in the middle, mix 02-NTF-300-2,5 shows an admixture with a 2,5% F/C ratio; on the right, mix 02-NTF-300-5 shows the slump of an admixture with a 5% F/C ratio.

On a density of 300kg/m^3, the addition of fibers makes the slump decrease significantly. However, the admixtures with the two different F/C ratios present a 20% deviation from each other, being the admixture with a 5% F/C ratio, the one with the lower slump.

For 500 kg/m^3, the slump decreased on average a 50% for admixtures with a 1,25% F/C ratio.

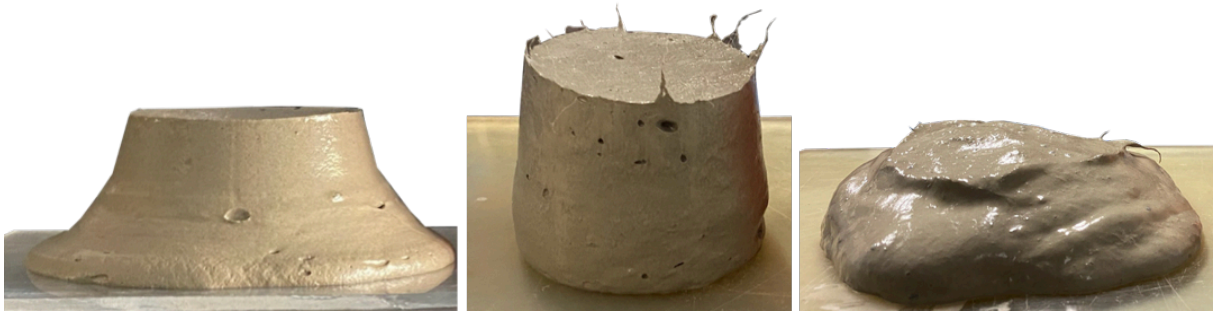

Figure 48. Image showing the influence of fiber addition on the slump for the second experimental campaign on the 500kg/m^3 density. On the left, mix 02-NF-500 represents the slump without fibers; in the middle, mix 02-NTF-500-1,25 shows an admixture with a 1,25% F/C ratio; on the right, mix 02-NTF-500-2,5 shows the slump of an admixture with a 2,5% F/C ratio.

At a density of 500kg/m^3, the addition of fibers significantly decreases the slump. Among the admixture without fibers and the one with a 1,25% F/C ratio, there is a variation of 50%. However, to obtain this result, the S/C ratio was modified from 1%, the one present on the other target densities analyzed, to 0,25%. This decision was motivated by the rheology of the admixture 02-NTF-500-2,5, which, as shown in Figure 48, was very fluid and did not maintain the original shape.

In addition, in the first part of the experimental campaign, the subsection about the fiber content choice shows that when the F/C content ratio increases, the slump decreases accordingly.

- Fiber length:

In the first part of the experimental campaign, the subsection about the fiber length choice shows that while 6mm fibers do not present a significant impact on the slump compared to the admixture without fibers, the admixtures with 12 and 20mm fibers present a similar advantage in slump reduction.

- Density and foam addition:

Figure 49. Image showing the influence of density on the slump for the second experimental campaign. On the left, mix 02-NF-100 presents a density of 100kg/m^3; in the middle, mix 02-NF-300 shows an admixture with a 300kg/m^3 density; on the right, mix 02-NF-500 shows the slump of an admixture with a 500kg/m3 density.

Figure 49 shows how a lower density, which translates into a higher foam/cement (Fo/C) ratio, decreases the slump, possibly because the cement paste gets more stability due to the higher foam content. However, this rule does not apply to the admixture 02-NF-500 because the superplasticizer content was reduced.

In concrete 3D printing, a lower slump value embodies an improved buildability because the 3D printed concrete needs to maintain its shape during the printing process and withstand the weight of successive layers [60]. Considering this, the addition of SWF is beneficial for the printability of the material.

5.2.2. Density variation

This research performed a density variation valuation on every admixture from the second part of the experimental campaign. The purpose of this analysis is to evaluate the variations in density between the different stages of each sample and the possible effects that the presence of the SWF in the mixtures may have on these variations.

The density variations were evaluated for:

1. The fresh state density: was measured on every admixture at the end of the mixing process.
2. The 28 days density: was measured after 20 days of maturation of the samples. The maturation took place at room temperature and natural humidity conditions.
3. The dry state density: after the 28 days of maturation, the samples were subjected to oven drying at 100°C for at least 72 hours or until reaching a constant weight. The measuring took place immediately after removing the samples from the oven.

The density in the fresh state was evaluated as the ratio between the weight and the volume of a glass full of admixture. In contrast, the 28 days and the dry density were evaluated as the ratio between the weight of the sample and its volume, calculated by measuring the dimensions of each side with a caliper, carried out as the average of three measurements (one central and two lateral) and also taking into account the hollowing caused by the exposure to air of the upper face of each sample.

The mean values obtained are reported in the following graphs for each admixture analyzed:

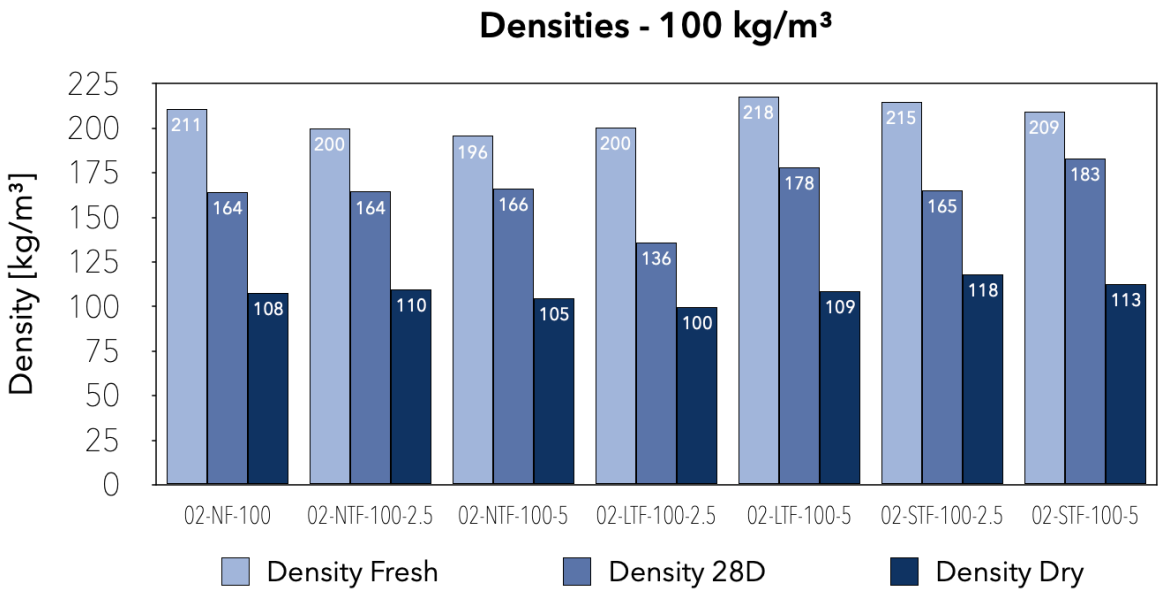

Figure 50. Image showing the density variation on the admixtures with 100kg/m^3 from the second part of the experimental campaign.

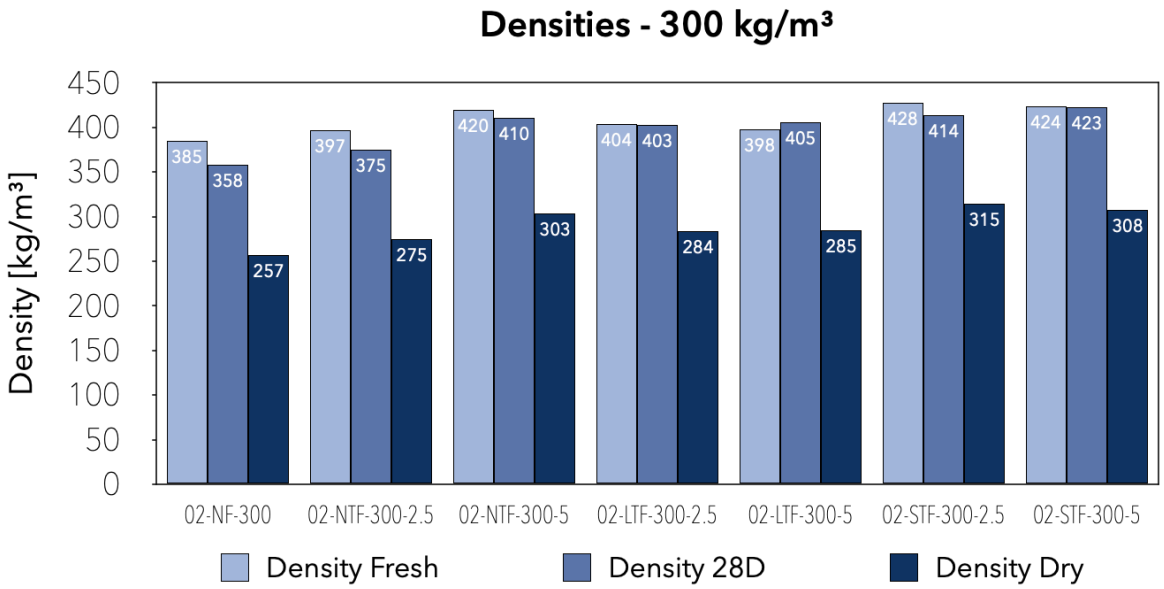

Figure 51. Image showing the density variation on the admixtures with 300kg/m³ from the second part of the experimental campaign.

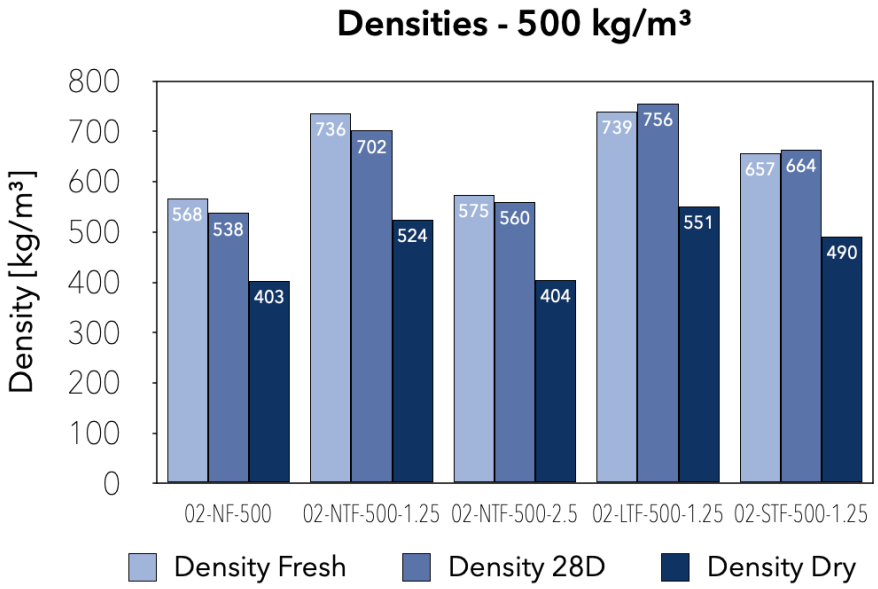

Figure 52. Image showing the density variation on the admixtures with 500kg/m³ from the second part of the experimental campaign.

From the comparison among the same density, it is noticeable that the admixtures with a lower density, 100kg/m³, lose more weight during the 28 days of maturation compared to the admixtures with higher densities, 300 and 500kg/m³. This variation might be attributed to the fact that the Fo/C ratio for admixtures with a target density of 100kg/m3 was around 125%, while that for 300 and 500kg/m3 was 55 and 45%, respectively. A higher amount of foam translates into a higher amount of water, which can explain the higher weight loss by a more significant contribution due to the evaporation of the liquid phase of the compounds.

5.2.3. Microstructural characterization

The microstructural analysis of printable foamed concrete is fundamental given that this characteristic influences, in addition to thermal performance, two of the main properties of the material in the hardened state, namely the mechanical performance and durability of the final element. As far as mechanical performance is concerned, what plays a central role is the size of the pores and their relative distribution; as far as durability is concerned, porosity is the characteristic that influences the material's permeability. Therefore, the main objective of the microstructural characterization is to evaluate the porosity and analyze the dimensional and distributive characteristics of the pores of each sample to identify any effects that the incorporation of SWF and their treatment may have had on the characteristics of the admixtures.

The microstructural analysis was performed on each sample from the second part of the experimental campaign. One of the 7cm cubic samples of each admixture got cut into three pieces after the maturation for 28 days and oven drying at 60°C for at least 72 hours or until reaching a constant weight. A highspeed circular saw cut the samples into three parts.

Following the cutting operation, a careful visual analysis of the parts made it possible to verify the distribution of pores in the entire sample and choose the most representative section of each sample, discarding the sections that had macro-voids caused by material packaging problems. Images of these selected surfaces were taken by a stereoscope, taking care to always guarantee the partial overlap between them in order to facilitate their subsequent union. In addition, the use of the stereoscope made it possible to create high-resolution images without any focusing problems despite the absence of a continuous flat surface due to cavities.

Subsequently, the various images taken with the stereoscope were superimposed and joined to form a single image of approximately 30 x 30 mm in size. A representative quadrangular portion was selected for each image, with dimensions equal to 15 x 15 mm for samples with a target density of 100kg/m^3, 12,5 x 12,5 mm for 300kg/m^3, 15 x 15 mm for 300kg/m^3. Furthermore, each portion was binarized on ImageJ by representing the solids in white and the voids in black.

Two types of microstructural analysis were carried out using the ImageJ software on the binarized images: the evaluation of porosity and the quantification of the size and relative distribution of the pores.

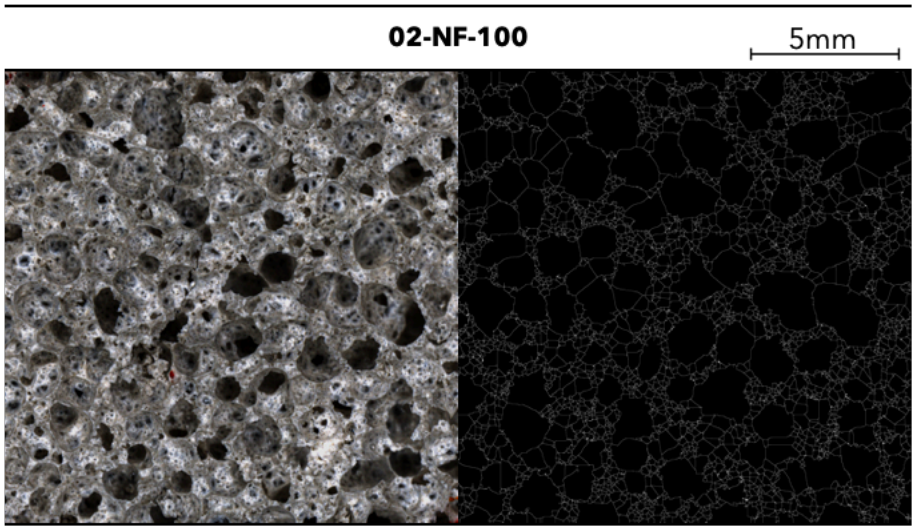

Figure 53. Original and binarized images employed to evaluate the porosity of mix 02-NF-100.

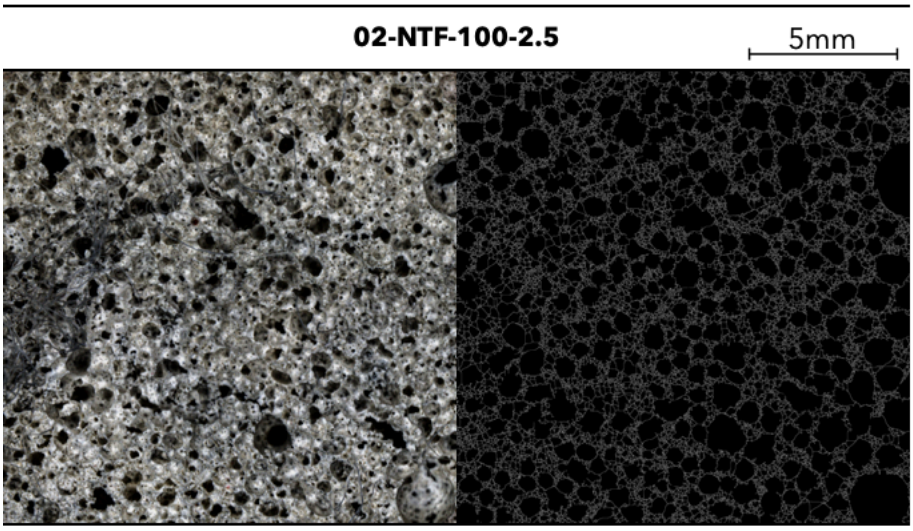

Figure 54. Original and binarized images employed to evaluate the porosity of mix 02-NTF-100-2,5.

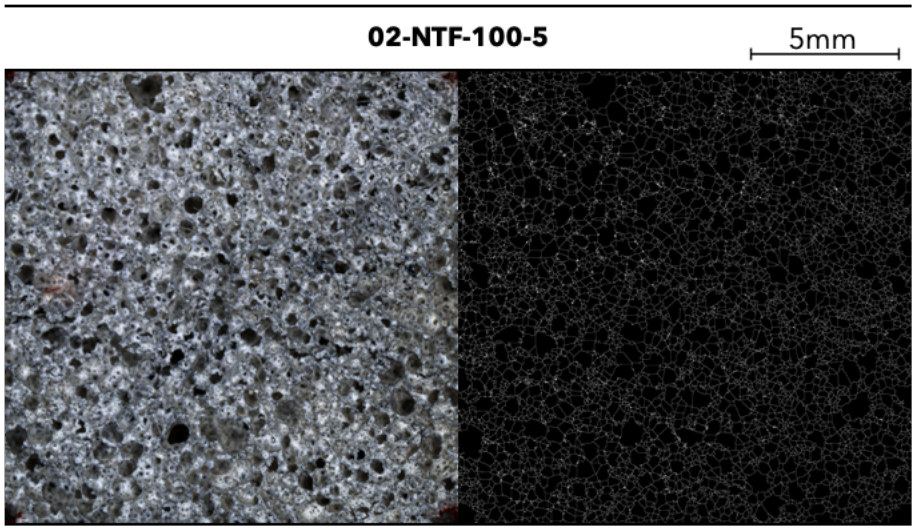

Figure 55. Original and binarized images employed to evaluate the porosity of mix 02-NTF-100-5.

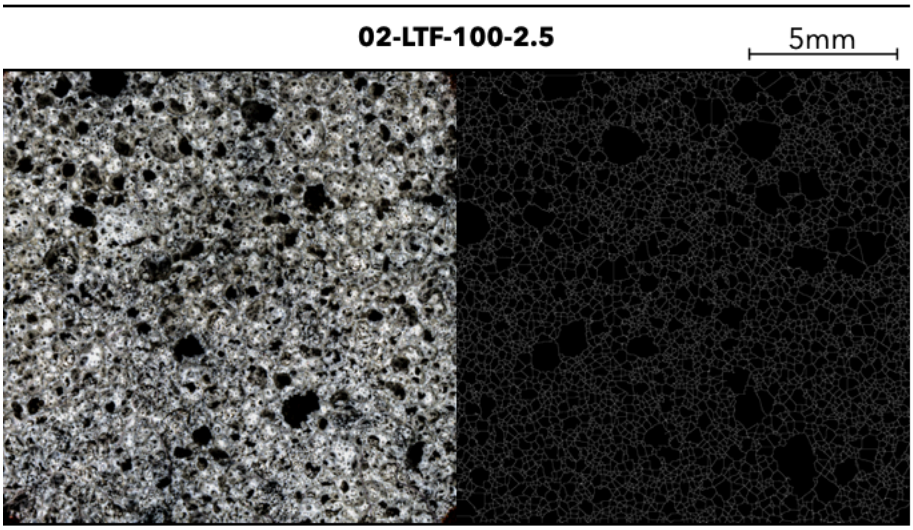

Figure 56. Original and binarized images employed to evaluate the porosity of mix 02-LTF-100-2,5.

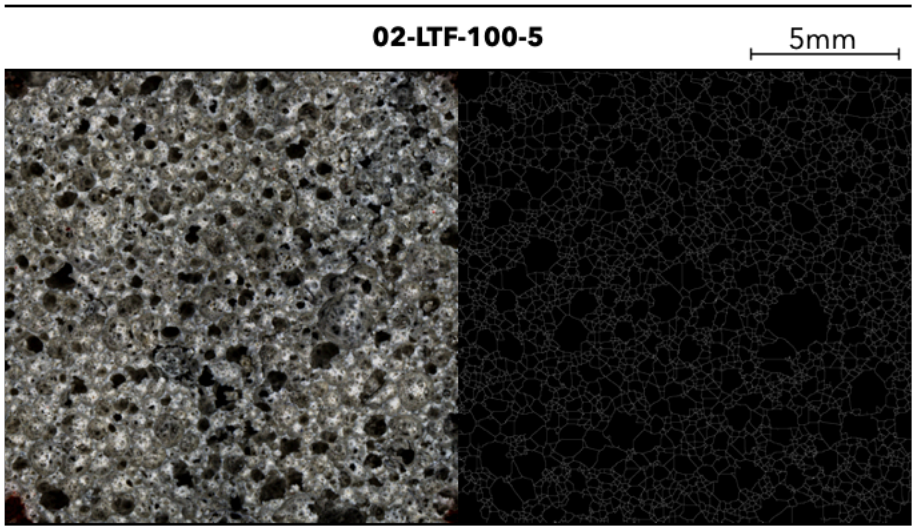

Figure 57. Original and binarized images employed to evaluate the porosity of mix 02-LTF-100-5.

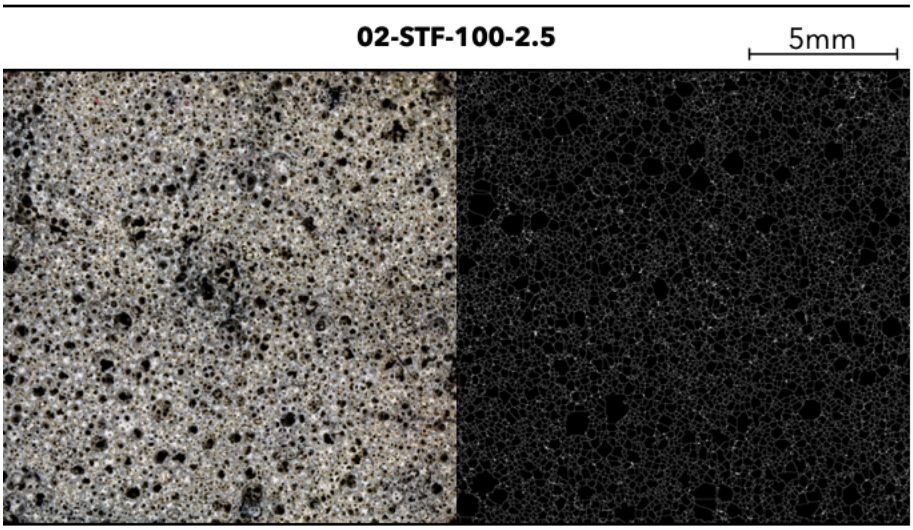

Figure 58. Original and binarized images employed to evaluate the porosity of mix 02-STF-100-2,5.

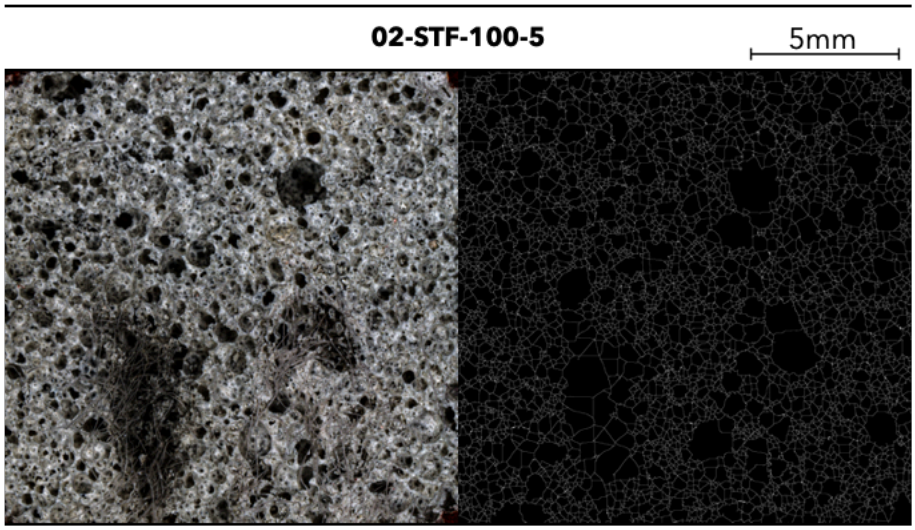

Figure 59. Original and binarized images employed to evaluate the porosity of mix 02-STF-100-5.

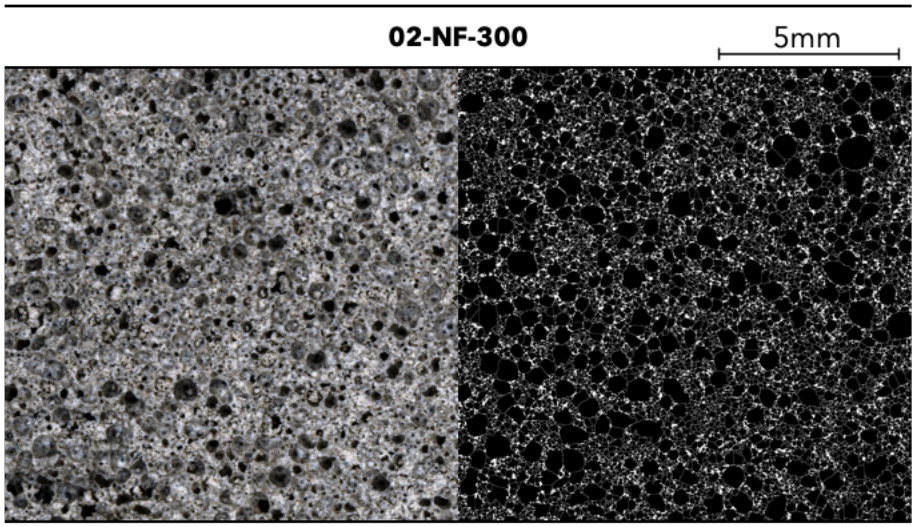

Figure 60. Original and binarized images employed to evaluate the porosity of mix 02-NF-300.

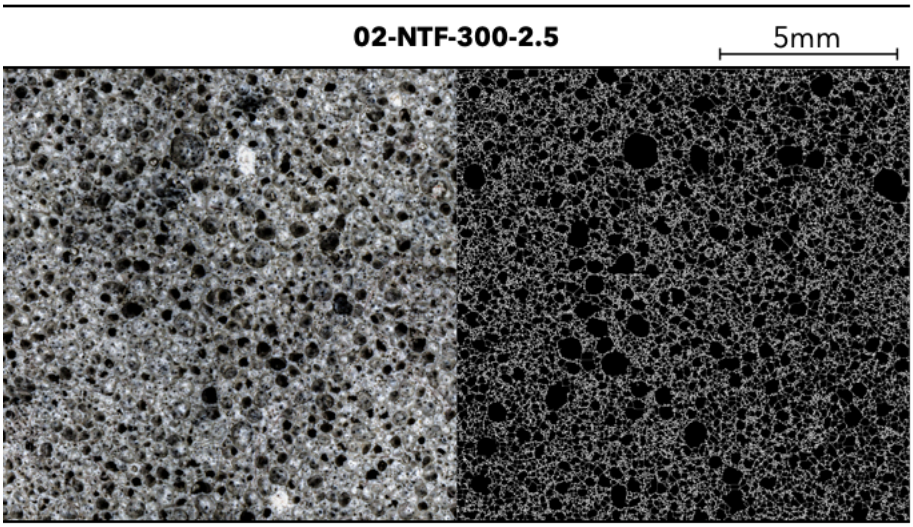

Figure 61. Original and binarized images employed to evaluate the porosity of mix 02-NTF-300-2,5.

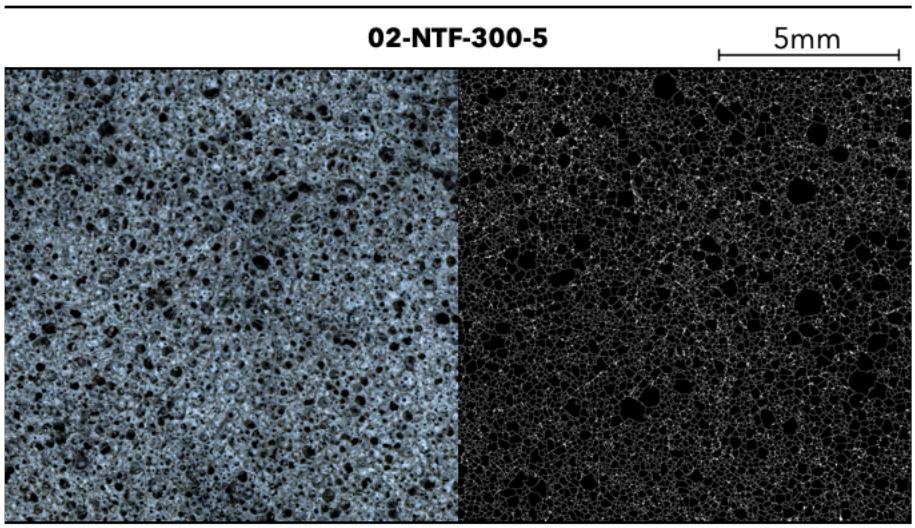

Figure 62. Original and binarized images employed to evaluate the porosity of mix 02-NTF-300-5.

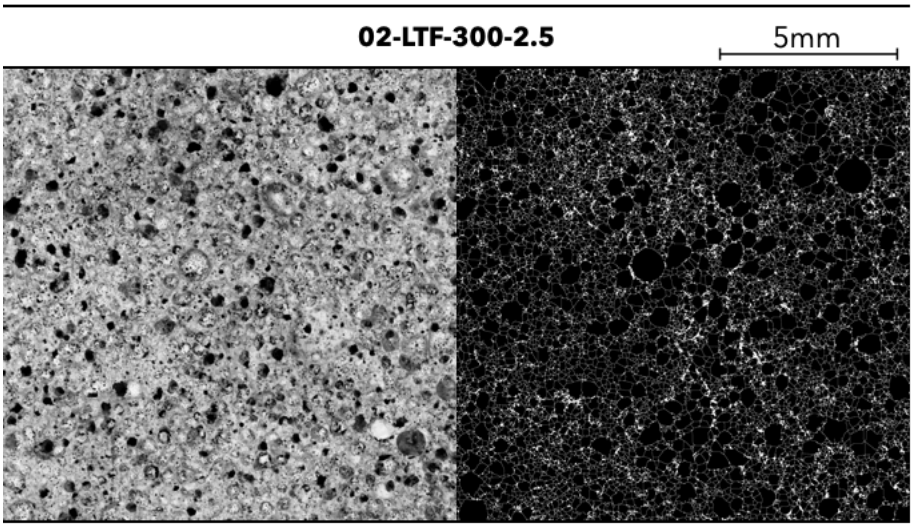

Figure 63. Original and binarized images employed to evaluate the porosity of mix 02-LTF-300-2,5.

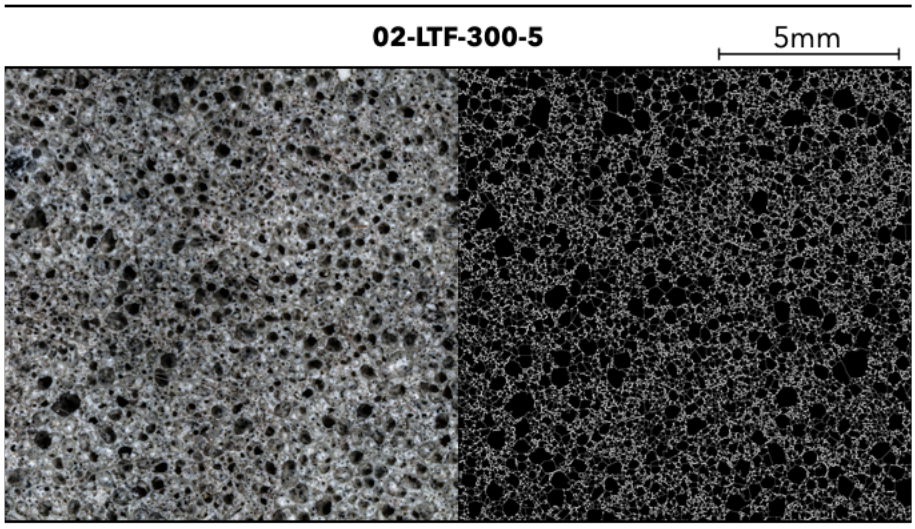

Figure 64. Original and binarized images employed to evaluate the porosity of mix 02-LTF-300-5.

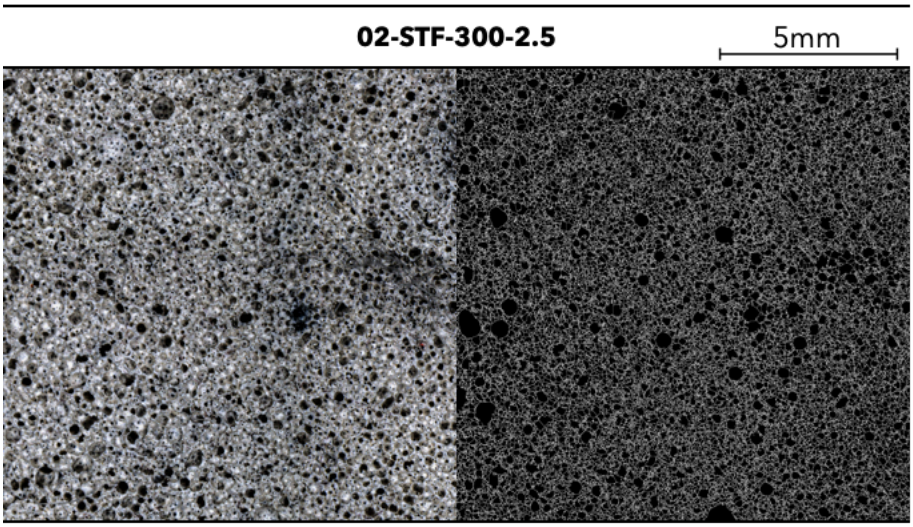

Figure 65. Original and binarized images employed to evaluate the porosity of mix 02-STF-300-2,5.

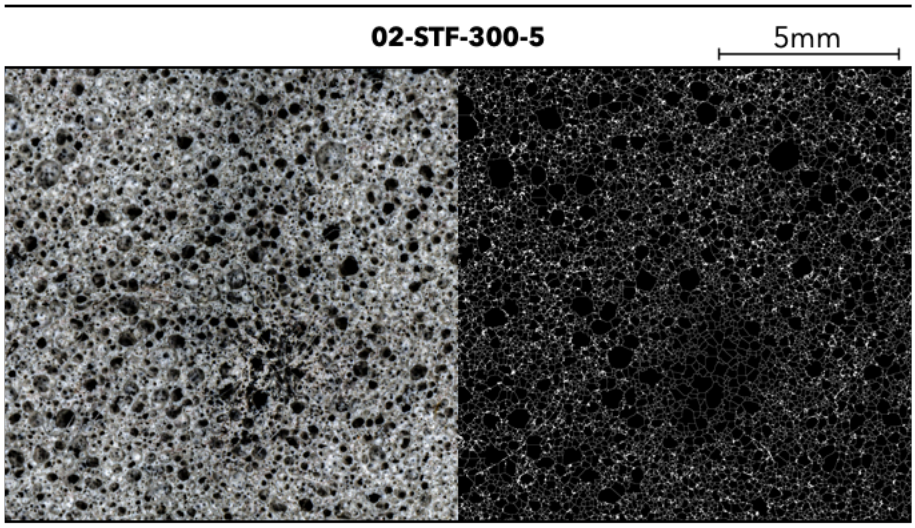

Figure 66. Original and binarized images employed to evaluate the porosity of mix 02-STF-300-5.

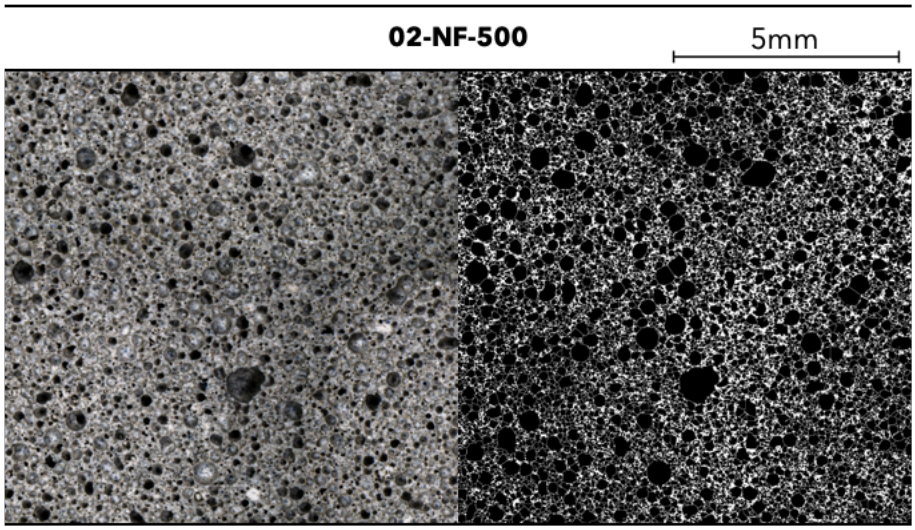

Figure 67. Original and binarized images employed to evaluate the porosity of mix 02-NF-500.

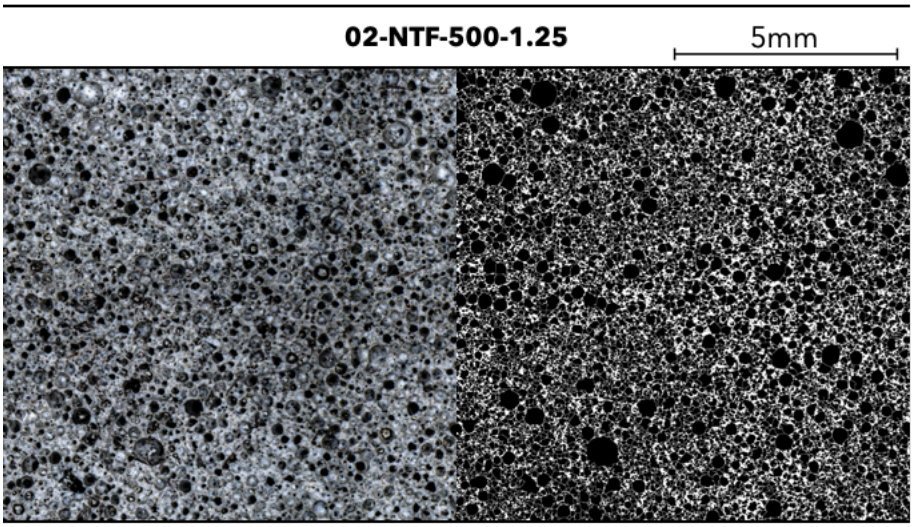

Figure 68. Original and binarized images employed to evaluate the porosity of mix 02-NTF-500-1,25.

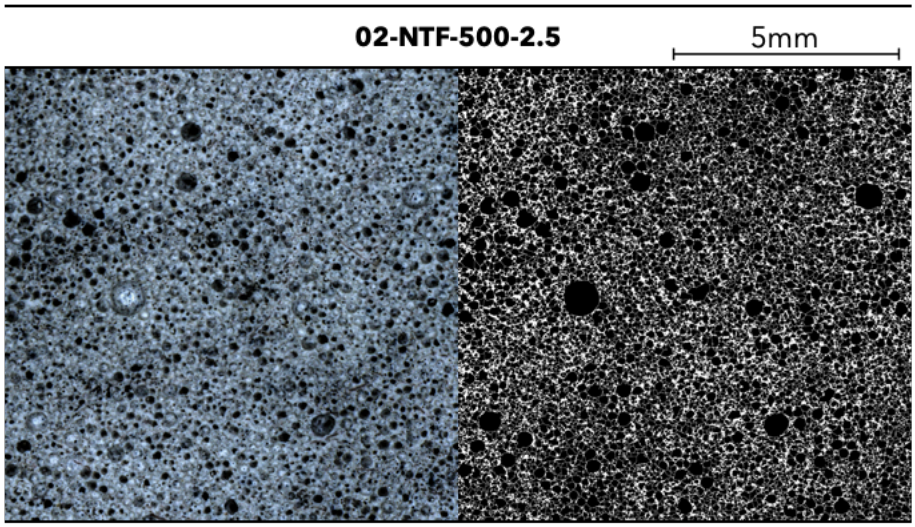

Figure 69. Original and binarized images employed to evaluate the porosity of mix 02-NTF-500-2,5.

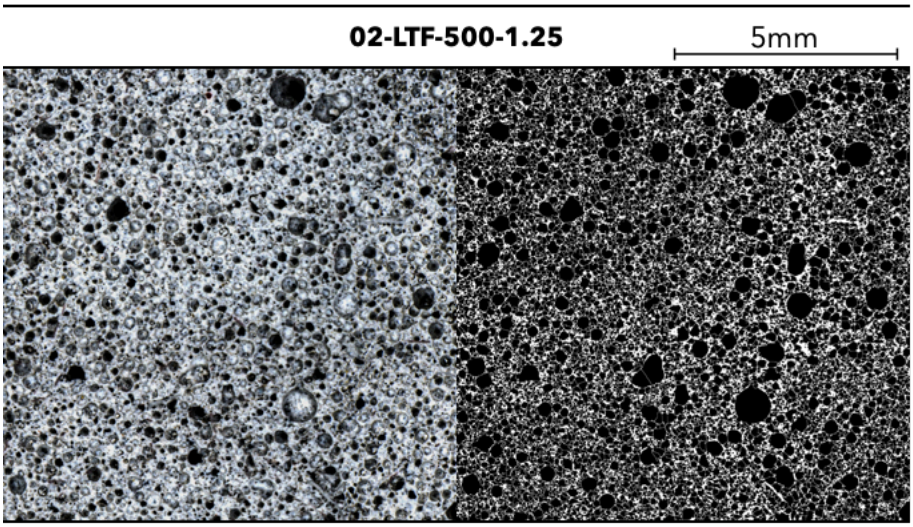

Figure 70. Original and binarized images employed to evaluate the porosity of mix 02-LTF-500-1,25.

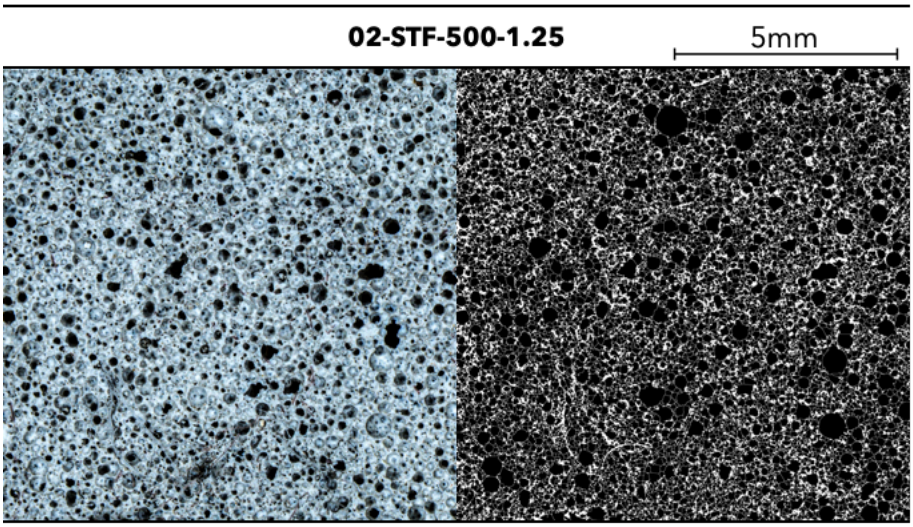

Figure 71. Original and binarized images employed to evaluate the porosity of mix 02-STF-500-1,25.

The porosity of every sample was quantified on the image binarized by the threshold function of ImageJ. This value was then confronted with the theoretical porosity obtained with the following formula:

$$\varepsilon = 1 - \frac{\gamma\ dry}{\gamma\ solid}$$

Where $\gamma\ dry$ is the density of the sample after 28 days of maturation in air and oven drying for 72 hours, on the other hand, $\gamma\ solid$ is the density of the cement paste without the addition of foam which is equal to 1850 kg/m^3.

Furthermore, the ImageJ software calculated through the analyze particles function the values relating to the area of each pore, excluding those placed on the edge of the image, and considering each pore as if it were a perfect circle. Finally, the equivalent diameter of each of them and the percentage distribution of the pore size were calculated using an Excel worksheet.

The results presented in the following table and graphs emerged from the evaluations carried out during the microstructural analyses.

Table 10. Summary of the results obtained from the microstructural analysis carried out on the image area selected for each evaluated admixture.

MIX ID	Dry Density γ_{dry} [kg/m³]	Theoretical Porosity [%]	Measured Porosity [%]
100 kg/m³			
02-NF-100	112.8	93.9 %	94.1 %
02-NTF-100-2.5	115.6	93.8 %	92.1 %
02-NTF-100-5	107.2	94.2 %	92.9 %
02-LTF-100-2.5	101.1	94.5 %	94.4 %
02-LTF-100-5	104.7	94.3 %	93.7 %
02-STF-100-2.5	118.7	93.6 %	91.8 %
02-STF-100-5	109.0	94.1 %	93.9 %
300 kg/m³			
02-NF-300	272.5	85.3 %	84.2 %
02-NTF-300-2.5	279.3	84.9 %	85.5 %
02-NTF-300-5	314.6	83.0 %	83.9 %
02-LTF-300-2.5	297.3	83.9 %	83.1 %
02-LTF-300-5	297.0	83.9 %	82.1 %
02-STF-300-2.5	309.0	83.3 %	82.4 %
02-STF-300-5	306.9	83.4 %	84.5 %
500 kg/m³			
02-NF-500	420.1	77.3 %	77.2 %
02-NTF-500-1.25	539.0	70.9 %	69.7 %
02-NTF-500-2.5	419.8	77.3 %	75.4 %
02-LTF-500-1.25	574.5	68.9 %	69.7 %
02-STF-500-1.25	507.9	72.5 %	72.3 %

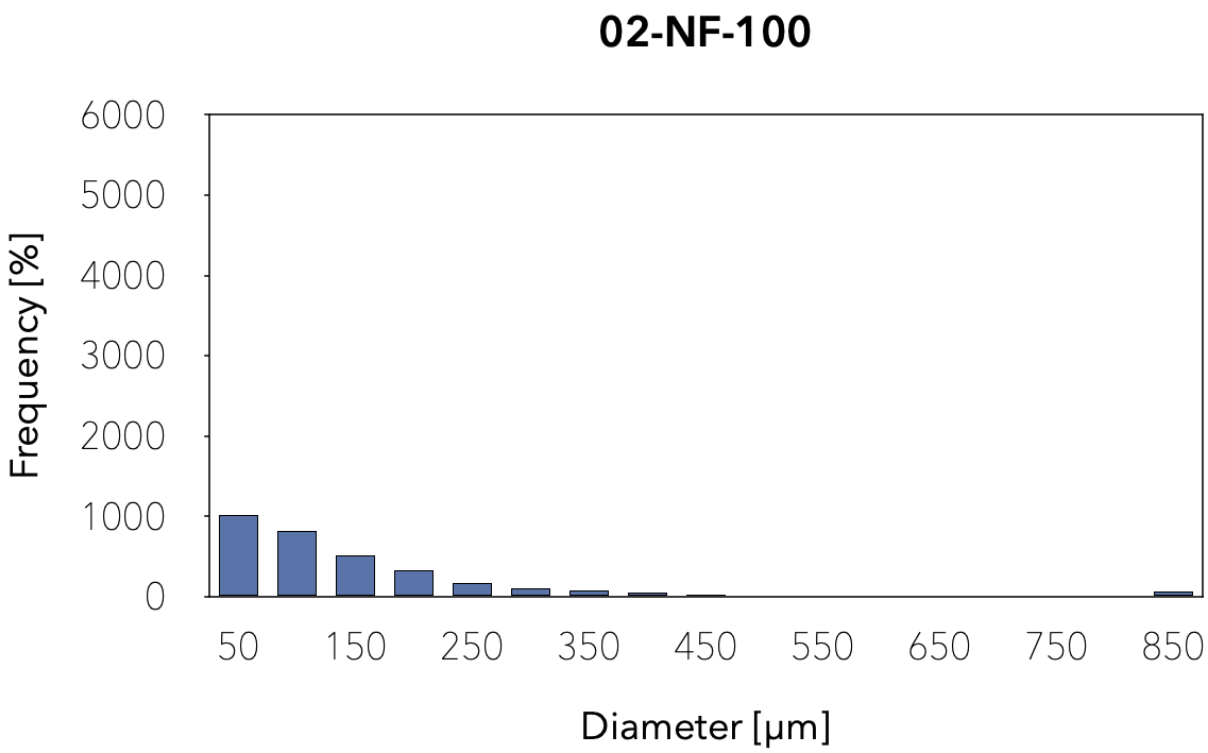

Figure 72. Graphic representation of the frequency with which the equivalent diameters of the pores are present in the samples made with admixture 02-NF-100.

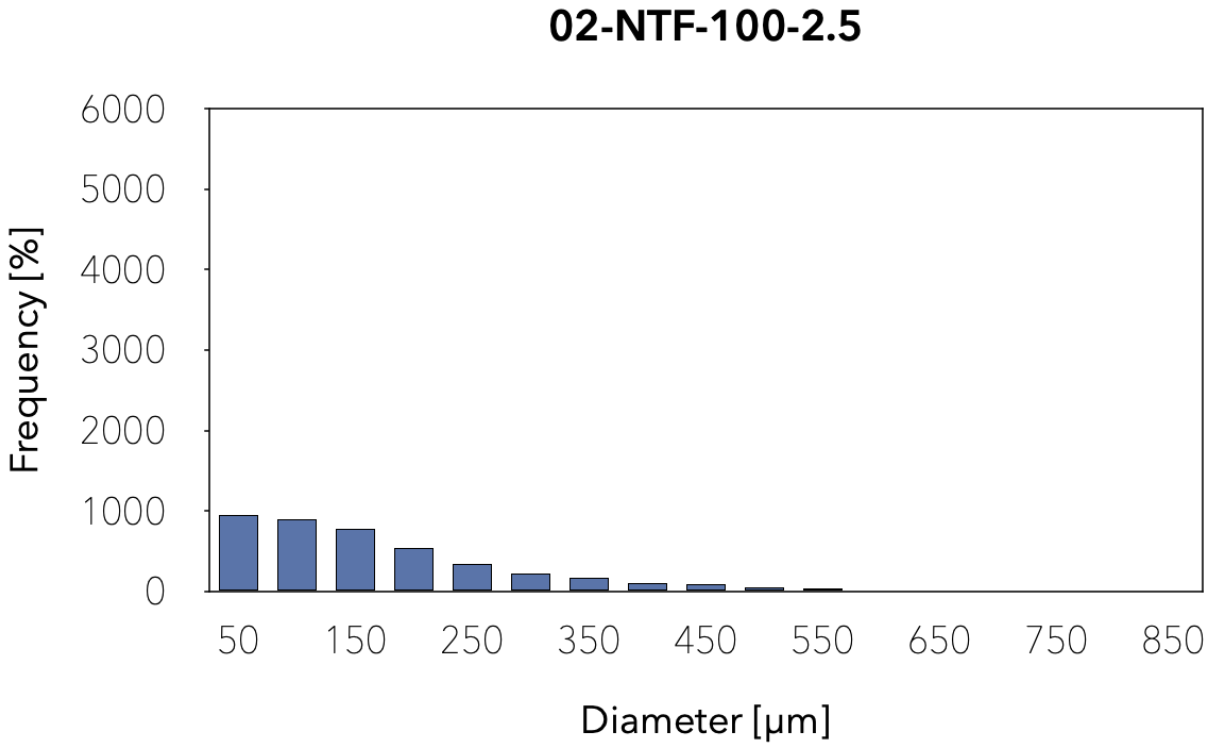

Figure 73. Graphic representation of the frequency with which the equivalent diameters of the pores are present in the samples made with admixture 02-NTF-100-2,5.

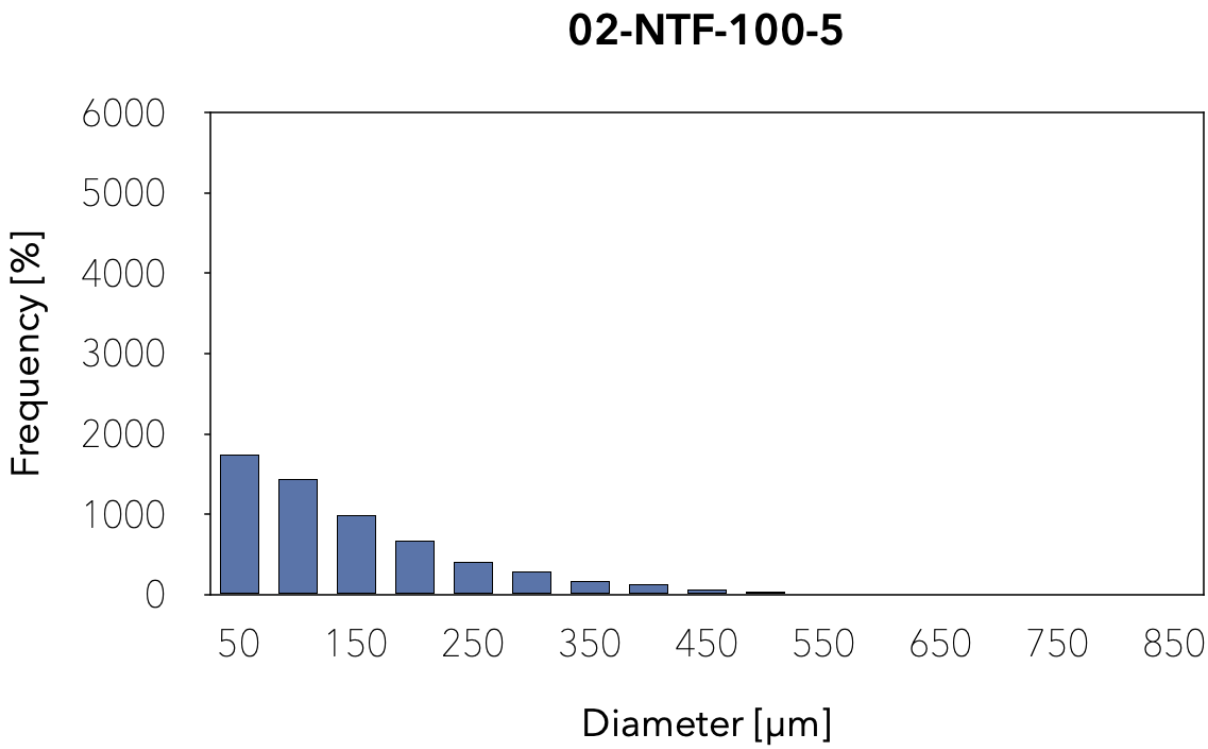

Figure 74. Graphic representation of the frequency with which the equivalent diameters of the pores are present in the samples made with admixture 02-NTF-100-5.

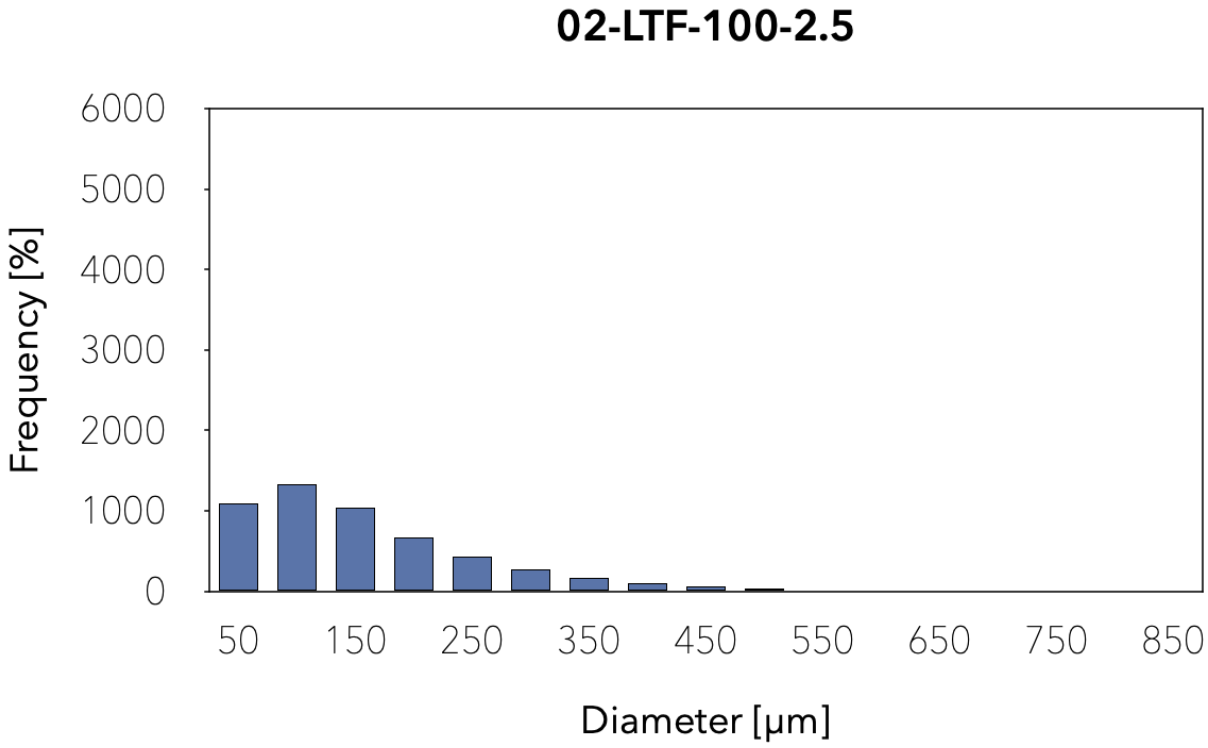

Figure 75. Graphic representation of the frequency with which the equivalent diameters of the pores are present in the samples made with admixture 02-LTF-100-2,5.

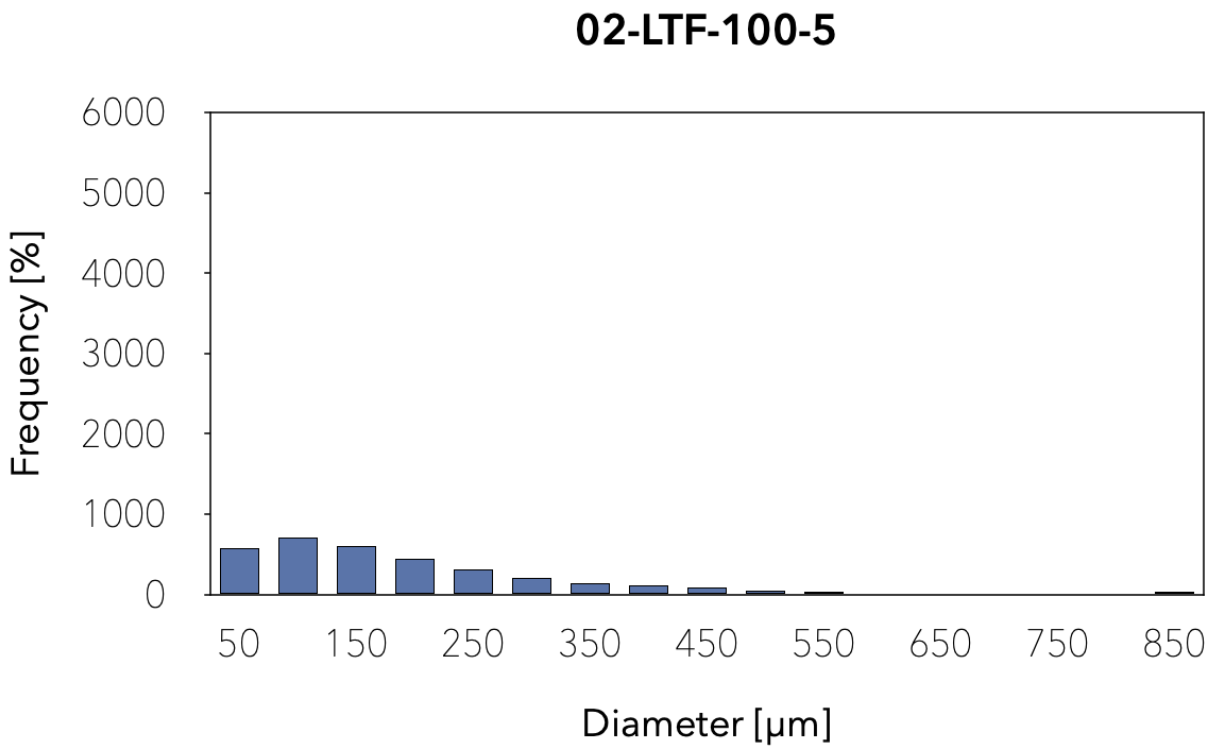

Figure 76. Graphic representation of the frequency with which the equivalent diameters of the pores are present in the samples made with admixture 02-LTF-100-5.

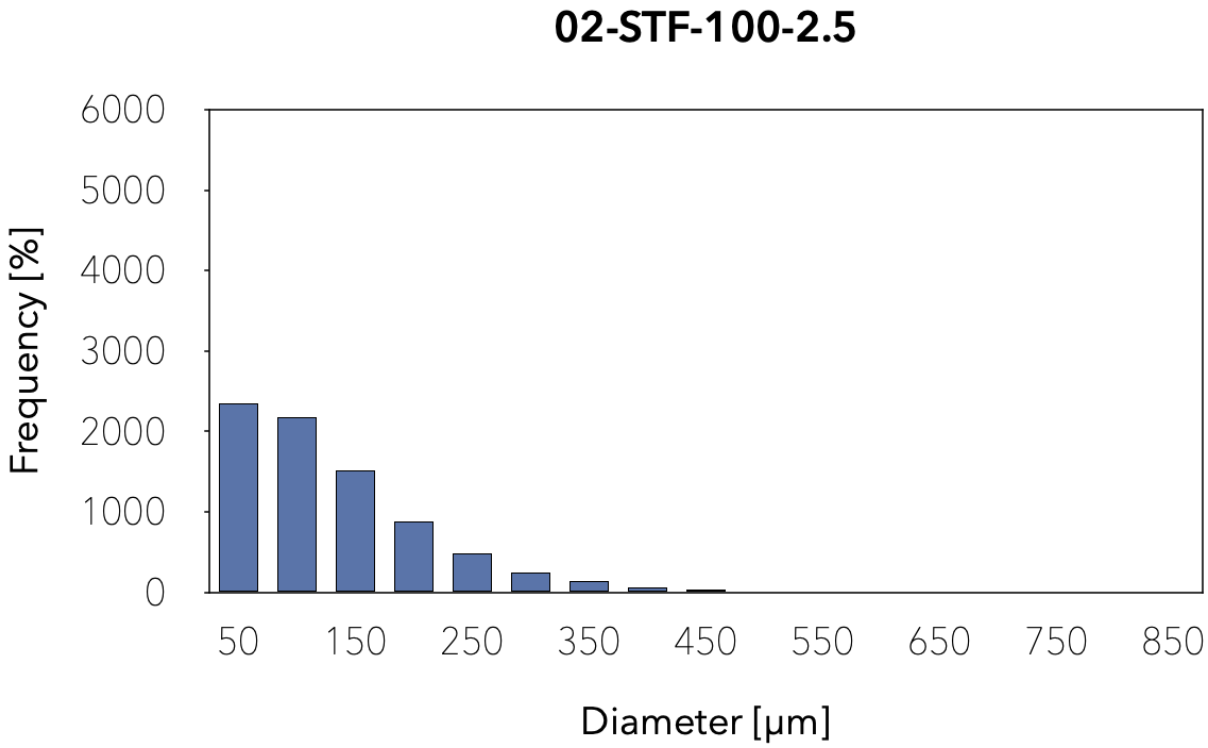

Figure 77. Graphic representation of the frequency with which the equivalent diameters of the pores are present in the samples made with admixture 02-STF-100-2,5.

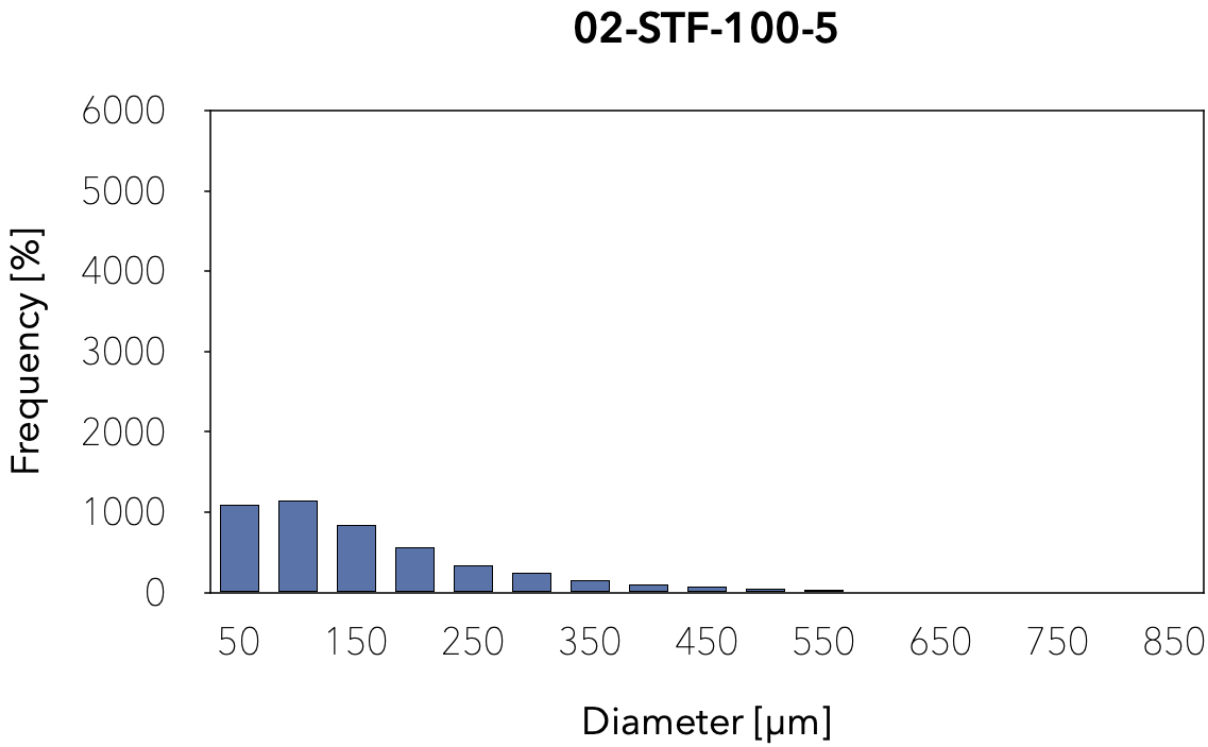

Figure 78. Graphic representation of the frequency with which the equivalent diameters of the pores are present in the samples made with admixture 02-STF-100-5.

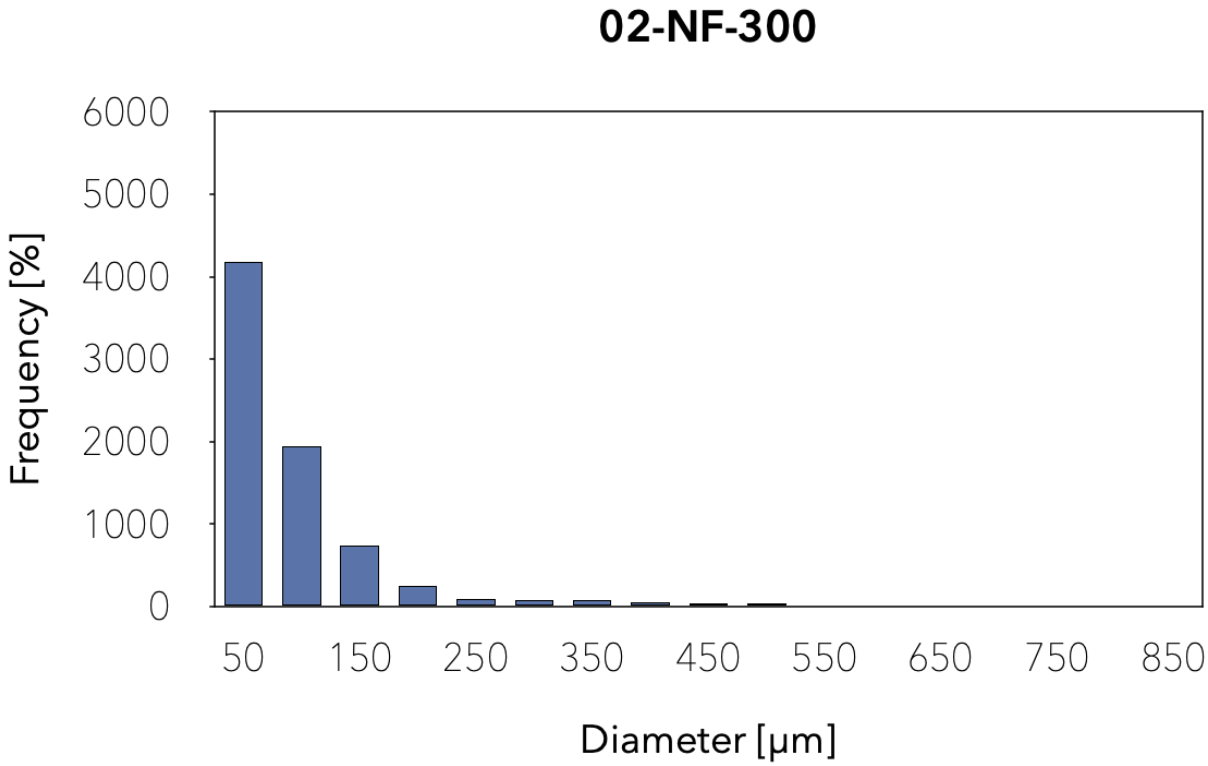

Figure 79. Graphic representation of the frequency with which the equivalent diameters of the pores are present in the samples made with admixture 02-NF-300.

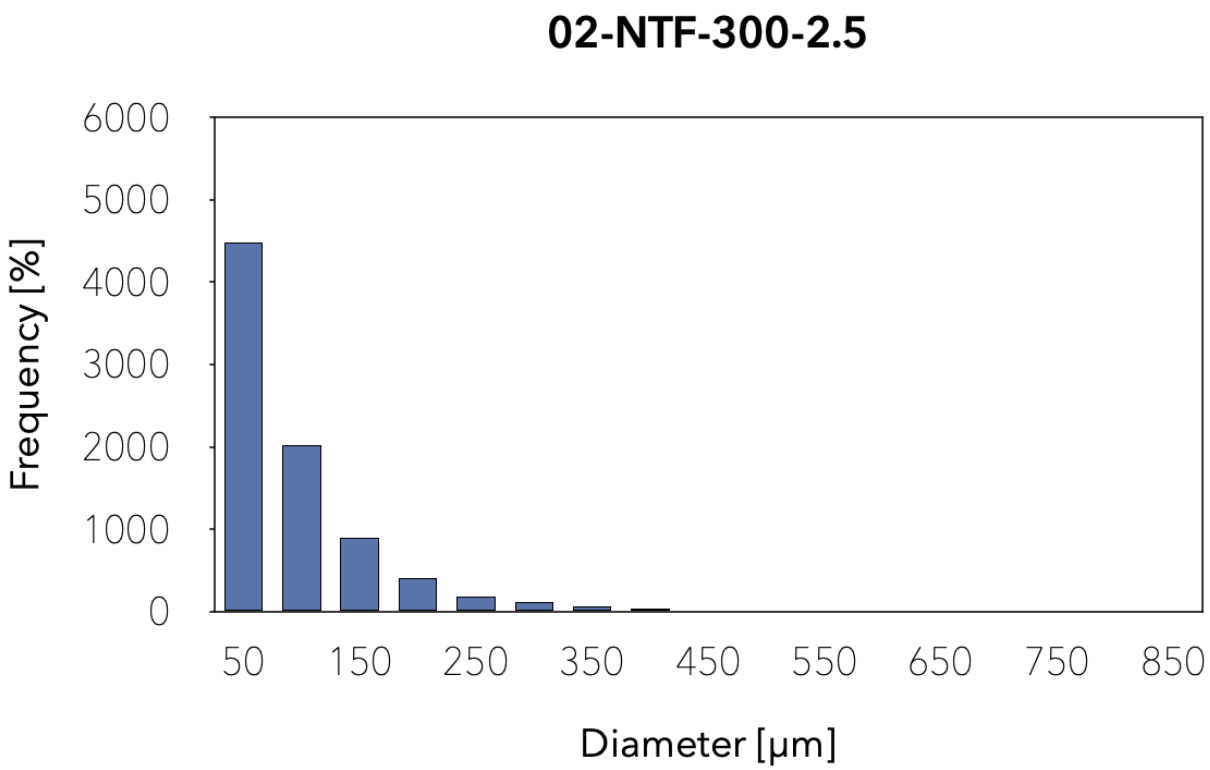

Figure 80. Graphic representation of the frequency with which the equivalent diameters of the pores are present in the samples made with admixture 02-NTF-300-2,5.

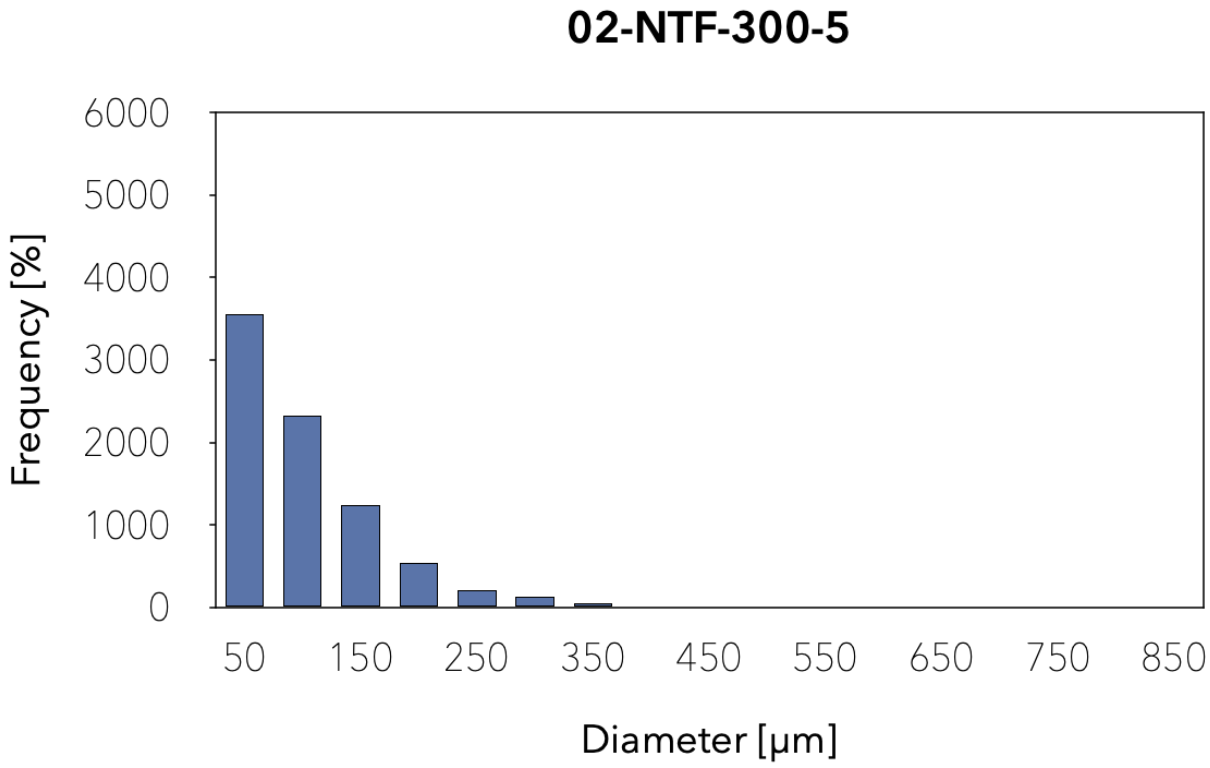

Figure 81. Graphic representation of the frequency with which the equivalent diameters of the pores are present in the samples made with admixture 02-NTF-300-5.

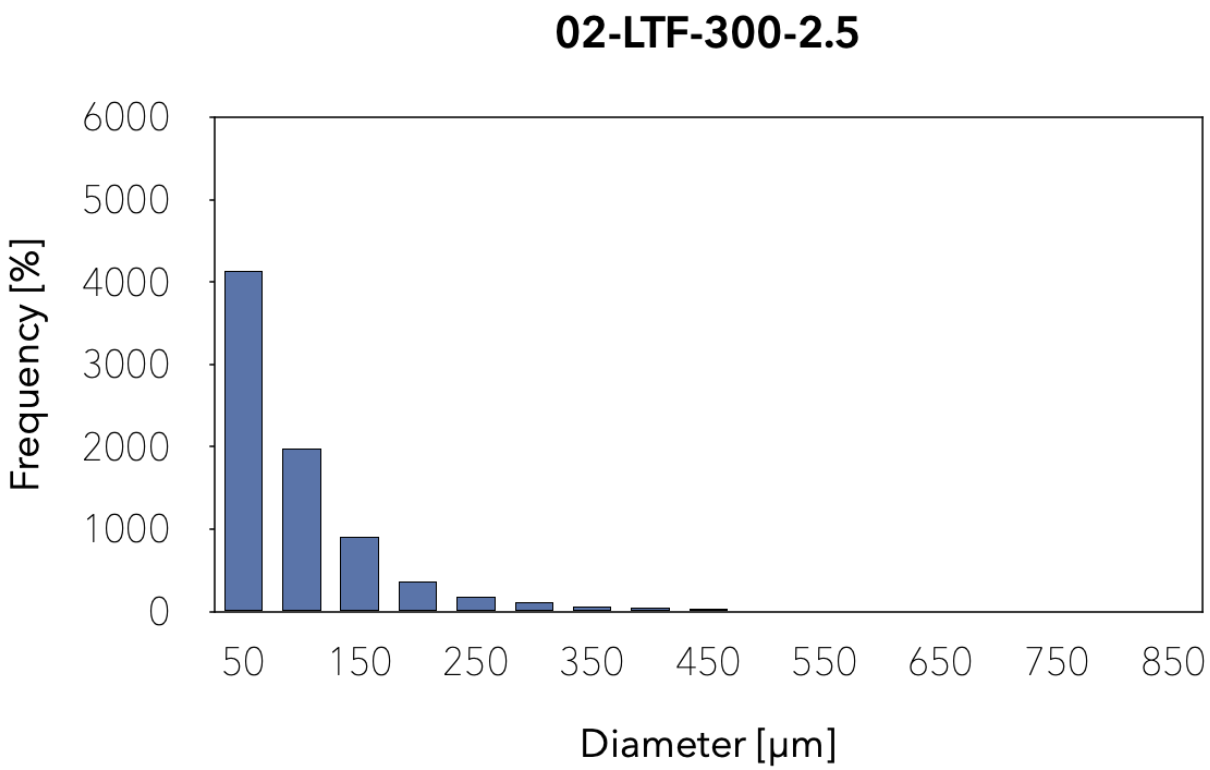

Figure 82. Graphic representation of the frequency with which the equivalent diameters of the pores are present in the samples made with admixture 02-LTF-300-2,5.

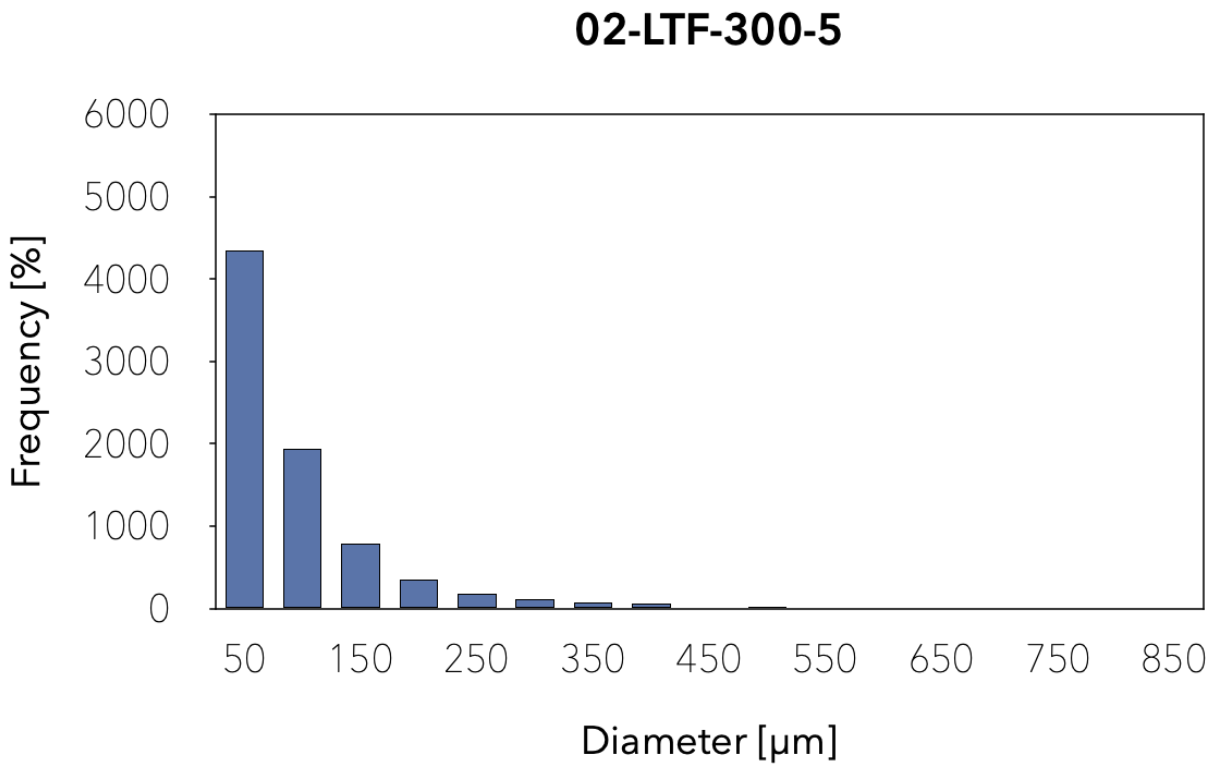

Figure 83. Graphic representation of the frequency with which the equivalent diameters of the pores are present in the samples made with admixture 02-LTF-300-5.

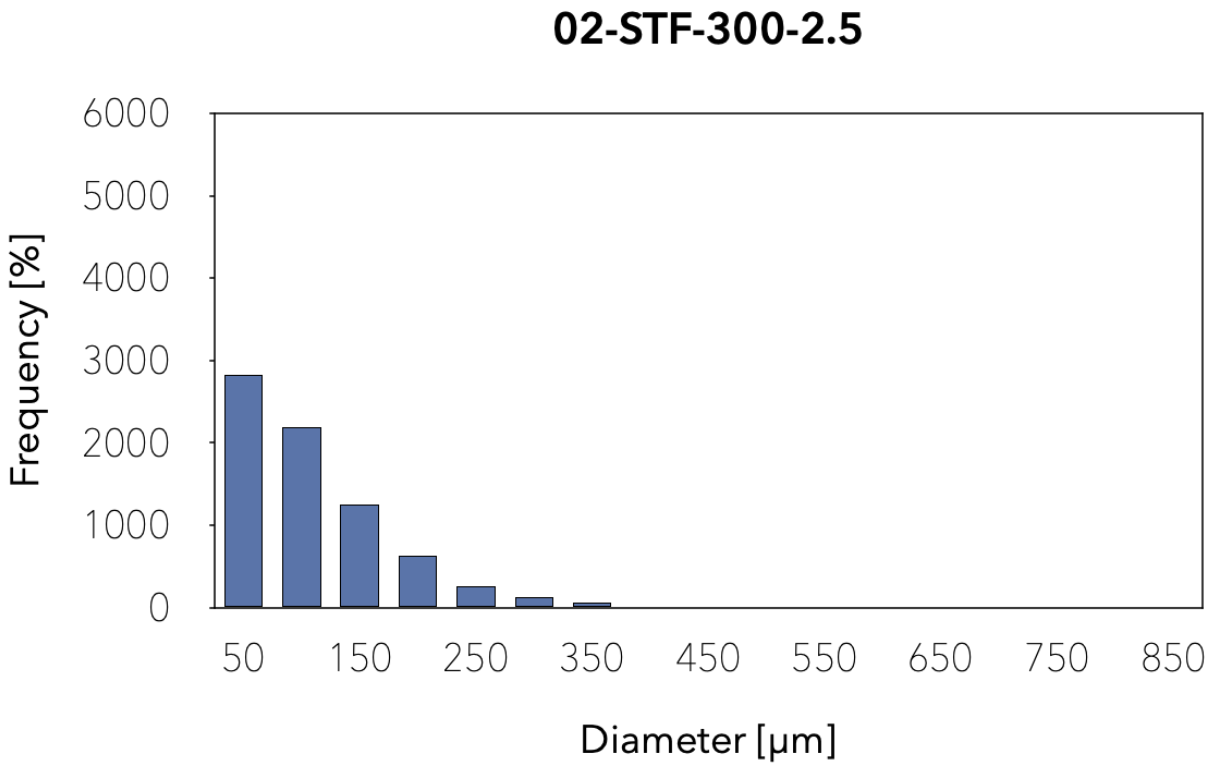

Figure 84. Graphic representation of the frequency with which the equivalent diameters of the pores are present in the samples made with admixture 02-STF-300-2,5.

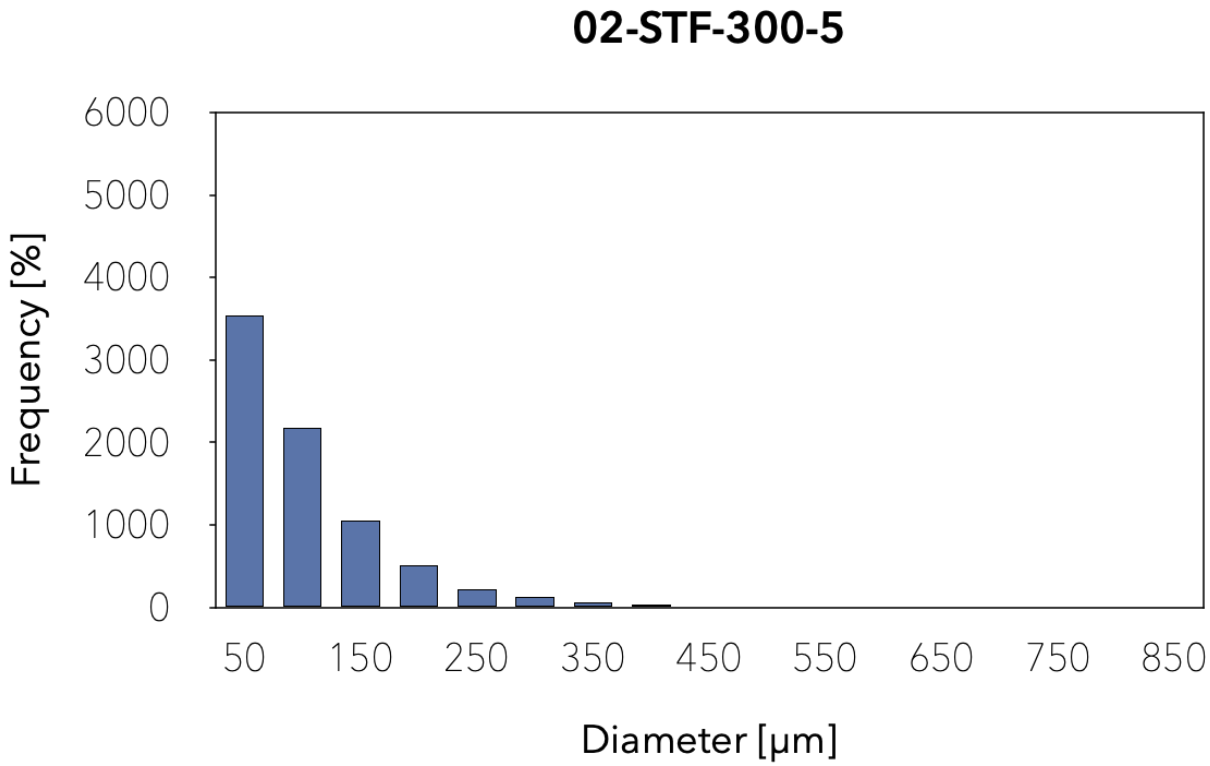

Figure 85. Graphic representation of the frequency with which the equivalent diameters of the pores are present in the samples made with admixture 02-STF-300-5.

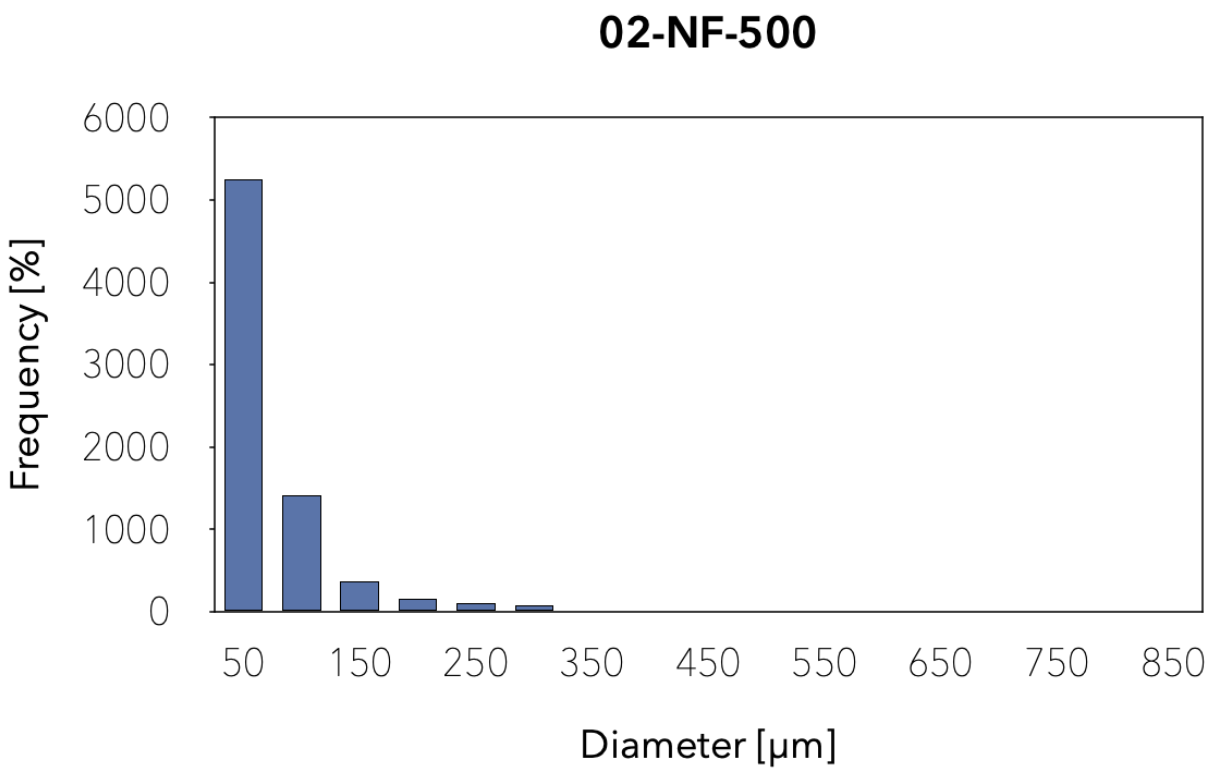

Figure 86. Graphic representation of the frequency with which the equivalent diameters of the pores are present in the samples made with admixture 02-NF-500.

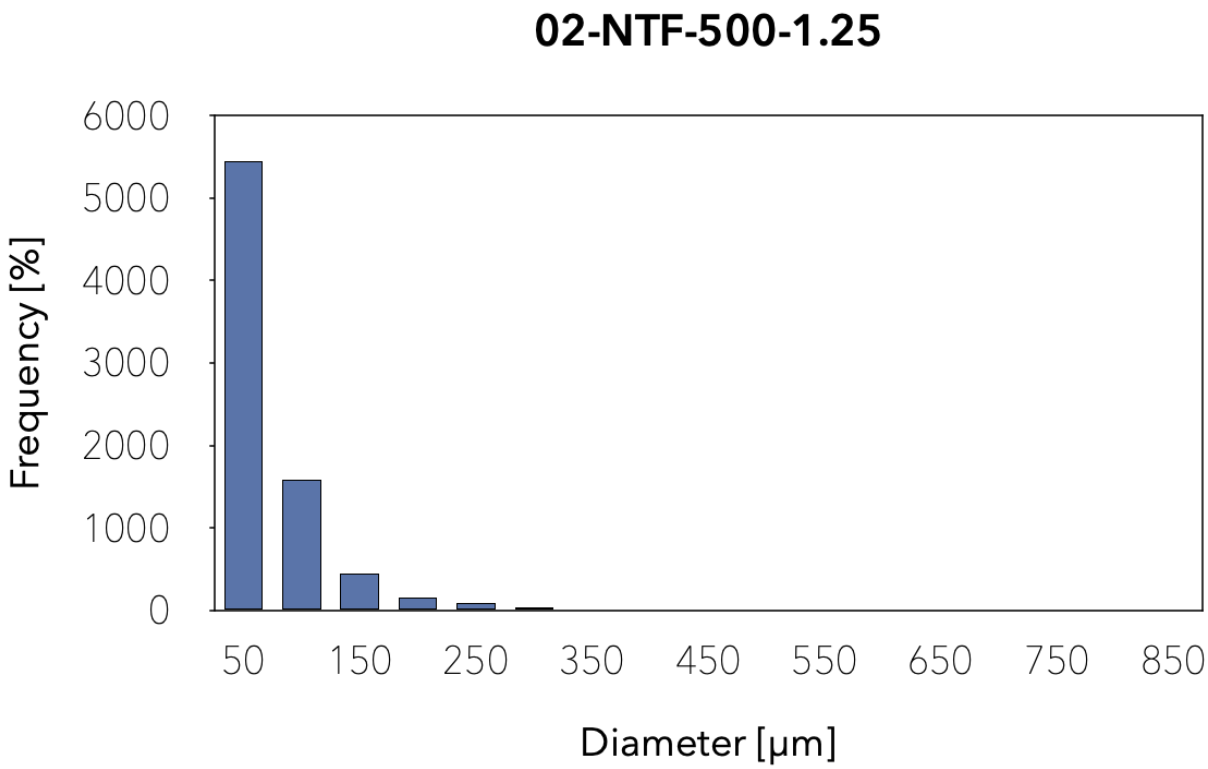

Figure 87. Graphic representation of the frequency with which the equivalent diameters of the pores are present in the samples made with admixture 02-NTF-500-1,25.

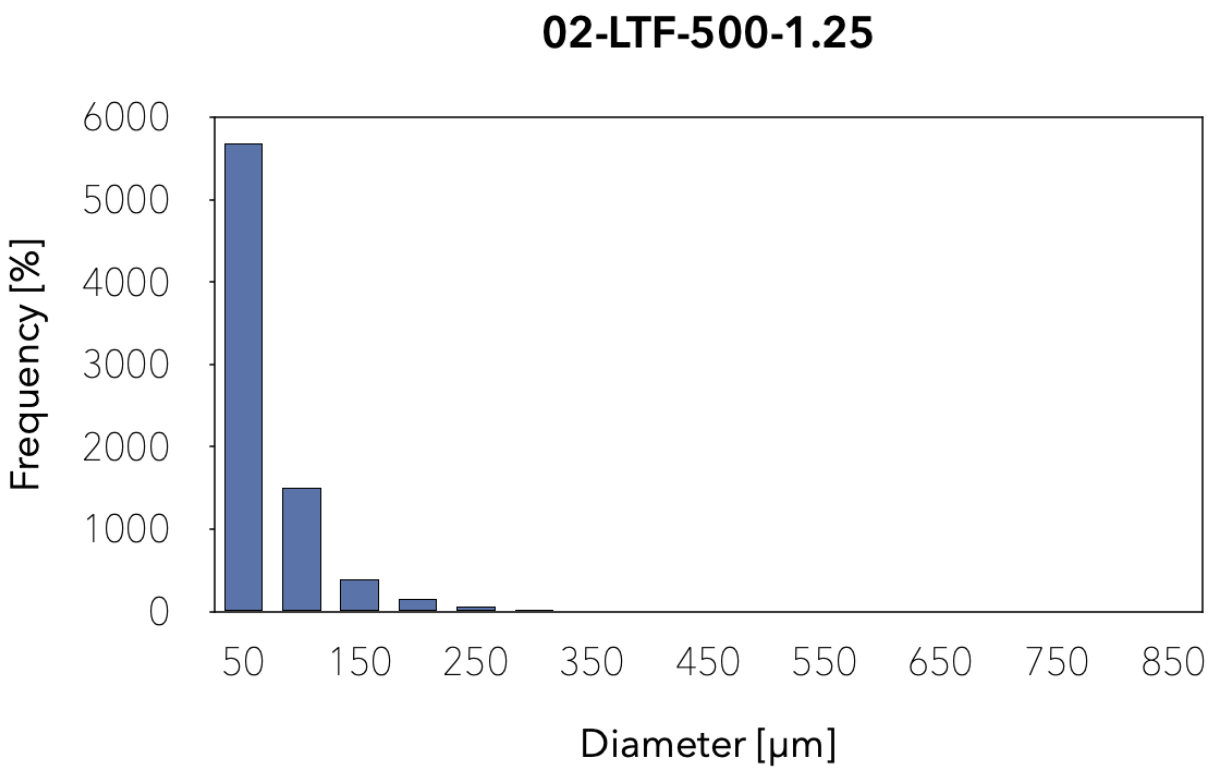

Figure 88. Graphic representation of the frequency with which the equivalent diameters of the pores are present in the samples made with admixture 02-LTF-500-1,25.

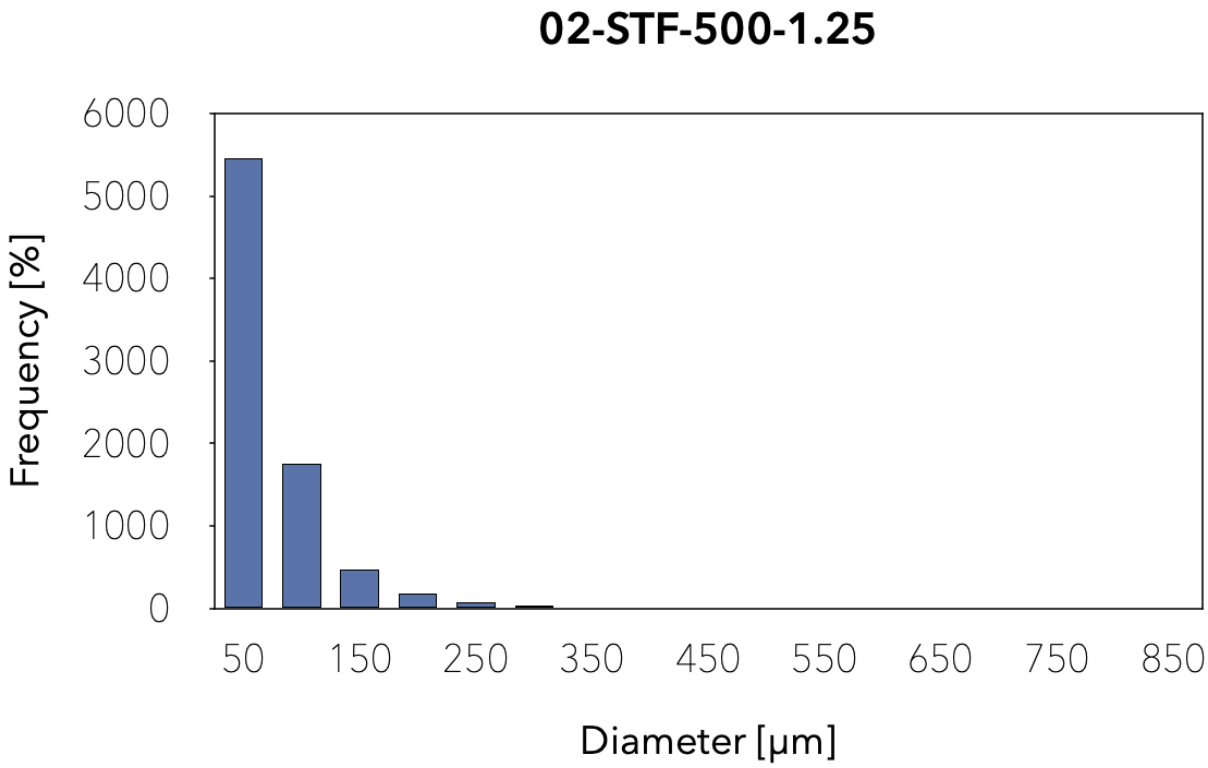

Figure 89. Graphic representation of the frequency with which the equivalent diameters of the pores are present in the samples made with admixture 02-STF-500-1,25.

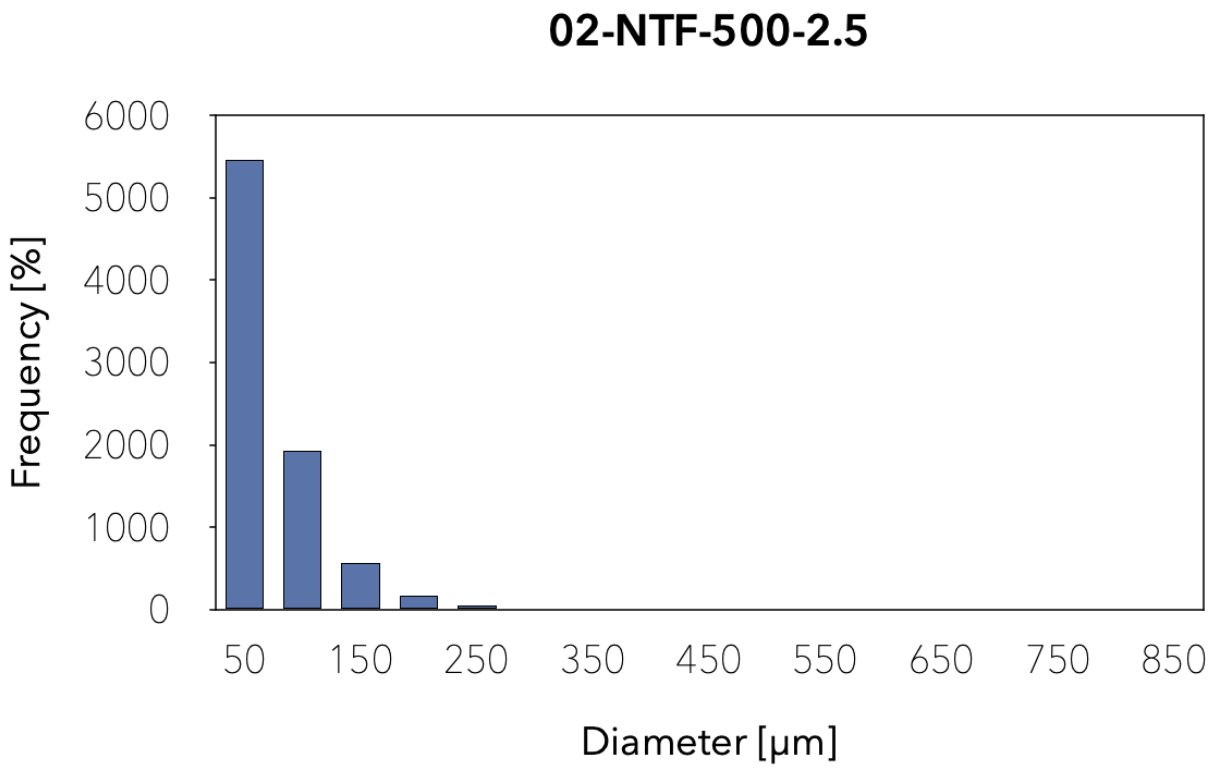

Figure 90. Graphic representation of the frequency with which the equivalent diameters of the pores are present in the samples made with admixture 02-NTF-500-2,5.

From the microstructural analysis, elevated and similar porosity values of the samples emerge, as was expected given the ultra-low density that characterizes them and is included in a very narrow range. From the observation of the images and the quantifications carried out with the ImageJ software, it is evident that every mixture characterizes by closed-cell porosity. The pores are easily distinguishable and are interconnected only in the few cases in which the phenomenon of coalescence occurs. However, some differences emerge between the various samples:

On a density of 100 kg/m^3, the admixtures 02-NTF-100-5 and 02-STF-100-2.5 characterize by smaller pores and a higher quantity of voids. As shown in Figure 59 the sample 02-STF-100-5 presents a fiber agglomeration.

On a density of 300 kg/m^3, the admixture 02-STF-300-2.5 characterizes a lower quantity of voids.

On a density of 500 kg/m^3, every admixture presents more or less the same amount and size of pores.

5.2.4. Mechanical properties after 28 days of maturation

The mechanical properties tests took place for every sample analyzed with the three prismatic samples of 4x4x16 cm. The compressive and flexural strength tests were developed in two different stages for the first and second parts of the experimental campaign.

5.2.4.1. Flexural strength

The flexural strength tests were carried out with the three-point bending method with a 10cm span and force control of 10 N/s for samples with a target density of 100kg/m^3 and 50N/s for 300 and 500kg/m^3.

For each admixture, three samples made in metal formwork with a prismatic shape of 4x4x16 cm, matured for 28 days, were tested. The analysis of three samples per admixture allowed the identification of a realistic behavior related to the tensile strength by carrying out three tests per sample.

Each specimen got tested by being positioned so that the surface exposed to the air during curing was in a frontal position so as not to be directly subjected to the pressure exerted by the machine through the three contact points, following the regulations.

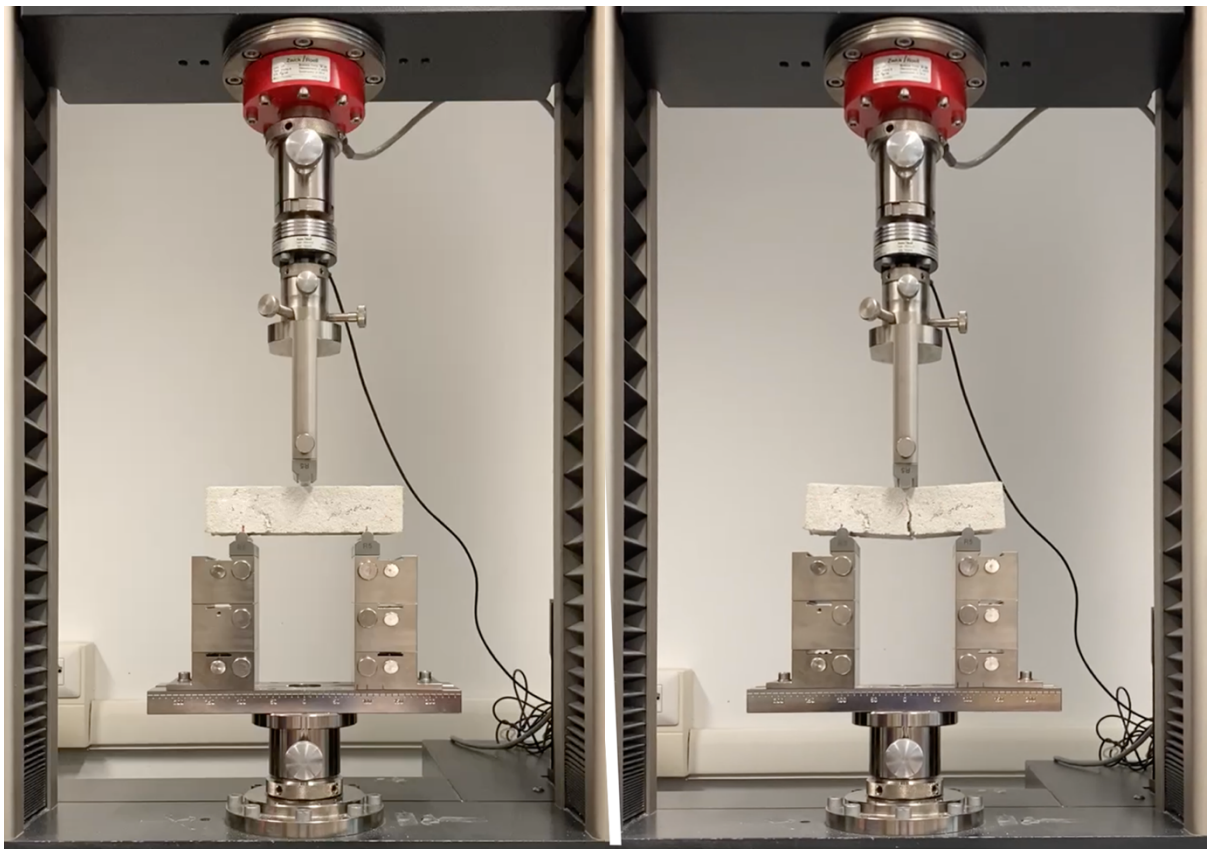

Figure 91. Image showing the sample positioning on the machine for the flexural strength tests.

- First part of the experimental campaign:

The first part of the experimental campaign consisted of finding the most efficient fiber treatment, length, and content. Bellow, the flexural strength test results for finding the fiber treatment are displayed graphically.

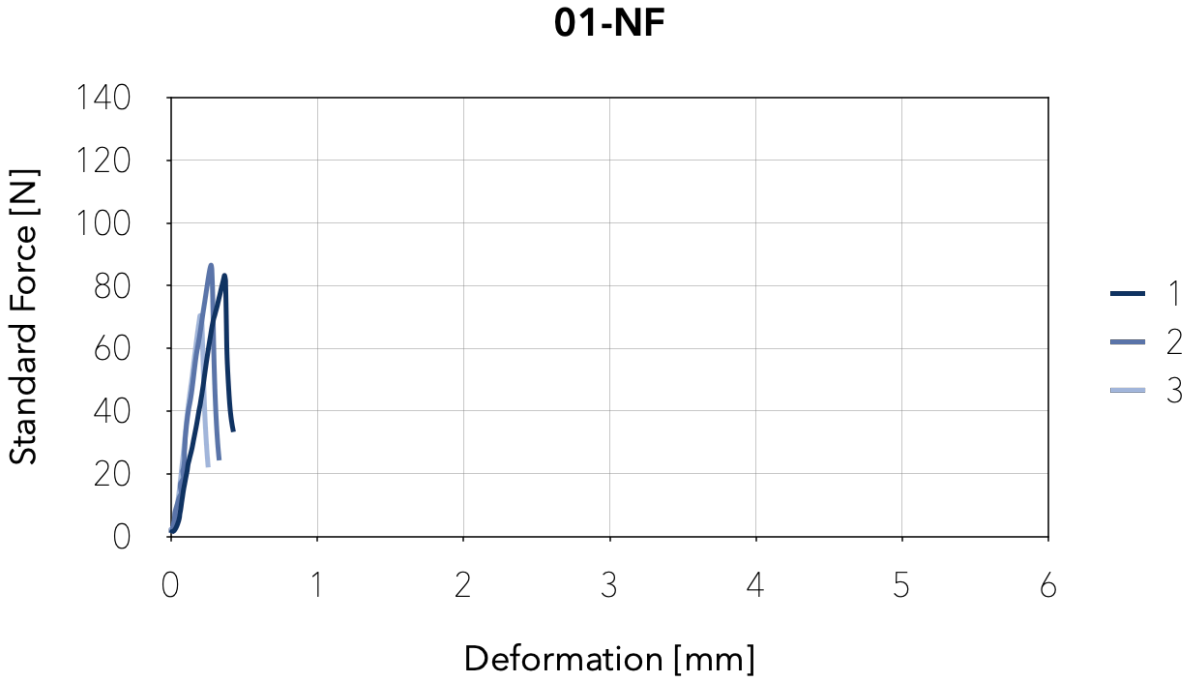

Figure 92. Image showing the flexural strength results of the three samples evaluated for the admixture without fibers (01-NF).

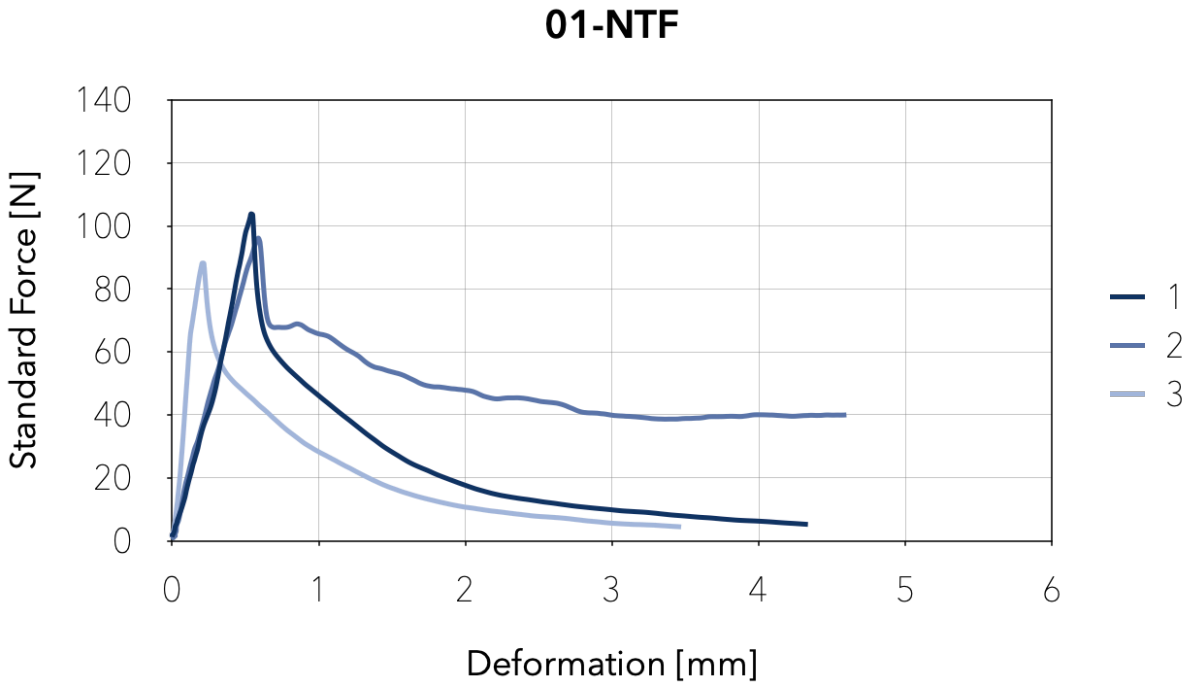

Figure 93. Image showing the flexural strength results of the three samples evaluated for the admixture with non-treated fibers (01-NTF).

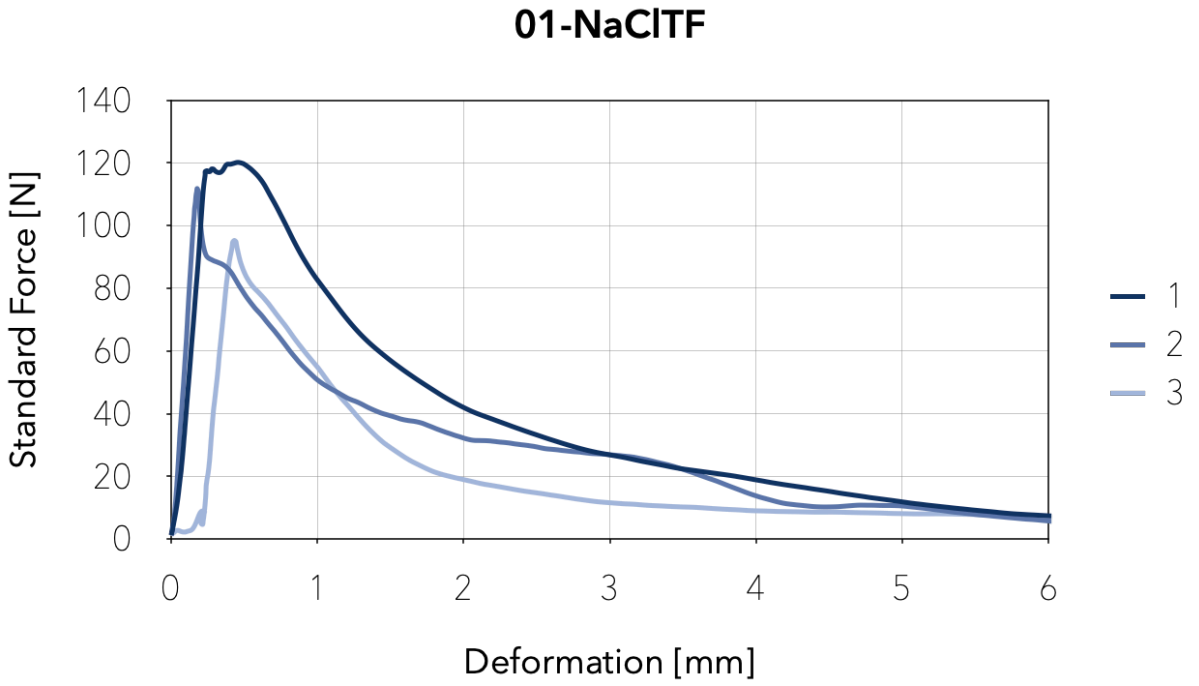

Figure 94. Image showing the flexural strength results of the three samples evaluated for the admixture with salt-treated fibers (01-NaClTF).

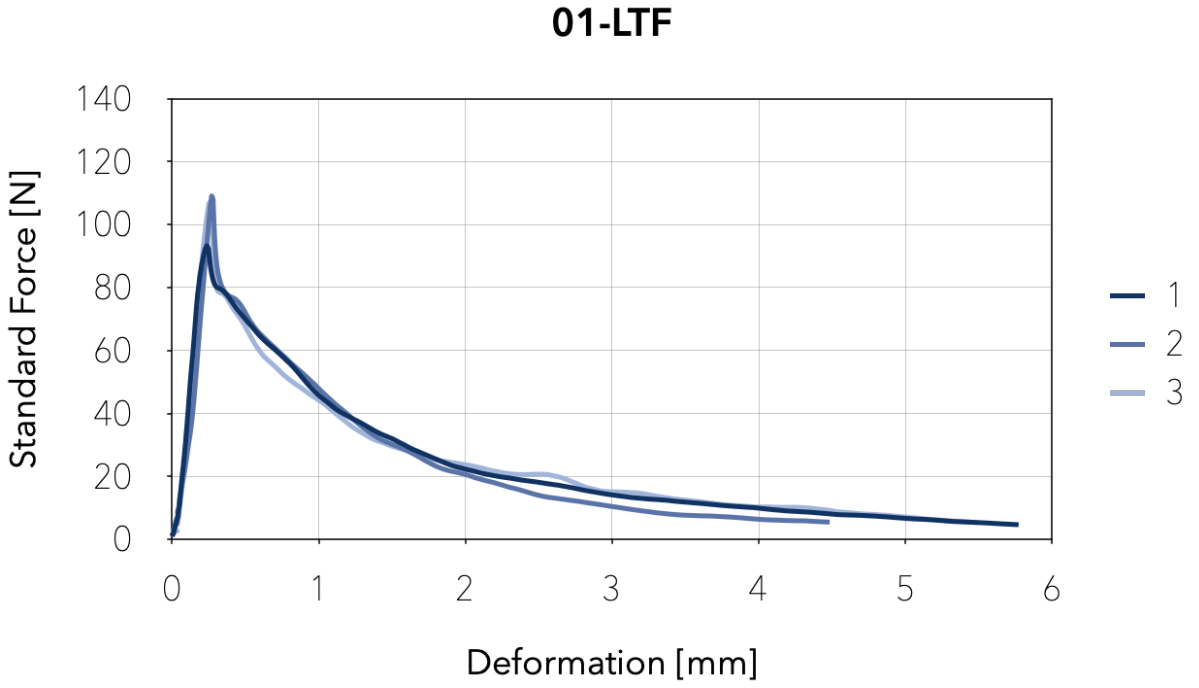

Figure 95. Image showing the flexural strength results of the three samples evaluated for the admixture with lime-treated fibers (01-LTF).

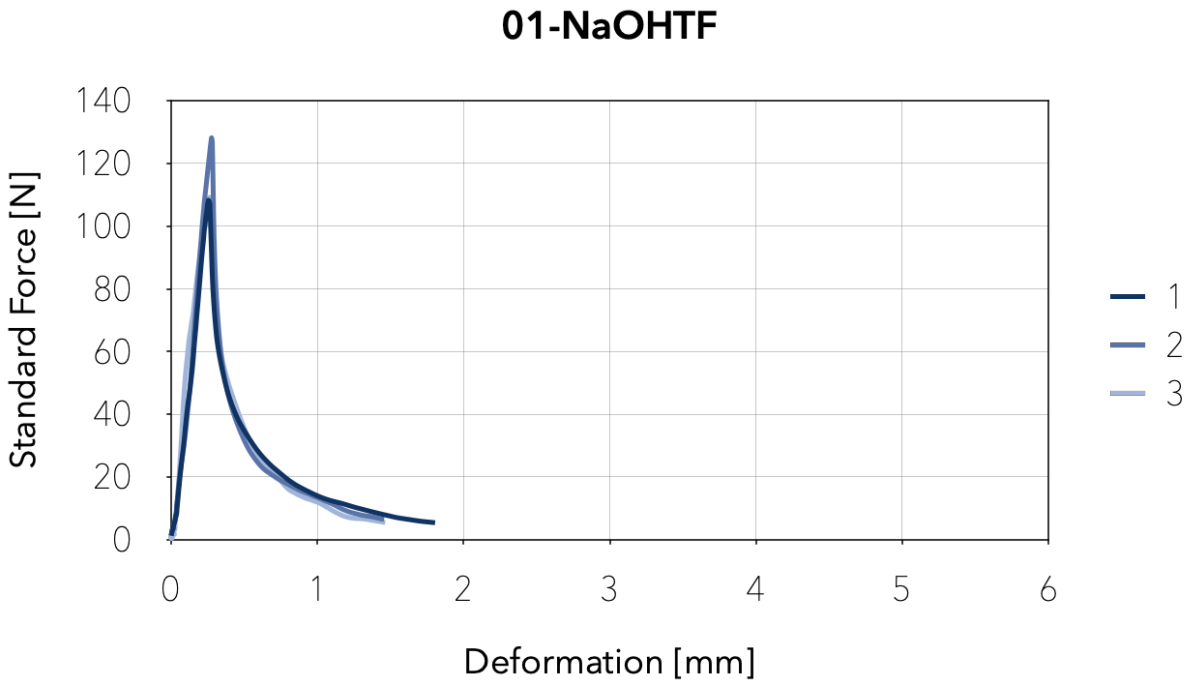

Figure 96. Image showing the flexural strength results of the three samples evaluated for the admixture with sodium hydroxide-treated fibers (01-NaOHTF).

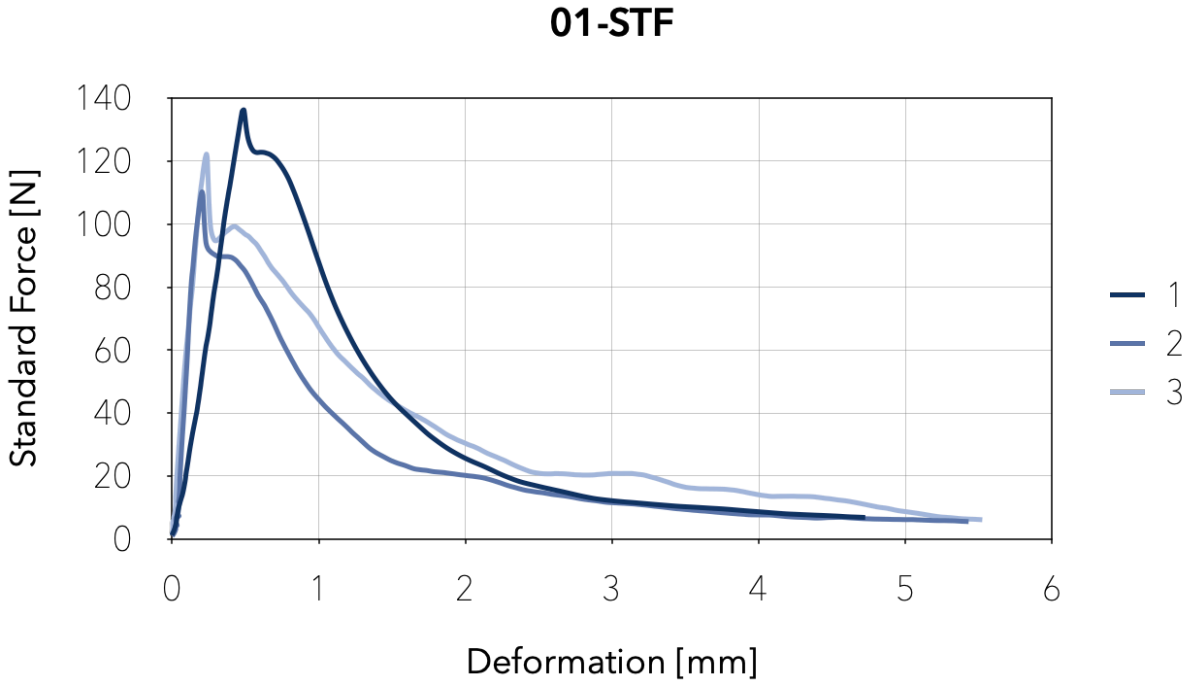

Figure 97. Image showing the flexural strength results of the three samples evaluated for the admixture with surfactant-treated fibers (01-STF).

In the previous images, it is observable that the flexural behavior of the samples with SWF reinforcement resulted in a more elastic deformation when compared to the samples without fibers. The NaOHTF samples presented a lower benefit in terms of brittleness reduction in comparison to the admixtures with other fiber treatments,

probably because of the damage caused to the fibers by the treatment; as observed in Figure 42, the fibers with this treatment lost elasticity.

Furthermore, a comparison between the average flexural strength is represented in the following graph.

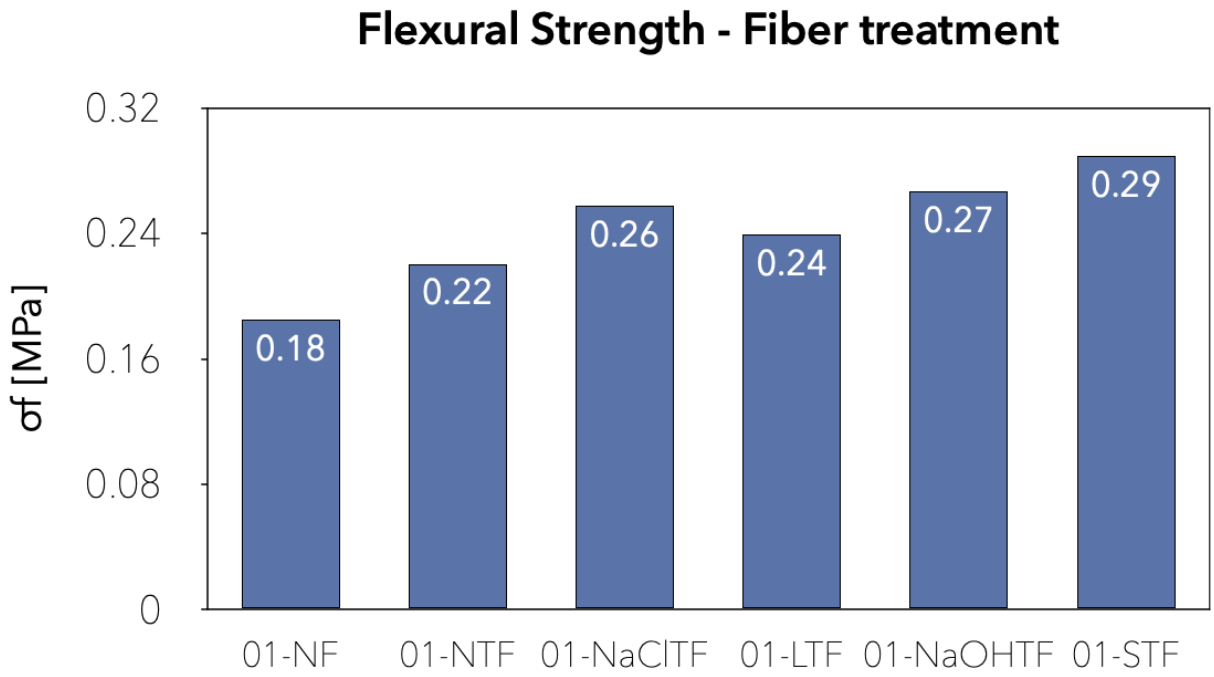

Figure 98. Graph with the average maximum flexural strength of the admixtures analyzed for fiber selection.

From Figure 98, it can be observed that the fibers treated with the foaming surfactant presented the highest average result in flexural strength, presenting an improvement of 61% concerning the samples without fibers. They were followed by the admixtures treated with salt and sodium hydroxide; the former presents a rise of 50% and the latter of 45%. Despite the lack of elasticity, the NaOHTF accomplished the second-highest flexural strength average. LTF follows with a 33% improvement from the original non-fiber composites. In addition, NTF admixtures were the ones that presented the lowest increment with a rate of 22%.

Considering the previous information, it is possible to determine that the addition of SWF significantly improves the flexural strength of foamed concrete. Furthermore, the evaluation of these results suggests an improvement in the flexural performance when the fibers are treated prior to their incorporation into the mix.

The following dispersion graph shows the average flexural strength of the samples on the Y-axis and the average density after 28 days of maturation on the X-axis.

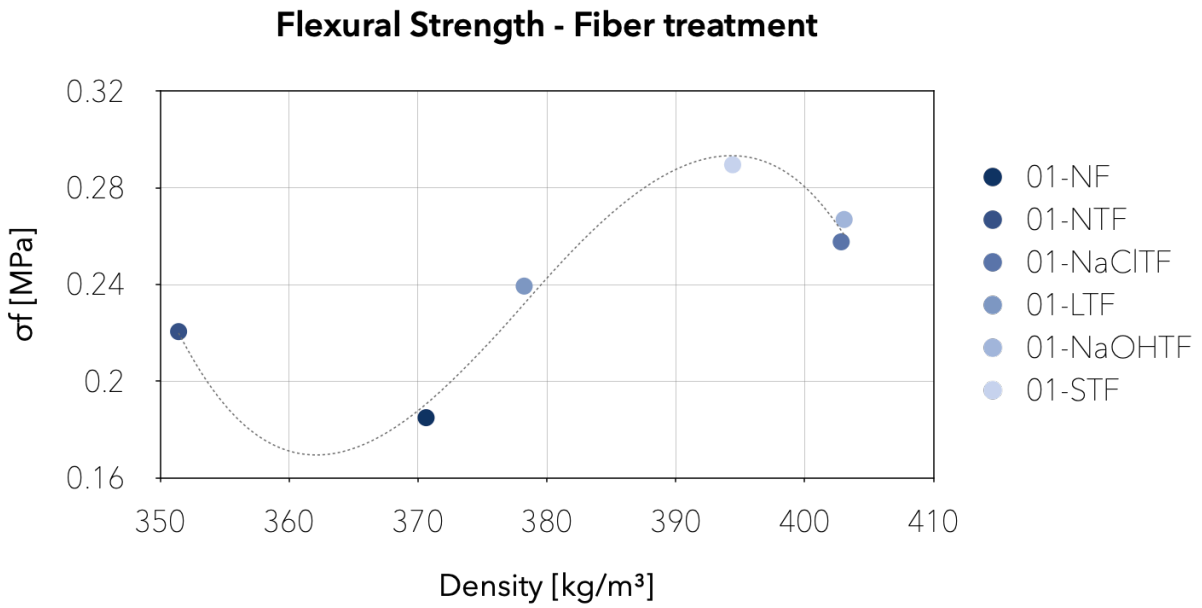

Figure 99. Dispersion graph of the average flexural strength of the admixtures analyzed for fiber treatment selection compared to the average density measured after 28 days of maturation.

Generally, a concrete admixture with a higher density also has a better mechanical performance. Therefore, an analysis considering both parameters is key to understanding the fundamental factors of the variation of the mechanical properties of each set of samples. For example, Figure 99 shows that as the density increases, the flexural strength increases as well, except for the samples from the admixtures 01-NaOHTH and 01-NaClTF, which, although having a higher density than 01-STF, have a lower flexural performance.

The following analysis focused on the fiber length. The experimentation focused on individuating the most performant length between 6, 12, and 20 mm. This analysis considered a density of 300kg/m^3 and the inclusion of NTF at a 2,5% F/C ratio. The following images display the results of the flexural strength measurements developed on the samples after 28 days of maturation.

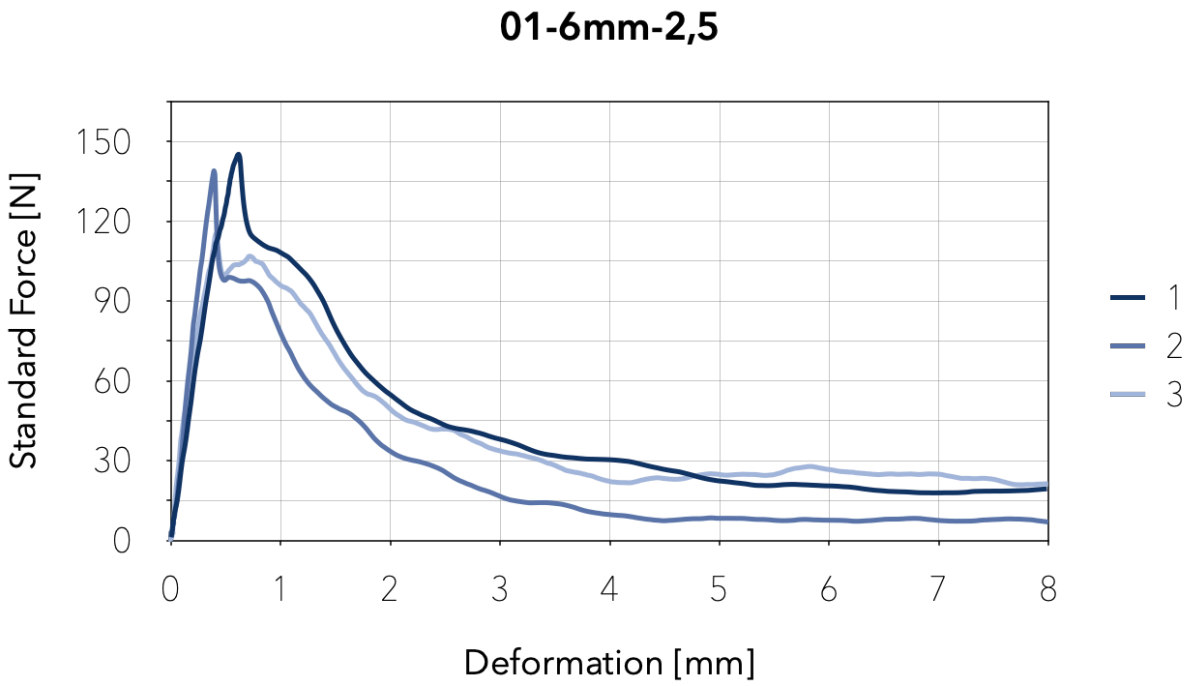

Figure 100. Image showing the flexural strength results of the three samples evaluated for the admixture with 6mm fibers and 2,5% F/C ratio (01-6mm-2,5).

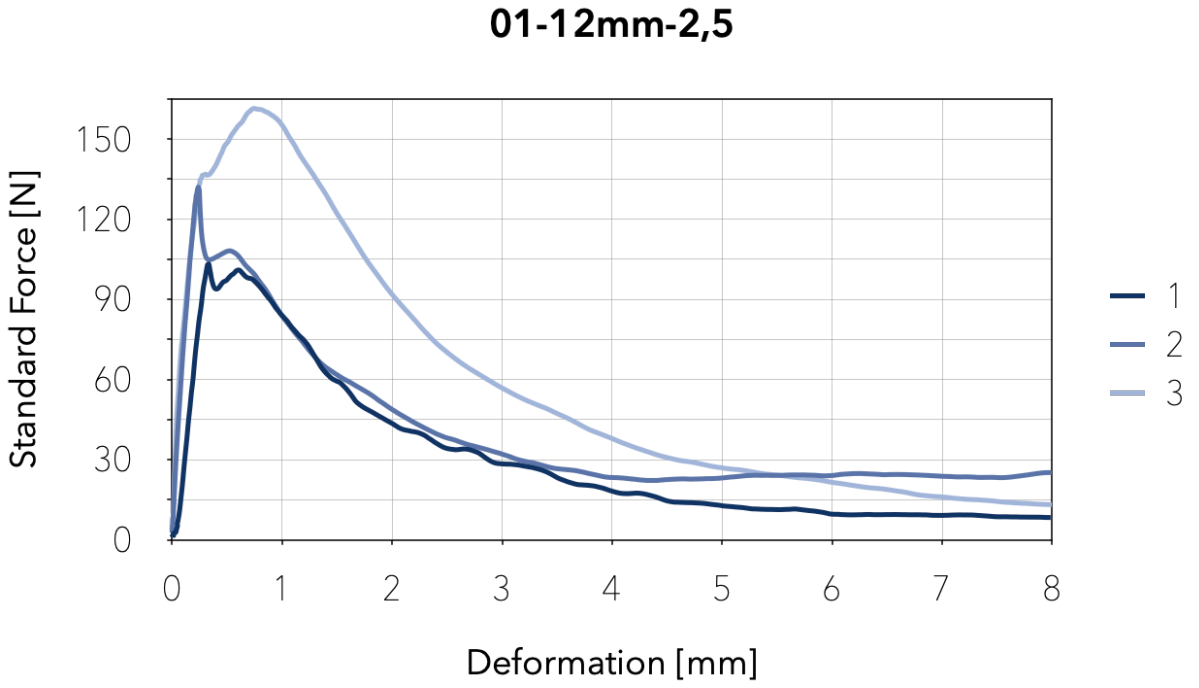

Figure 101. Image showing the flexural strength results of the three samples evaluated for the admixture with 12mm fibers and 2,5% F/C ratio (01-12mm-2,5).

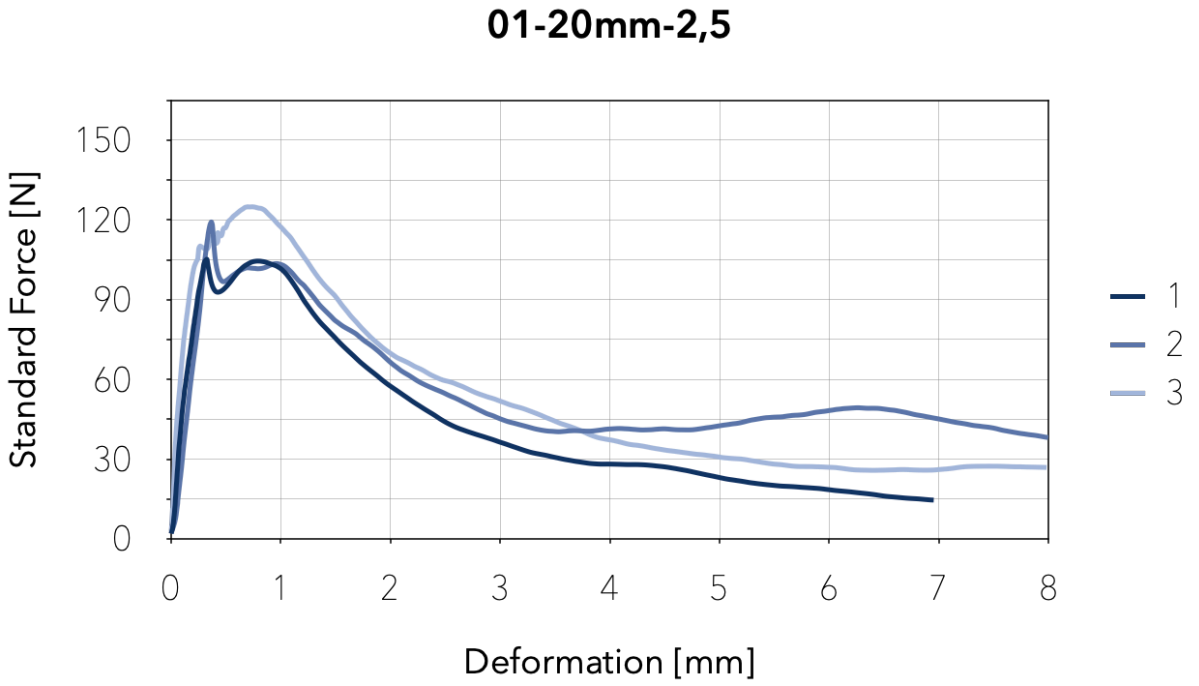

Figure 102. Image showing the flexural strength results of the three samples evaluated for the admixture with 20mm fibers and 2,5% F/C ratio (01-20mm-2,5).

The previous images show a similar behavior between the admixtures with 12 and 20mm fibers in terms of brittleness. In comparison, the samples with 6mm fibers have a more brittle behavior.

Furthermore, a comparison between the average flexural strength is represented in the following graph.

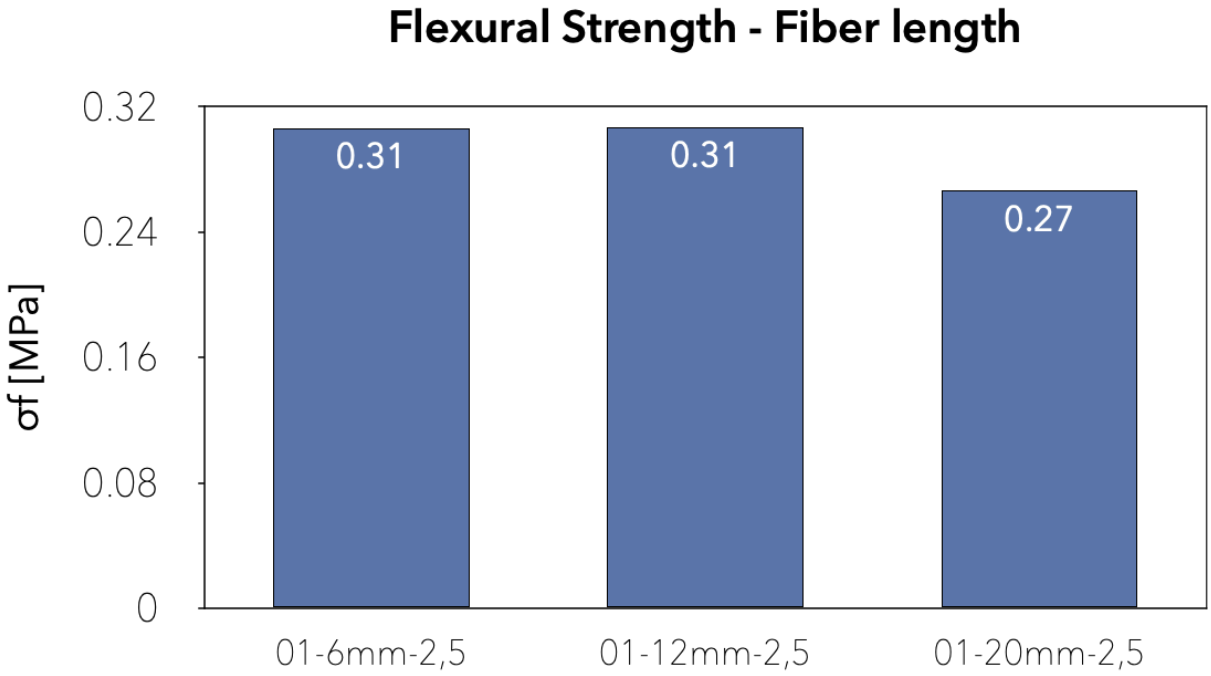

Figure 103. Graph with the average maximum flexural strength of the admixtures analyzed for fiber length selection.

Figure 103 shows that the flexural strength is a 13% higher in the admixtures with 6 and 12 mm than that of 20mm. In addition, the following dispersion graph shows the average flexural strength of the samples on the Y-axis and the average density after 28 days of maturation on the X-axis.

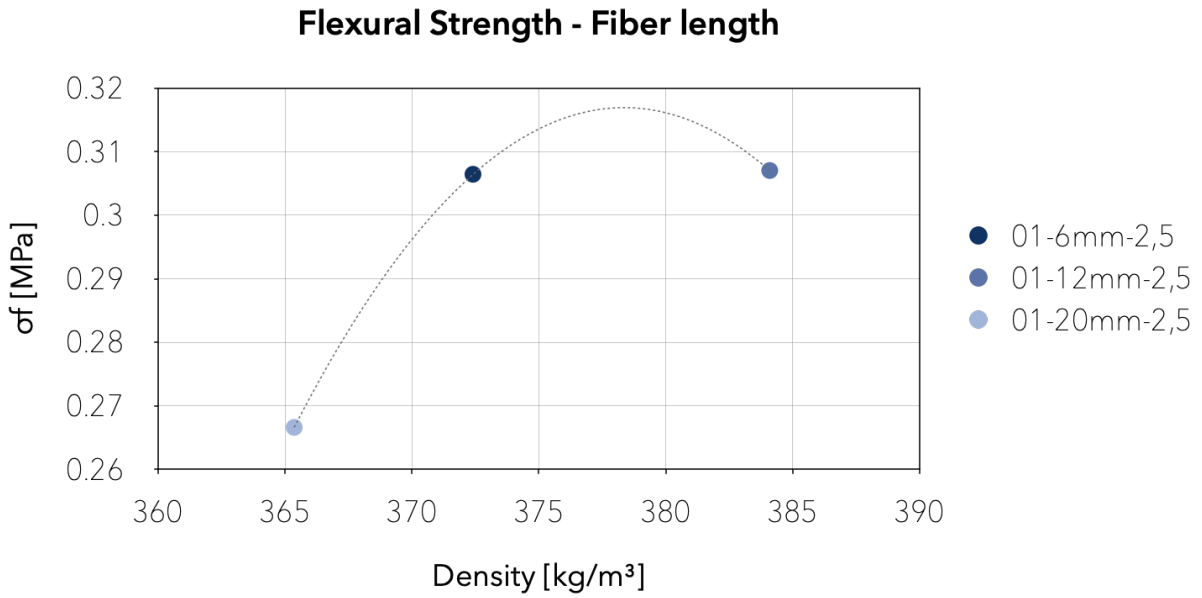

Figure 104. Dispersion graph of the average flexural strength of the admixtures analyzed for fiber length selection compared to the average density measured after 28 days of maturation.

The dispersion graph above shows that even though the admixtures 01-6mm-2,5 and 01-12mm-2,5 have a similar flexural strength, their density differs, which means that on similar densities, the 6mm admixture is expected to have a higher resistance.

Additionally, the experimentation focused on individuating the most performant F/C ratio between 2,5, 5, and 10%. This analysis considered a density of 300kg/m^3 and the inclusion of 12mm NTF. The following images display the results of the flexural strength measurements developed on the samples after 28 days of maturation. The admixture 01-12mm-2,5 used on the fiber length analysis also contributes to finding the F/C ratio.

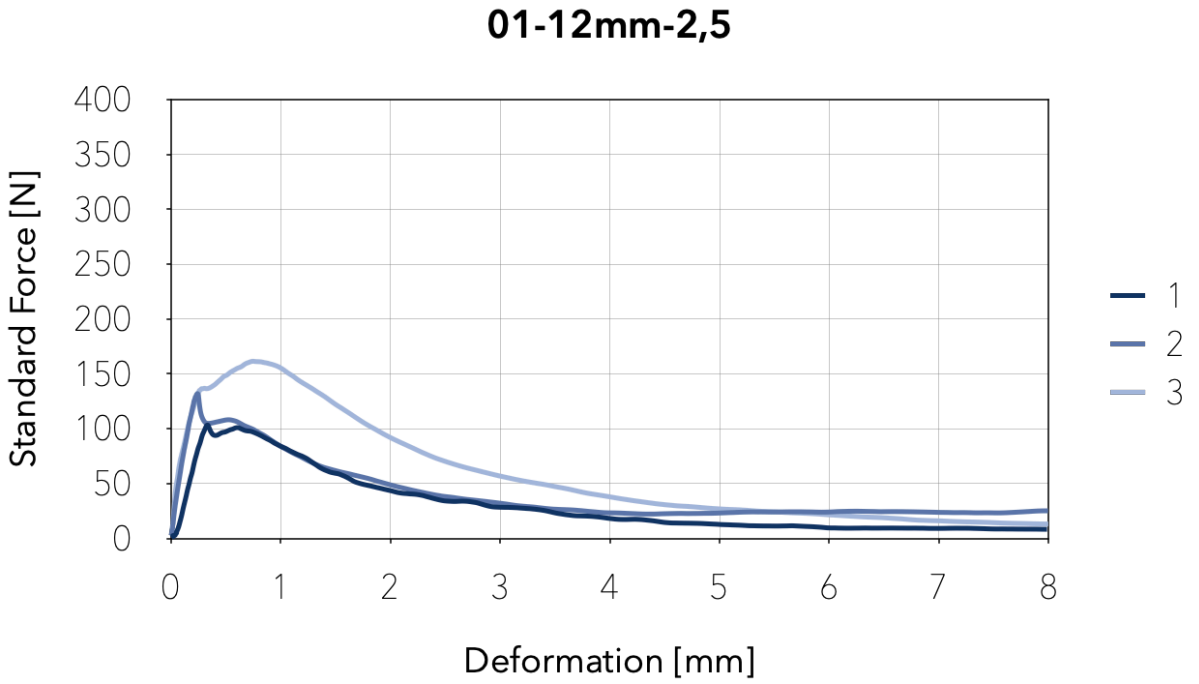

Figure 105. Image showing the flexural strength results of the three samples evaluated for the admixture with 12mm fibers and 2,5% F/C ratio (01-12mm-2,5).

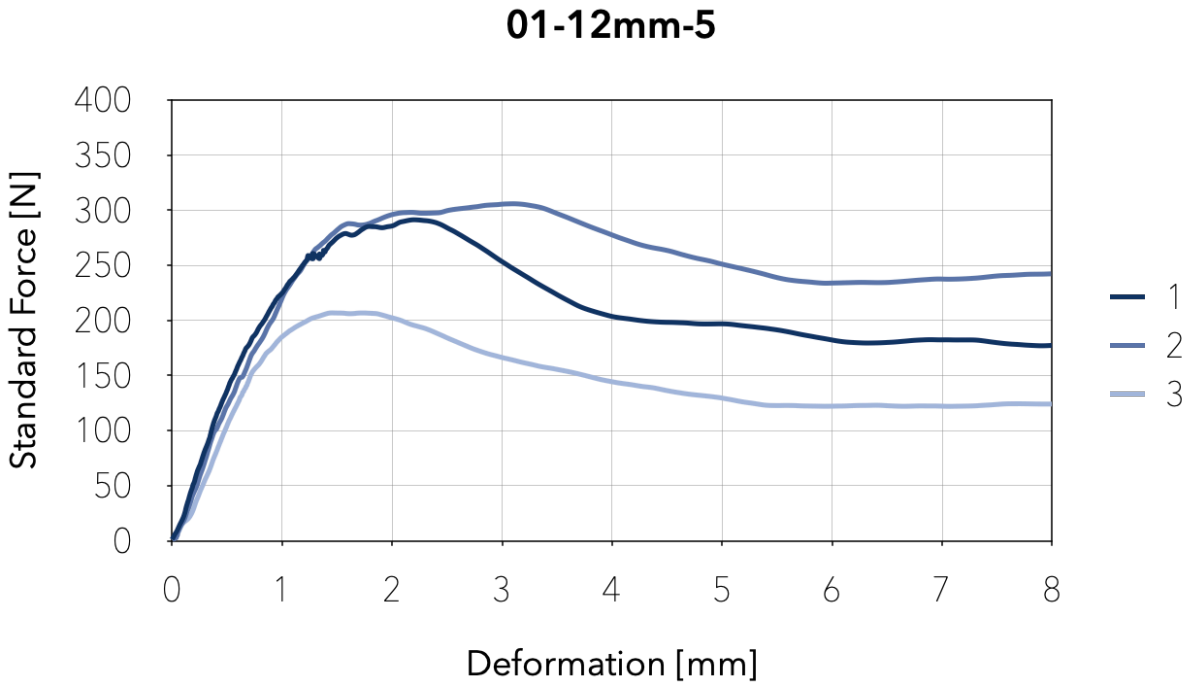

Figure 106. Image showing the flexural strength results of the three samples evaluated for the admixture with 12mm fibers and 2,5% F/C ratio (01-12mm-5).

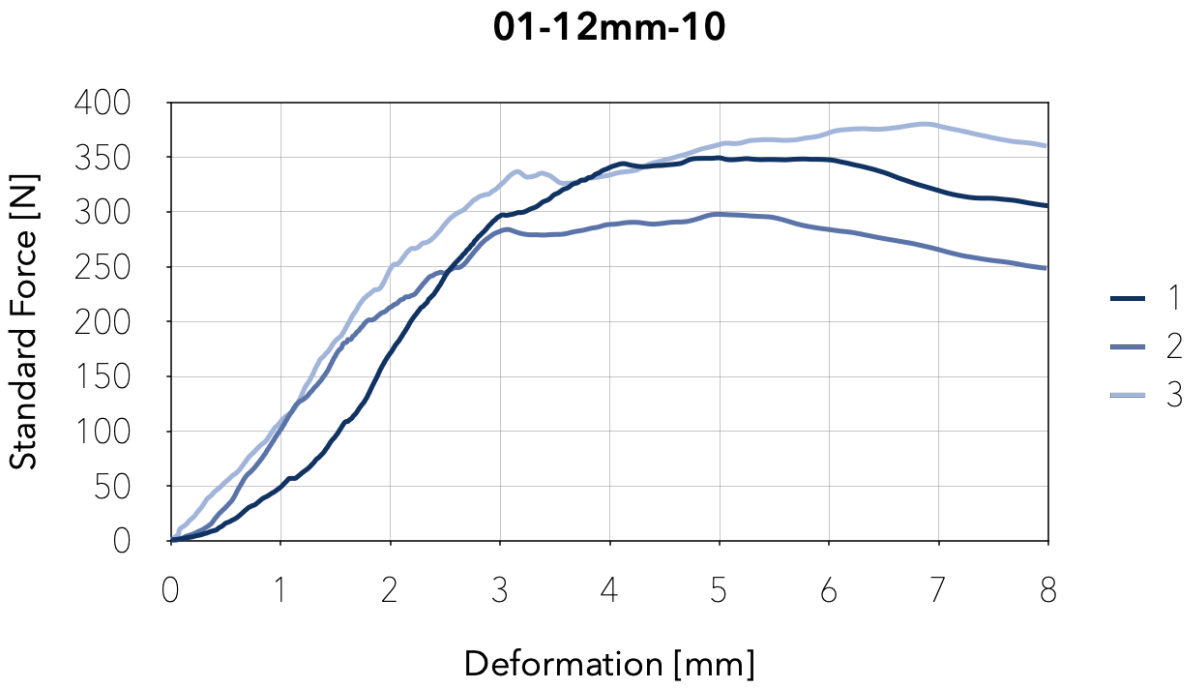

Figure 107. Image showing the flexural strength results of the three samples evaluated for the admixture with 12mm fibers and 2,5% F/C ratio (01-12mm-10).

The preceding images show that when the amount of fibers increases, so does the samples' elasticity and flexural strength. The admixture 01-12mm-2,5 presents the most brittle behavior; Figure 105 shows how the samples reach the maximum flexural strength during the first 0,5mm of deformation. On the other hand, 01-12mm-5 admixtures reach the maximum flexural strength at around 2mm of deformation while 01-12mm-10 do so around 5-7mm. After reaching the maximum flexural strength, the samples with a 2,5% F/C ratio lose the flexural strength up to almost zero during the first 8mm of deformation. The samples with 5% fiber content present a slight reduction, and the ones with 10% fiber content tend to maintain the flexural strength reached.

Furthermore, a comparison between the average flexural strength is represented in the following graph, showing that the flexural strength increases when the F/C ratio is higher.

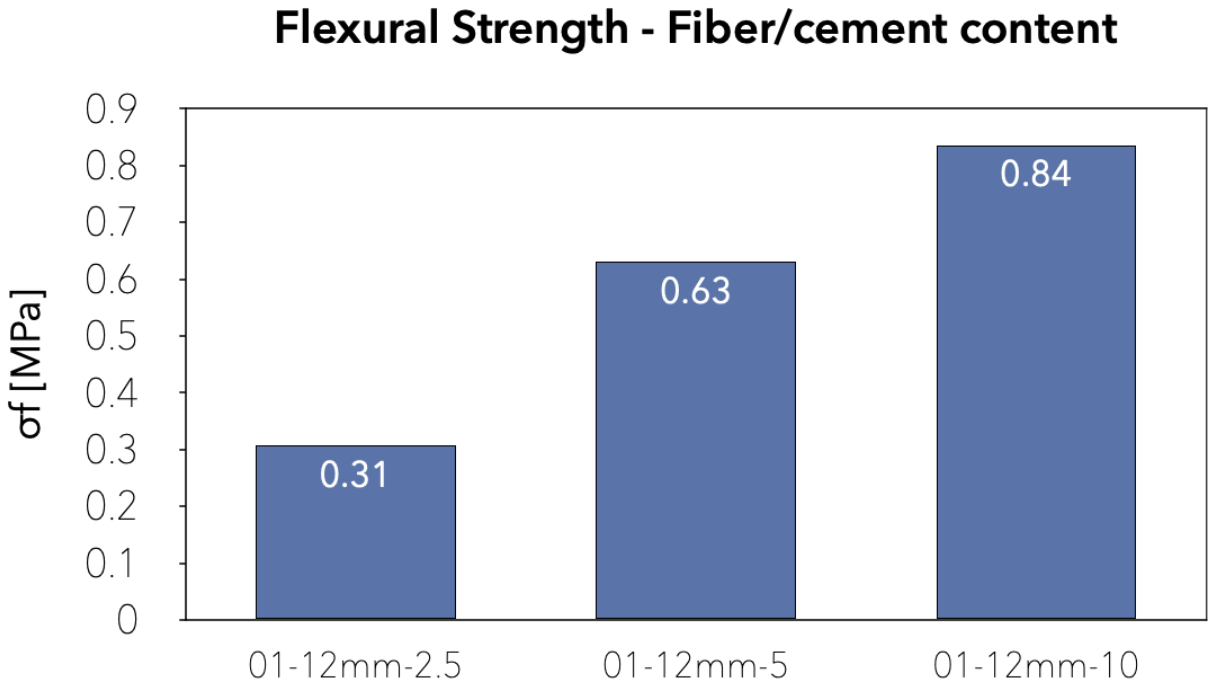

Figure 108. Graph with the average maximum flexural strength of the admixtures analyzed for fiber content selection.

The following dispersion graph shows the average flexural strength of the samples on the Y-axis and the average density after 28 days of maturation on the X-axis. The 01-12mm-2,5 resistance is 50% higher than the 01-12mm-5; therefore, doubling the fibers doubled the resistance when the F/C content changed from 2,5 to 5%. However, when it increased from 5 to 10%, the benefit reduced to 33%.

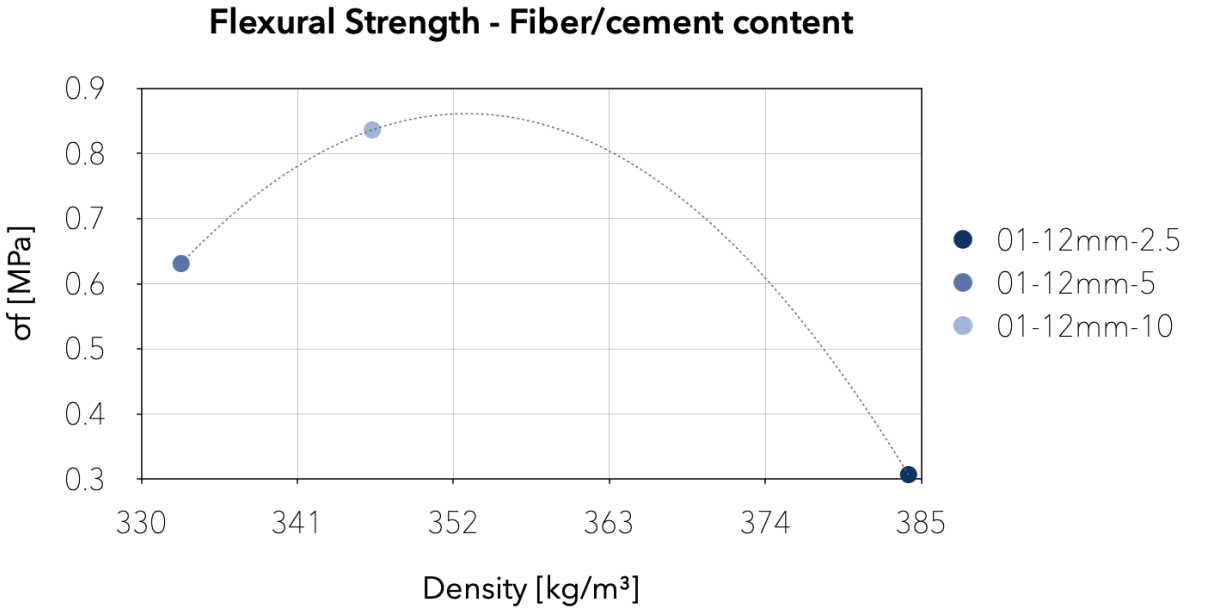

Figure 109. Dispersion graph of the average flexural strength of the admixtures analyzed for fiber content selection compared to the average density measured after 28 days of maturation.

- Second part of the experimental campaign:

The second part of this research consisted of applying the chosen fiber properties to admixtures with different target densities (100, 300, and 500kg/m^3). Bellow, the flexural strength test results for a 100kg/m^3 target density are displayed graphically.

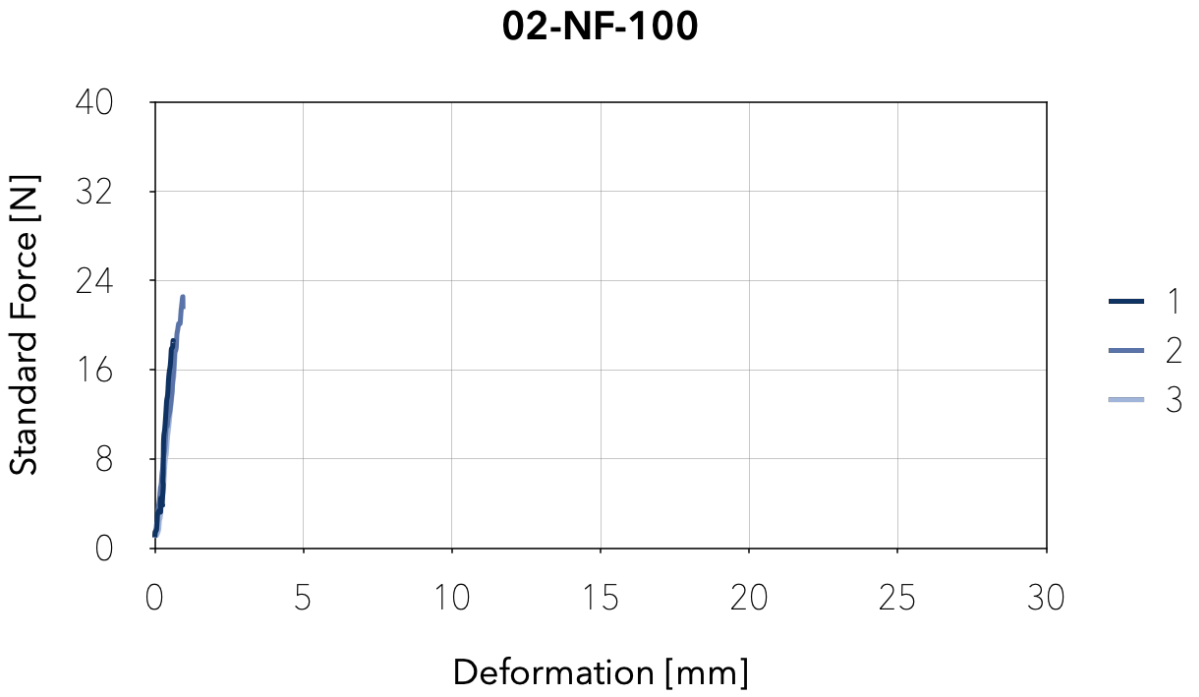

Figure 110. Image showing the flexural strength results of the three samples evaluated for the admixture 02-NF-100.

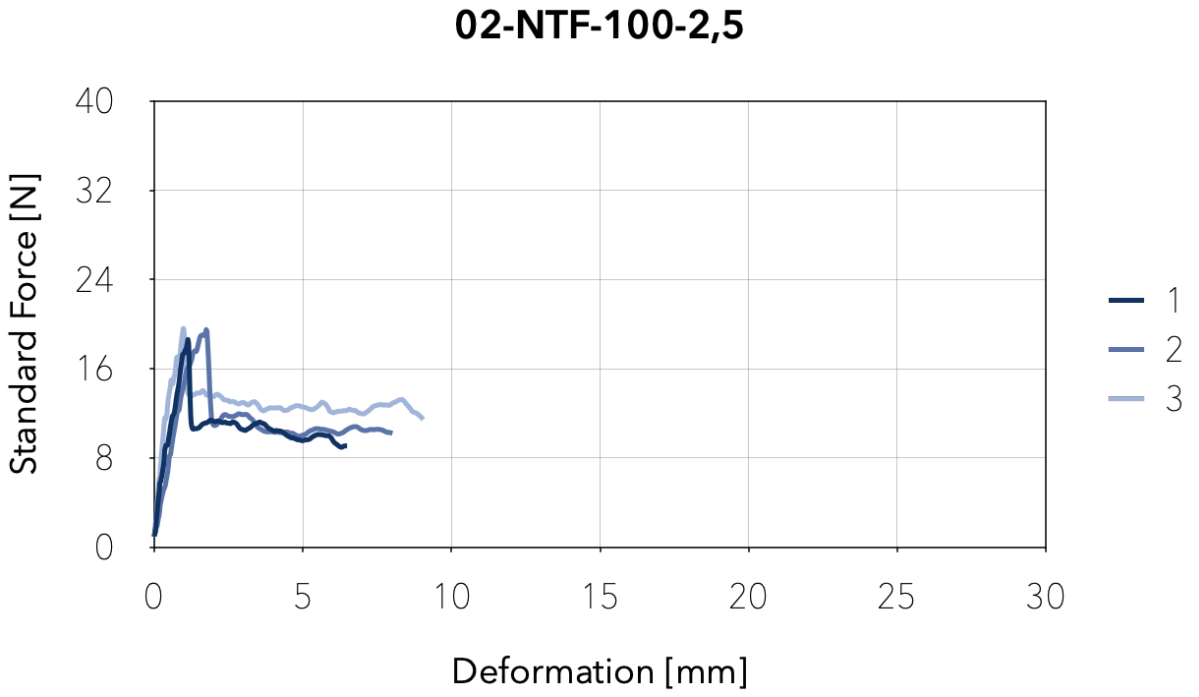

Figure 111. Image showing the flexural strength results of the three samples evaluated for the admixture 02-NTF-100-2,5.

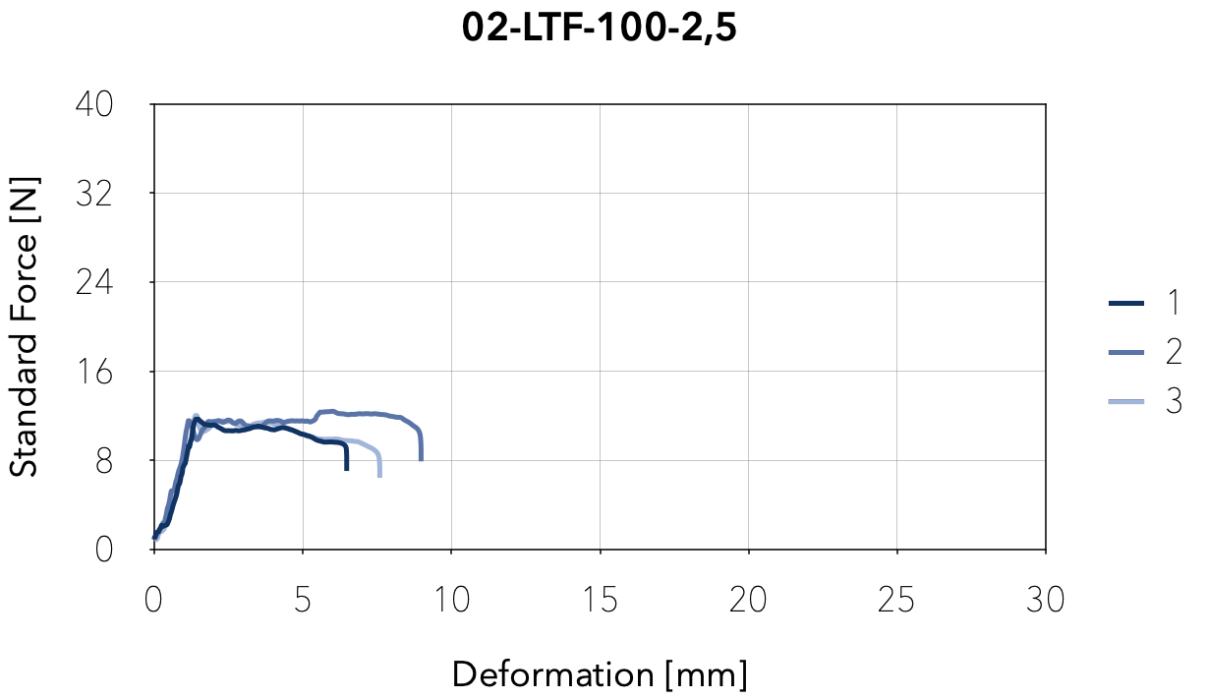

Figure 112. Image showing the flexural strength results of the three samples evaluated for the admixture 02-LTF-100-2,5.

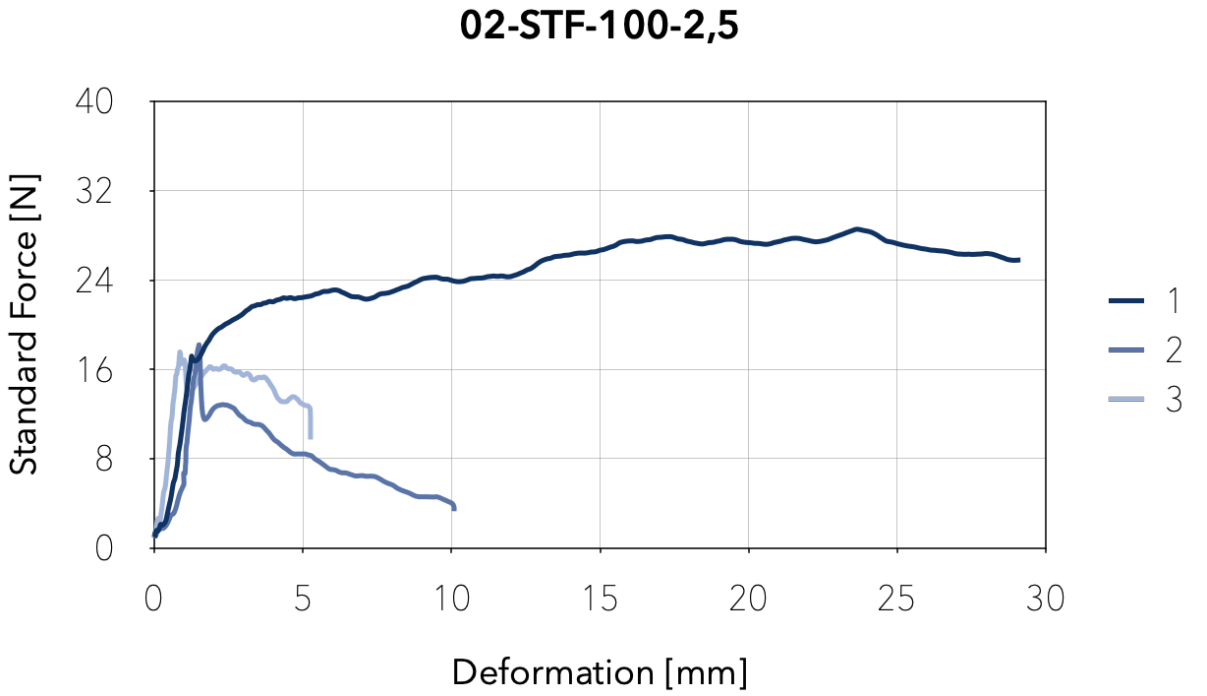

Figure 113. Image showing the flexural strength results of the three samples evaluated for the admixture 02-STF-100-2,5.

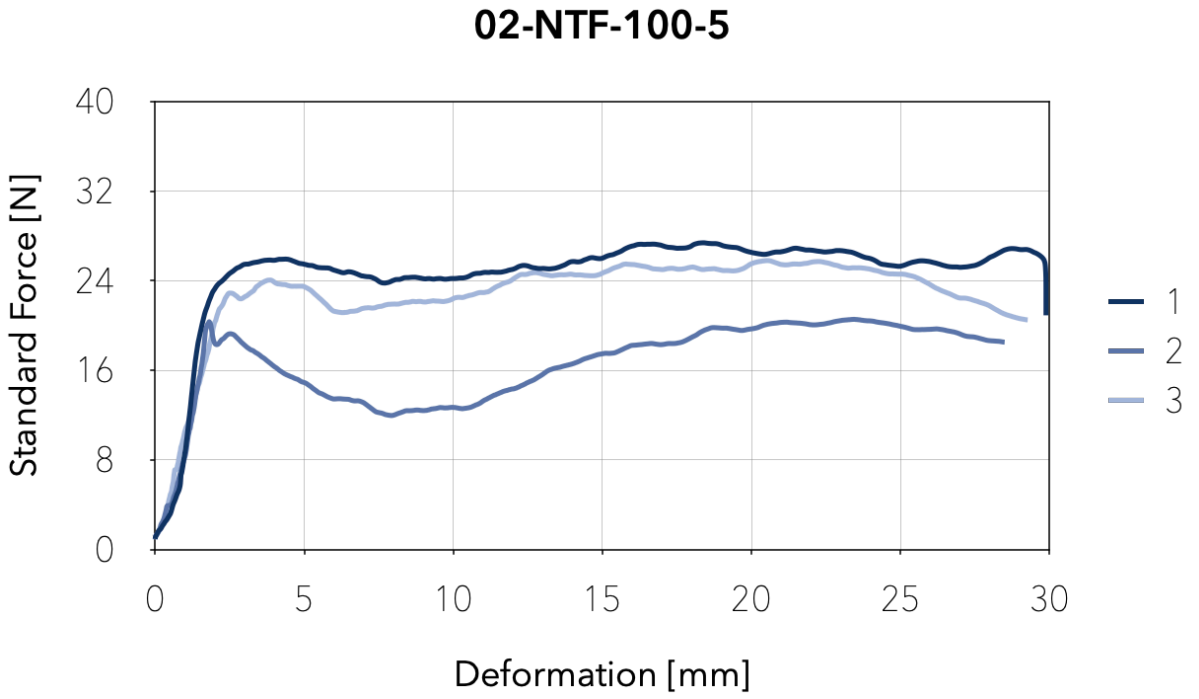

Figure 114. Image showing the flexural strength results of the three samples evaluated for the admixture 02-NTF-100-5.

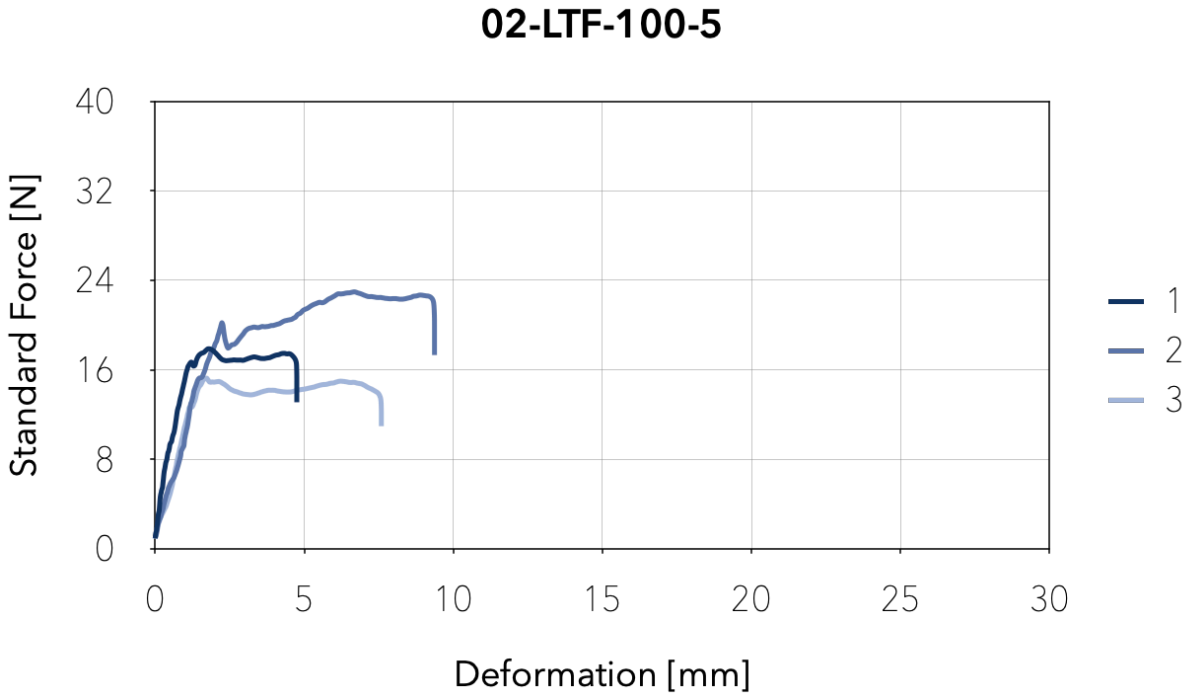

Figure 115. Image showing the flexural strength results of the three samples evaluated for the admixture 02-LTF-100-5.

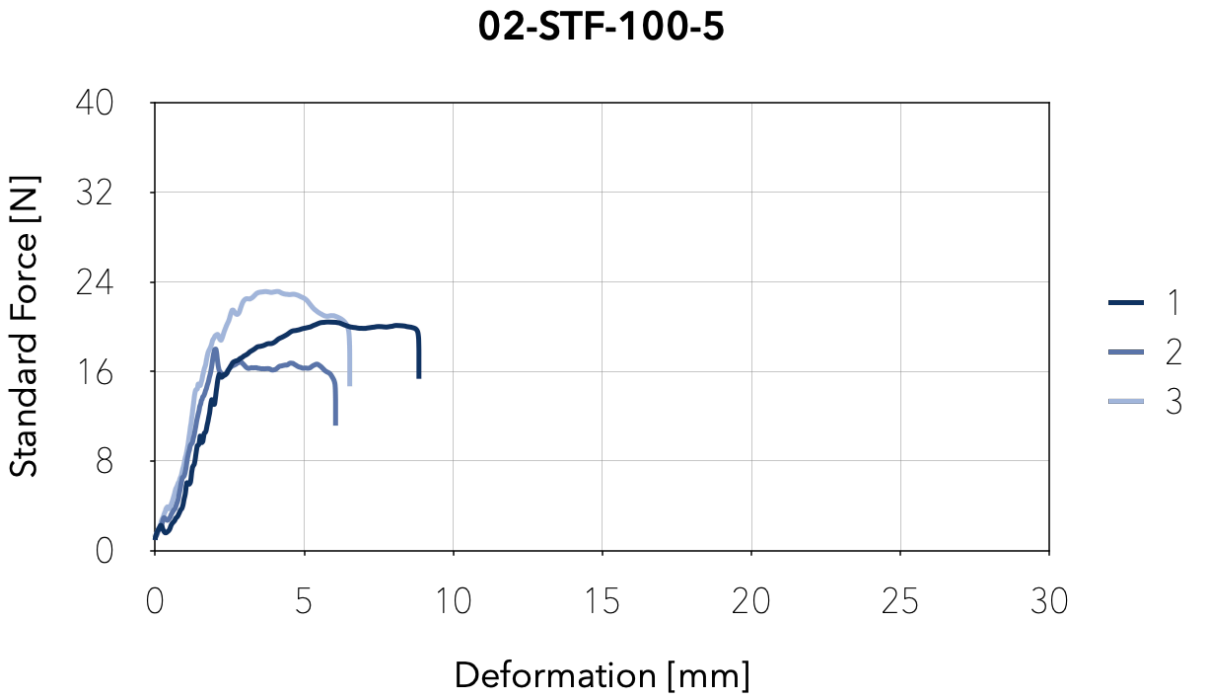

Figure 116. Image showing the flexural strength results of the three samples evaluated for the admixture 02-STF-100-5.

In the previous images, it is observable that the brittle behavior of the admixtures without fibers reduced considerably with the addition of SWF. For example, while the samples of the admixture 02-NF-100 broke with about 0,1mm of deformation, the samples with fibers resisted a deformation of about 5-10mm. However, some samples presented the following irregularities:

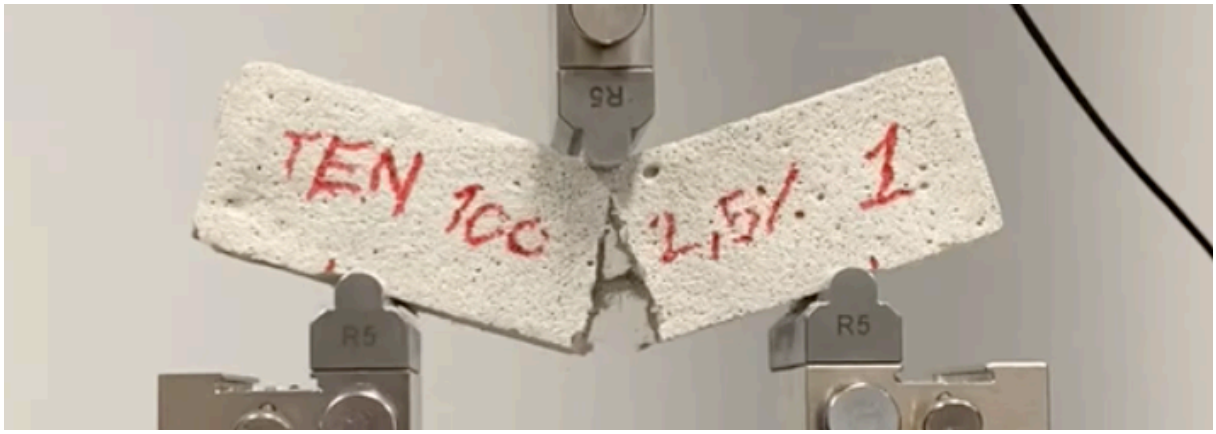

Figure 117. Flexural strength test photograph of 02-STF-100-2,5 sample1.

On the admixture 02-STF-100-2,5 sample 1, Figure 113 shows an atypical behavior; this sample resisted more than the others from the same admixture. In Figure 117, an agglomeration of fibers at the point of rupture explains the incremented flexural strength of this particular sample.

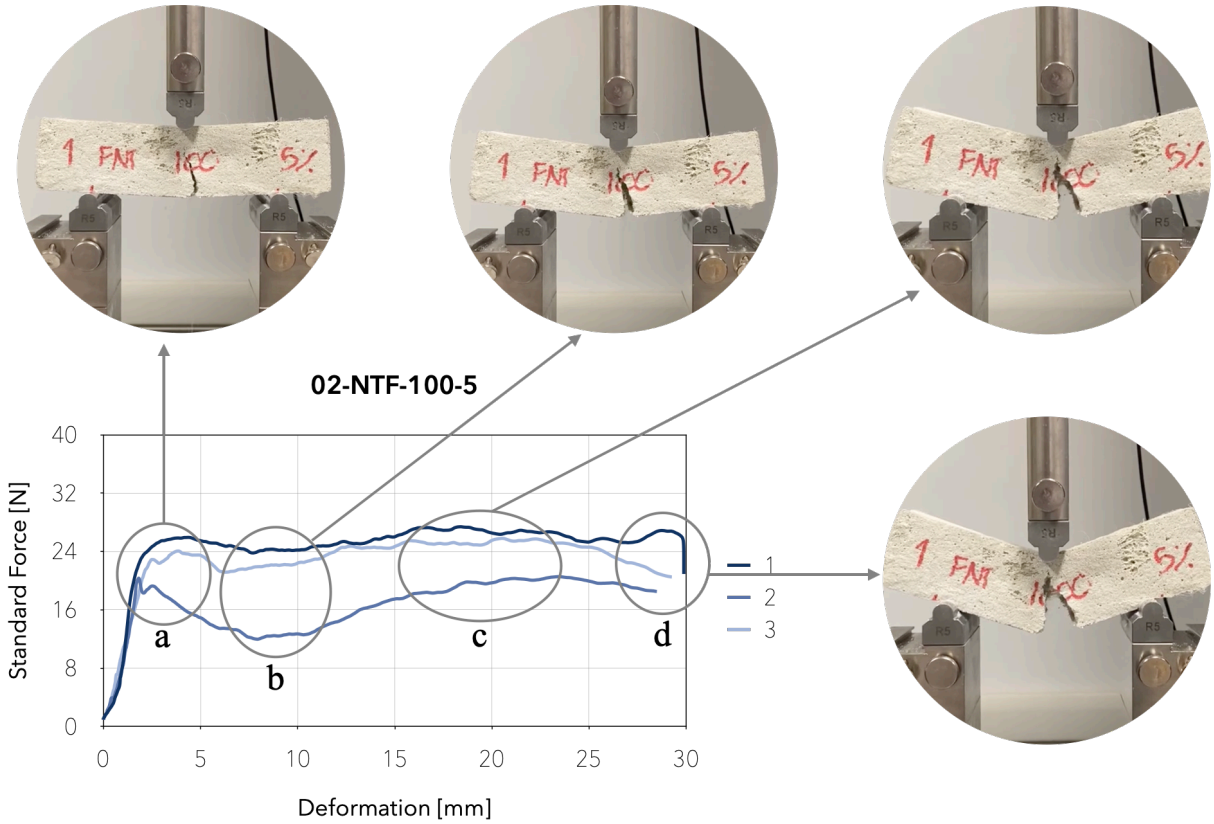

Figure 118. Image explaining the flexural strength/deformation behavior of admixture 02-NTF-100-5.

Most admixtures with a target density of 100kg/m^3 presented a point of rupture of around 5-10mm; however, every sample of admixture 02-NTF-100-5 reached almost 30mm because of fiber agglomerations located at the breaking point. Figure 118 explains this behavior graphically:

a. First crack: load corresponding to the tensile strength of foamed concrete material.
b. The force level decreases until the fiber reinforcement is entirely involved in the tensile resistance.
c. The force rises to a new maximum point. This resistance belongs to the fiber reinforcements that still hold the crack together
d. The fiber's failure point is reached, and the force decreases accordingly.

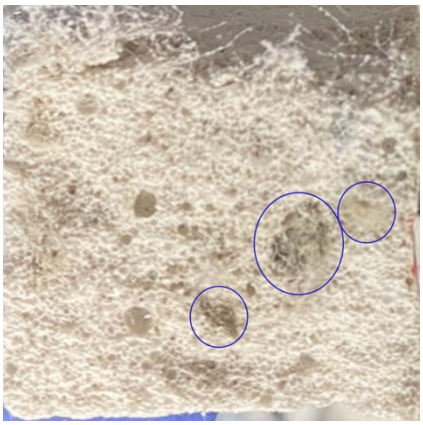

Figure 119. Section with the fiber agglomerations found at the breaking point on sample 2 admixture 02-NTF-100-5.

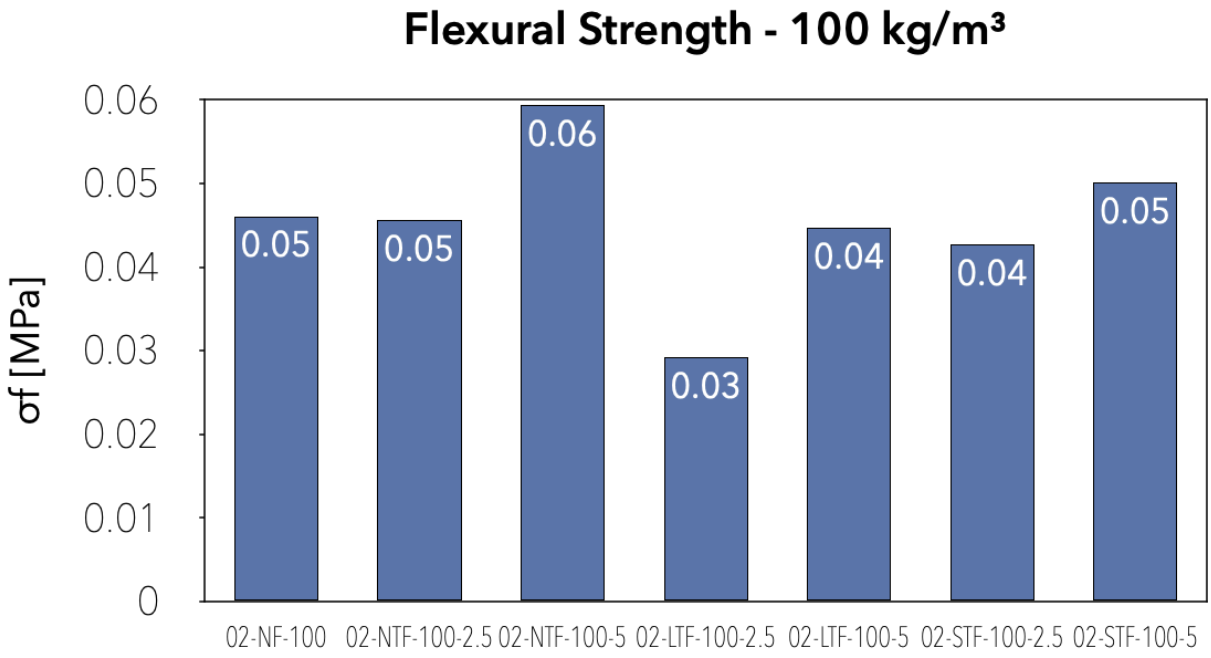

Figure 120. Graph showing the average maximum flexural strength of the admixtures with a 100kg/m³ target density.

Figure 120 shows the average flexural strength of each admixture with a target density of 100kg/m^3. 02-NF-100, 02-NTF-100-2,5, 02-LTF-100-5, 02-STF-100-2,5, and 02-STF-100-5 have a similar flexural strength. However, 02-NTF-100-5 is around 20% higher than the others, while 02-LTF-100-2,5 is about 40% lower.

It is fundamental to analyze how the fiber and cement content influences the flexural strength of each admixture. The following graphs display the results of this analysis.

Figure 121 shows that with a target density of 100kg/m^3 and NTF, the flexural strength of the admixture with a 2,5% F/C ratio has almost the same resistance as the samples without fibers, but with a 5% F/C ratio, the flexural strength increases by 20%. Figure 122 shows the results for LTF; in this case, the flexural strength is

almost equal for the samples without fibers and those with a 5% F/C ratio; however, the admixture with a 2,5% F/C ratio has a 33% lower flexural strength. Figure 123 shows that with STF, the flexural strength of the admixture with a 2,5% F/C ratio decreases by 7%, while with a 5% ratio, it increases by 9% compared to the admixture without fibers.

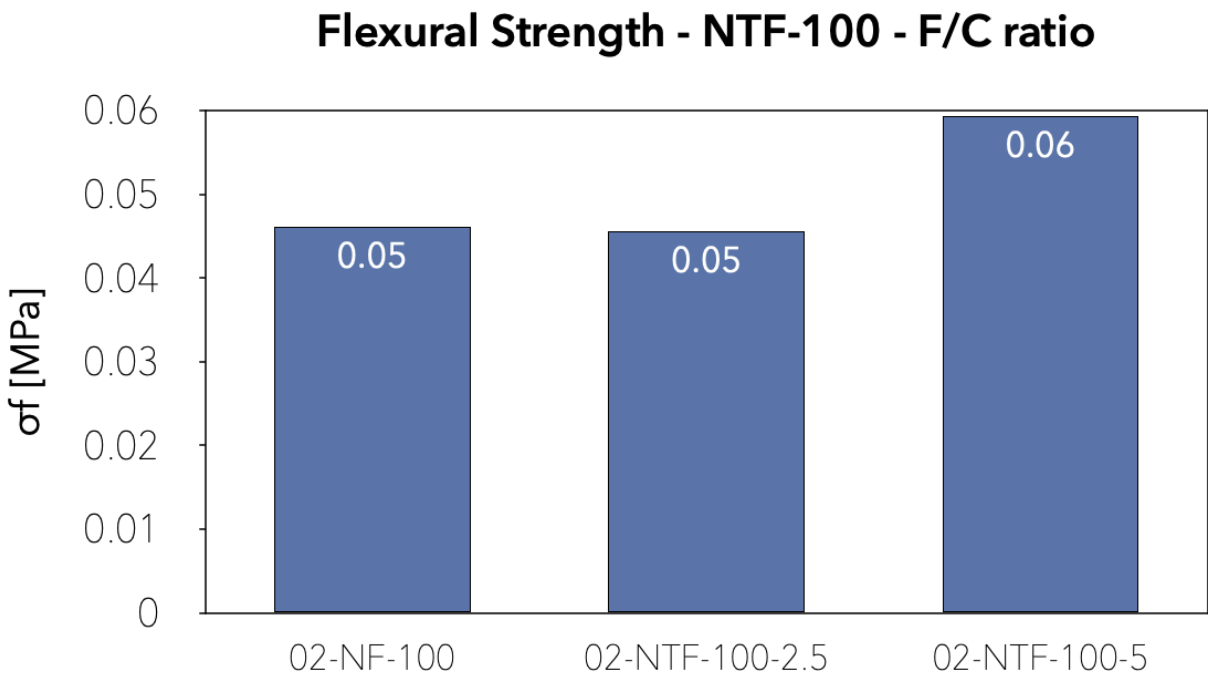

Figure 121. Graph showing the average maximum flexural strength of the admixtures with NTF and a 100kg/m³ target density.

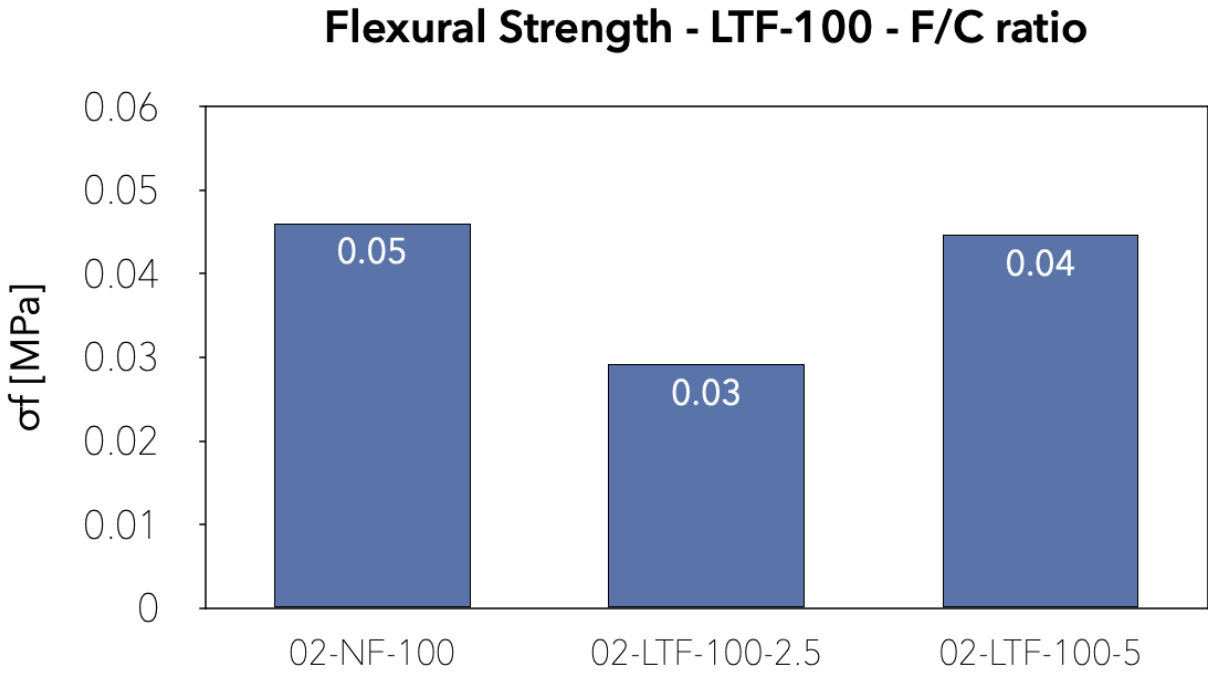

Figure 122. Graph showing the average maximum flexural strength of the admixtures with LTF and a 100kg/m³ target density.

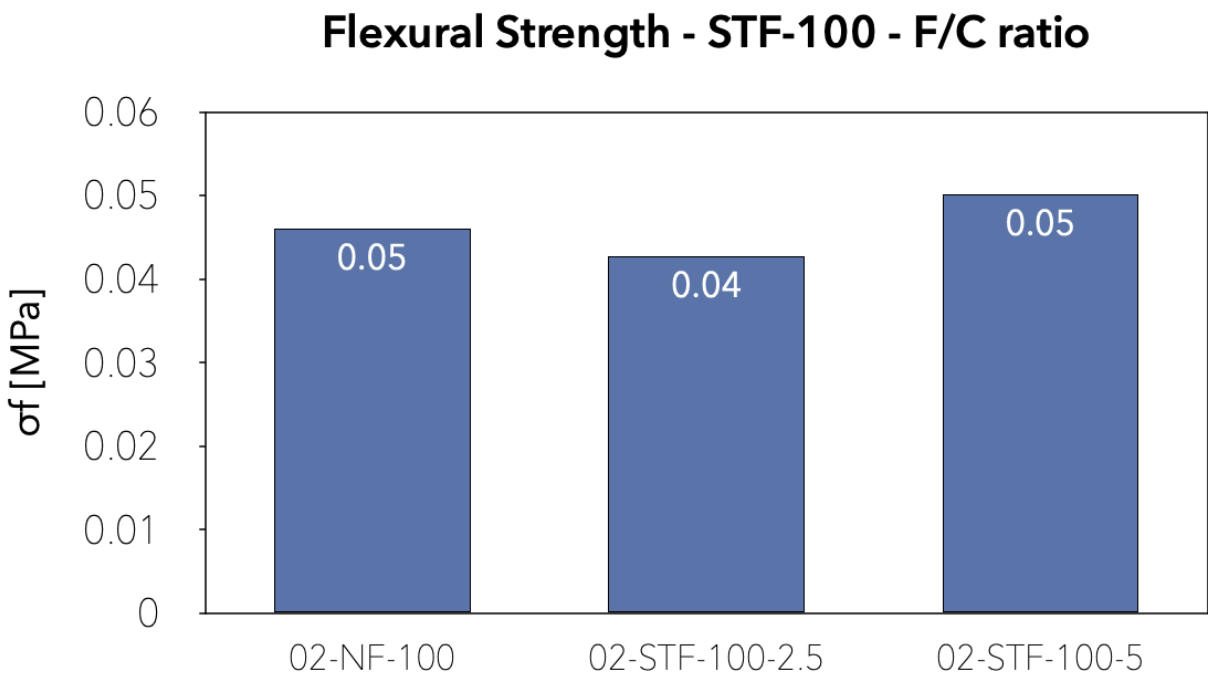

Figure 123. Graph showing the average maximum flexural strength of the admixtures with STF and a 100kg/m³ target density.

The following images show the flexural strength test results of the admixtures with a 300kg/m³ target density.

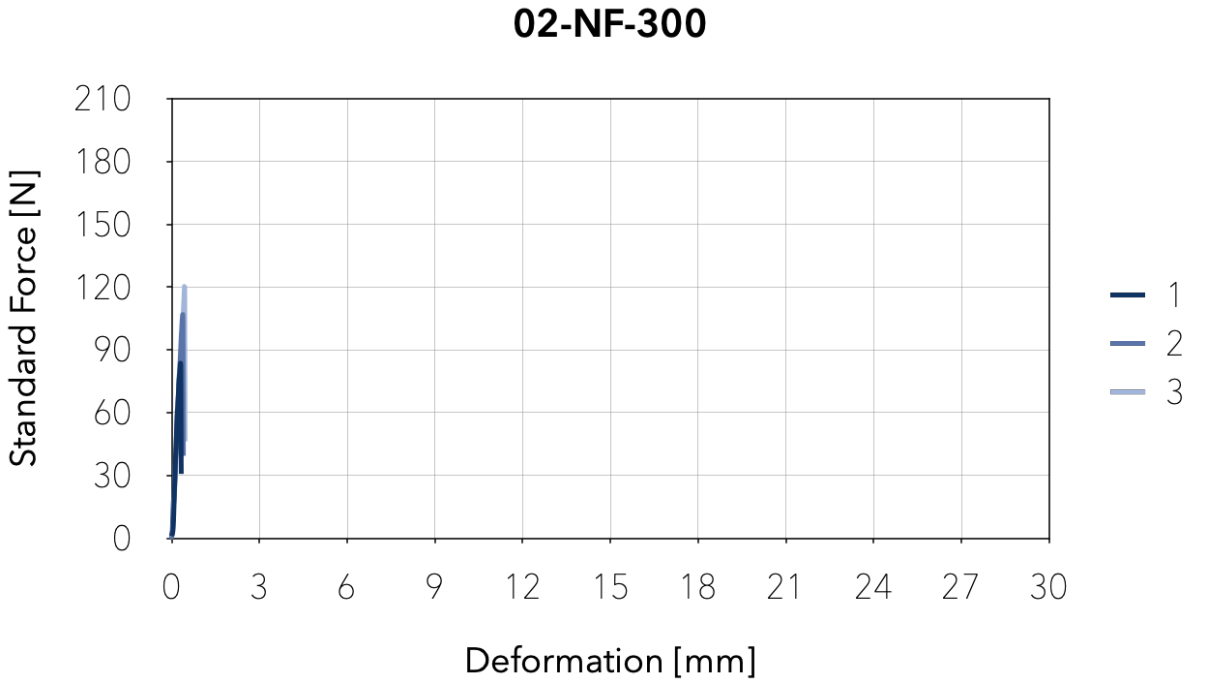

Figure 124. Image showing the flexural strength results of the three samples evaluated for the admixture 02-NF-300.

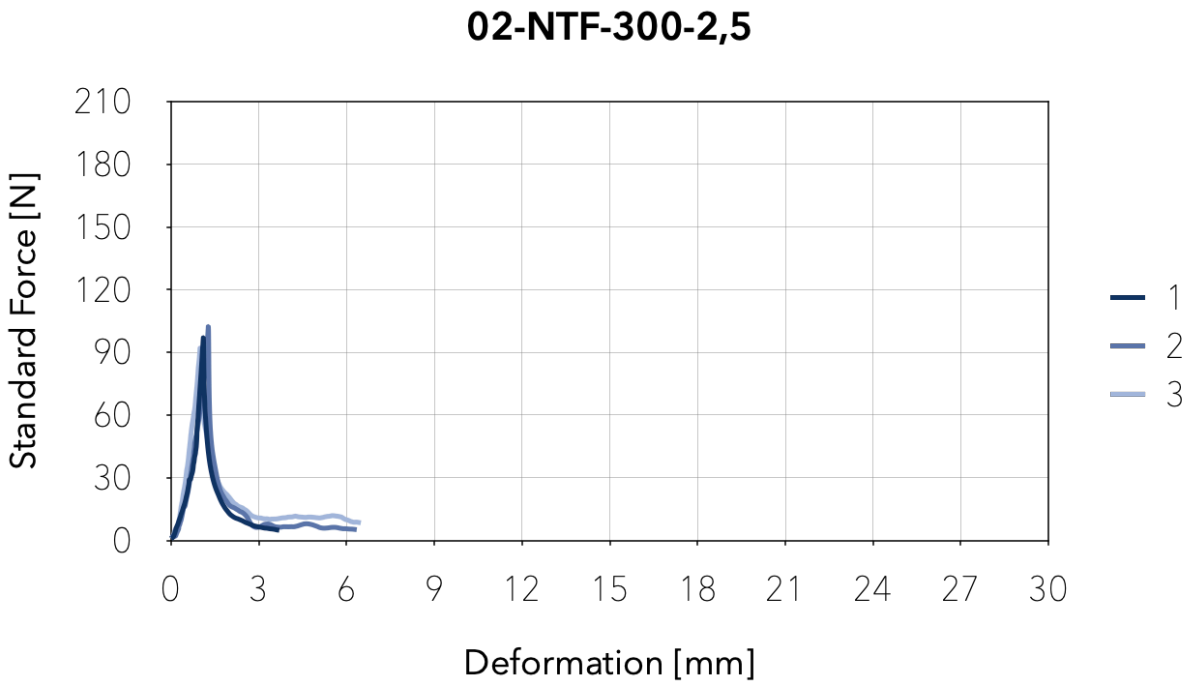

Figure 125. Image showing the flexural strength results of the three samples evaluated for the admixture 02-NTF-300-2,5.

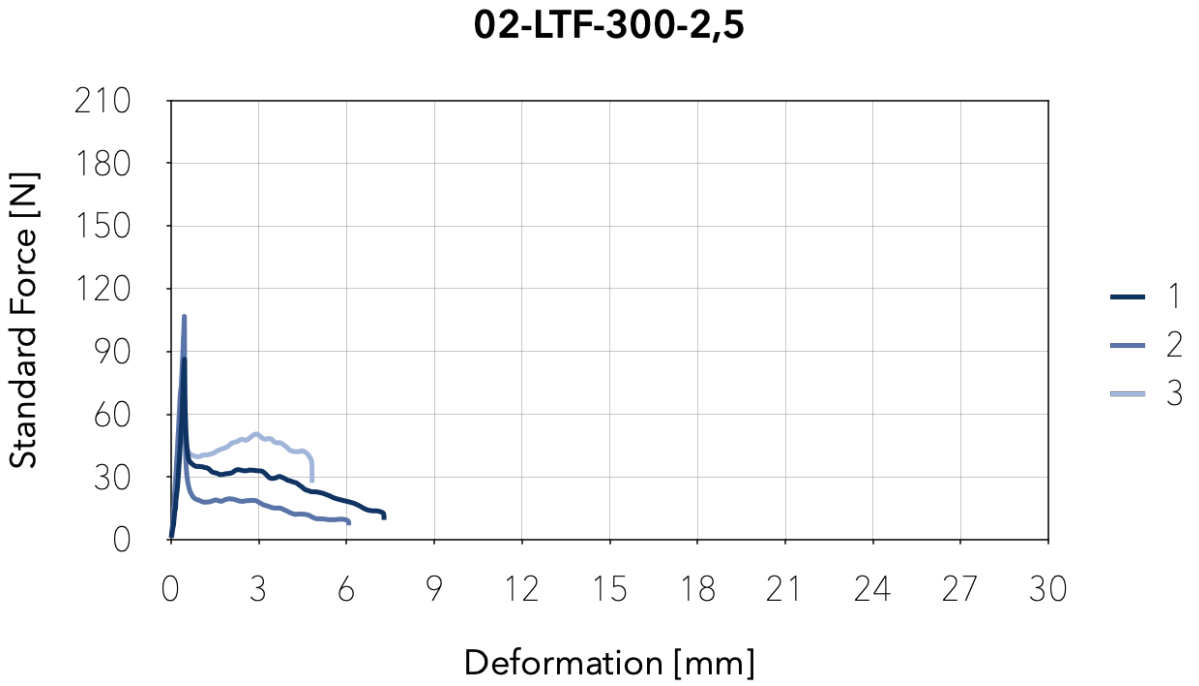

Figure 126. Image showing the flexural strength results of the three samples evaluated for the admixture 02-LTF-300-2,5.

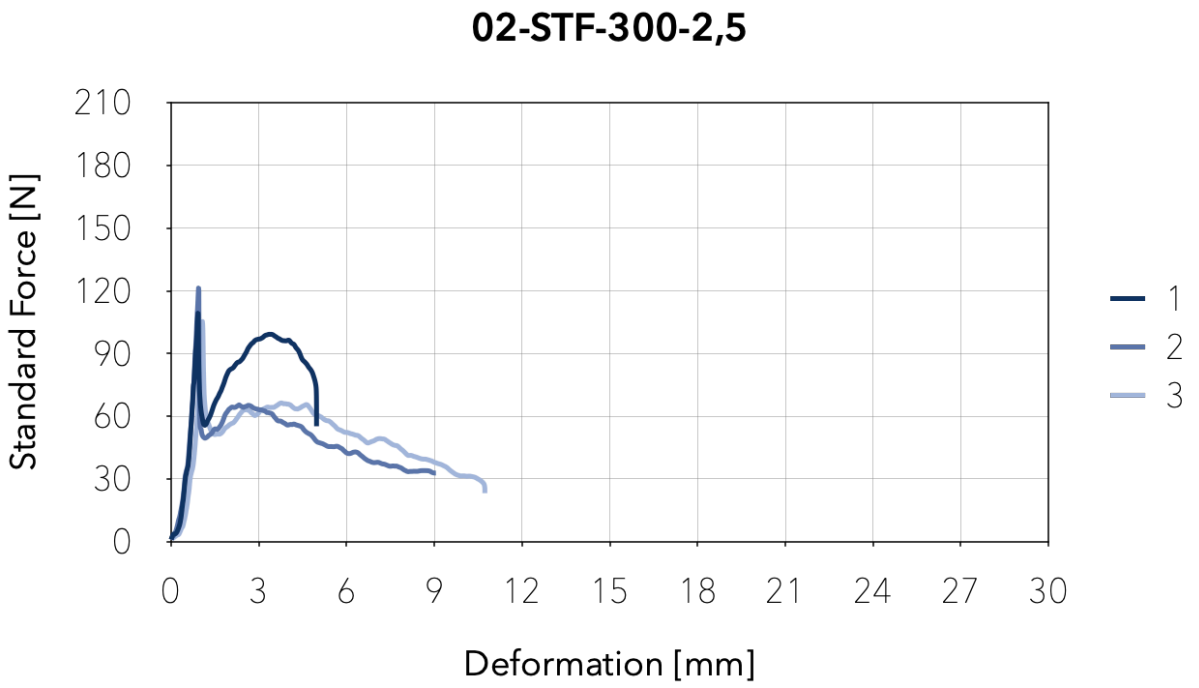

Figure 127. Image showing the flexural strength results of the three samples evaluated for the admixture 02-STF-300-2,5.

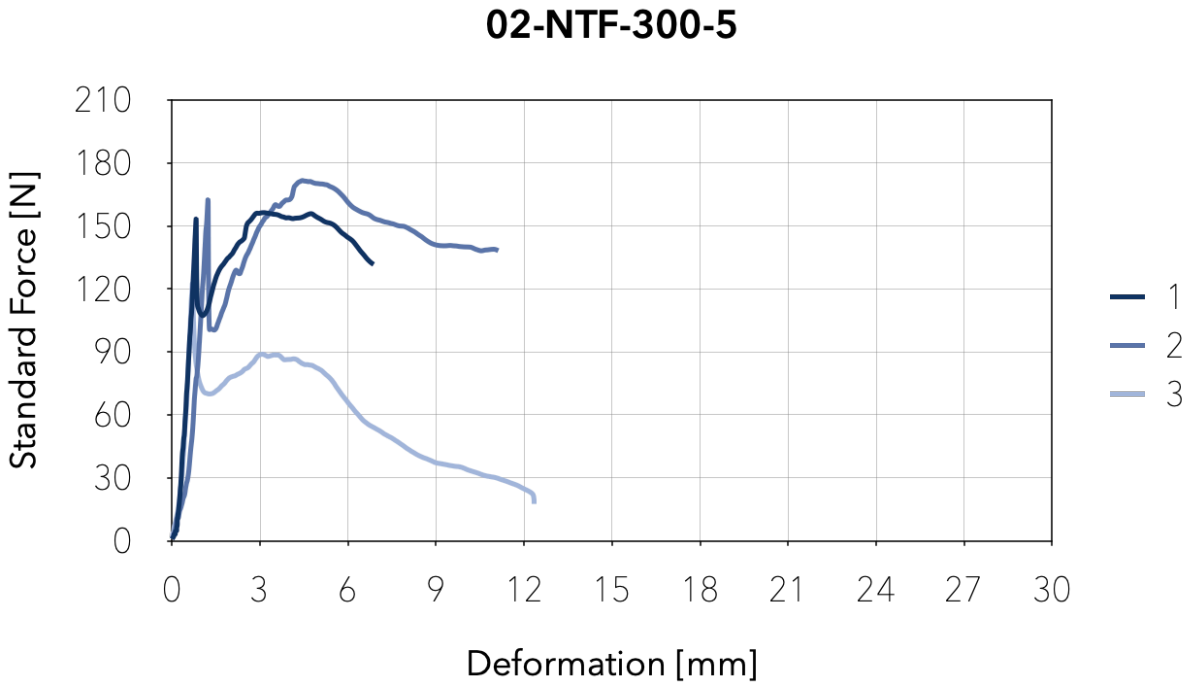

Figure 128. Image showing the flexural strength results of the three samples evaluated for the admixture 02-NTF-300-5.

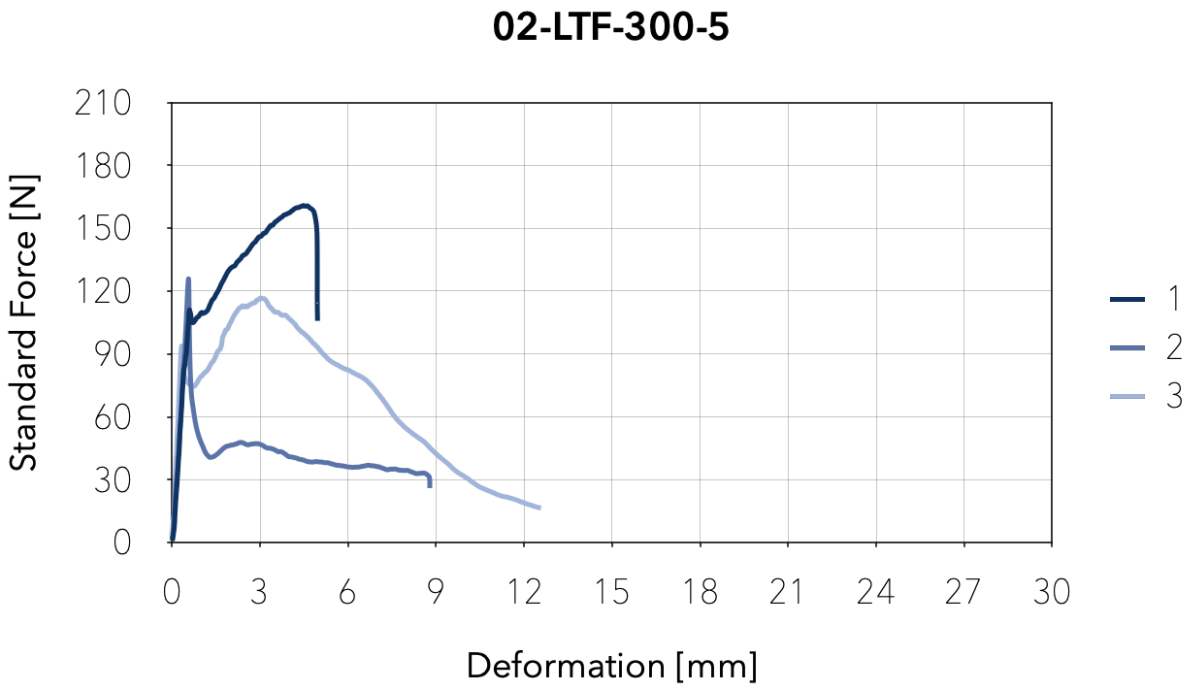

Figure 129. Image showing the flexural strength results of the three samples evaluated for the admixture 02-LTF-300-5.

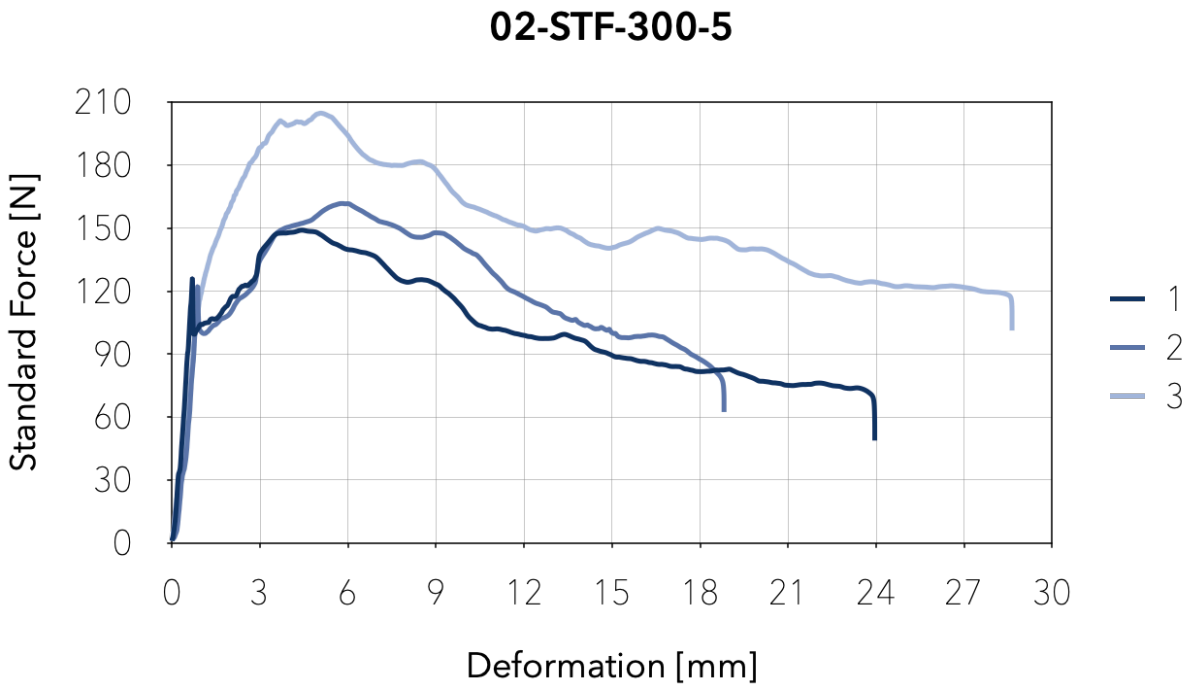

Figure 130. Image showing the flexural strength results of the three samples evaluated for the admixture 02-STF-300-5.

In the previous images, it is observable that the brittleness of the admixtures without fibers reduced considerably with the addition of SWF. For example, while the samples of the admixture 02-NF-300 broke with about 0,4mm of deformation, the

samples with fibers resisted a deformation of about 6-12mm. However, the samples of the admixture 02-STF-300-5 presented the following irregularities:

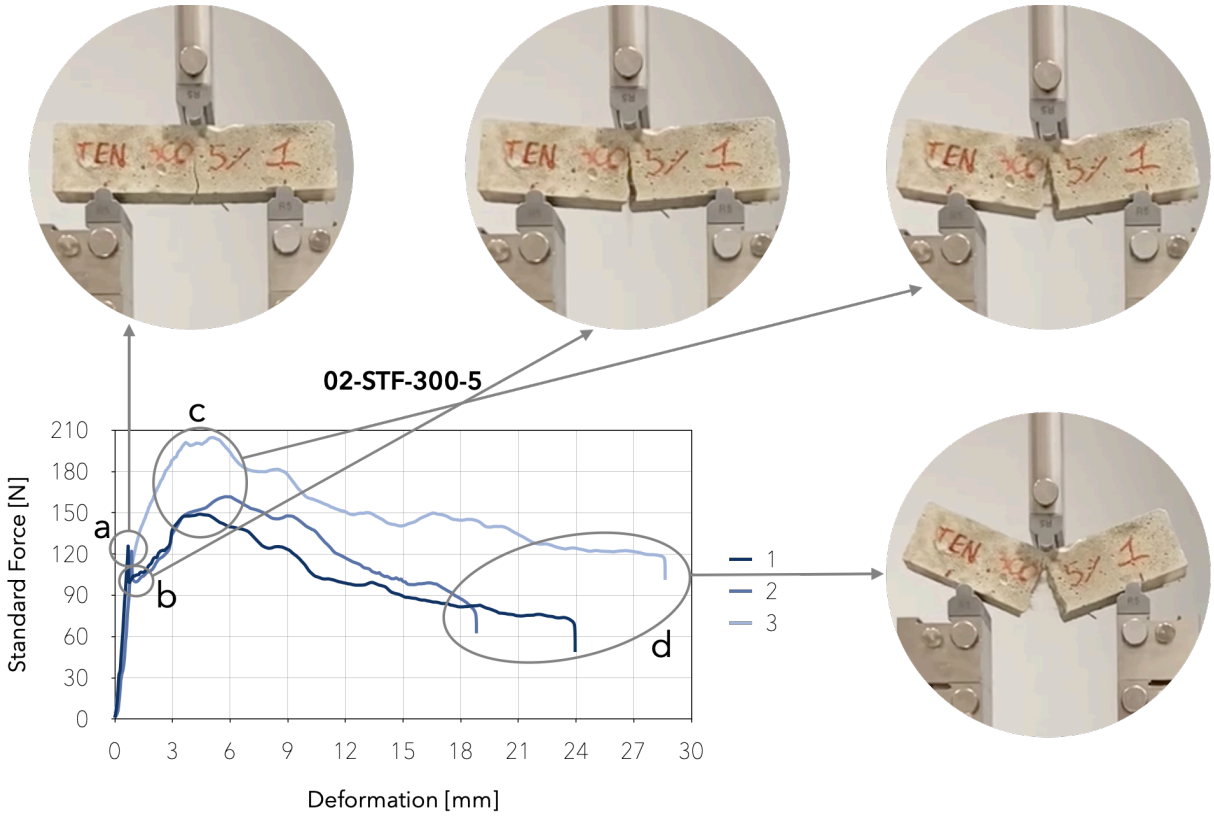

Figure 131. Image explaining the flexural strength/deformation behavior of admixture 02-STF-300-5.

Most admixtures with a target density of 300kg/m^3 presented a point of rupture of around 6-12mm; however, every sample of admixture 02-STF-300-5 reached a deformation of 19-28mm because of fiber agglomerations located at the breaking point. Figure 131 explains this behavior graphically:

1. First crack: load corresponding to the tensile strength of foamed concrete material.
2. Theforceleveldecreasesuntilthefiberreinforcementisentirelyinvolved in the tensile resistance.
3. The force rises to a new maximum point. This resistance belongs to the fiber reinforcements that still hold the crack together
4. The fiber's failure point is reached, and the force decreases accordingly.

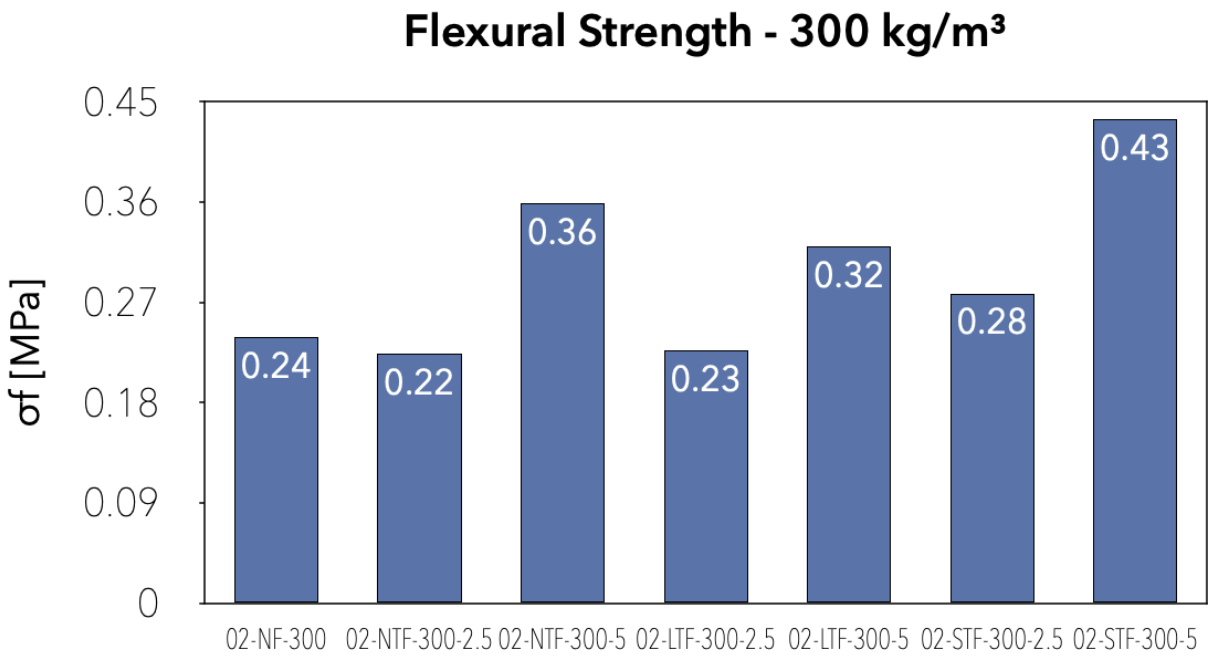

Figure 132. Graph showing the average maximum flexural strength of the admixtures with a 300kg/m³ target density.

Figure 132 shows the average flexural strength of each admixture with a target density of 300kg/m^3. 02-NF-300, 02-NTF-300-2,5, and 02-LTF-300-5 have a similar flexural strength being the admixtures with fibers slightly less resistant to flexural stress. For example, 02-STF-300-2,5 presented a 17% increment in flexural strength compared to the admixture without fibers; this was the only admixture with a 2,5% fiber content that presented an augmented flexural strength with respect to the admixture without fibers. However, admixtures with a 5% F/C ratio resulted in a higher resistance, especially the admixture with STF, in which the influence of fiber agglomerations translates into a higher average resistance.

It is fundamental to analyze how the fiber and cement content influences the flexural strength of each admixture. The following graphs display the results of this analysis.

Figure 133 shows that with a target density of 300kg/m^3 and NTF, the flexural strength of the admixture with a 2,5% F/C ratio has a 7% lower resistance than the samples without fibers, but with a 5% F/C ratio, the flexural strength increases by 50%. Figure 134 shows the results for LTF; in this case, the flexural strength is similar to that of NTF, being the admixture with a 2,5%F/C ratio lower by 5% and the 5% F/C ratio higher by 34%. Figure 135 shows that with STF, the flexural strength of the admixture with a 2,5% F/C ratio increases by 17%, while with a 5% ratio, it increases by 82% compared to the admixture without fibers.

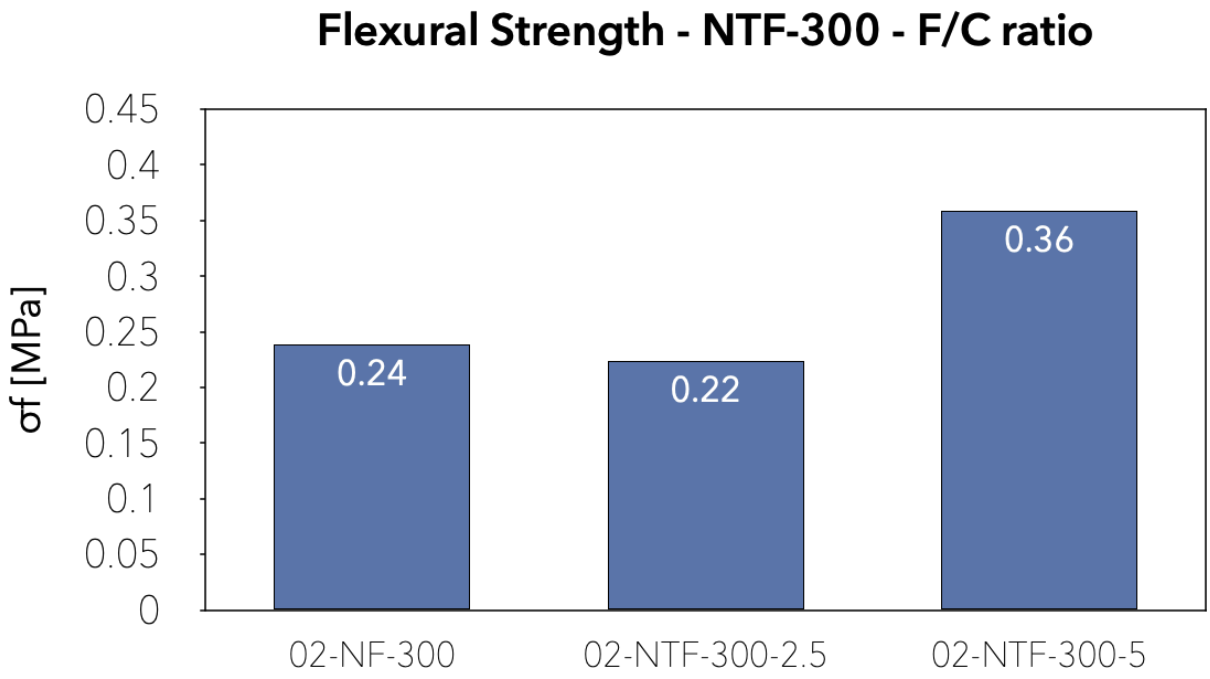

Figure 133. Graph showing the average maximum flexural strength of the admixtures with NTF and a 300kg/m³ target density.

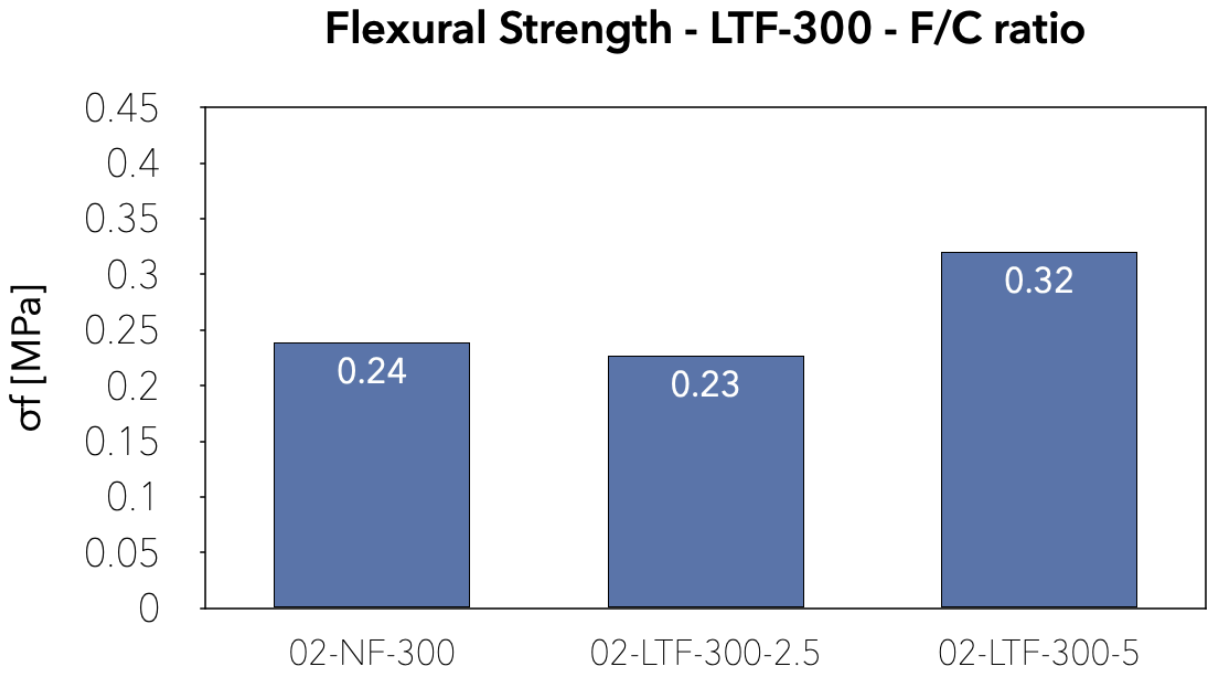

Figure 134. Graph showing the average maximum flexural strength of the admixtures with LTF and a 300kg/m³ target density.

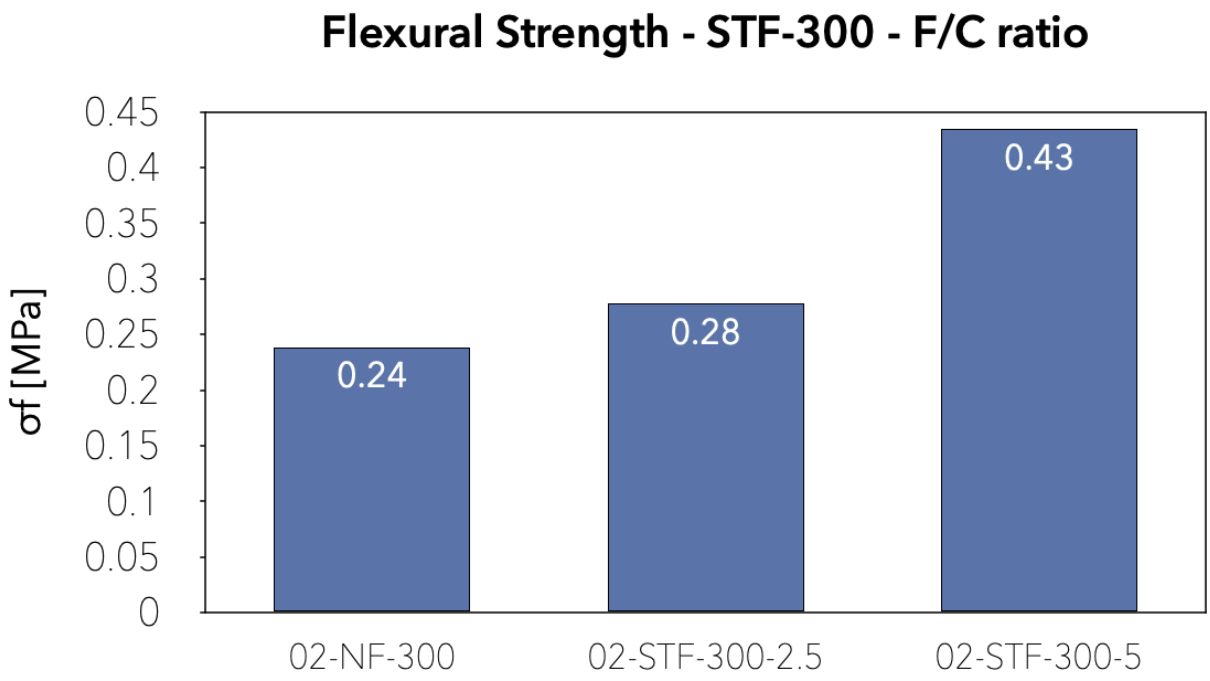

Figure 135. Graph showing the average maximum flexural strength of the admixtures with STF and a 300kg/m³ target density.

The following images show the flexural strength test results of the admixtures with a 500kg/m^3 target density.

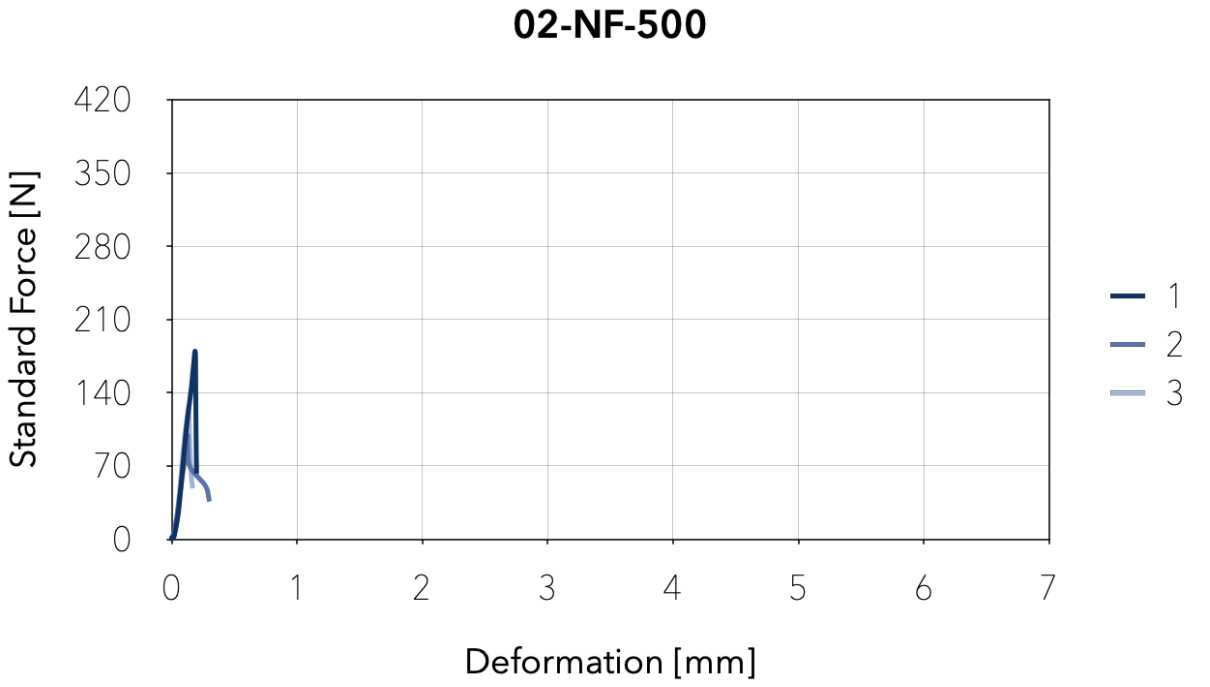

Figure 136. Image showing the flexural strength results of the three samples evaluated for the admixture 02-NF-500.

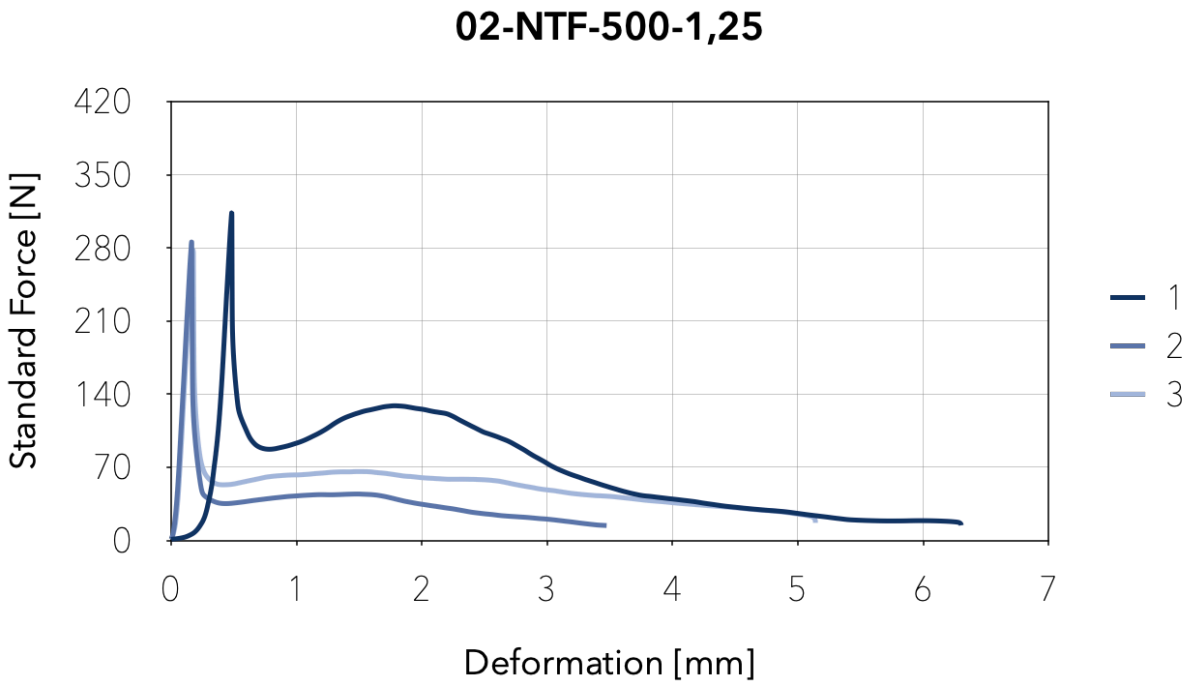

Figure 137. Image showing the flexural strength results of the three samples evaluated for the admixture 02-NTF-500-1,25.

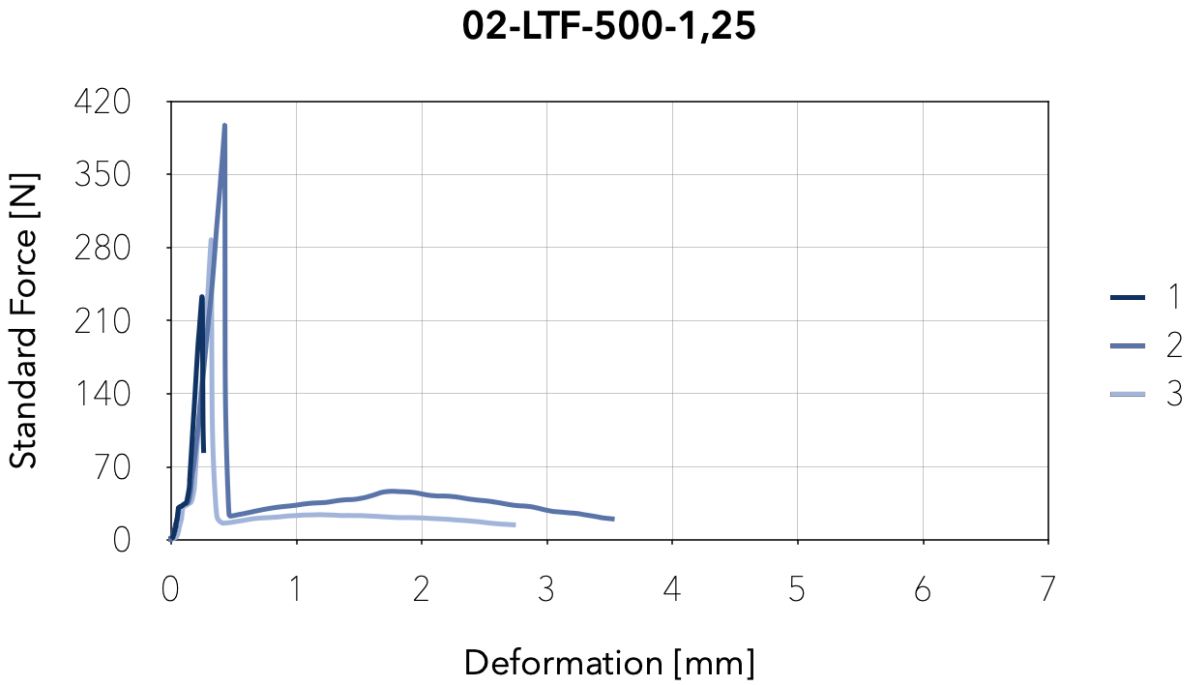

Figure 138. Image showing the flexural strength results of the three samples evaluated for the admixture 02-LTF-500-1,25.

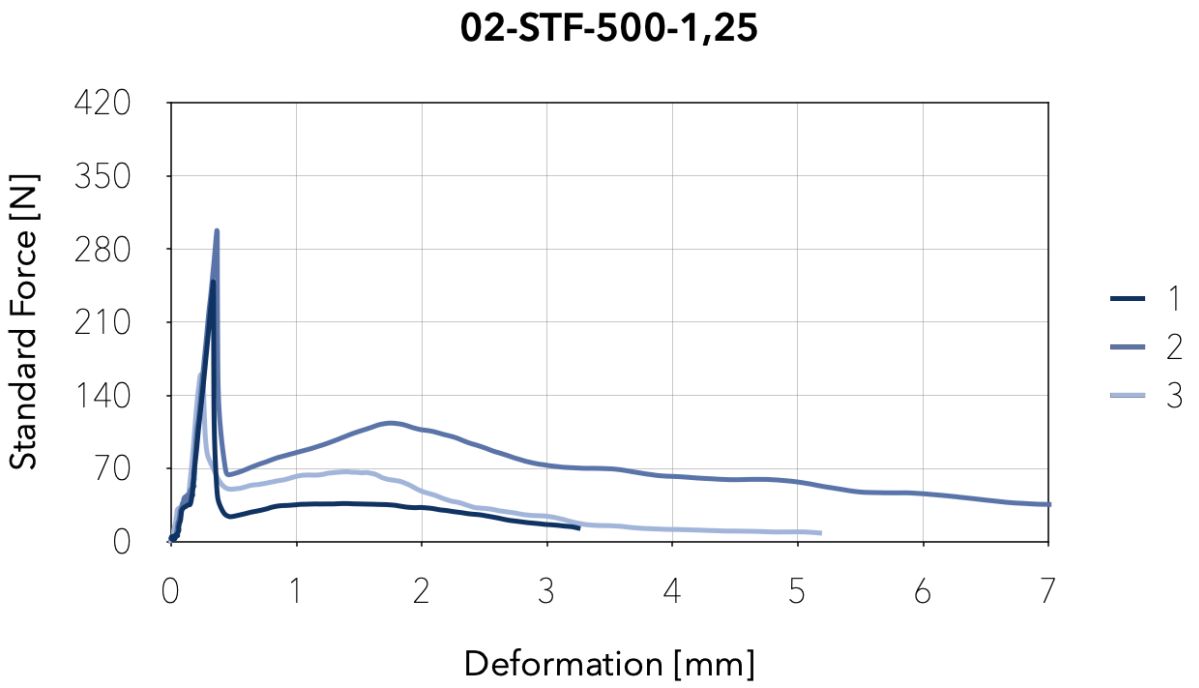

Figure 139. Image showing the flexural strength results of the three samples evaluated for the admixture 02-STF-500-1,25.

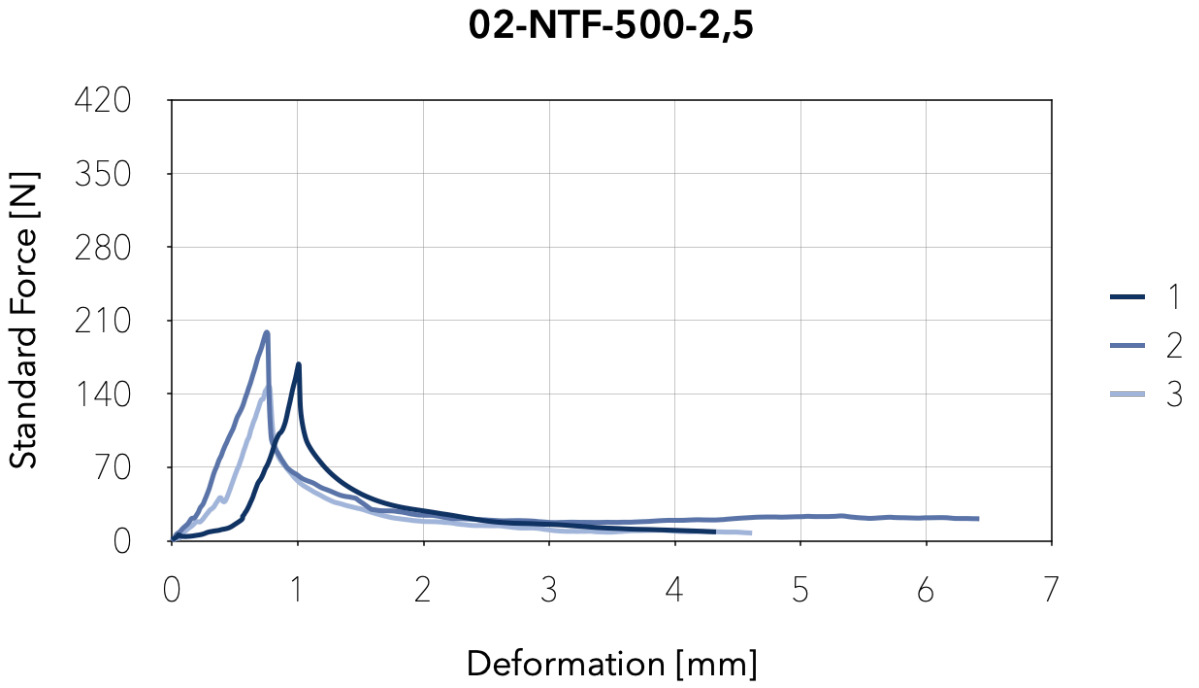

Figure 140. Image showing the flexural strength results of the three samples evaluated for the admixture 02-NTF-500-2,5.

In the previous images, it is observable that the brittle behavior of the admixtures without fibers reduced considerably with the addition of SWF. For example, while the samples of the admixture 02-NF-500 broke with about 0,2-0,3mm of deformation, the samples with fibers resisted a deformation of about 3-7mm. Furthermore, the samples with fibers presented an increment to a new maximum

point that belongs to the fiber agglomerations. At this density, the increment due to fibers is lower than that of admixtures with target densities of 100 and 300kg/m^3.

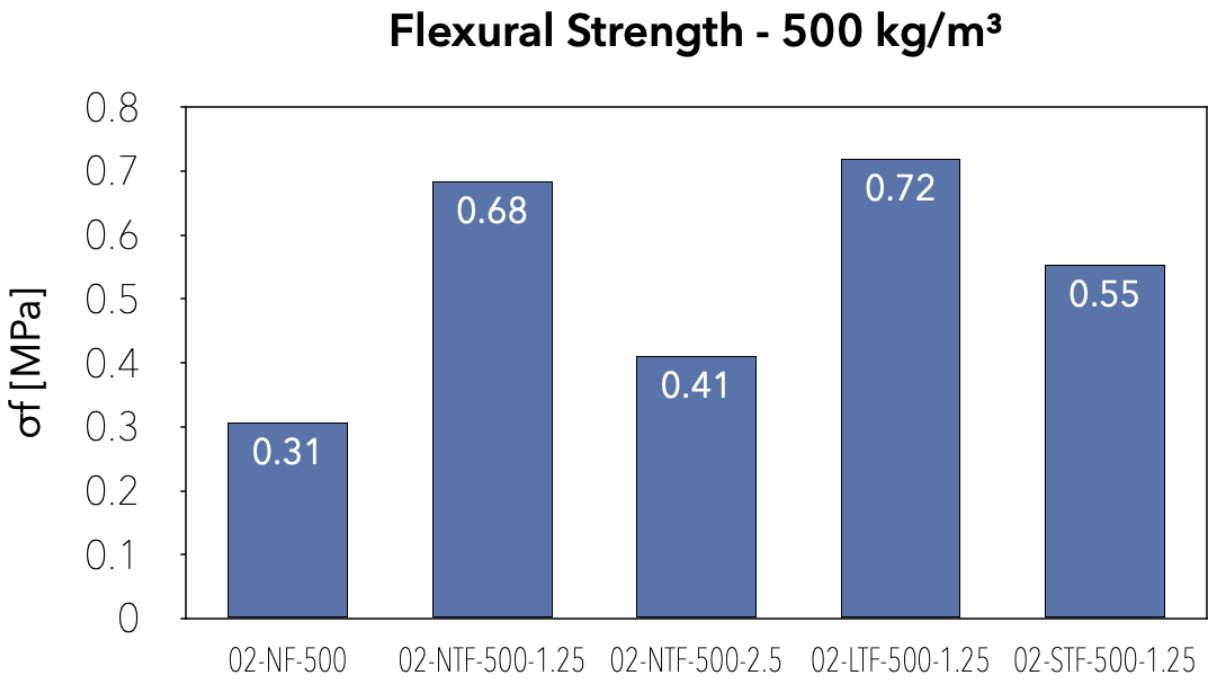

Figure 141. Graph showing the average maximum flexural strength of the admixtures with a 500kg/m³ target density.

Figure 141 shows the average flexural strength of each admixture with a target density of 500kg/m^3. In comparison to 02-NF-500, 02-NTF-500-1,25 had an improvement of about 120%, 02-LTF-500-1,25 was the most performant, increasing by around 132%, and 02-STF-500-1,25 showed a flexural strength higher by 77%. 02-NTF-500-2,5 had different characteristics because it contained a 1% S/C ratio; however, it still presented a 32% improvement in flexural strength.

The following graphs show the flexural strength in terms of density, considering a similar fiber content in volume instead of cement. In this case, the admixtures with a target density of 100kg/m^3 with a 5% F/C ratio, 300kg/m^3 with a 2,5% F/C ratio, and 500kg/m^3 with a 1,25% F/C ratio present a similar fiber content per volume unit of about 4,5kg/m^3. A higher density translates into a higher resistance which is listed below. The first percentage of the increase rate between admixtures of 100 and 300kg/m^3 and the second between 300 and 500kg/m^3:

- NF 420% and 30%
- NTF 280% and 210%
- LTF 400% and 220%
- STF 450% and 100%

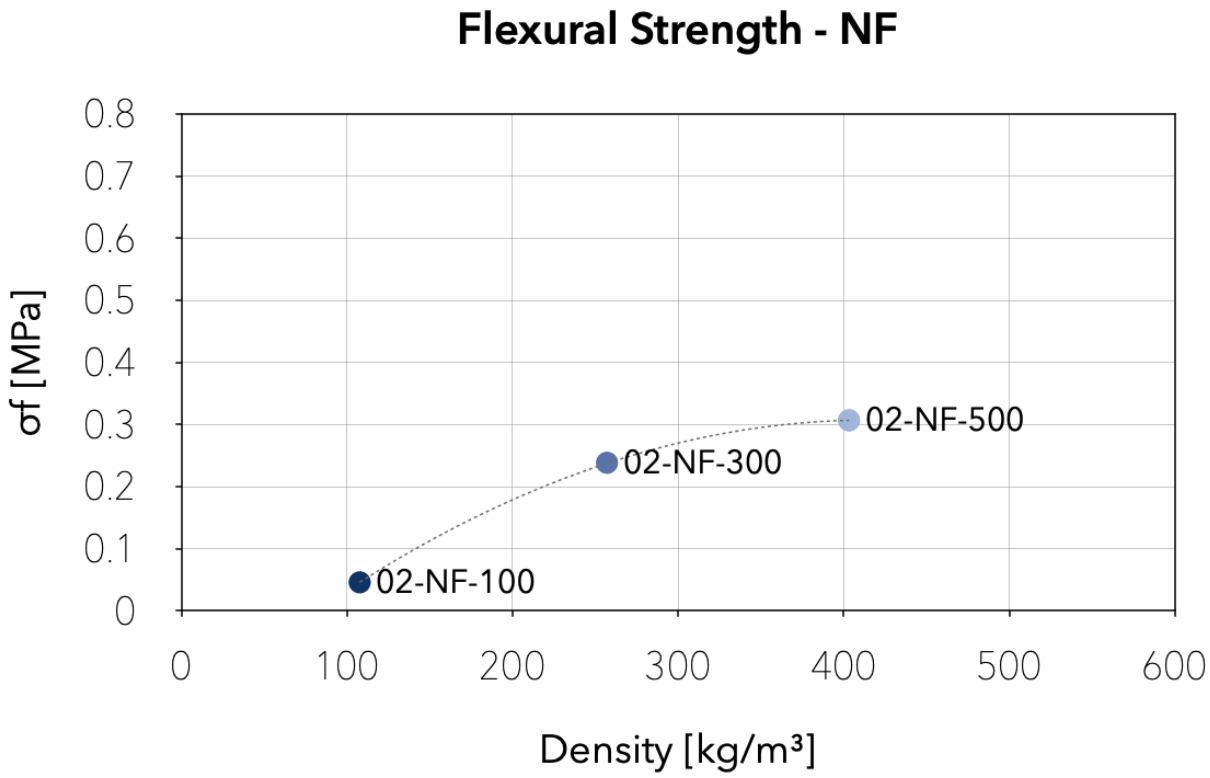

Figure 142. Dispersion graph of the average flexural strength of the NF admixtures compared to the average dry density.

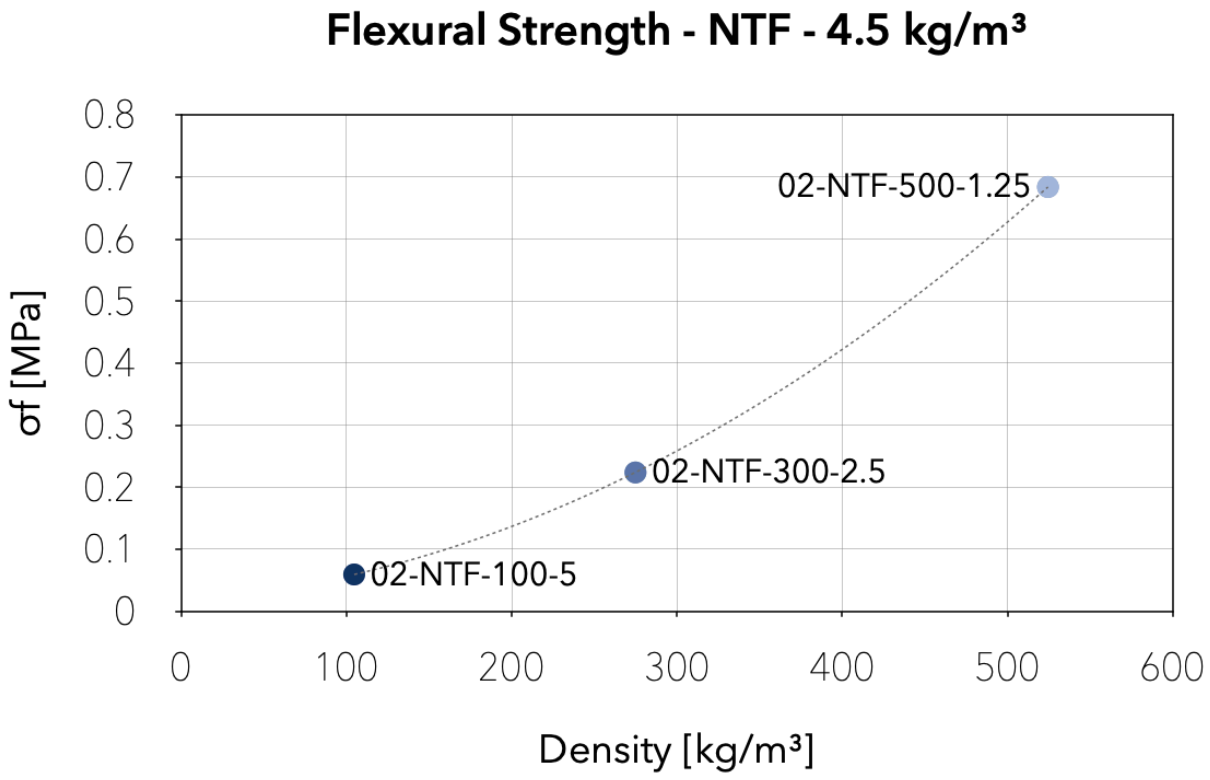

Figure 143. Dispersion graph of the average flexural strength of the NTF admixtures with 4,5kg/m³ of fibers compared to the average dry density.

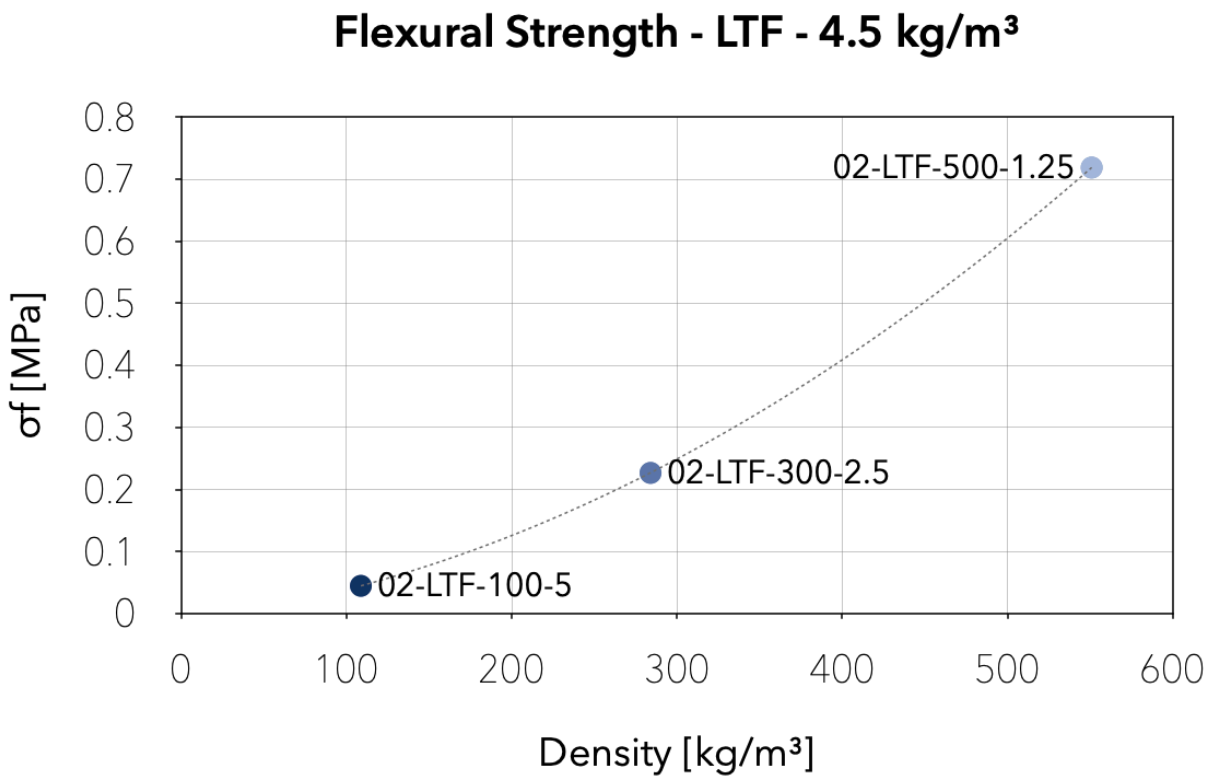

Figure 144. Dispersion graph of the average flexural strength of the LTF admixtures with 4,5kg/m³ of fibers compared to the average dry density.

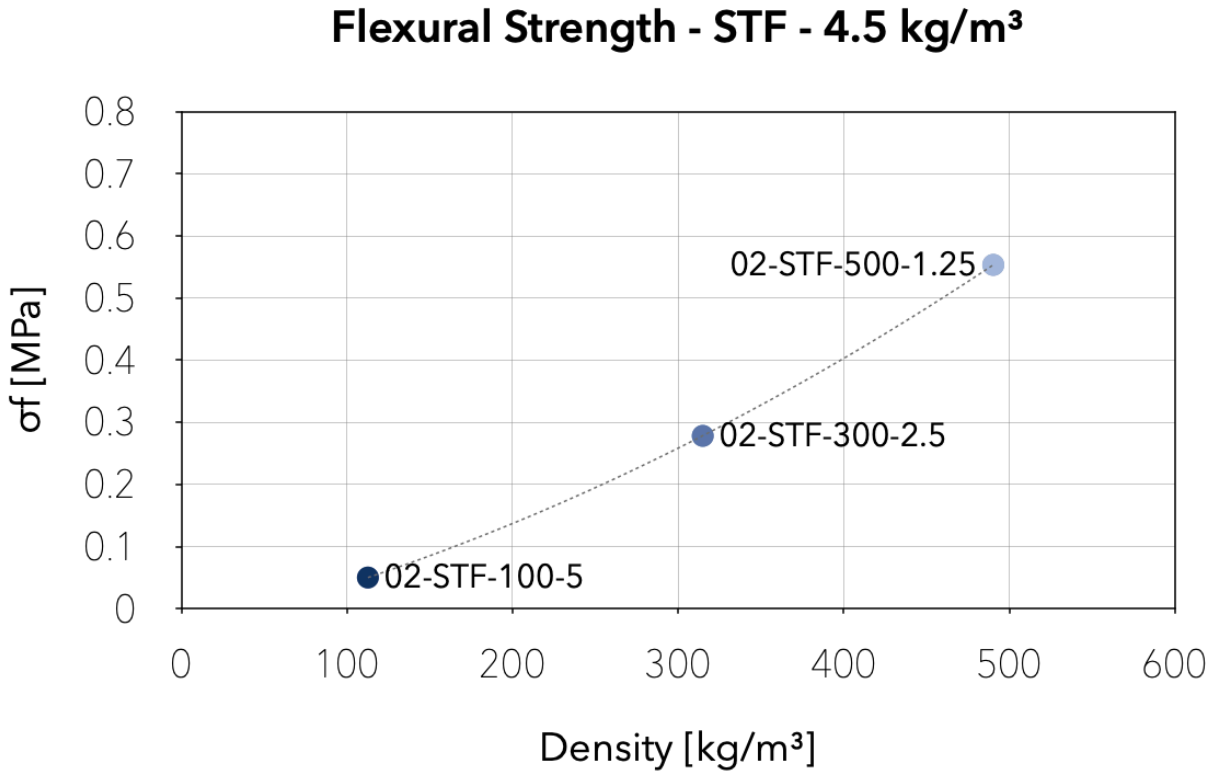

Figure 145. Dispersion graph of the average flexural strength of the STF admixtures with 4,5kg/m³ of fibers compared to the average dry density.

NF, LTF, and STF increased by at least 400% from 100 to 300 kg/m^{3,} but NTF only presented an improvement of 280%. On the other hand, from 300 to 500 kg/m^{3,} NTF and LTF increased by about 200%, STF by 100%, and NF only by 30%. This analysis shows that each fiber treatment presents a different behavior on different densities. This should be considered a fundamental factor in the selection process depending on the needs of each particular scenario.

5.2.4.2. Compressive strength

The compressive strength test was performed on the samples matured in air at room temperature (20 ± 3 °C) and natural humidity. In particular, the fragments of the prisms generated following the bending test were subjected to the test; for each mixture, the test was carried out on a total of 6 elements. The high number of tests made it possible to identify a representative and realistic behavior relating to the compressive strength of the material used for each type of mixture. For carrying out the tests, the force control mode was used according to the UNI EN 196-1 standard, but, unlike it, a force equal to 50 N/s was used for samples with a target density of 100kg/m^3 and 100 N/s for 300 and 500kg/m^3. Given the characteristics and specifications of the material under analysis, very low compressive strengths were foreseen pre-trial.

Each specimen got tested by being positioned so that the surface exposed to the air during curing was in a frontal position so as not to be directly subjected to the pressure exerted by the machinery, following the regulations.

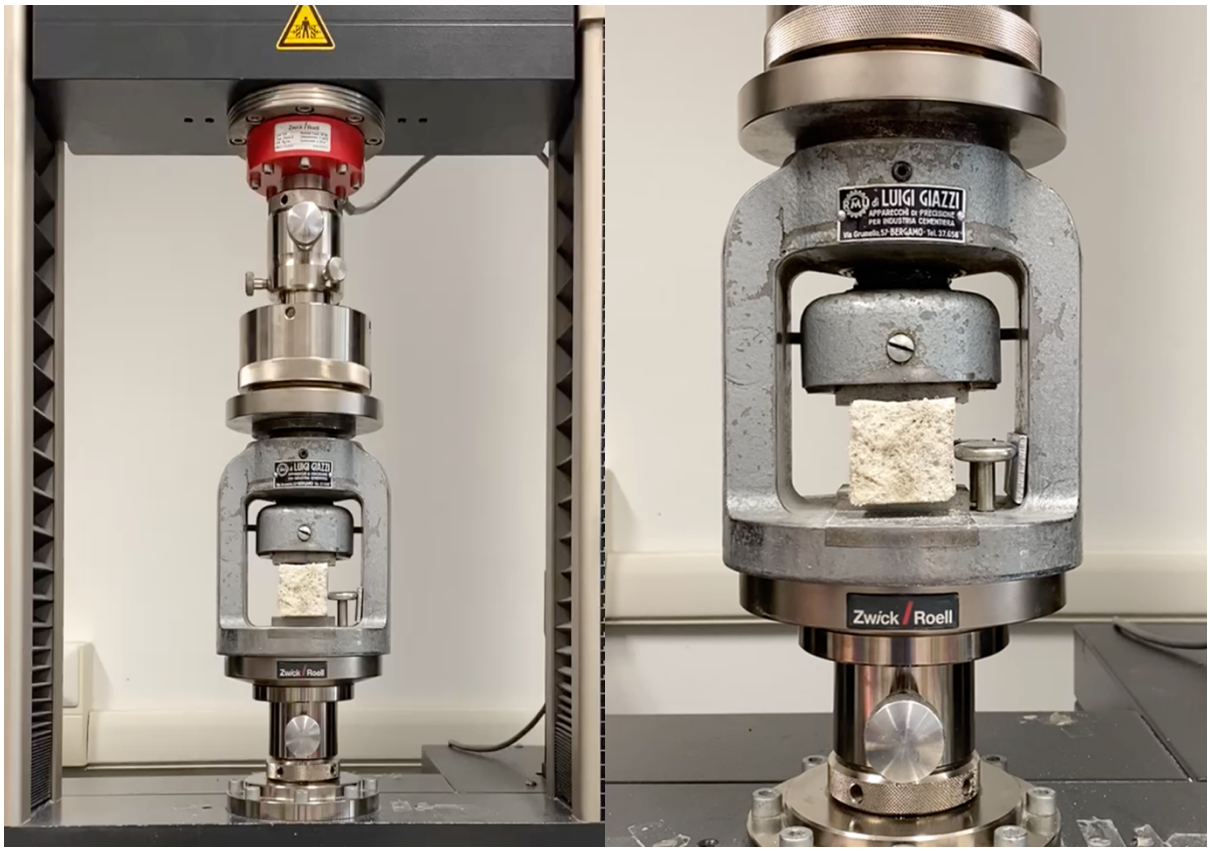

Figure 146. Image showing the sample positioning on the machine for the compressive strength tests.

- First part of the experimental campaign:

The first part of the experimental campaign consisted of finding the most efficient fiber treatment, length, and content. Bellow, the compressive strength test results for finding the fiber treatment are displayed graphically.

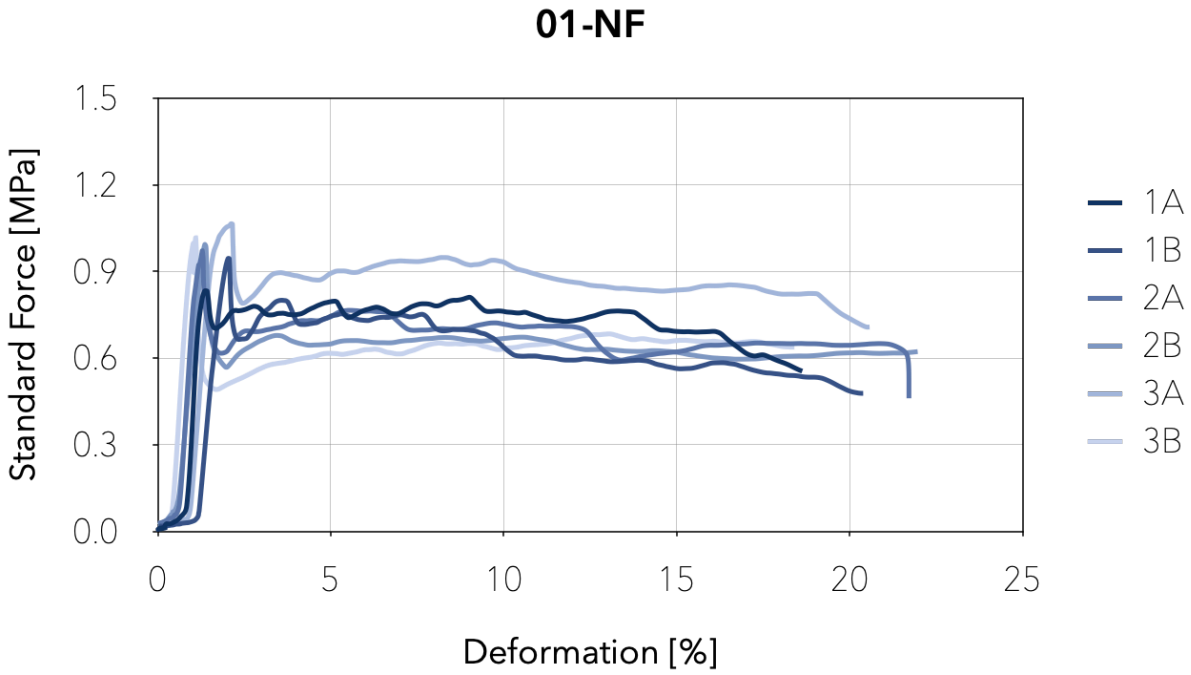

Figure 147. Image showing the compressive strength results of the three samples evaluated for the admixture without fibers (01-NF).

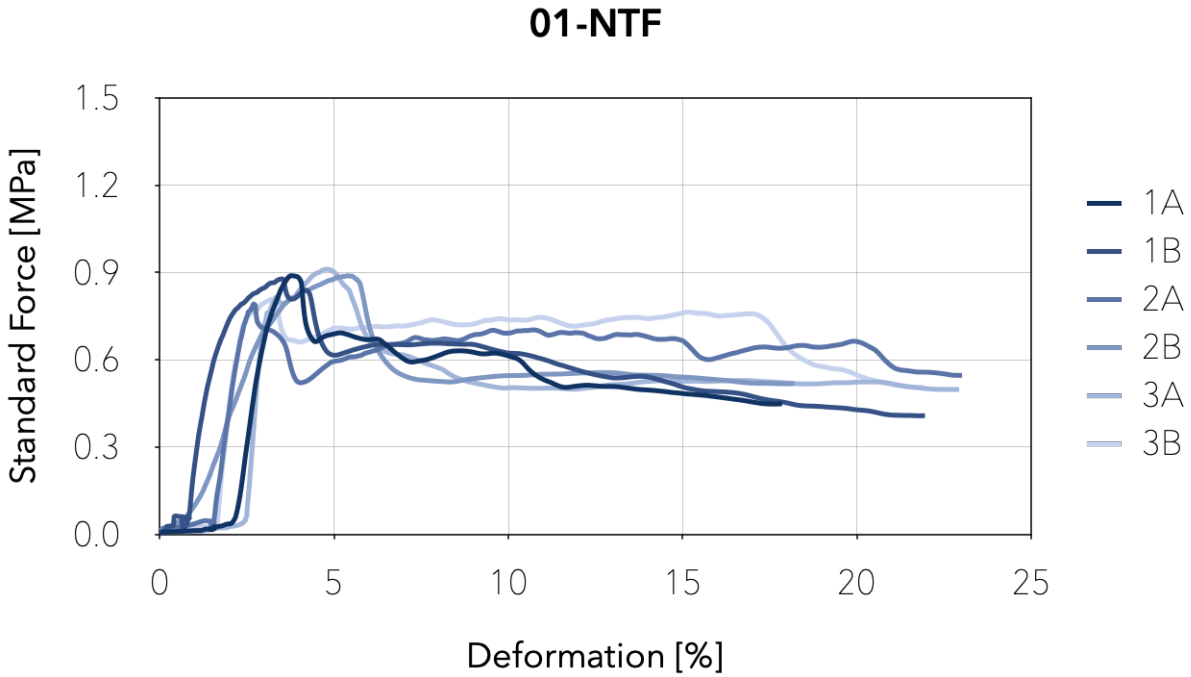

Figure 148. Image showing the compressive strength results of the three samples evaluated for the admixture with non-treated fibers (01-NTF).

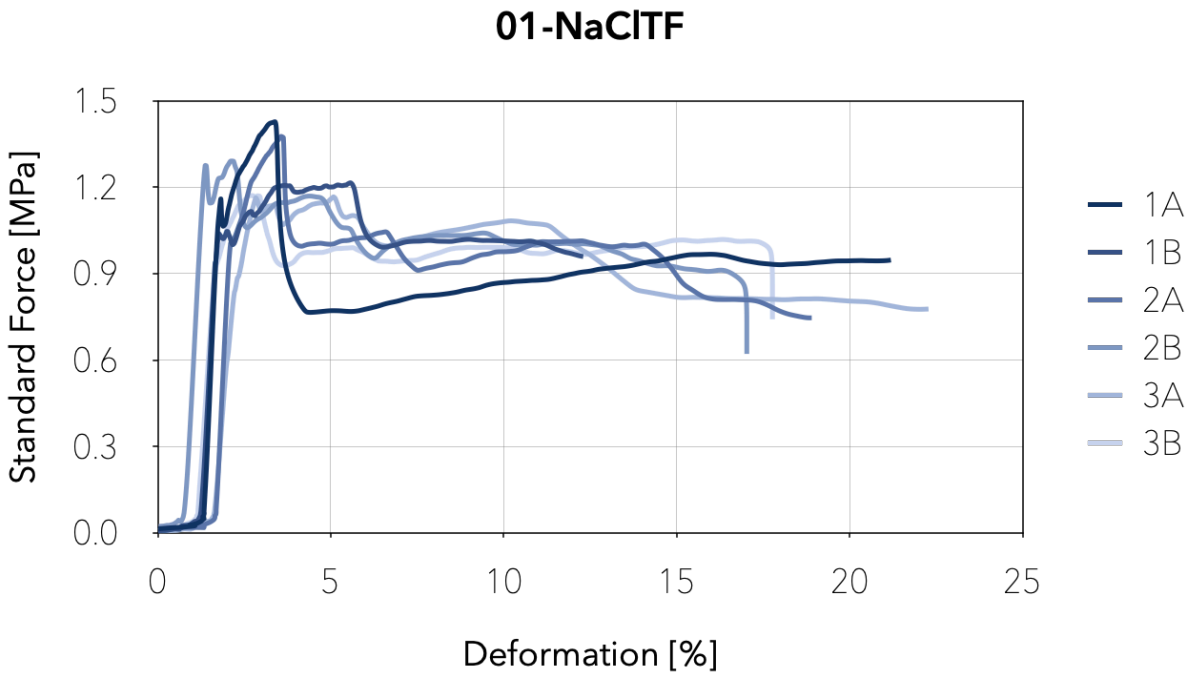

Figure 149. Image showing the compressive strength results of the three samples evaluated for the admixture with salt-treated fibers (01-NaClTF).

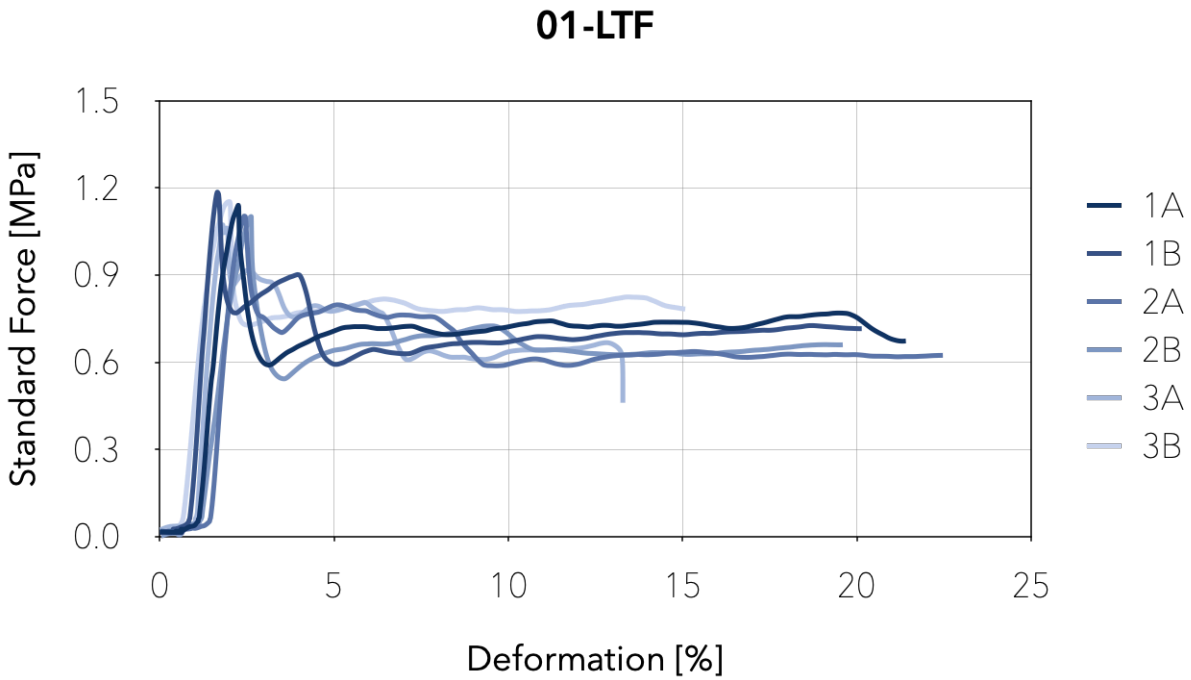

Figure 150. Image showing the compressive strength results of the three samples evaluated for the admixture with lime-treated fibers (01-LTF).

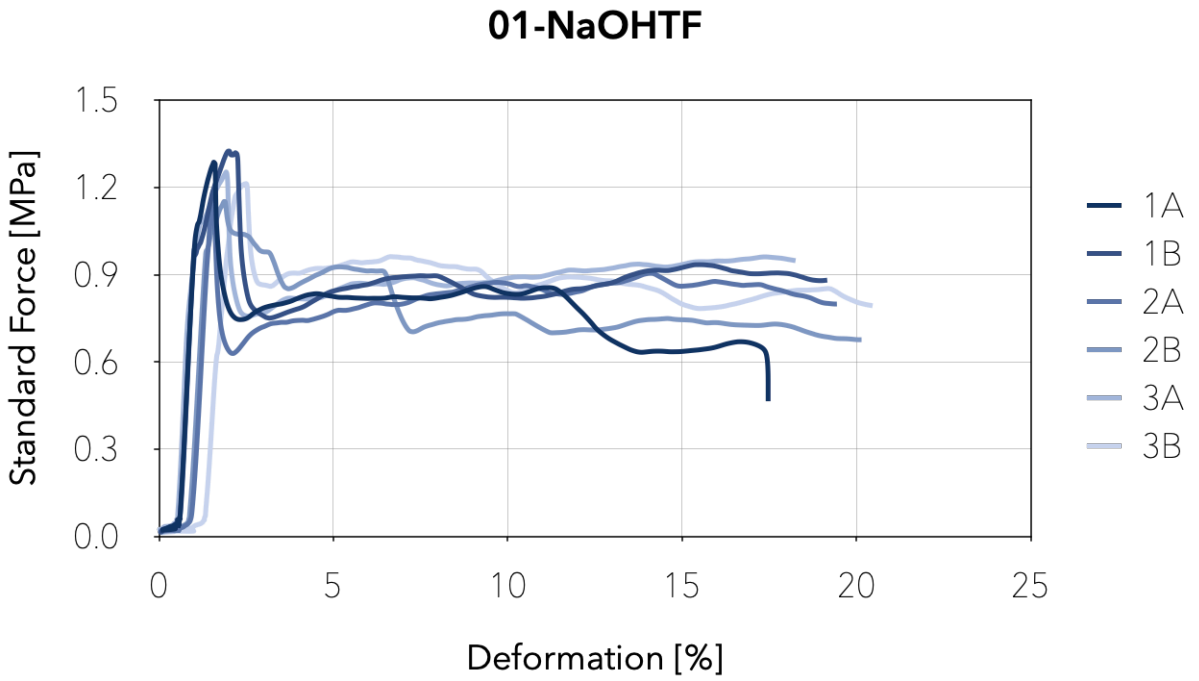

Figure 151. Image showing the compressive strength results of the three samples evaluated for the admixture with sodium hydroxide-treated fibers (01-NaOHTF).

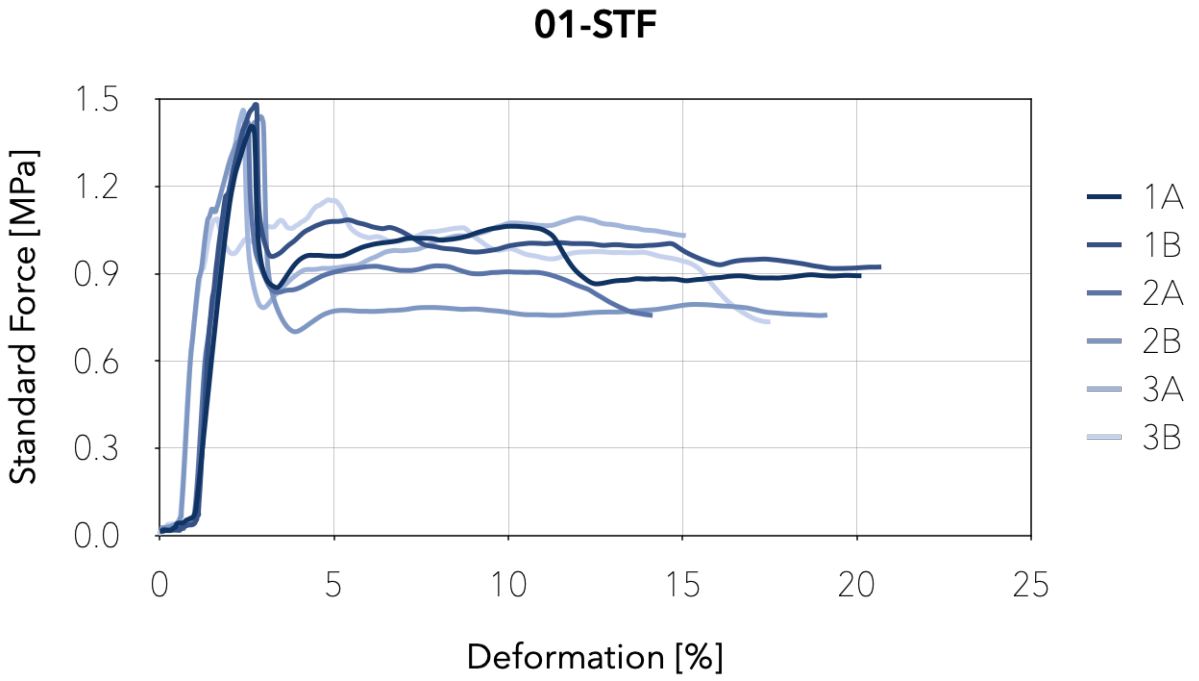

Figure 152. Image showing the compressive strength results of the three samples evaluated for the admixture with surfactant-treated fibers (01-STF).

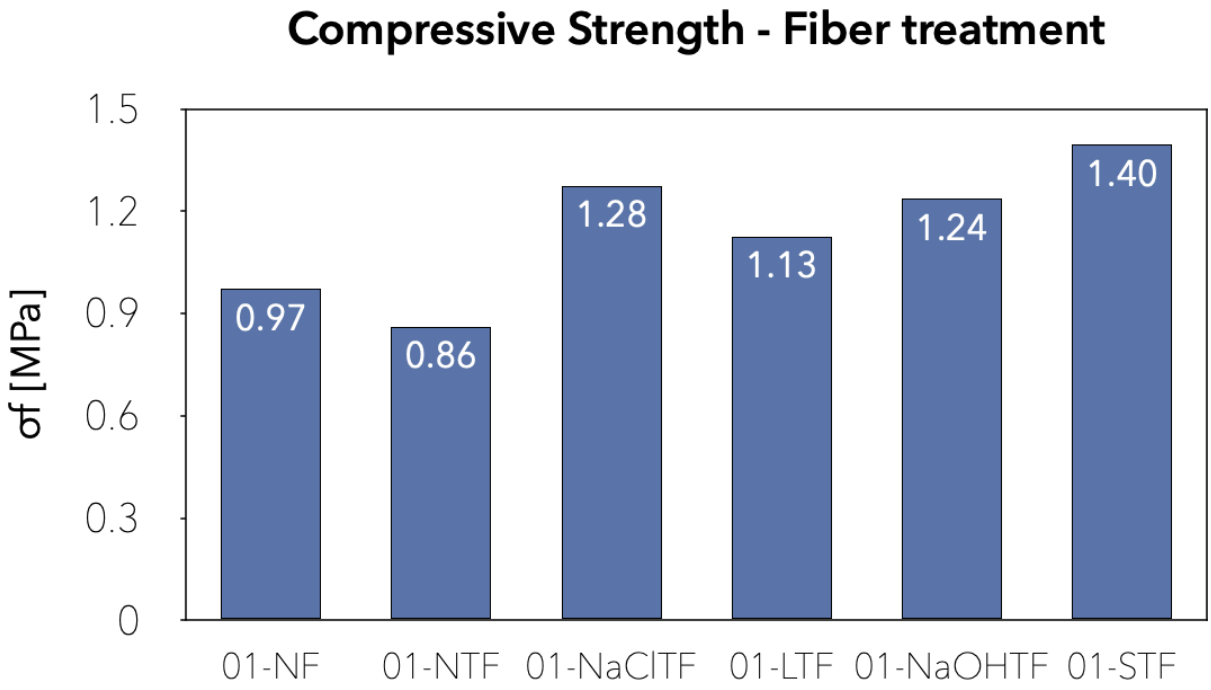

Figure 153. Graph with the average maximum compressive strength of the admixtures analyzed for fiber selection.

In the previous graphs, it can be observed that the admixtures with treated SWF present a higher compressive strength than the admixtures without fibers and with NTF. The fibers treated with the foaming surfactant presented the highest average result in compressive strength, presenting an improvement of 44% concerning the samples without fibers. They were followed by the admixtures treated with salt and sodium hydroxide; the former presents a rise of 32% and the latter of 29%. Despite losing its resistance properties, the NaOHTF accomplished the third-highest flexural strength average. LTF follows with a 17% improvement from the original non-fiber composites. In addition, NTF admixtures presented the lowest compressive strength decreasing by 11%.

Considering the previous information, it is possible to determine that the addition of treated SWF significantly improves the compressive strength of foamed concrete. Furthermore, the evaluation of these results suggests an improvement in the compressive performance only exists when the fibers are treated prior to their incorporation into the mix.

The following dispersion graph shows the average compressive strength of the samples on the Y-axis and the average density after 28 days of maturation on the X-axis.

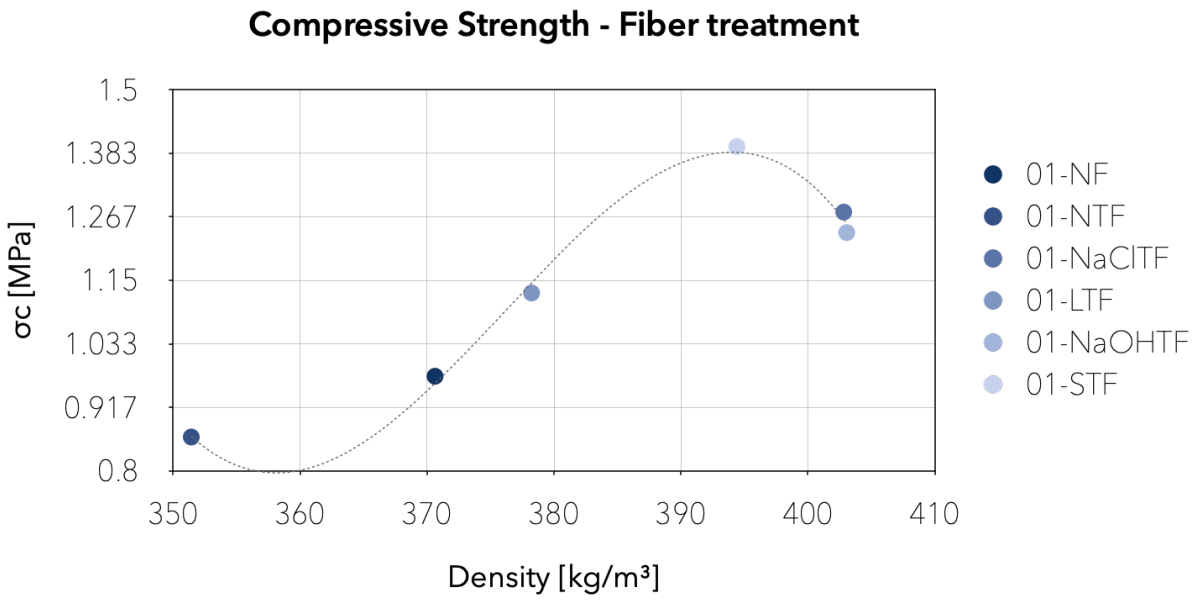

Figure 154. Dispersion graph of the average compressive strength of the admixtures analyzed for fiber treatment selection compared to the average density measured after 28 days of maturation.

Generally, a concrete admixture with a higher density also has a better mechanical performance. Therefore, an analysis considering both parameters is key to understanding the fundamental factors of the variation of the mechanical properties of each set of samples. For example, Figure 154 shows that as the density increases, the compressive strength increases as well, except for the samples from the admixtures 01-NaOHTH and 01-NaClTF, which, although having a higher density than 01-STF, have a lower compressive performance.

The following analysis focused on the fiber length. The experimentation focused on individuating the most performant length between 6, 12, and 20 mm. This analysis considered a density of 300kg/m^3 and the inclusion of NTF at a 2,5% F/C ratio. The following images display the results of the flexural strength measurements developed on the samples after 28 days of maturation.

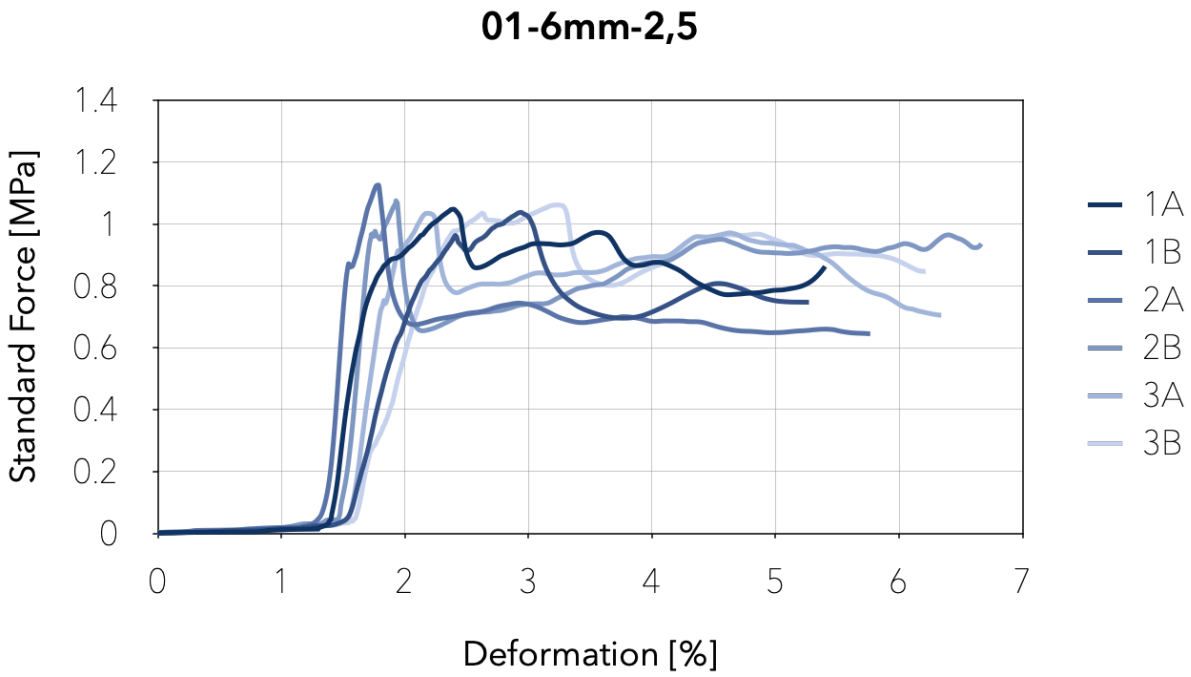

Figure 155. Image showing the compressive strength results of the three samples evaluated for the admixture with 6mm fibers and 2,5% F/C ratio (01-6mm-2,5).

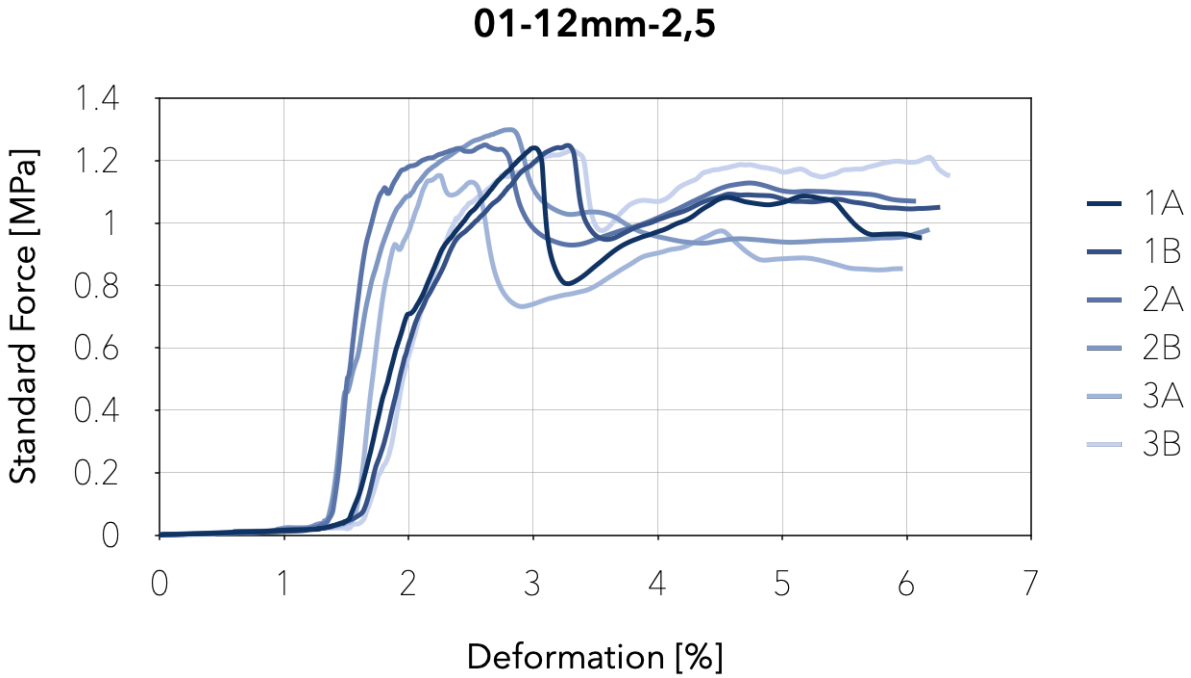

Figure 156. Image showing the compressive strength results of the three samples evaluated for the admixture with 12mm fibers and 2,5% F/C ratio (01-12mm-2,5).

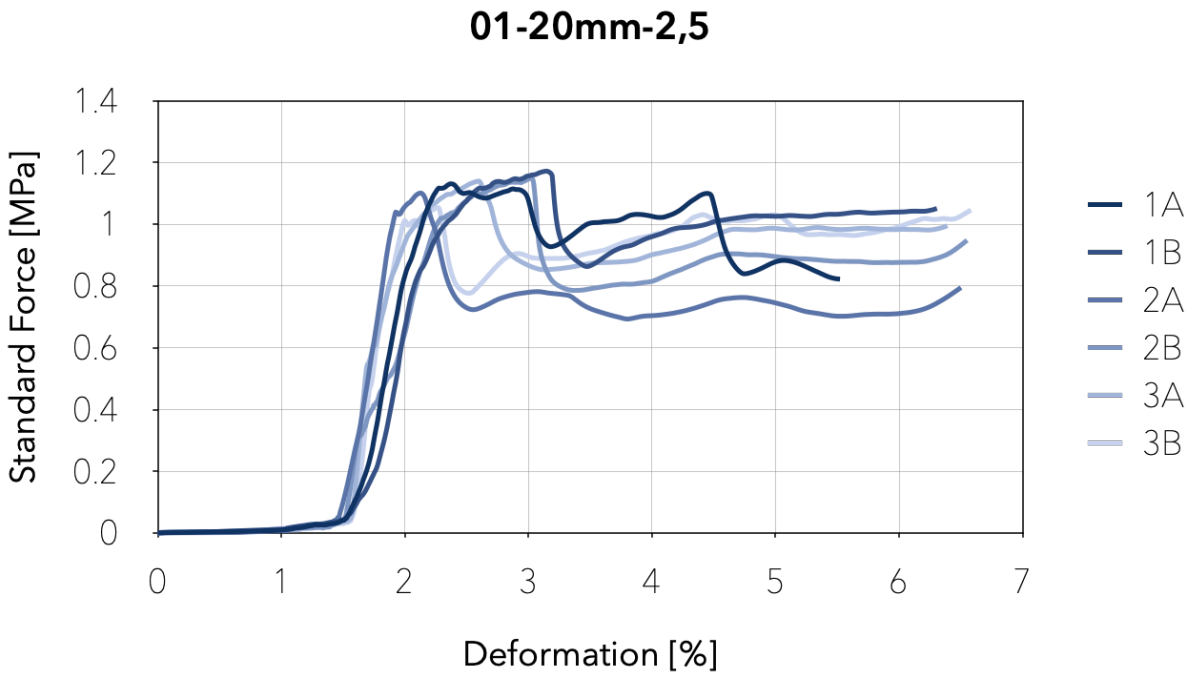

Figure 157. Image showing the compressive strength results of the three samples evaluated for the admixture with 20mm fibers and 2,5% F/C ratio (01-20mm-2,5).

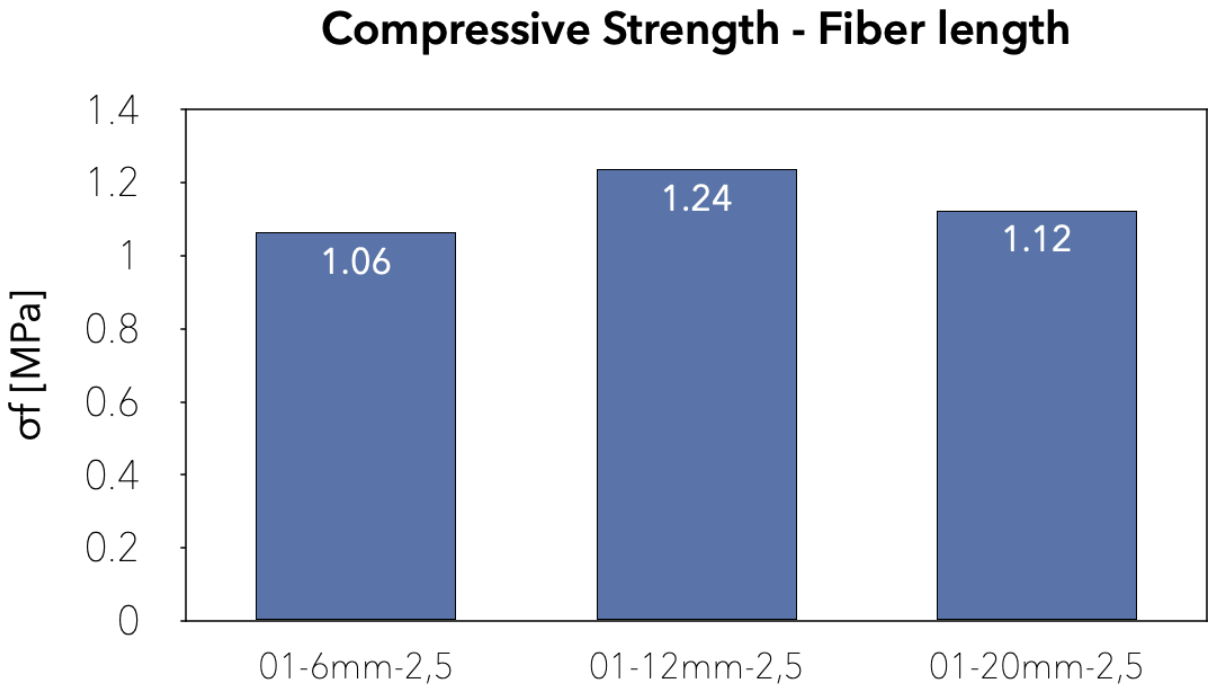

Figure 158. Graph with the average maximum compressive strength of the admixtures analyzed for fiber length selection.

The previous images show a similar behavior between the admixtures with 6 and 20mm. In comparison, the samples with 12mm fibers have a higher compressive strength. In addition, the following dispersion graph shows the average compressive strength of the samples on the Y-axis and the average density after 28 days of maturation on the X-axis.

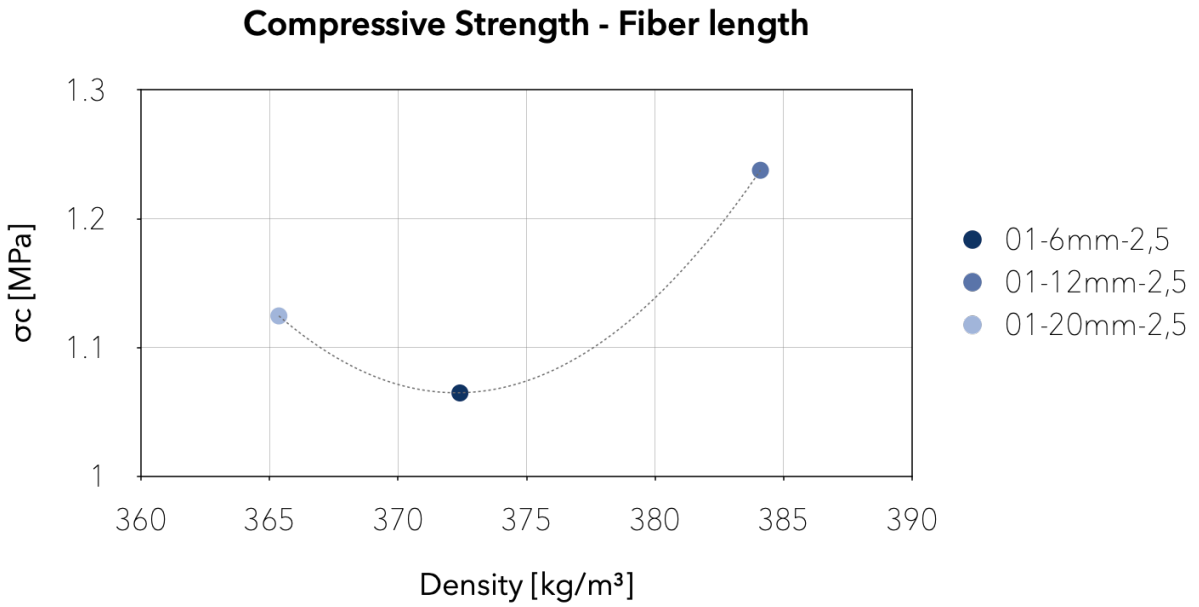

Figure 159. Dispersion graph of the average compressive strength of the admixtures analyzed for fiber length selection compared to the average density measured after 28 days of maturation.

The dispersion graph above shows that even though the 01-12mm-2,5 has a 16% higher flexural strength than 01-6mm-2,5. However, their density only differs by 3%, meaning that the 12mm fibers present the highest advantage for compressive strength.

Additionally, the experimentation focused on individuating the most performant F/C ratio between 2,5, 5, and 10%. This analysis considered a density of 300kg/m^3 and the inclusion of 12mm NTF. The following images display the results of the compressive strength measurements developed on the samples after 28 days of maturation. The admixture 01-12mm-2,5 used on the fiber length analysis also contributes to finding the F/C ratio.

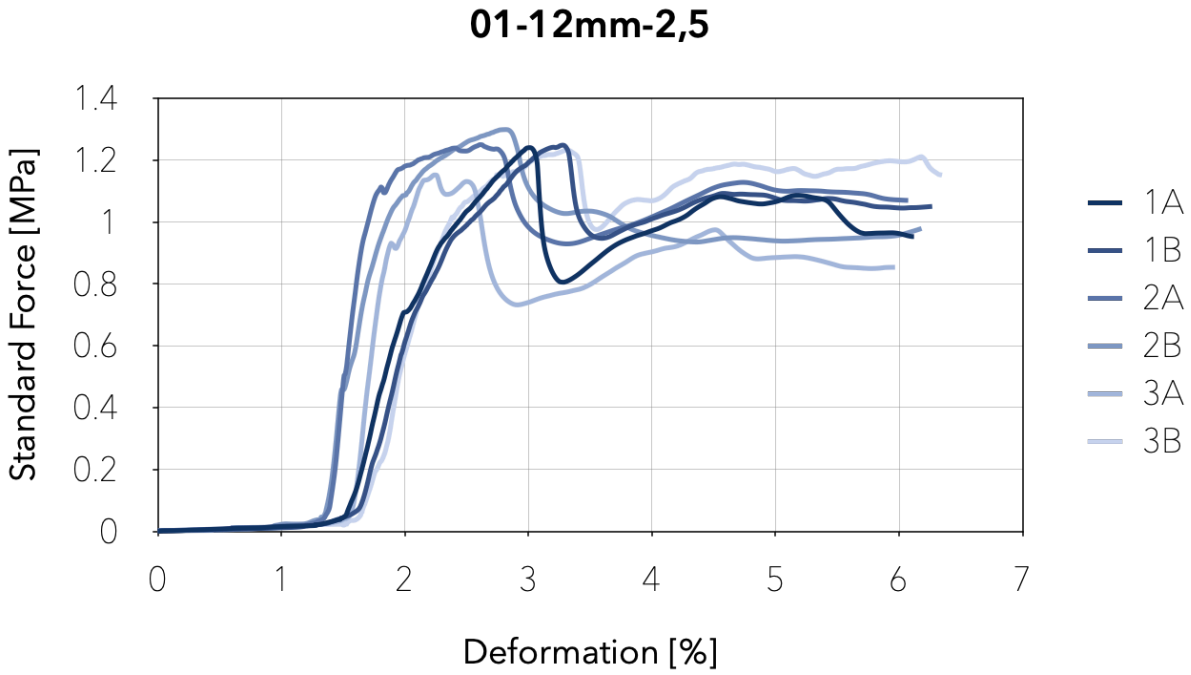

Figure 160. Image showing the compressive strength results of the three samples evaluated for the admixture with 12mm fibers and 2,5% F/C ratio (01-12mm-2,5).

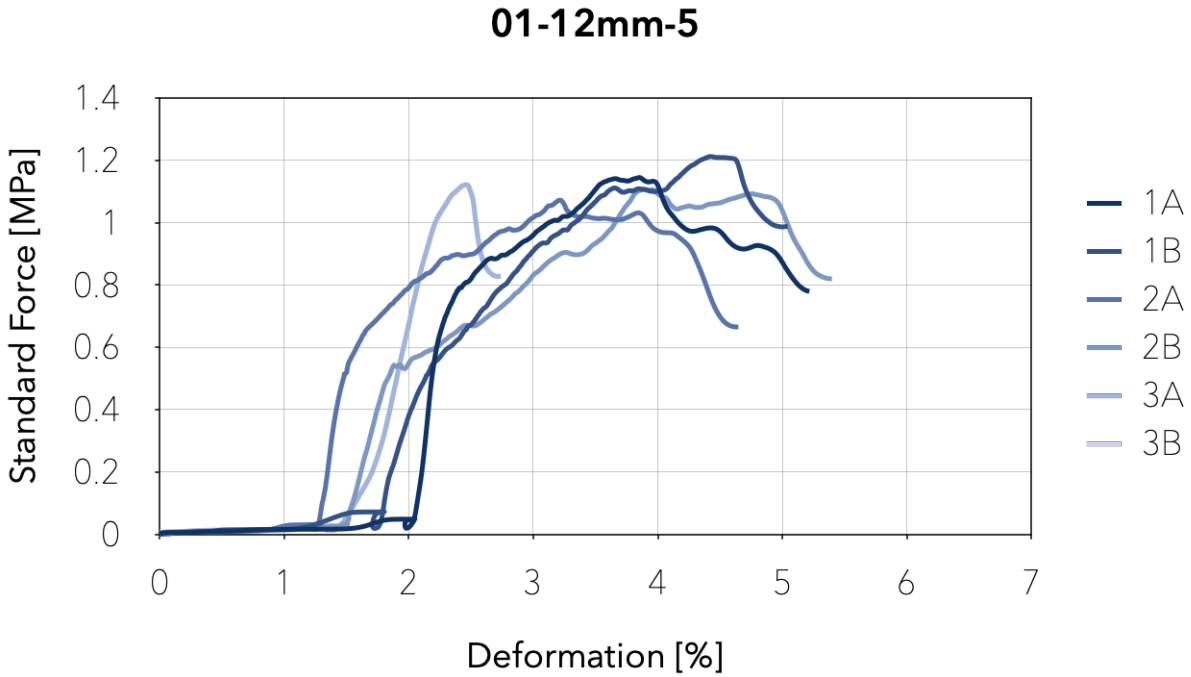

Figure 161. Image showing the compressive strength results of the three samples evaluated for the admixture with 12mm fibers and 5% F/C ratio (01-12mm-5).

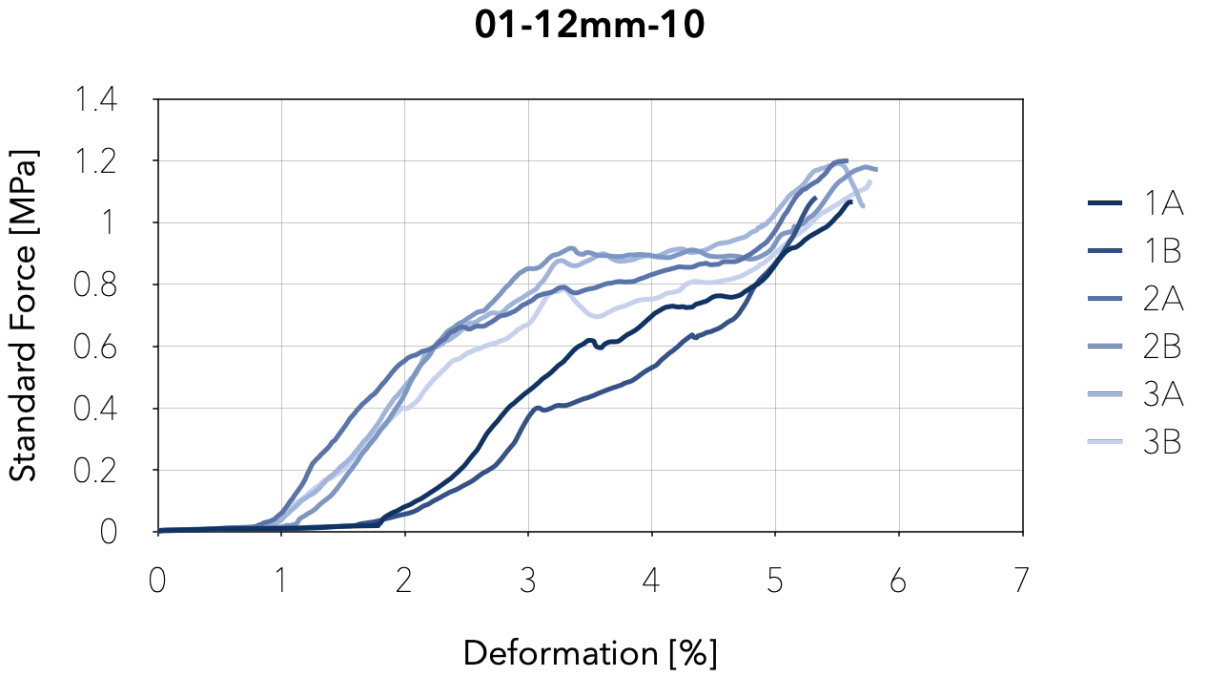

Figure 162. Image showing the compressive strength results of the three samples evaluated for the admixture with 12mm fibers and 10% F/C ratio (01-12mm-10).

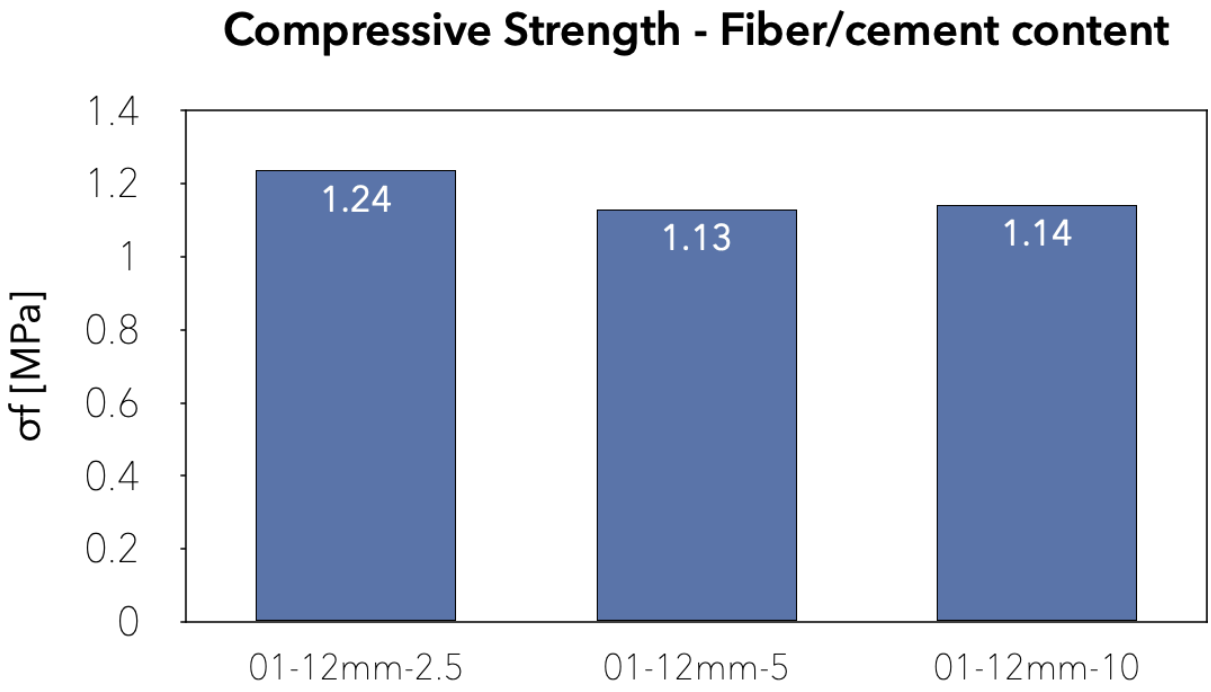

Figure 163. Graph with the average maximum compressive strength of the admixtures analyzed for fiber content selection.

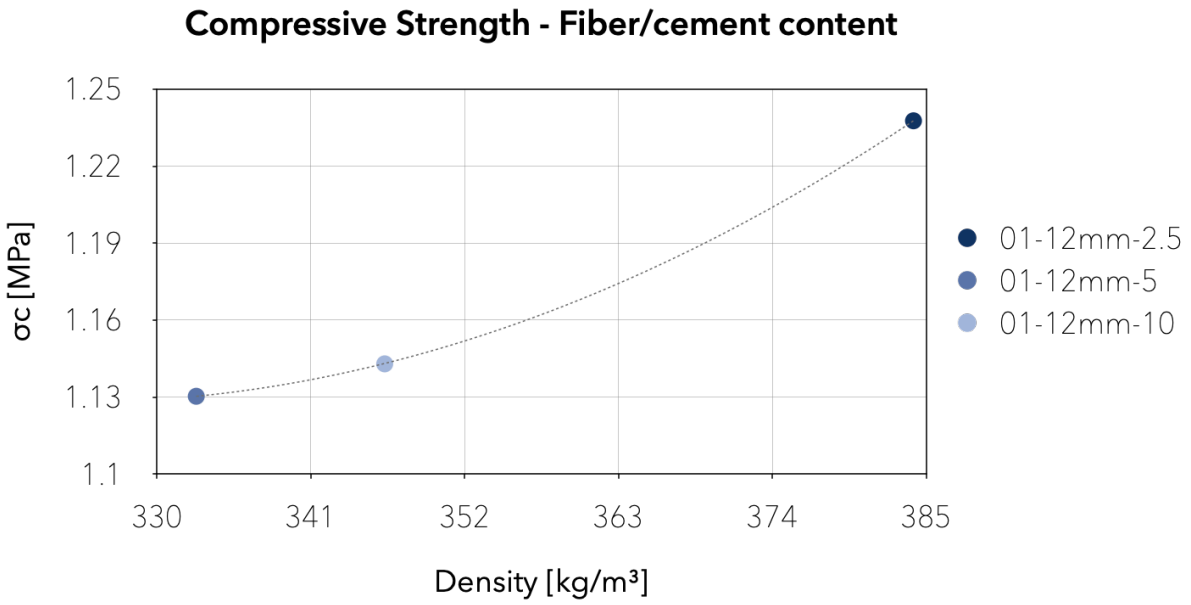

Figure 164. Dispersion graph of the average compressive strength of the admixtures analyzed for fiber content selection compared to the average density measured after 28 days of maturation.

The previous graphs show that the admixture 01-12mm-2,5 presents a higher compressive strength and a higher deformation capacity, making this the best option for compressive strength in terms of F/C ratio.

- Second part of the experimental campaign:

The second part of this research consisted of applying the chosen fiber properties to admixtures with different target densities (100, 300, and 500kg/m^3). Bellow, the compressive strength test results for a 100kg/m^3 target density are displayed graphically.

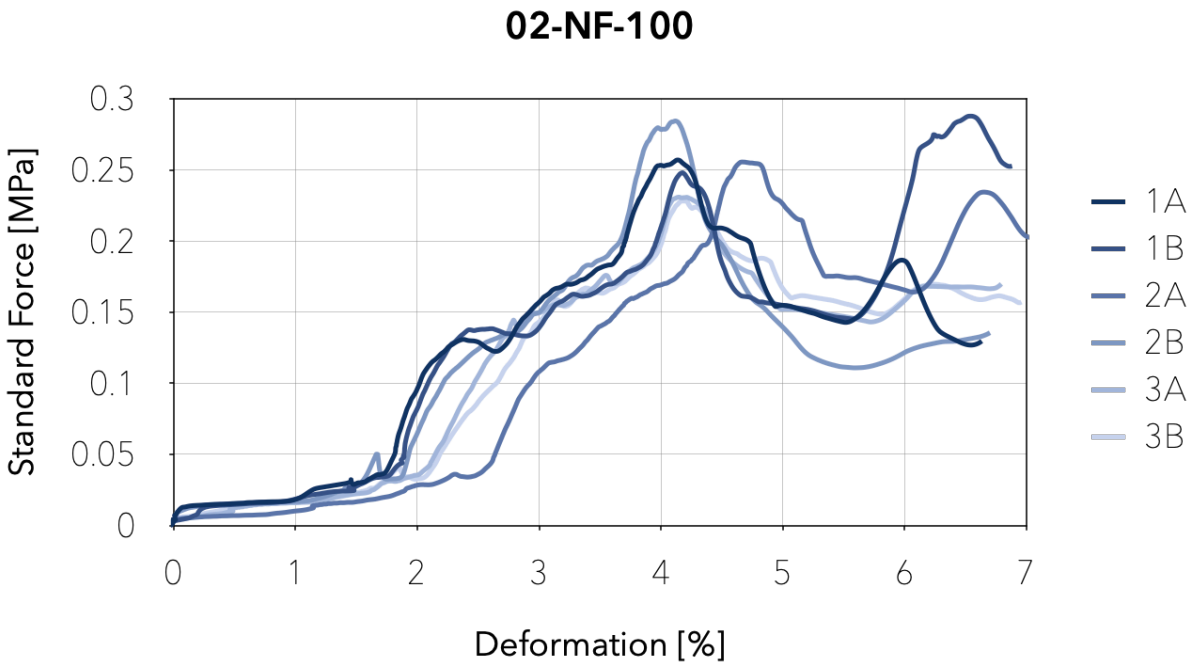

Figure 165. Image showing the compressive strength results of the three samples evaluated for the admixture 02-NF-100.

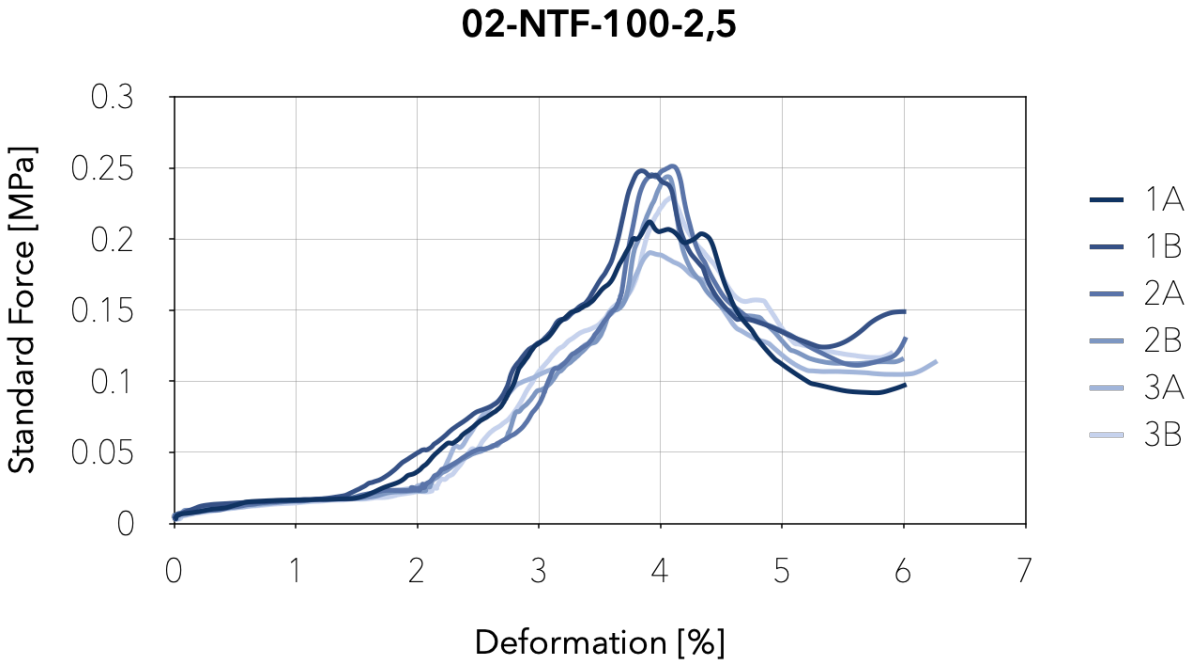

Figure 166. Image showing the compressive strength results of the three samples evaluated for the admixture 02-NTF-100-2,5.

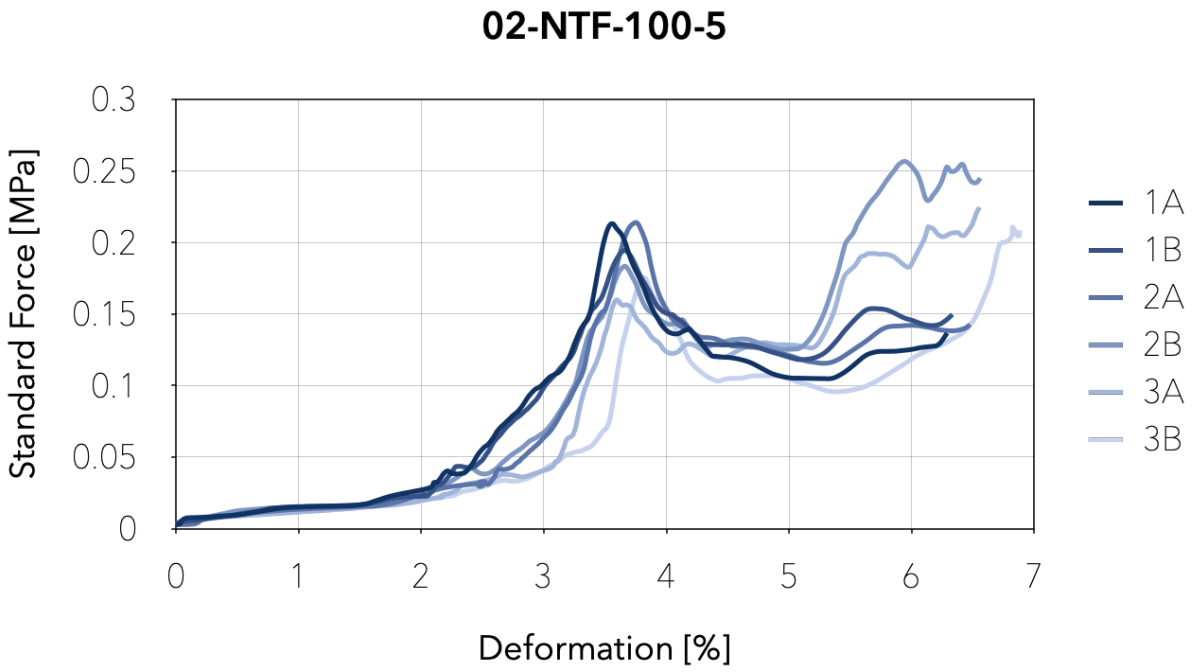

Figure 167. Image showing the compressive strength results of the three samples evaluated for the admixture 02-NTF-100-5.

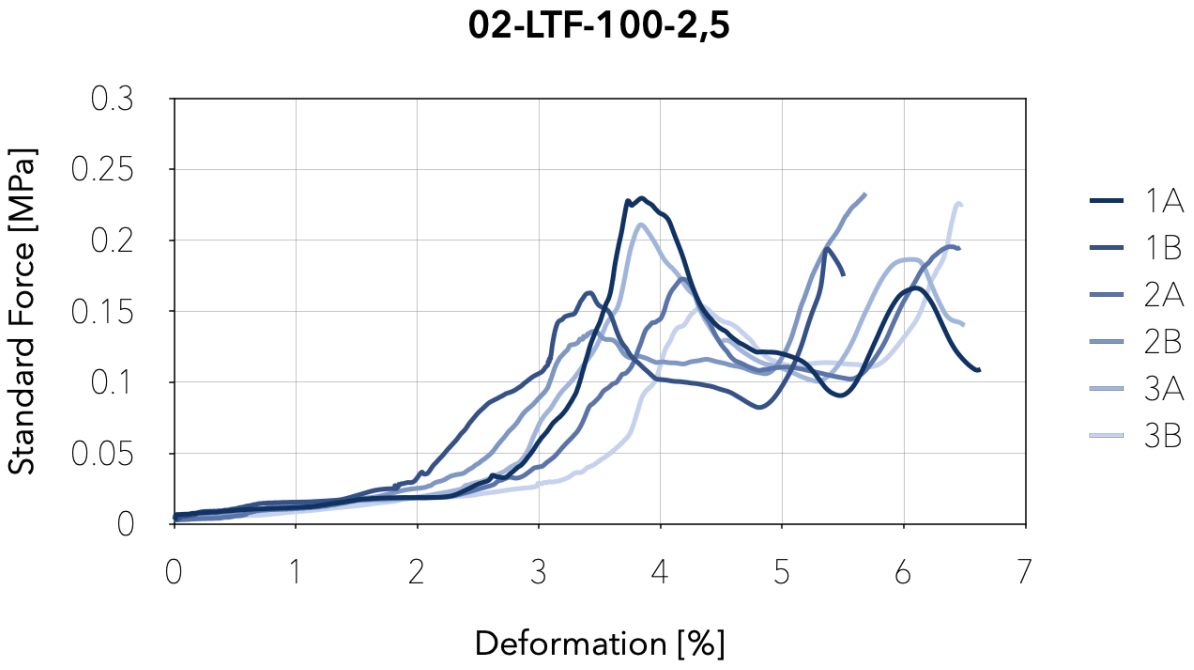

Figure 168. Image showing the compressive strength results of the three samples evaluated for the admixture 02-LTF-100-2,5.

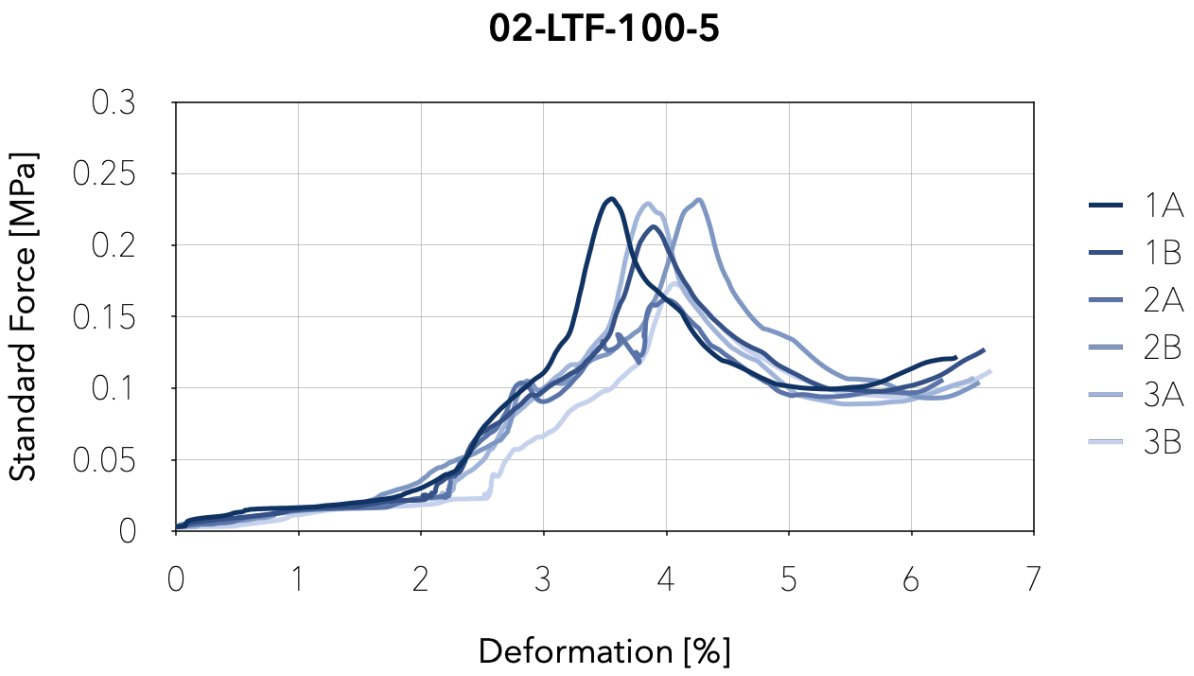

Figure 169. Image showing the compressive strength results of the three samples evaluated for the admixture 02-LTF-100-5.

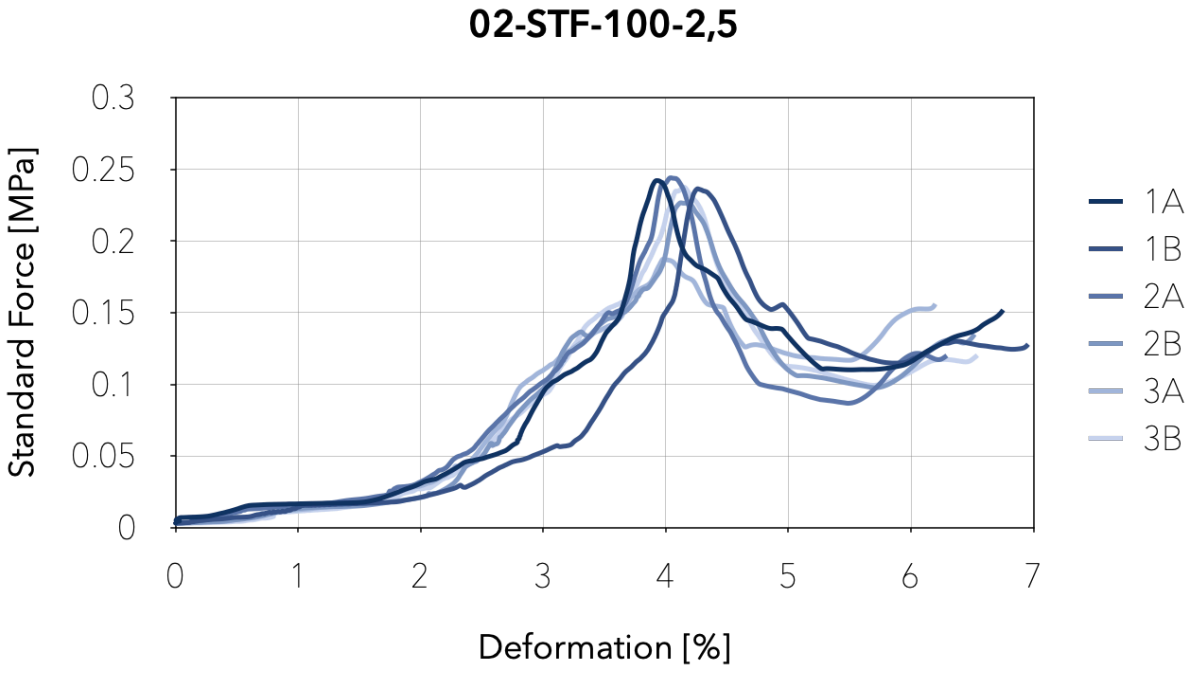

Figure 170. Image showing the compressive strength results of the three samples evaluated for the admixture 02-STF-100-2,5.

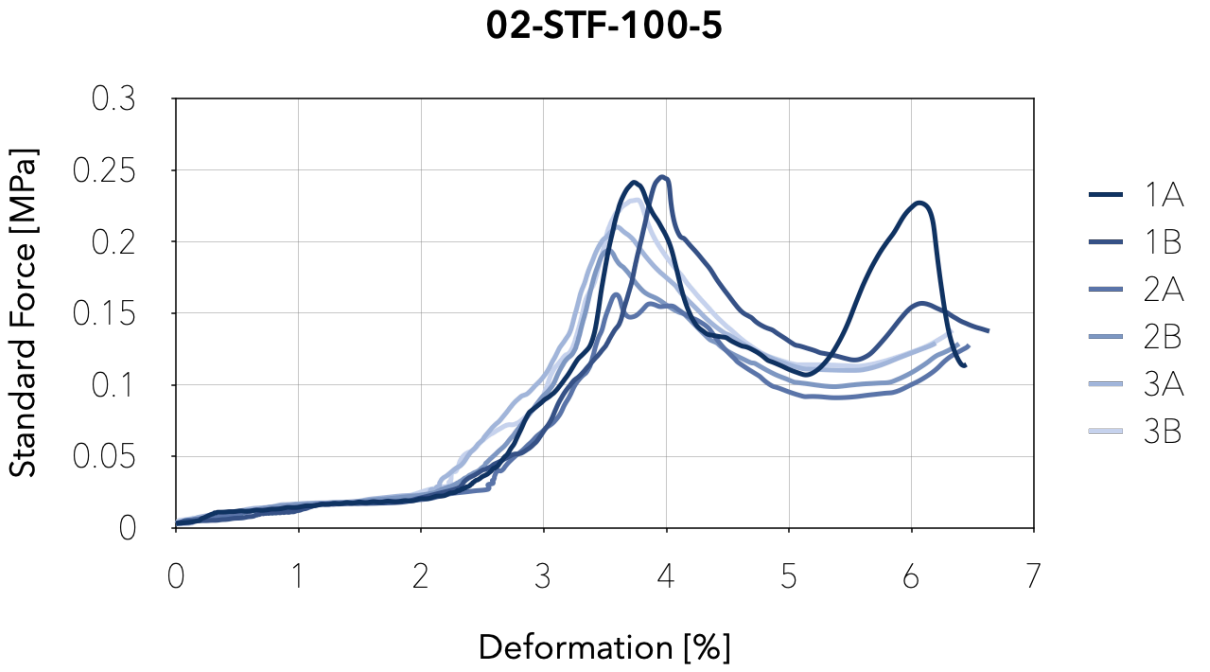

Figure 171. Image showing the compressive strength results of the three samples evaluated for the admixture 02-STF-100-5.

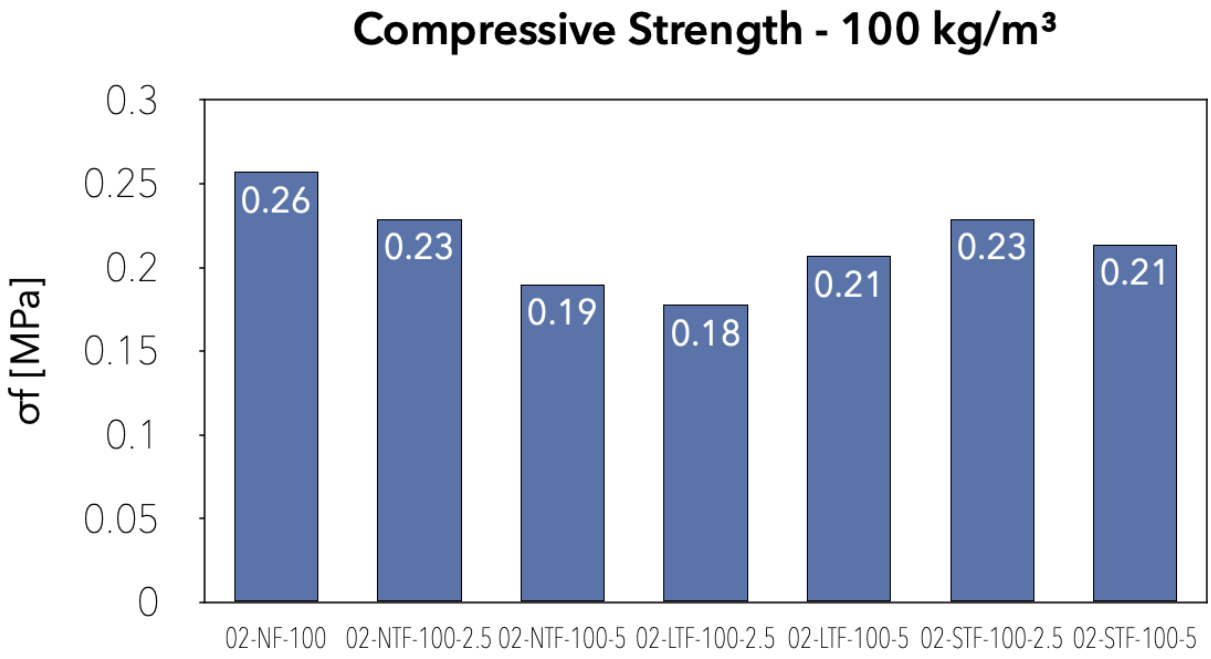

Figure 172. Graph showing the average maximum compressive strength of the admixtures with a 100kg/m³ target density.

The previous images show that the compressive strength decreases when adding fibers at a target density of 100kg/m^3. By analyzing admixtures 02-NTF-100-2,5 and 02-STF-100-2,5, the highest result with SWF, it comes out that the compressive strength of these admixtures is 12% lower than that of 01-NF-100. 02-LTF-100-5 and 02-STF-100-5 follow with a 19% lower resistance. Finally, 02-NTF-100-5 and 02-LTF-

100-2,5 are the least resistant to compressive pressing charges, the former by 27% and the latter by 30%.

It is fundamental to analyze how the fiber and cement content influences the compressive strength of each admixture. The following graphs display the results of this analysis.

Figure 173 shows that with a target density of 100kg/m^3 and NTF, the compressive strength of the admixture with a 2,5% F/C ratio decreases by 12%, but with a 5% F/C ratio, the compressive strength decreases by 27%. Figure 174 shows the results for LTF; in this case, the compressive strength is higher for the samples with a 2,5% F/C ratio and lower with a 5% F/C ratio; the admixture with a 2,5% F/C ratio has a 30% lower flexural strength while the one with a 5% F/C ratio a 19%. Figure 175 shows that with STF, the compressive strength of the admixture with a 2,5% F/C ratio decreases by 12%, while with a 5% ratio, it decreases by 19% compared to the admixture without fibers.

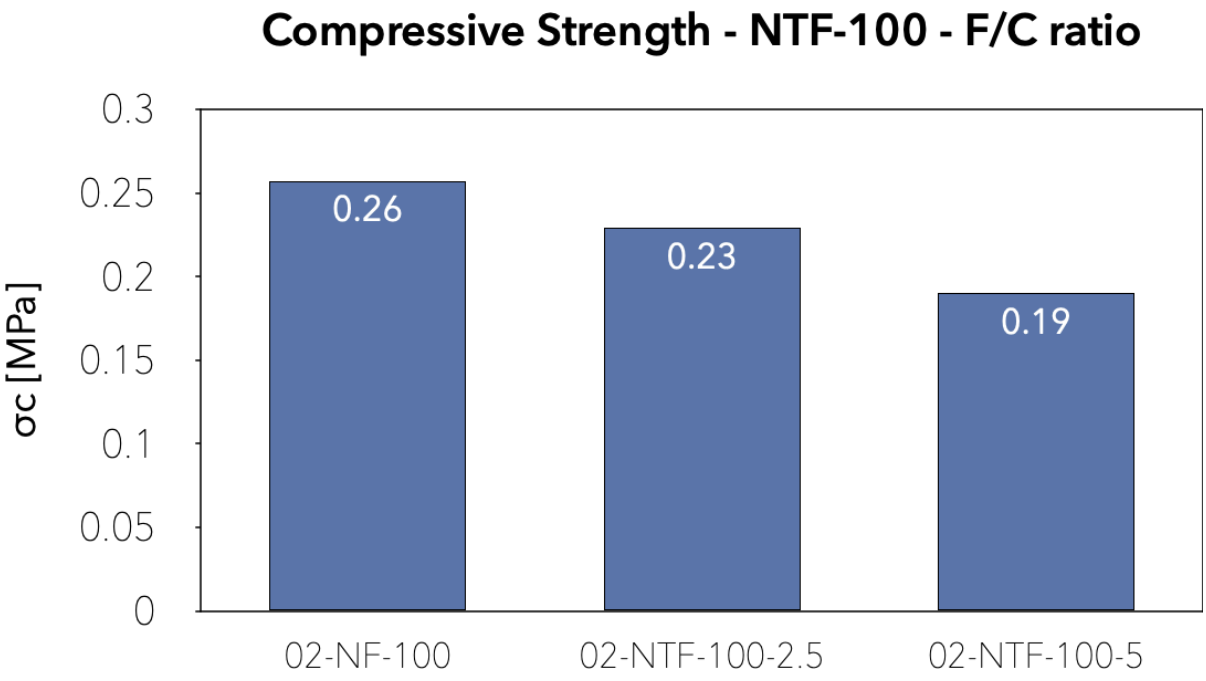

Figure 173. Graph showing the average maximum flexural strength of the admixtures with NTF and a 100kg/m³ target density.

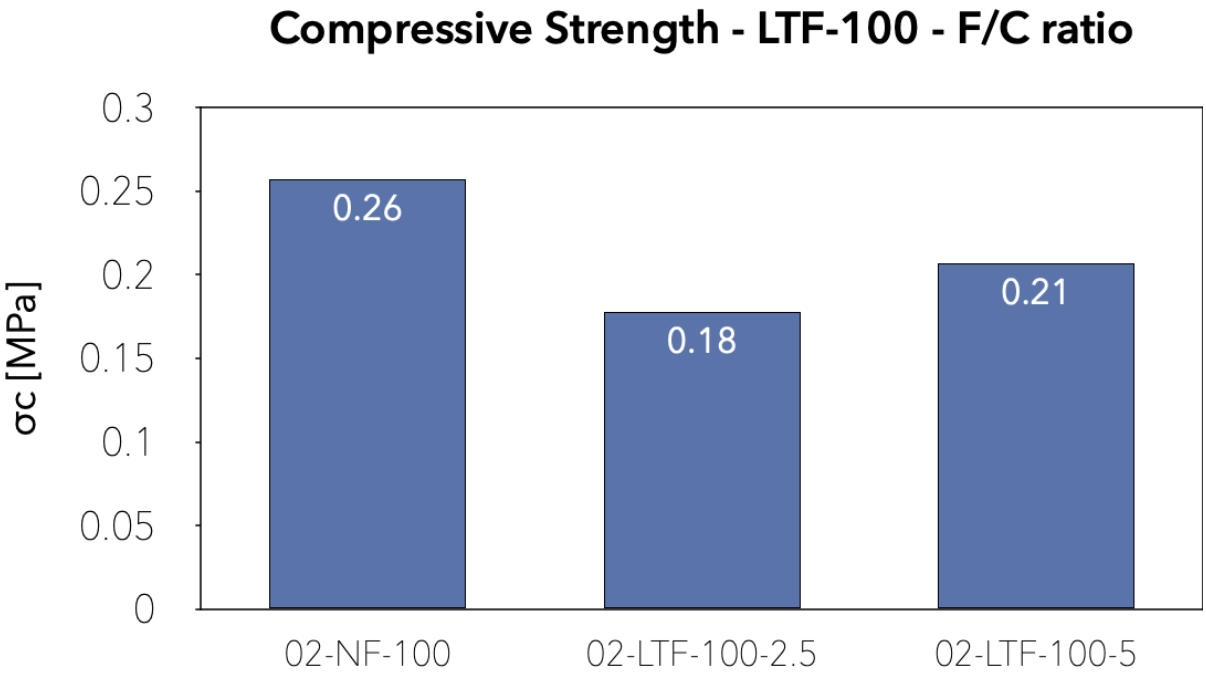

Figure 174. Graph showing the average maximum flexural strength of the admixtures with LTF and a 100kg/m³ target density.

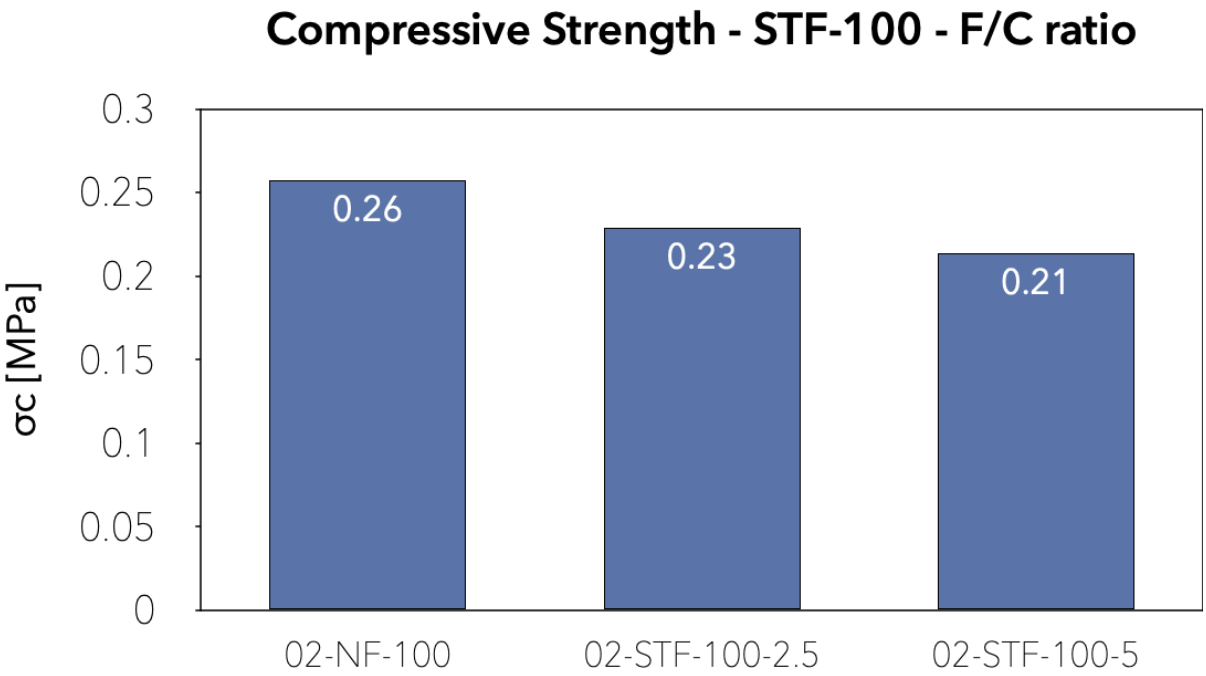

Figure 175. Graph showing the average maximum flexural strength of the admixtures with STF and a 100kg/m³ target density.

The following images show the flexural strength test results of the admixtures with a 300kg/m^3 target density.

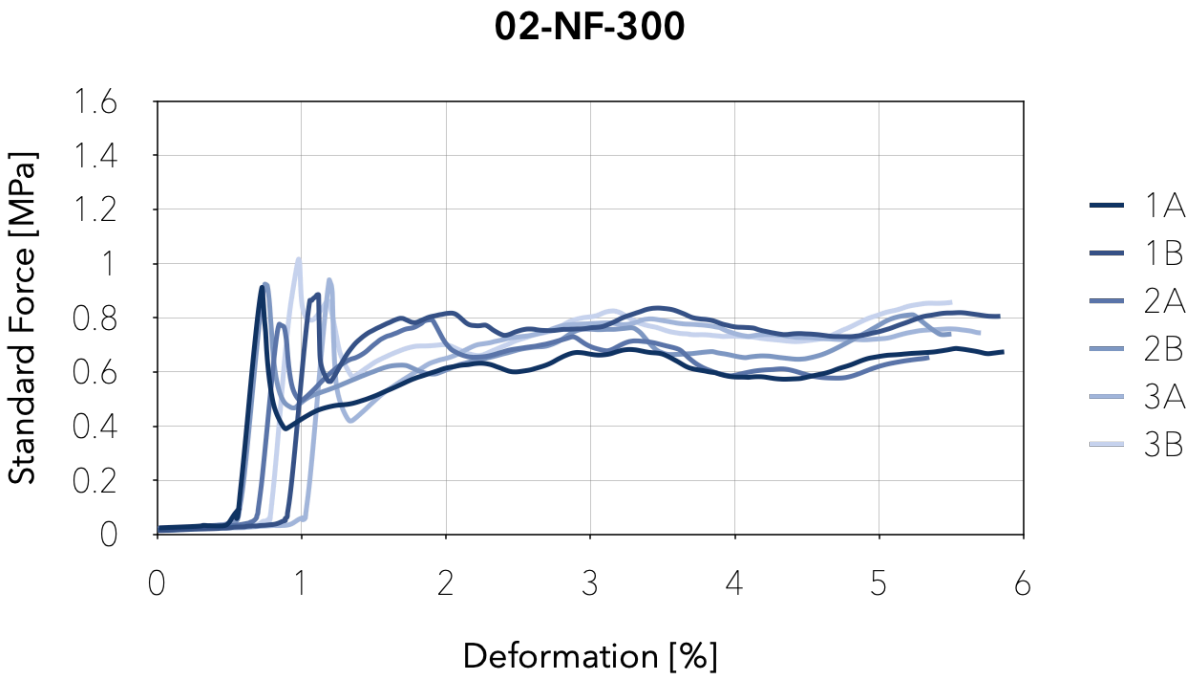

Figure 176. Image showing the compressive strength results of the three samples evaluated for the admixture 02-NF-300.

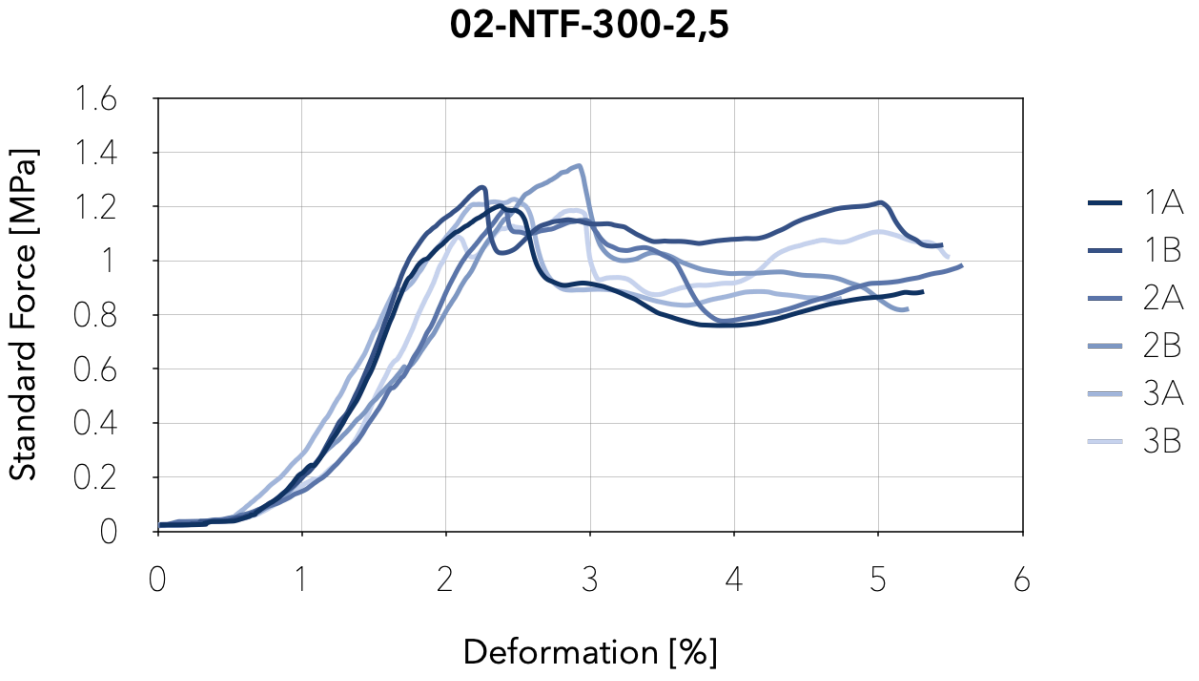

Figure 177. Image showing the compressive strength results of the three samples evaluated for the admixture 02-NTF-300-2,5.

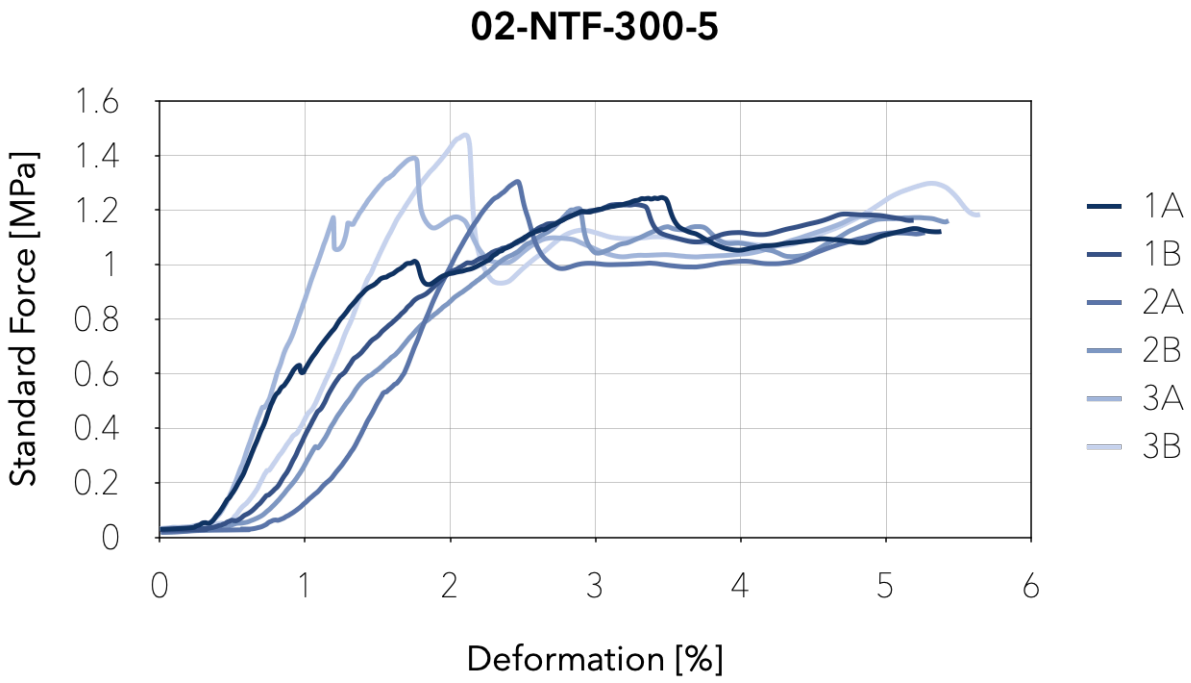

Figure 178. Image showing the compressive strength results of the three samples evaluated for the admixture 02-NTF-300-5.

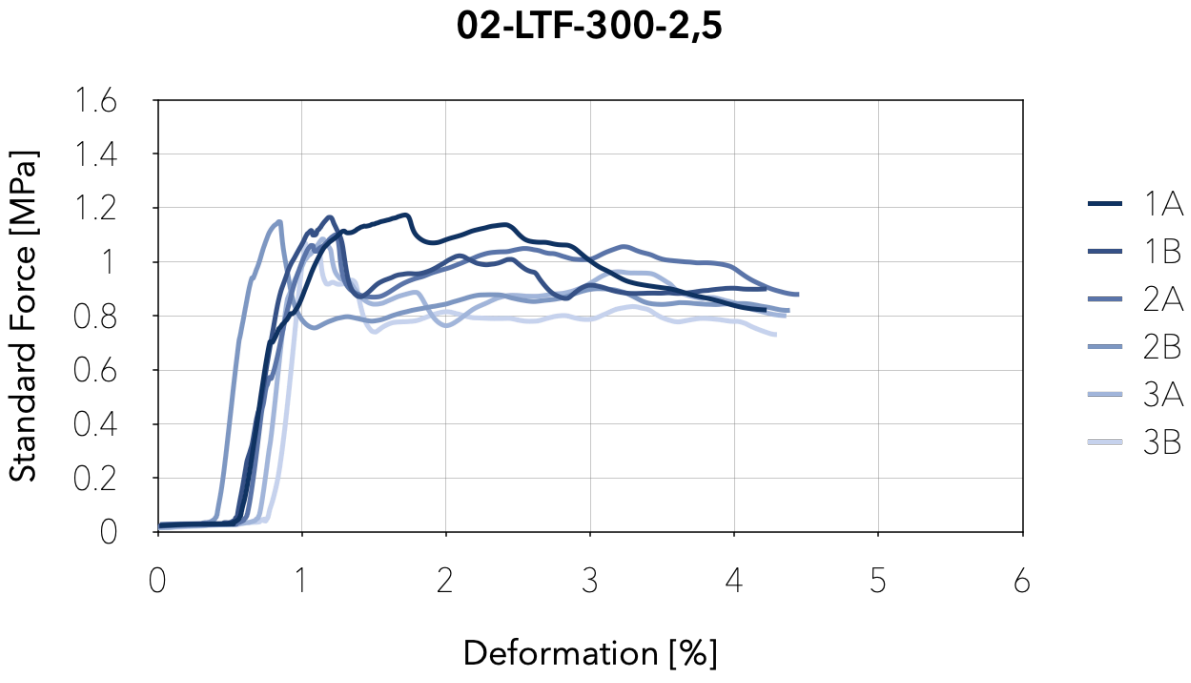

Figure 179. Image showing the compressive strength results of the three samples evaluated for the admixture 02-LTF-300-2,5.

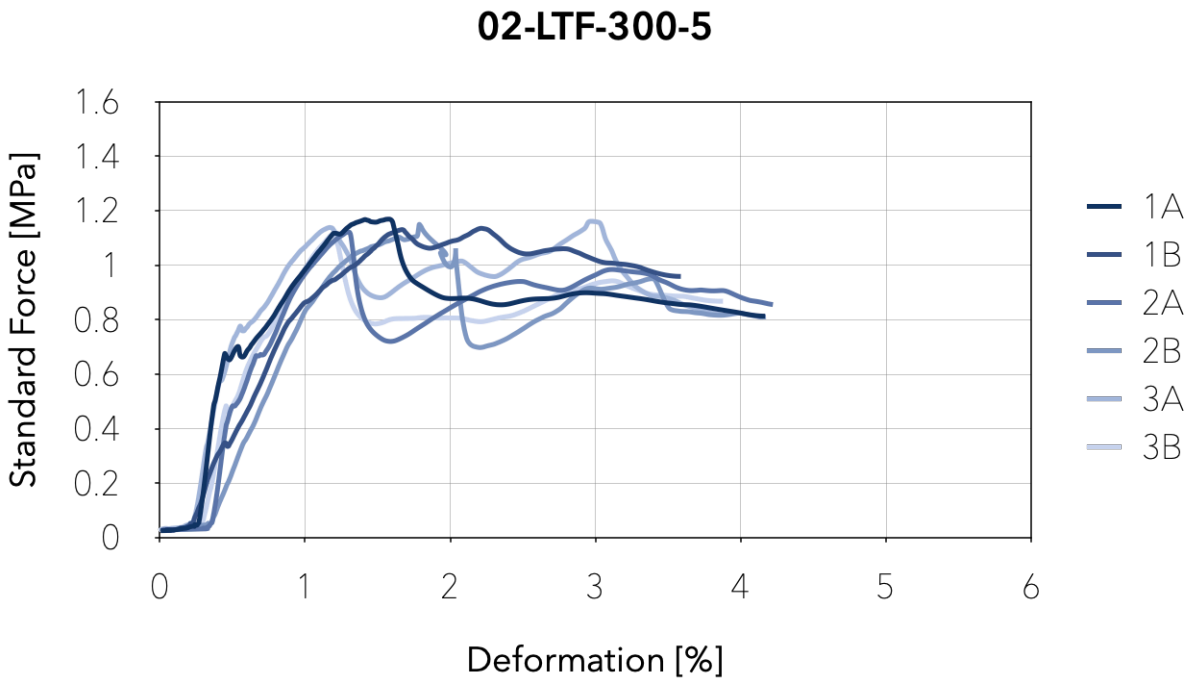

Figure 180. Image showing the compressive strength results of the three samples evaluated for the admixture 02-LTF-300-5.

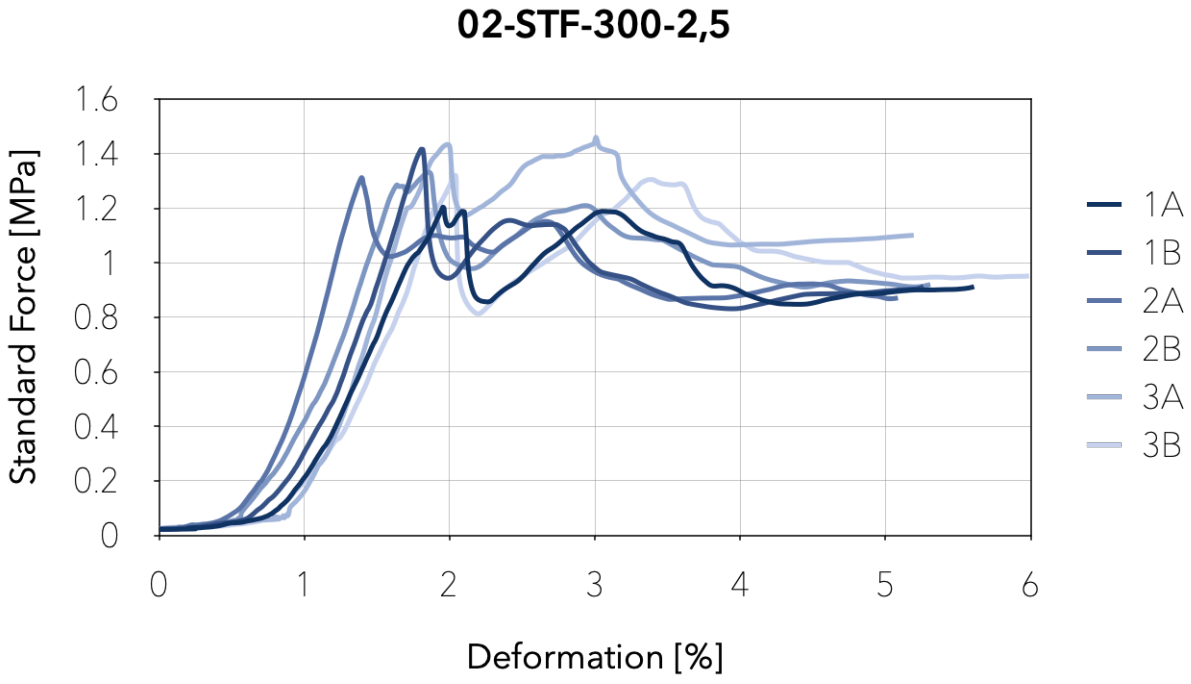

Figure 181. Image showing the compressive strength results of the three samples evaluated for the admixture 02-STF-300-2,5.

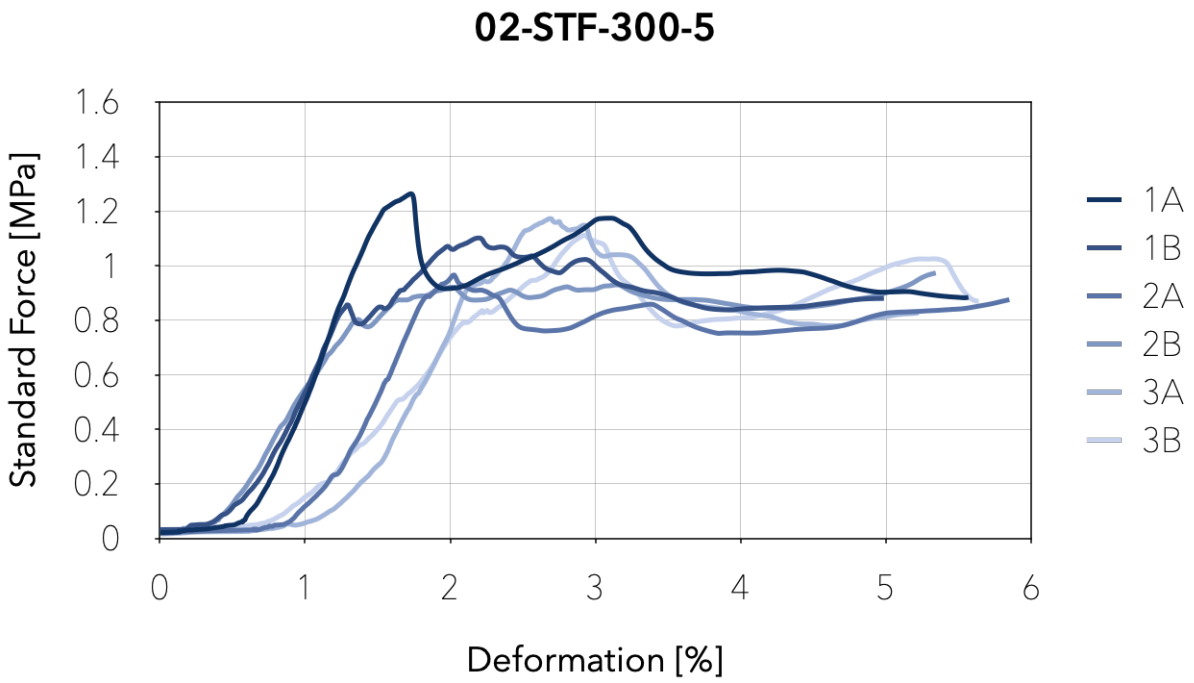

Figure 182. Image showing the compressive strength results of the three samples evaluated for the admixture 02-STF-300-5.

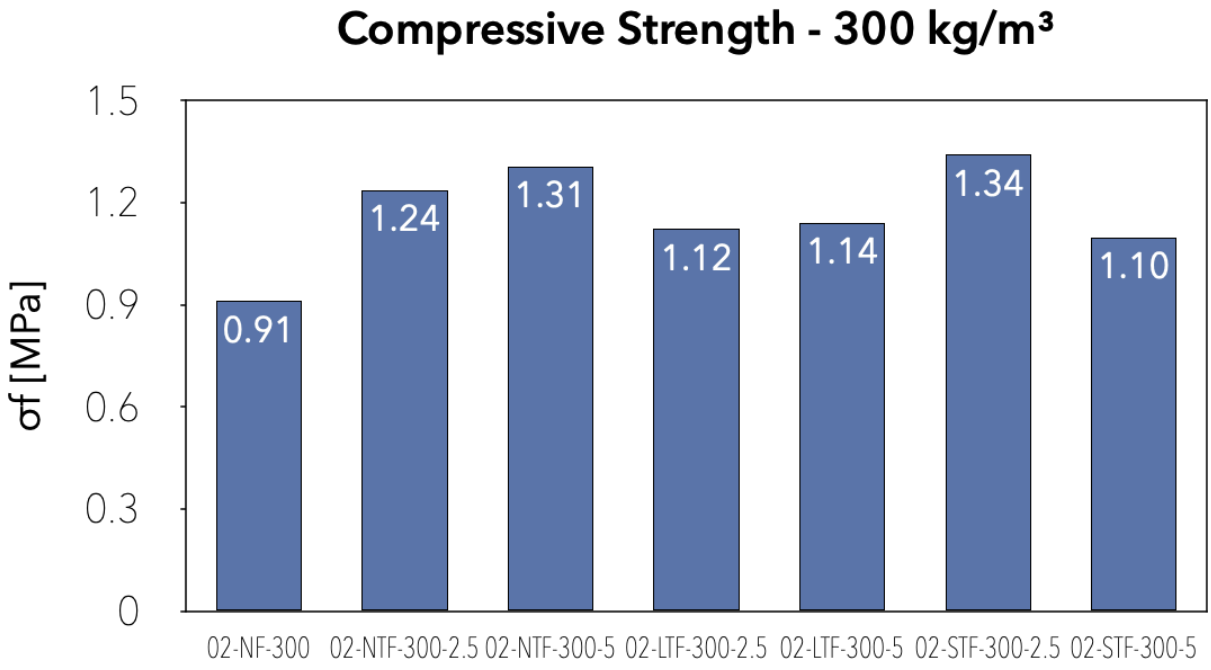

Figure 183. Graph showing the average maximum compressive strength of the admixtures with a 300kg/m³ target density.

The previous images show the average flexural strength of each admixture with a target density of 300kg/m³. Admixtures with SWF have a higher compressive strength than 02-NF-300. The results listed below show, from highest compressive

strength to lowest compressive strength, the percentage of increment each admixture with fibers present compared to the admixture without fibers:

- 02-STF-300-2,5 augmented by 47%.
- 02-NTF-300-5 augmented by 44%.
- 02-NTF-300-2,5 augmented by 36%.
- 02-LTF-300-5 augmented by 25%.
- 02-LTF-300-2,5 augmented by 23%.
- 02-STF-300-5 augmented by 21%.

It is fundamental to analyze how the fiber and cement content influences the compressive strength of each admixture. The following graphs display the results of this analysis, where the compressive strength increases significantly on admixtures with NTF when adding a 2,5% F/C ratio but from that point on tends to maintain. Admixtures with LTF present a similar behavior; however, with STF, the compressive strength for a 2,5% F/C ratio is higher than that for a 5% F/C ratio.

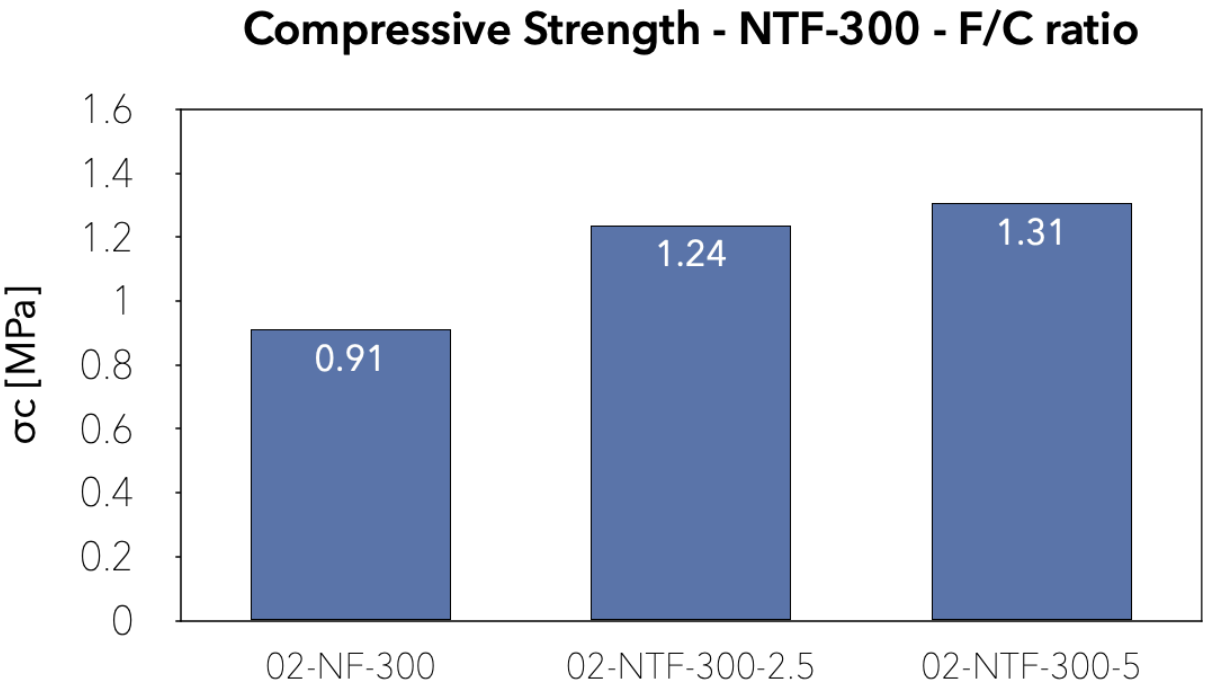

Figure 184. Graph showing the average maximum compressive strength of the admixtures with NTF and a 300kg/m³ target density.

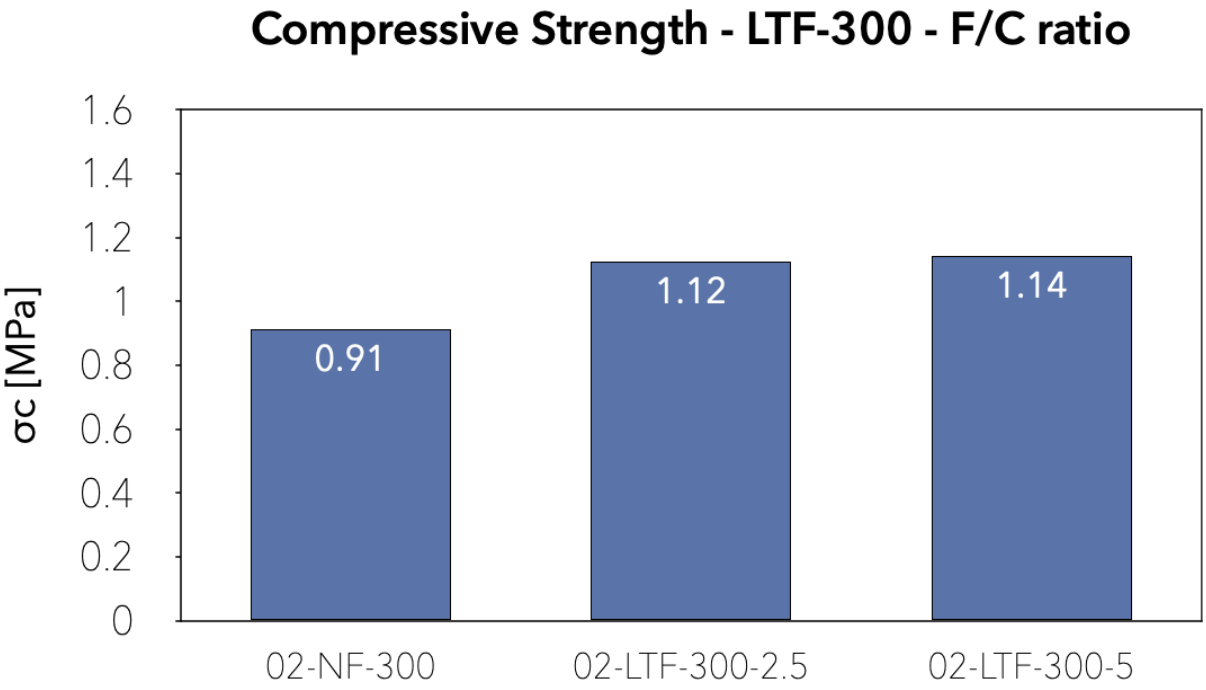

Figure 185. Graph showing the average maximum compressive strength of the admixtures with LTF and a 300kg/m³ target density.

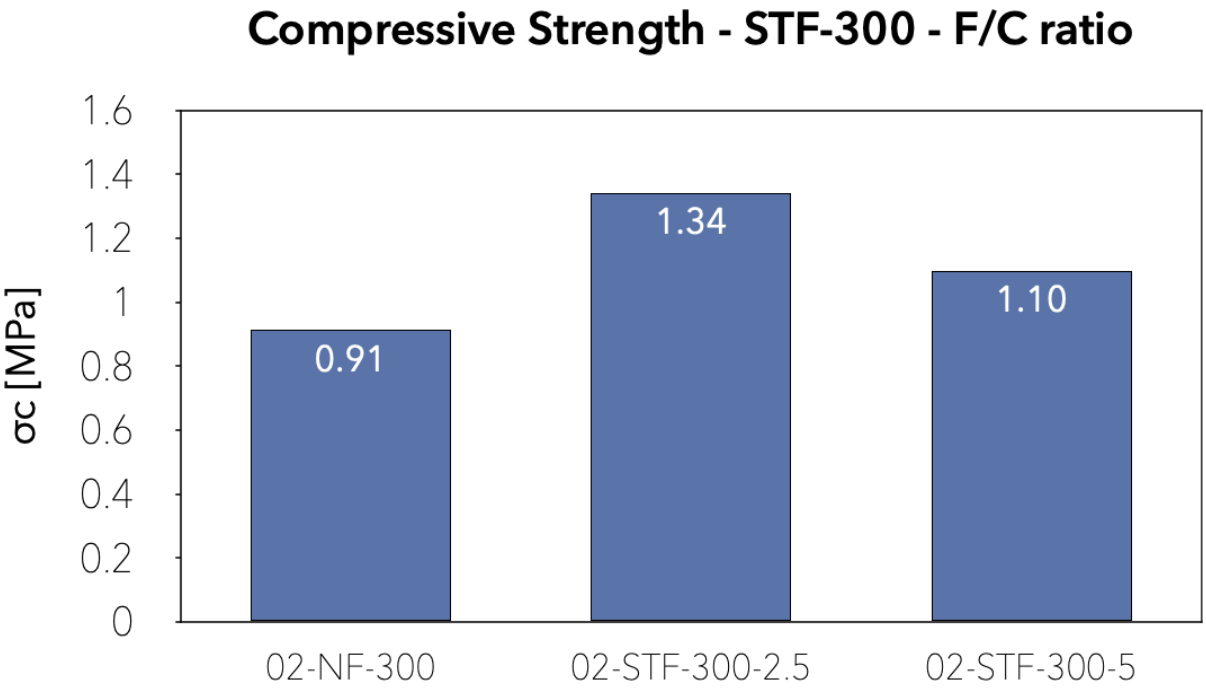

Figure 186. Graph showing the average maximum compressive strength of the admixtures with STF and a 300kg/m³ target density.

The following images show the flexural strength test results of the admixtures with a 500kg/m^3 target density.

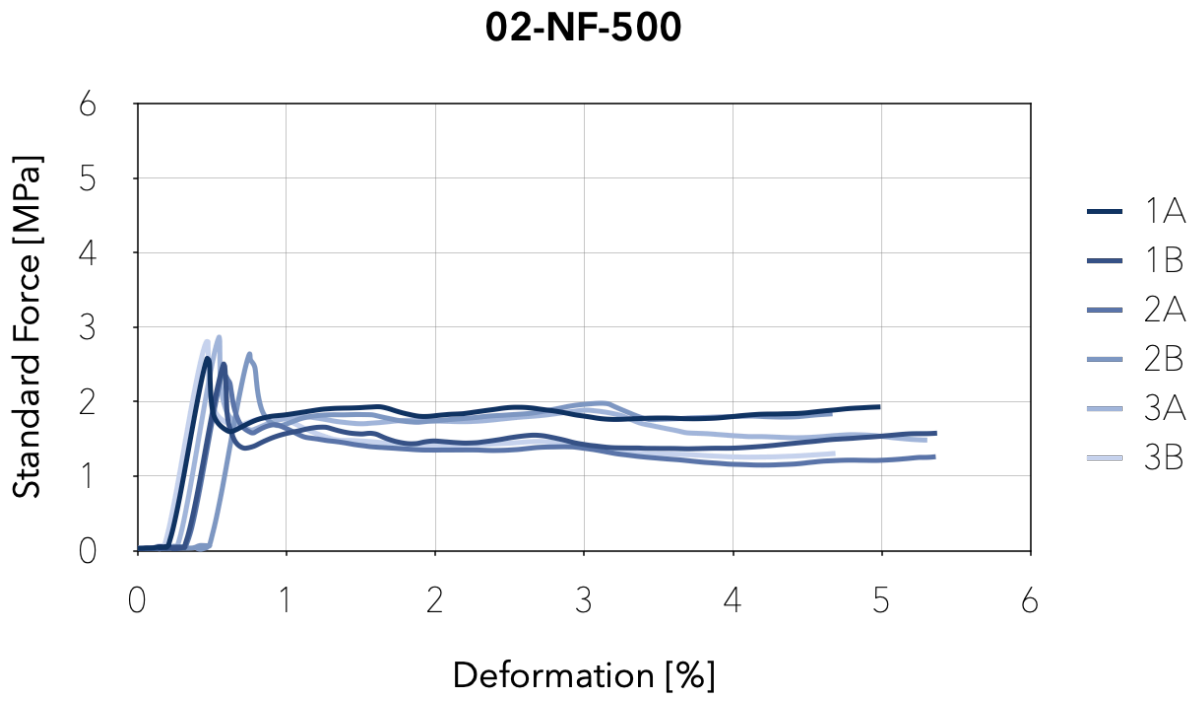

Figure 187. Image showing the compressive strength results of the three samples evaluated for the admixture 02-NF-500.

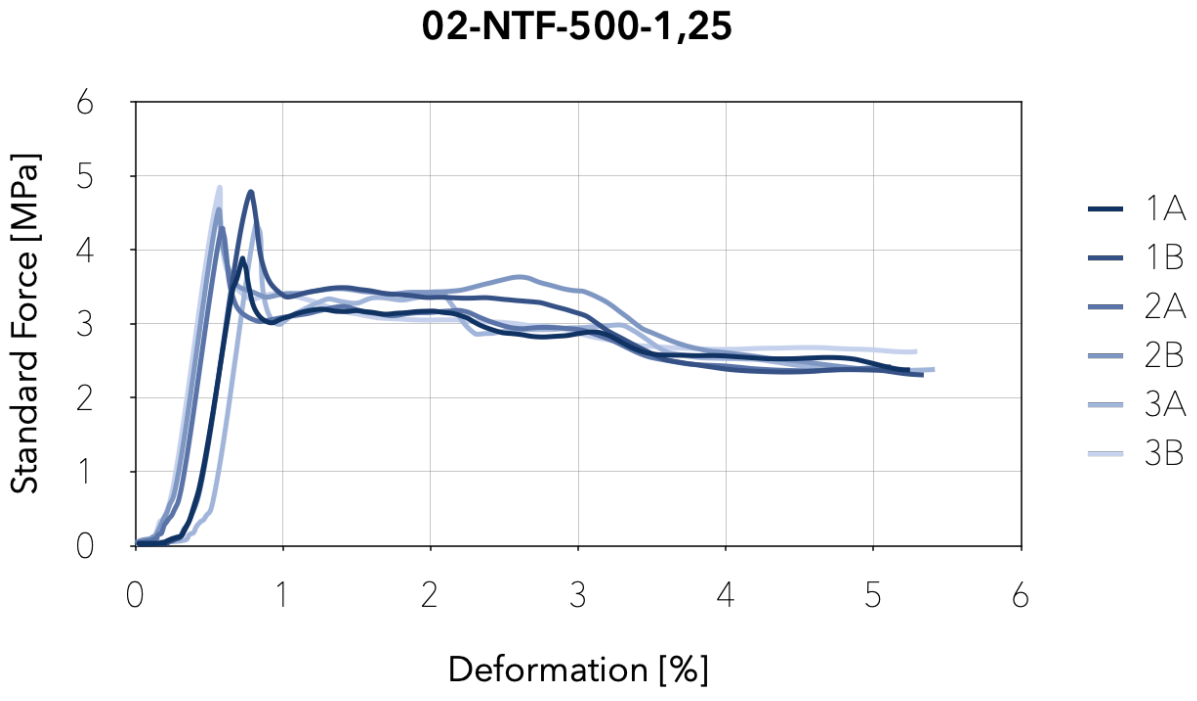

Figure 188. Image showing the compressive strength results of the three samples evaluated for the admixture 02-NTF-500-1,25.

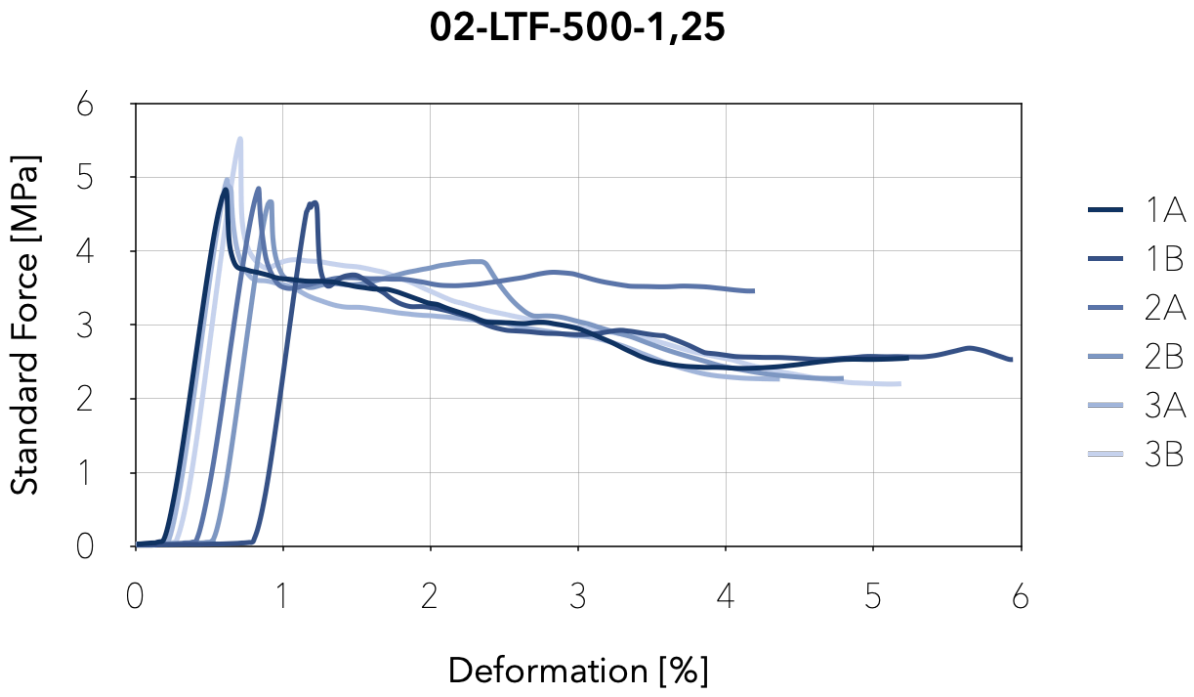

Figure 189. Image showing the compressive strength results of the three samples evaluated for the admixture 02-LTF-500-1,25.

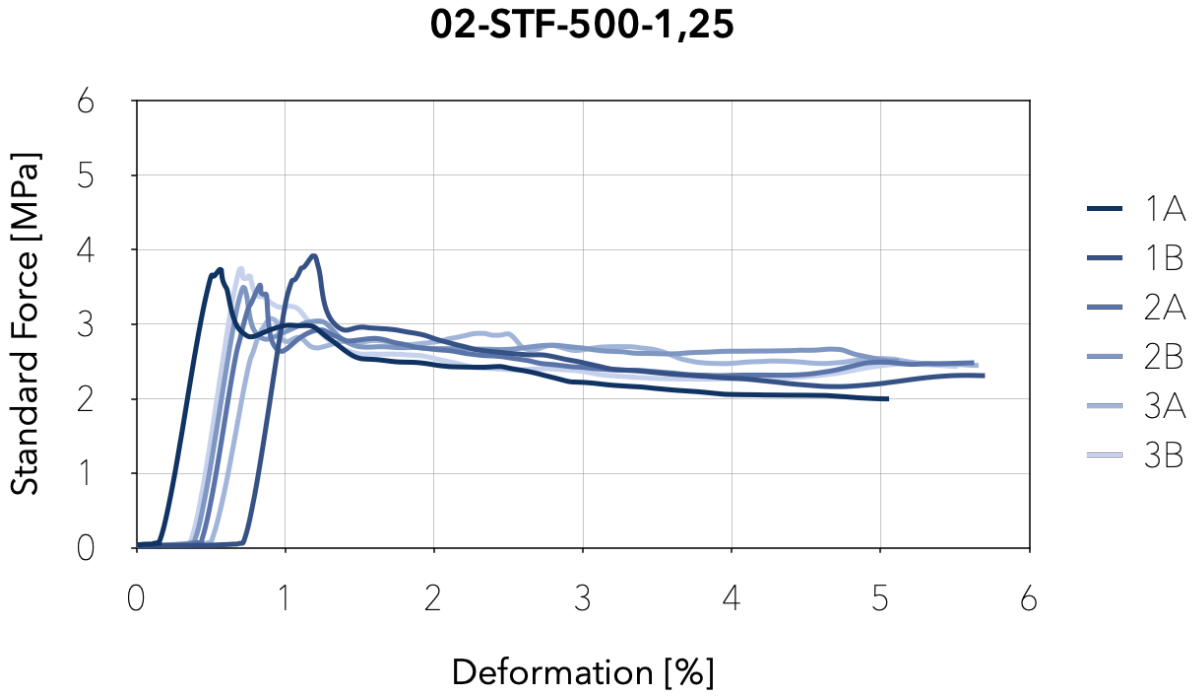

Figure 190. Image showing the compressive strength results of the three samples evaluated for the admixture 02-STF-500-1,25.

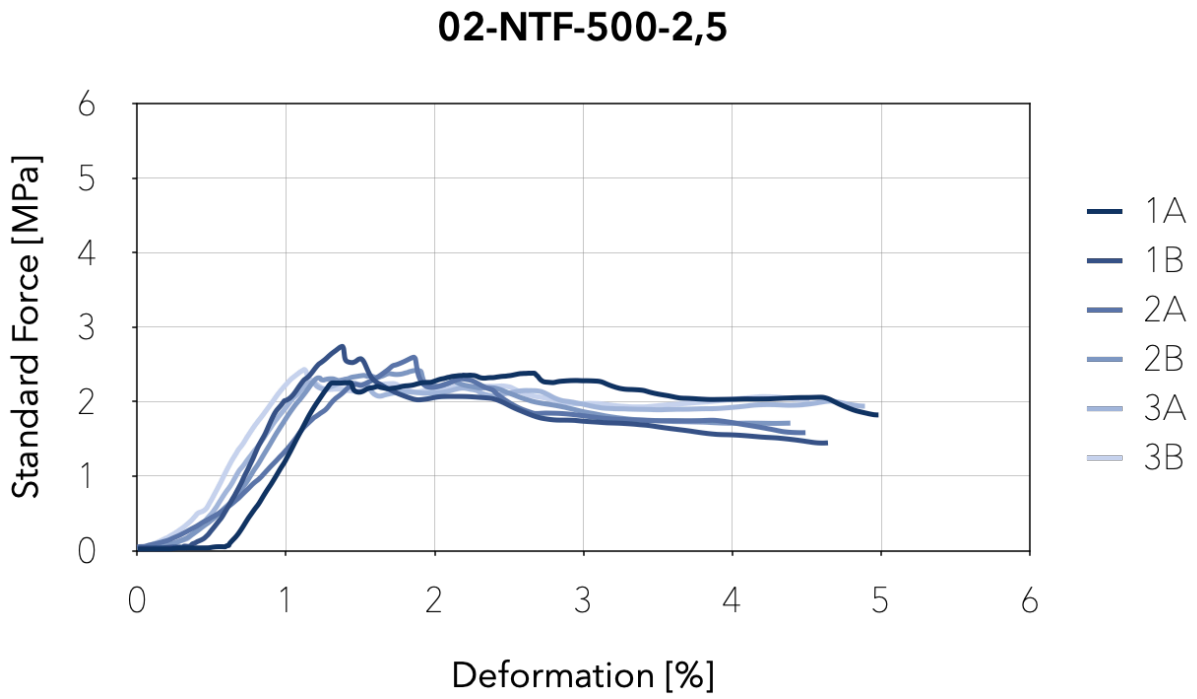

Figure 191. Image showing the compressive strength results of the three samples evaluated for the admixture 02-NTF-500-2,5.

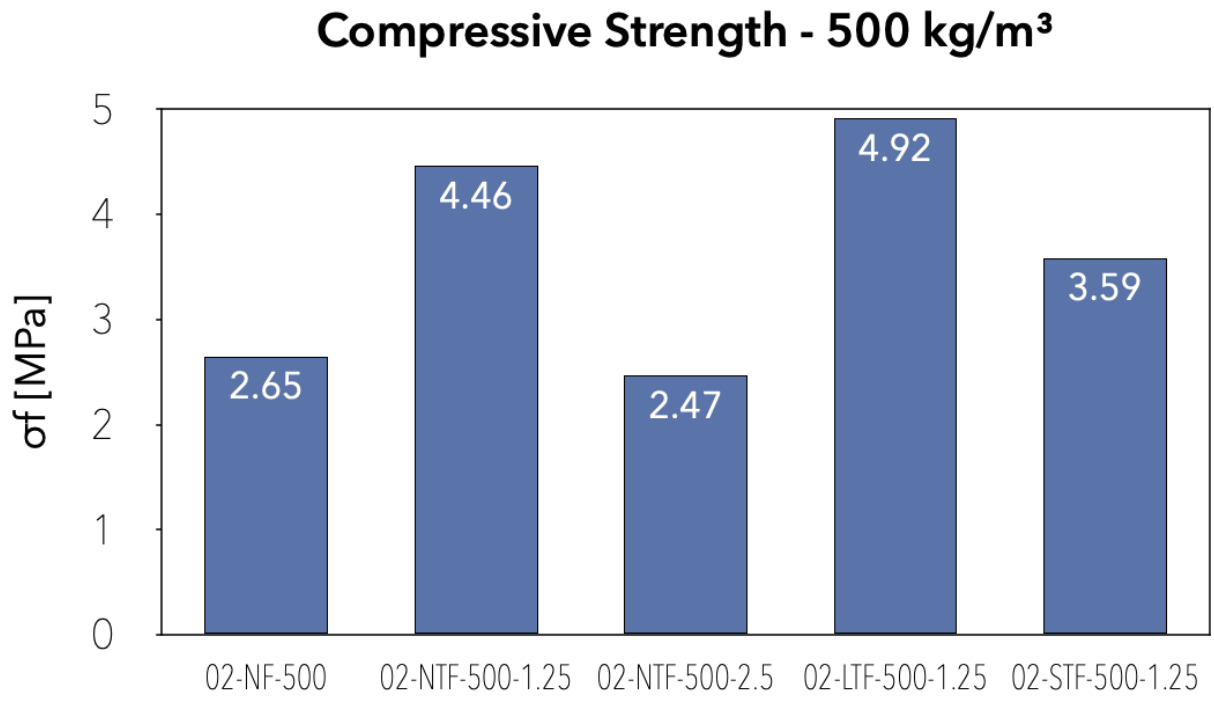

Figure 192. Graph showing the average maximum compressive strength of the admixtures with a 500kg/m³ target density.

The previous graphs show the average compressive strength of each admixture with a target density of 500kg/m³. In comparison to 02-NF-500, 02-NTF-500-1,25 had an

improvement of about 68%, 02-LTF-500-1,25 was the most performant, increasing by around 86%, and 02-STF-500-1,25 showed a compressive strength higher by 36%. On the other hand, 02-NTF-500-2,5 had different characteristics because it contained a 1% S/C ratio; however, it presented a 7% reduction in compressive strength.

The following graphs show the compressive strength in terms of density, considering a similar fiber content in terms of volume instead of cement. In this case, the admixtures with a target density of 100kg/m^3 with a 5% F/C ratio, 300kg/m^3 with a 2,5% F/C ratio, and 500kg/m^3 with a 1,25% F/C ratio present a similar fiber content per volume unit of about 4,5kg/m^3. A higher density translates into a higher resistance which is listed below. The first percentage is the increase rate between admixtures of 100 and 300kg/m^3 and the second between 300 and 500kg/m^3:

- NF 254% and 190%
- NTF 552% and 261%
- LTF 443% and 337%
- STF 527% and 167%

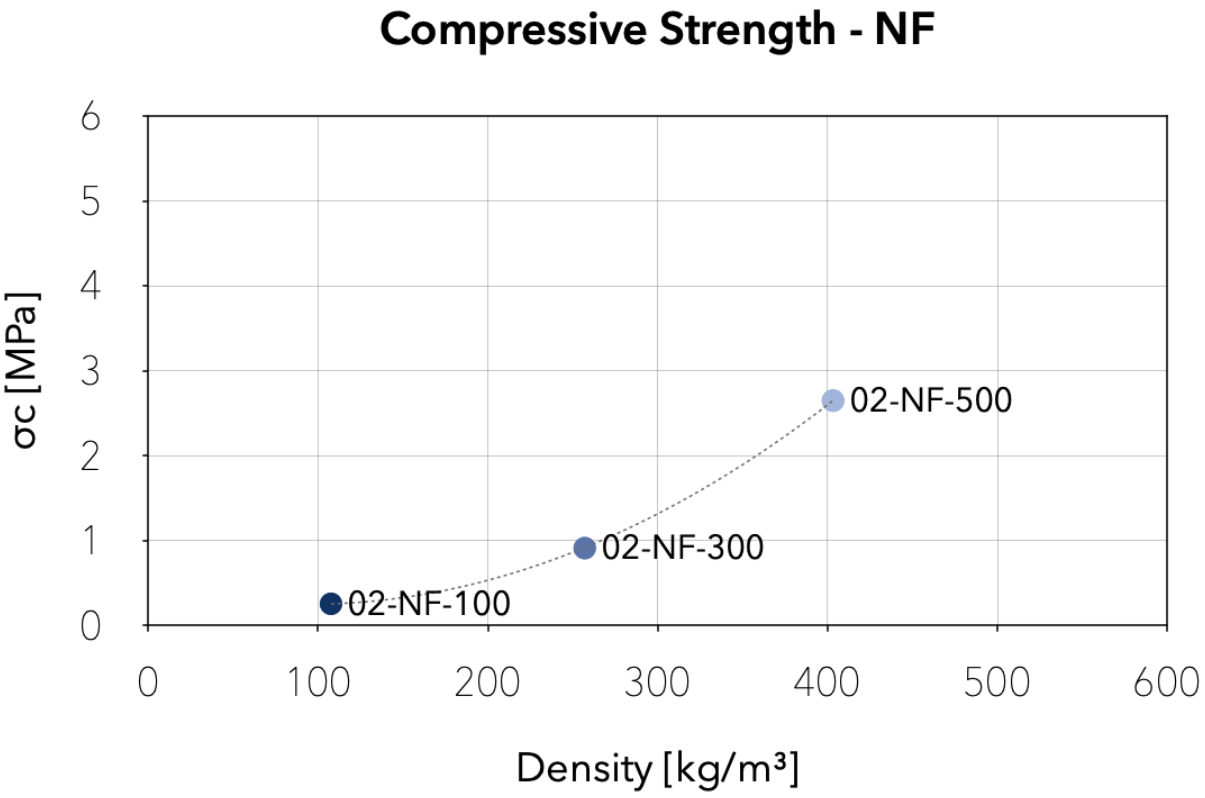

Figure 193. Dispersion graph of the average compressive strength of the NF admixtures compared to the average dry density.

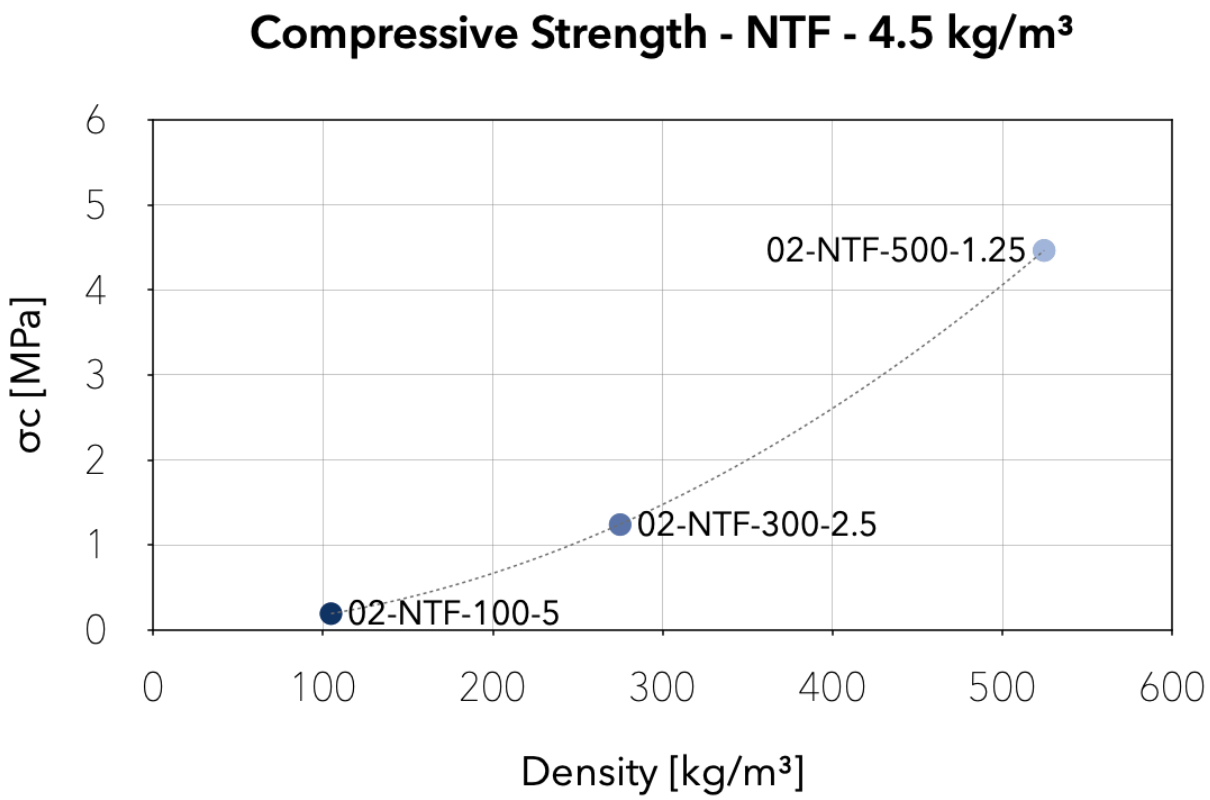

Figure 194. Dispersion graph of the average compressive strength of the NTF admixtures compared to the average dry density.

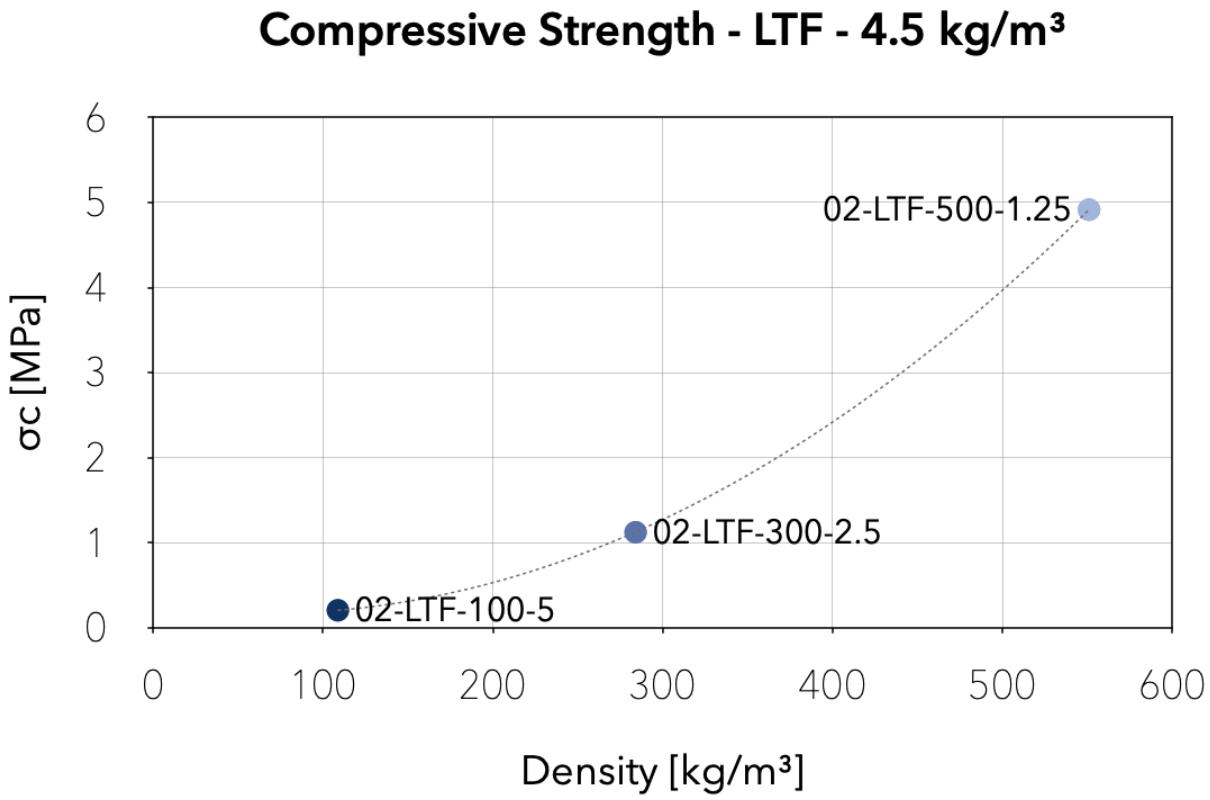

Figure 195. Dispersion graph of the average compressive strength of the LTF admixtures compared to the average dry density.

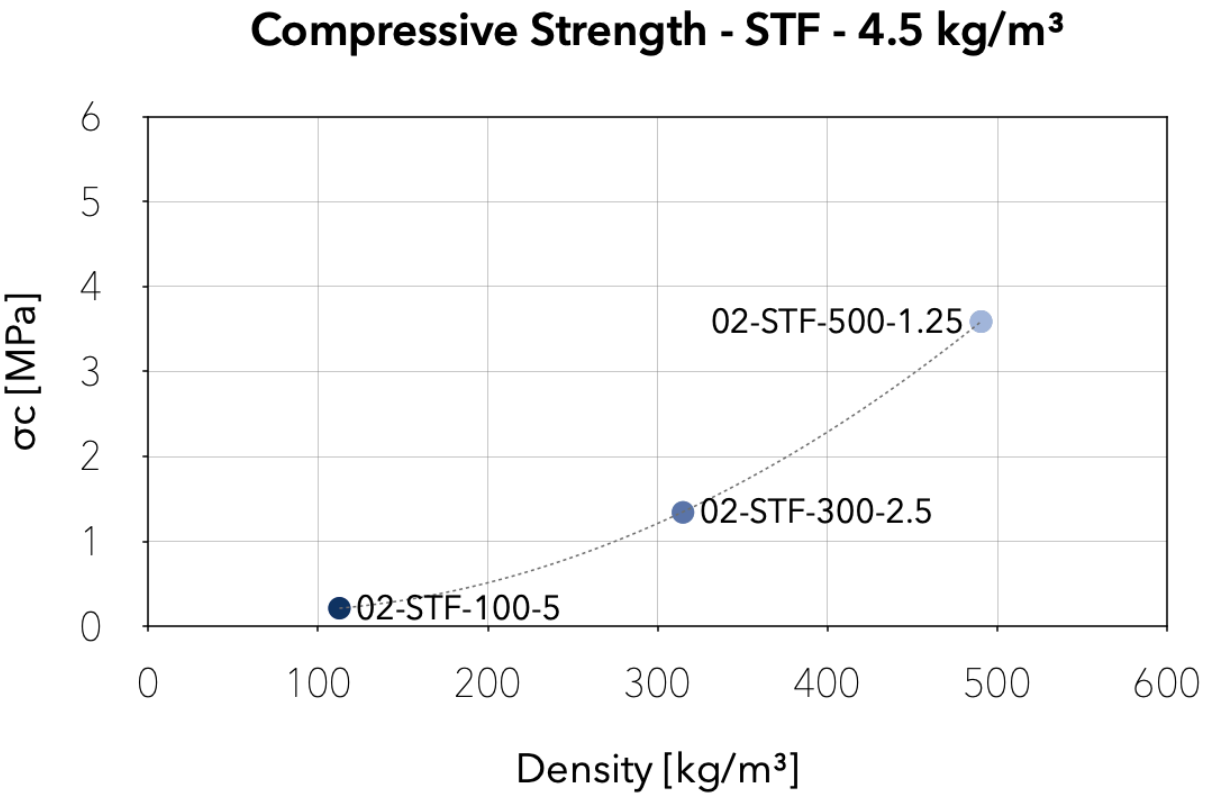

Figure 196. Dispersion graph of the average compressive strength of the STF admixtures compared to the average dry density.

NTF, LTF, and STF increased by at least 400% from 100 to 300 kg/m^3, but NF only presented an improvement of 254%. On the other hand, from 300 to 500 kg/m^3, NF increased by about 190%, NTF by 261%, LTF by 337%, and STF only by 167%. This analysis shows that each fiber treatment presents a different behavior on different densities. This should be considered a fundamental factor in the selection process depending on the needs of each particular scenario.

5.2.5. Thermal conductivity

The evaluation of the thermal conductivity of the samples made in the present experimentation represents a fascinating area to be analyzed in terms of an ultra-light material characterized by an extremely low density. Although no tests have been performed, it is still possible to predict indicative thermal conductivity values. Thanks to an experimental study published in 2019 [59], it was possible to hypothesize indicative thermal conductivity values for the samples made in this experiment. Of course, the actual validity of these values must be verified at a practical level for the specific case under study, but in the circumstances just outlined, this strategy allowed to put forward some hypotheses in this regard. The latter are essentially based on the assumption of being able to extend the curve defined by fresh density and thermal conductivity highlighted during the experimental study and obtained from the analysis of extrudable foamed concrete

samples matured in air and with humid density included in the range between 316 and 828 kg/m^3 even for samples characterized by lower densities [59]. In the study, the samples subjected to this evaluation were made in dimensions of 50x50x3 cm and analyzed in a context of ambient temperature of 25°C employing the heat flow meter method with a cold plate at a temperature of 15°C and a hot plate at a temperature of 40°C. From this experiment, it emerged that the thermal conductivity reduces significantly with the reduction in the density of the sample and that, in the density section analyzed, this reduction follows a trend that can be described through the exponential regression curve identified by the formula represented in the following graph.

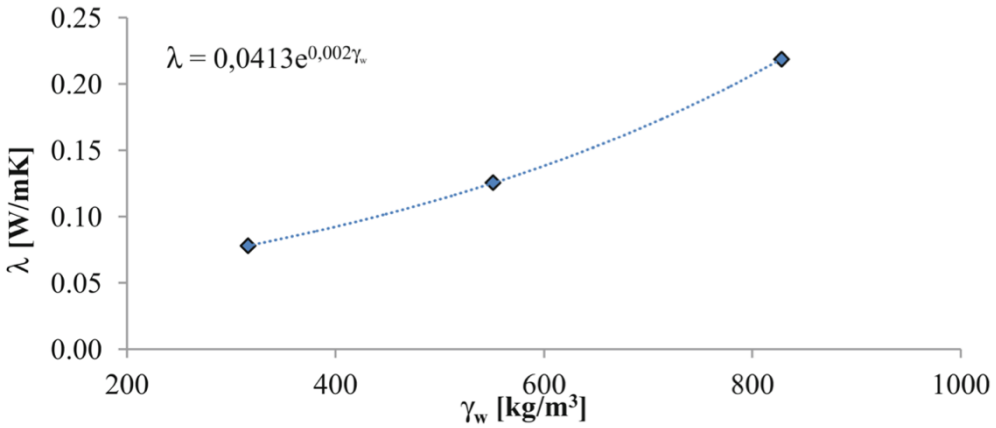

Figure 197. Graphical representation of the exponential regression curve obtained from the values of thermal conductivity (X-axis) and wet density (Y-axis) in the experimental study carried out on extrudable foamed concrete samples with a humid density in the range 316-828 kg/m³.

Starting from the behavior that emerged from this study and assuming that the regression continues with the same trend even for humid densities below 316 kg/m^3 up to including the range of wet densities covered by this thesis, it was possible to hypothesize the thermal conductivity values of the samples made in this study. The differences between the experimental study [59] from the present work, in terms of the composition of the admixtures and the analyzed density range, make the actual validity of the values shown in the following table undetermined but at least allow us to put forward a hypothesis. If they coincide with the performance offered, the conductivity values shown in the following table concerning the extrudable foam concrete samples would be optimal for carrying out the thermal insulation function to which the innovative material under study is mainly addressed.

Table 11. Hypothesized thermal conductivity values for samples made with admixtures from the first part of the experimental campaign.

MIX ID	Fresh Density γ_{ua} [kg/m³]	Thermal Conductivity λ [W/mK]
Fiber treatment choice		
01-NF	398.50	0.0916
01-NTF	425.00	0.0966
01-NaClTF	420.60	0.0958
01-LTF	405.00	0.0928
01-NaOHTF	403.00	0.0925
01-STF	425.00	0.0966
Fiber length and fiber content choice		
01-6mm-2.5	392.40	0.0905
01-12mm-2.5	422.20	0.0961
01-20mm-2.5	408.50	0.0935
01-12mm-5	392.80	0.0906
01-12mm-10	382.10	0.0887

Table 12. Hypothesized thermal conductivity values for samples made with admixtures from the second part of the experimental campaign.

MIX ID	Fresh Density γ_{ua} [kg/m³]	Thermal Conductivity λ [W/mK]
100 kg/m³		
02-NF-100	210.81	0.0630
02-NTF-100-2.5	199.90	0.0616
02-NTF-100-5	195.75	0.0611
02-LTF-100-2.5	200.40	0.0617
02-LTF-100-5	217.73	0.0638
02-STF-100-2.5	215.00	0.0635
02-STF-100-5	209.46	0.0628
300 kg/m³		
02-NF-300	384.97	0.0892
02-NTF-300-2.5	396.80	0.0913
02-NTF-300-5	420.00	0.0957
02-LTF-300-2.5	403.70	0.0926
02-LTF-300-5	397.65	0.0915
02-STF-300-2.5	427.50	0.0971
02-STF-300-5	423.50	0.0963
500 kg/m³		
02-NF-500	567.57	0.1285
02-NTF-500-1.25	735.57	0.1798
02-NTF-500-2.5	574.60	0.1303
02-LTF-500-1.25	739.35	0.1812
02-STF-500-1.25	657.41	0.1538

Chapter 6

Conclusions and possible scenarios from experimentation

6.1. Considerations and conclusions

The construction sector is still closely linked to traditional practices, often inefficient, costly, and with a high environmental impact. Therefore, the growing demand for efficient, economical, and sustainable materials, processes, and products capable of promoting a turnaround to the current building practice could represent a challenge to be met precisely by using extrudable foamed concrete reinforced with SWF.

In addition to the considerations already expressed in each specific analysis, there are further aspects to highlight. For example, some admixtures present porosity results that differ from the average of the others; however, these variations do not present any correlation between the mechanical resistance. On the other hand, the addition of SWF influences several aspects of the material. For example, the rheological analysis proves that adding SWF significantly reduces the slump, an essential characteristic for extrudable concrete because it needs to keep its shape during the printing process. In addition, the mechanical resistance, for both compressive and flexural strength, benefits from the fiber addition.

From the first part of the experimental campaign, the following conclusions can be outlined:

- With SWF, longer fibers create agglomerations, but shorter fibers present a lower compressive strength. Therefore, 12mm fibers result in optimal mechanical properties and applicability.

- In the preliminary study, fibers treated with the foaming surfactant presented an increment of 60% for flexural strength and 50% in compressive strength with respect to the admixture without fibers. In addition, an increment of 30% for flexural strength and 60% in compressive strength was achieved when comparing STF with NTF.

From the second part of the experimental campaign, the following conclusions can be outlined:

- In contrast with conclusion b from the preliminary study, in the detailed study, the admixture 02-STF-300-4.5, which shared similar characteristics to the one analyzed in the preliminary study, was 16% higher in flexural strength and 50% in compressive strength than 02-NF-300; also, it was 24% higher in flexural strength and 8% in compressive strength than 02-NTF-300-4.5. Therefore, changing the mixing methodology affected the benefits provided by this type of treatment, probably because the amount of foam required to achieve the target density increased to the same levels as the other types of fiber. Furthermore, in the preliminary study, the surfactant embedded in the fibers probably contributed to foam formation because they were added during the mixing process. In contrast, for the detailed study, fibers were added afterward. Adding fibers during the mixing process helps reduce the foam and water added; therefore, the mechanical properties increase. However, adding fibers during the high speed (1500 rpm) mixing process causes them to get entangled on the mixing paddle; therefore, it is not advisable to invert the process.

- At a density of 100kg/m^3, the benefits obtained from adding SWF are lower than those of the other densities. Admixture 02-NTF-100-4.5 presents the highest flexural strength with a 20% higher resistance than 02-NF-100. However, the highest compressive strength is shared by 02-NTF-100-2 and 02-STF-100-2, but it is 12% lower than the admixture without fibers.

- At a 300kg/m^3 density, both compressive and flexural strength improve when SWFs are added to the admixture. For example, admixture 02-STF-300-9 presents the highest flexural strength with an 82% higher resistance than 02-NF-300, and 02-STF-300-4.5 has the highest compressive strength results surpassing the admixture without fibers by a 47%.

- At a density of 500kg/m^3, the benefits obtained from the addition of SWF are higher than those of the other densities, meaning that the impact of the fibers in extrudable foamed concrete is higher when density increases. Admixture 02-LTF-500-4.5 presents the highest flexural strength with a 132% higher resistance than 02-NF-100, and 02-LTF-500-4.5 shows the highest compressive strength results surpassing the admixture without fibers by 68%.

- The addition of SWF to ultralightweight foamed concrete proves to improve the mechanical properties of the material and to be directly proportional to the material's density.

- The hypothesized thermal conductivity predicts that the material studied in this research can be applied in construction as insulation. This material can be poured inside cast or printed concrete voids or form panels to be installed

onsite. However, it is necessary to deepen the research on the printability of foamed concrete.

6.2. Research and possible future scenarios

In order to continue the study carried out on extrudable ultra-light foamed concrete with a target density in the range of 100-500kg/m^3 reinforced with natural fibers, it would be appealing to deepen on diverse subjects. For example, the general knowledge of ultra-light foamed concrete which is scarcely present in research studies. In addition, the inclusion of SWF as reinforcement in ultralight foamed concrete which, until now, has only been applied to regular concrete admixtures and mortars.

The pumpability of foamed concrete has been studied in previous articles. Cho et al. demonstrated that the "cushioning effect," prominent in materials with higher foam/volume ratio, prevents foam degradation [61]. This suggests that low-density foamed concretes should maintain foam stability; however, future research projects should deepen on this topic to confirm or refute this hypothesis. The improvement of foam stability during concrete extrusion is still a topic to study. Also, the inclusion of SWF during the extrusion should be analyzed; given that these fibers tend to entangle during the mixing process, they may affect the pumpability of the material.

The most intriguing evaluations for the completion of this research work could be:

- The slump flow analysis of the admixtures would contribute to determining the flowability of the material and, therefore, its pumpability. Such analysis would complement the slump tests so that the material could be considered pumpable and capable of keeping its shape. It will also establish if SWF affect the flowability of the material.

- Determine the pumpability of the material, the properties it has during the printing process, and if the foam stability is, in any way, affected by the pumping procedure.

- Measuring the thermal conductivity actually offered: It would be worthwhile to identify the actual thermal conductivity values of the samples made in this study, both to deepen the knowledge relating to this specific topic and to confirm or deny the assumption of the continuity of the trend of the exponential regression curve of the graph of fresh density and thermal conductivity highlighted in the experimental study of 2019 regarding the wet density range between 316 and 828 kg/m^3 and also hypothesized for the density range analyzed in this work.

- Durability and permeability of the material: this research should be complemented with a study of the durability and permeability of the material. This is a fundamental step because adding natural fibers implies a possible degradation in time. Therefore, further research should also consider each fiber treatment's influence on its durability.

A further step should consider the application of this material in automated production processes. These experiments should be carried out using the 3D Concrete Printing methodology. In this regard, it would be interesting to use the ultra-light material for the realization of the low-density portions of multi-functional and multi-density engineered components made entirely of extrudable foam concrete and possibly made with the use of a machine capable of simultaneously applying both the high-density material constituting the resistant skeleton of the element and the low-density material for filling the cavities. In this context, any unsolved problems inherent to the production process's performance and the components' characteristics, properties, and performance in the hardened state could be identified.

List of figures

Figure 1. Life cycle stages of concrete and its respective strategies for sustainability [3]. 4

Figure 2. Distribution of CO2 emissions released during the different phases of the cement production process [3]. 5

Figure 3. Iron and steel production [3]. 6

Figure 4. Various types of artificial fibers [21]. 17

Figure 5. Various types of natural fibers [21]. 19

Figure 6. Ordinary sheep wool fibers used in concrete reinforcement [34]. 20

Figure 7. Non-treated sheep wool filament on the left and plasma treated sheep wool fiber on the right [38]. 20

Figure 8. Sheep wool fibers with 20 (a), 6 (b), and 1 (c) mm length [35]. 21

Figure 9. SWF reinforced mortar stored on air with visible wool filaments [34]. 22

Figure 10. SWF reinforced mortar stored in water with visible empty holes where the wool filaments used to be [34]. 22

Figure 11. Classification of light-weight cellular concrete [46]. 24

Figure 12. Example of instability in ultralightweight foamed concrete. From left to right, density is equal to 300, 200, and 150 kg/m³ [48]. 28

Figure 13. Graphical representation of the forces acting on a single air bubble inside a foamed concrete fresh admixture [48]. 28

Figure 14. High density foamed concrete on the left and low density on the right. The second presents macro-bubbles [48]..... 30

Figure 15. Schematic comparison between the bubbles in 300 and 600 kg/m³ foamed concrete [48]..... 30

Figure 16. Graphic representation of the gas diffusion process in 600 kg/m³ foamed concrete above and 300 kg/m³ below. On the second, the instability phenomenon leads to the composite's segregation [48]..... 31

Figure 17. Outline of AM processes and methods used in the construction sector [50]..... 32

Figure 18. CC operating model on the left, rectilinear and curvilinear CC built walls on the right [50]..... 35

Figure 19. Construction and result of the Apis Corp Dubai project (www.apis-cor.com/dubai-project)..... 36

Figure 20. CP construction process (left), CP built wall-bench (center), and façade element projected parametrically by Bruil (2019) (right) [50]..... 36

Figure 21. Examples of 3D Concrete Printing with different printing typologies and orientations [51]..... 37

Figure 22. Example of a printability test to identify the time window when the material can create a self-sustaining structure. Being 0, the time when the cement first came in contact with water [51]..... 39

Figure 23. Example of an element characterized by cold-joints on the left and another without cold-joints on the right [51]..... 42

Figure 24. Elements characterized by variable filament density on the left and constant filament density on the right. In the first case, the various layers and voids of various sizes are recognized, while in the second, the element is homogeneous [51]. 42

Figure 25. Example of shrinkage cracks in an element made using 3D Concrete Printing [53]. 43

Figure 26. Example of a hatch created by an internal path on the left [51] and a perimeter filled with casted material on the right (3dcp.dk). 45

Figure 27. 2D slicing method on the left and tangential continuity method on the right. The latter has a constant contact surface between layers which reduces the risk of collapse [51]. 46

Figure 28. Example of the integration of classic reinforcements to a 3D printed formwork. 47

Figure 29. Comparison between the traditional curved reinforced wall on the left and the Mesh Model Metal case study of ETH Zurich on the right [54]. 47

Figure 30. Specimens with bi-directional reinforcement in fiberglass and dispersed fibers after the flexural strength test [55]. 48

Figure 31. Example of a 3D printed beam with steel reinforcements integrated after the printing process [49]. 48

Figure 32. Structural element designed through topological optimization on the left [56] and element with hollow sections designed through functional hybridization on the right [57]. 50

Figure 33. Global warming potential compared to complexity. Advantage of digital fabrication against conventional construction [53]. 51

Figure 34. Schematic of the topological or structural optimization system [53]. 51

Figure 35. Schematics of the functional hybridization system [53]. 52

Figure 36. Quality comparison in terms of consistency, cohesion and viscosity in the fresh state between an extrudable foamed concrete mix (above) and a classic foamed concrete mix (below) both made to obtain a final density of 600 kg/m³ [55]. 53

Figure 37. Comparison of the final configuration following extrusion tests and after a rest time of 5 minutes between mixtures of different densities made with classic foamed concrete (above) and with extrudable foamed concrete (below). In the second case we are with the consequent maintenance of the shape following extrusion [58]. 54

Figure 38. Comparison in size and distribution of pores between cross-sections made on a classic foamed concrete element on the left and an extrudable foamed concrete one with the same final density, mixing speed, and hardening conditions on the right. Pore size diminished, and the distribution is more homogeneous on the latter [58]. 55

Figure 39. Comparison in terms of size and distribution of pores between cross-sections made on an extrudable foamed concrete element on the left and one in autoclaved aerated concrete with the same final density on the right. The first image shows that the pore size reduced, and the distribution became more homogeneous [59]. 56

Figure 40. Images of the base ingredients of every admixture: cement and viscosity modifier on the left, water and superplasticizer in the center, and pre-formed foam made with water and a surfactant agent on the right 63

Figure 41. mages of final mixture with fibers: 100Kg/m^3 on the left, 300Kg/m^3 in the center, and 500Kg/m^3 on the right..... 63

Figure 42. Images of the employed SWF with different treatments: a=NTF, b=NaClTF, c=LTF, d=NaOHTF, and e=STF 63

Figure 43. Images of the confectioning process of the prismatic samples above and confectioned cubic samples bellow..... 64

Figure 44. Image indicating how the slump test was measured to obtain the vertical and horizontal slump results. 65

Figure 45. Image showing the influence of fiber addition on the slump for the first experimental campaign on the fiber treatment choice. On the left, mix 01-NF represents the slump without fibers; on the right, mix 01-NTF shows the slump of an admixture containing fibers. 68

Figure 46. Image showing the influence of fiber addition on the slump for the second experimental campaign on the 100kg/m^3 density. On the left, mix 02-NF-100 represents the slump without fibers; in the middle, mix 02-NTF-100-2,5% shows an admixture with a 2,5% F/C ratio; on the right, mix 02-NTF-100-5% shows the slump of an admixture with a 5% F/C ratio. 68

Figure 47. Image showing the influence of fiber addition on the slump for the second experimental campaign on the 300kg/m^3 density. On the left, mix 02-NF-300 represents the slump without fibers; in the middle, mix 02-NTF-300-2,5 shows an admixture with a 2,5% F/C ratio; on the right, mix 02-NTF-300-5 shows the slump of an admixture with a 5% F/C ratio..... 69

Figure 48. Image showing the influence of fiber addition on the slump for the second experimental campaign on the 500kg/m^3 density. On the left, mix 02-NF-500 represents the slump without fibers; in the middle, mix 02-NTF-500-1,25 shows an

admixture with a 1,25% F/C ratio; on the right, mix 02-NTF-500-2,5 shows the slump of an admixture with a 2,5% F/C ratio. 69

Figure 49. Image showing the influence of density on the slump for the second experimental campaign. On the left, mix 02-NF-100 presents a density of 100kg/m^3; in the middle, mix 02-NF-300 shows an admixture with a 300kg/m^3 density; on the right, mix 02-NF-500 shows the slump of an admixture with a 500kg/m3 density. 70

Figure 50. Image showing the density variation on the admixtures with 100kg/m^3 from the second part of the experimental campaign. 71

Figure 51. Image showing the density variation on the admixtures with 300kg/m^3 from the second part of the experimental campaign. 72

Figure 52. Image showing the density variation on the admixtures with 500kg/m^3 from the second part of the experimental campaign. 72

Figure 53. Original and binarized images employed to evaluate the porosity of mix 02-NF-100. 74

Figure 54. Original and binarized images employed to evaluate the porosity of mix 02-NTF-100-2,5. 74

Figure 55. Original and binarized images employed to evaluate the porosity of mix 02-NTF-100-5. 74

Figure 56. Original and binarized images employed to evaluate the porosity of mix 02-LTF-100-2,5. 75

Figure 57. Original and binarized images employed to evaluate the porosity of mix 02-LTF-100-5. 75

Figure 58. Original and binarized images employed to evaluate the porosity of mix 02-STF-100-2,5. 75

Figure 59. Original and binarized images employed to evaluate the porosity of mix 02-STF-100-5. 76

Figure 60. Original and binarized images employed to evaluate the porosity of mix 02-NF-300. 76

Figure 61. Original and binarized images employed to evaluate the porosity of mix 02-NTF-300-2,5. 76

Figure 62. Original and binarized images employed to evaluate the porosity of mix 02-NTF-300-5. 77

Figure 63. Original and binarized images employed to evaluate the porosity of mix 02-LTF-300-2,5. 77

Figure 64. Original and binarized images employed to evaluate the porosity of mix 02-LTF-300-5. 77

Figure 65. Original and binarized images employed to evaluate the porosity of mix 02-STF-300-2,5. 78

Figure 66. Original and binarized images employed to evaluate the porosity of mix 02-STF-300-5. 78

Figure 67. Original and binarized images employed to evaluate the porosity of mix 02-NF-500. 78

Figure 68. Original and binarized images employed to evaluate the porosity of mix 02-NTF-500-1,25. 79

Figure 69. Original and binarized images employed to evaluate the porosity of mix 02-NTF-500-2,5. 79

Figure 70. Original and binarized images employed to evaluate the porosity of mix 02-LTF-500-1,25. 79

Figure 71. Original and binarized images employed to evaluate the porosity of mix 02-STF-500-1,25 80

Figure 72. Graphic representation of the frequency with which the equivalent diameters of the pores are present in the samples made with admixture 02-NF-100. 82

Figure 73. Graphic representation of the frequency with which the equivalent diameters of the pores are present in the samples made with admixture 02-NTF-100-2,5. 82

Figure 74. Graphic representation of the frequency with which the equivalent diameters of the pores are present in the samples made with admixture 02-NTF-100-5. 83

Figure 75. Graphic representation of the frequency with which the equivalent diameters of the pores are present in the samples made with admixture 02-LTF-100-2,5. 83

Figure 76. Graphic representation of the frequency with which the equivalent diameters of the pores are present in the samples made with admixture 02-LTF-100-5. 84

Figure 77. Graphic representation of the frequency with which the equivalent diameters of the pores are present in the samples made with admixture 02-STF-100-2,5. 84

Figure 78. Graphic representation of the frequency with which the equivalent diameters of the pores are present in the samples made with admixture 02-STF-100-5. 85

Figure 79. Graphic representation of the frequency with which the equivalent diameters of the pores are present in the samples made with admixture 02-NF-300. 85

Figure 80. Graphic representation of the frequency with which the equivalent diameters of the pores are present in the samples made with admixture 02-NTF-300-2,5. 86

Figure 81. Graphic representation of the frequency with which the equivalent diameters of the pores are present in the samples made with admixture 02-NTF-300-5. 86

Figure 82. Graphic representation of the frequency with which the equivalent diameters of the pores are present in the samples made with admixture 02-LTF-300-2,5. 87

Figure 83. Graphic representation of the frequency with which the equivalent diameters of the pores are present in the samples made with admixture 02-LTF-300-5. 87

Figure 84. Graphic representation of the frequency with which the equivalent diameters of the pores are present in the samples made with admixture 02-STF-300-2,5. 88

Figure 85. Graphic representation of the frequency with which the equivalent diameters of the pores are present in the samples made with admixture 02-STF-300-5. 88

Figure 86. Graphic representation of the frequency with which the equivalent diameters of the pores are present in the samples made with admixture 02-NF-500. 89

Figure 87. Graphic representation of the frequency with which the equivalent diameters of the pores are present in the samples made with admixture 02-NTF-500-1,25. 89

Figure 88. Graphic representation of the frequency with which the equivalent diameters of the pores are present in the samples made with admixture 02-LTF-500-1,25. 90

Figure 89. Graphic representation of the frequency with which the equivalent diameters of the pores are present in the samples made with admixture 02-STF-500-1,25. 90

Figure 90. Graphic representation of the frequency with which the equivalent diameters of the pores are present in the samples made with admixture 02-NTF-500-2,5. 91

Figure 91. Image showing the sample positioning on the machine for the flexural strength tests. 92

Figure 92. Image showing the flexural strength results of the three samples evaluated for the admixture without fibers (01-NF). 93

Figure 93. Image showing the flexural strength results of the three samples evaluated for the admixture with non-treated fibers (01-NTF). 93

Figure 94. Image showing the flexural strength results of the three samples evaluated for the admixture with salt-treated fibers (01-NaClTF). 94

Figure 95. Image showing the flexural strength results of the three samples evaluated for the admixture with lime-treated fibers (01-LTF). 94

Figure 96. Image showing the flexural strength results of the three samples evaluated for the admixture with sodium hydroxide-treated fibers (01-NaOHTF). 95

Figure 97. Image showing the flexural strength results of the three samples evaluated for the admixture with surfactant-treated fibers (01-STF)..... 95

Figure 98. Graph with the average maximum flexural strength of the admixtures analyzed for fiber selection. 96

Figure 99. Dispersion graph of the average flexural strength of the admixtures analyzed for fiber treatment selection compared to the average density measured after 28 days of maturation..... 97

Figure 100. Image showing the flexural strength results of the three samples evaluated for the admixture with 6mm fibers and 2,5% F/C ratio (01-6mm-2,5).... 98

Figure 101. Image showing the flexural strength results of the three samples evaluated for the admixture with 12mm fibers and 2,5% F/C ratio (01-12mm-2,5). 98

Figure 102. Image showing the flexural strength results of the three samples evaluated for the admixture with 20mm fibers and 2,5% F/C ratio (01-20mm-2,5). 99

Figure 103. Graph with the average maximum flexural strength of the admixtures analyzed for fiber length selection. 99

Figure 104. Dispersion graph of the average flexural strength of the admixtures analyzed for fiber length selection compared to the average density measured after 28 days of maturation..... 100

Figure 105. Image showing the flexural strength results of the three samples evaluated for the admixture with 12mm fibers and 2,5% F/C ratio (01-12mm-2,5). 101

Figure 106. Image showing the flexural strength results of the three samples evaluated for the admixture with 12mm fibers and 2,5% F/C ratio (01-12mm-5). 101

Figure 107. Image showing the flexural strength results of the three samples evaluated for the admixture with 12mm fibers and 2,5% F/C ratio (01-12mm-10). 102

Figure 108. Graph with the average maximum flexural strength of the admixtures analyzed for fiber content selection. 103

Figure 109. Dispersion graph of the average flexural strength of the admixtures analyzed for fiber content selection compared to the average density measured after 28 days of maturation..... 103

Figure 110. Image showing the flexural strength results of the three samples evaluated for the admixture 02-NF-100. 104

Figure 111. Image showing the flexural strength results of the three samples evaluated for the admixture 02-NTF-100-2,5..... 104

Figure 112. Image showing the flexural strength results of the three samples evaluated for the admixture 02-LTF-100-2,5..... 105

Figure 113. Image showing the flexural strength results of the three samples evaluated for the admixture 02-STF-100-2,5. 105

Figure 114. Image showing the flexural strength results of the three samples evaluated for the admixture 02-NTF-100-5..... 106

Figure 115. Image showing the flexural strength results of the three samples evaluated for the admixture 02-LTF-100-5. 106

Figure 116. Image showing the flexural strength results of the three samples evaluated for the admixture 02-STF-100-5. 107

Figure 117. Flexural strength test photograph of 02-STF-100-2,5 sample1 107

Figure 118. Image explaining the flexural strength/deformation behavior of admixture 02-NTF-100-5. 108

Figure 119. Section with the fiber agglomerations found at the breaking point on sample 2 admixture 02-NTF-100-5. 109

Figure 120. Graph showing the average maximum flexural strength of the admixtures with a 100kg/m³ target density. 109

Figure 121. Graph showing the average maximum flexural strength of the admixtures with NTF and a 100kg/m³ target density. 110

Figure 122. Graph showing the average maximum flexural strength of the admixtures with LTF and a 100kg/m³ target density. 110

Figure 123. Graph showing the average maximum flexural strength of the admixtures with STF and a 100kg/m³ target density. 111

Figure 124. Image showing the flexural strength results of the three samples evaluated for the admixture 02-NF-300. 111

Figure 125. Image showing the flexural strength results of the three samples evaluated for the admixture 02-NTF-300-2,5. 112

Figure 126. Image showing the flexural strength results of the three samples evaluated for the admixture 02-LTF-300-2,5. 112

Figure 127. Image showing the flexural strength results of the three samples evaluated for the admixture 02-STF-300-2,5. 113

Figure 128. Image showing the flexural strength results of the three samples evaluated for the admixture 02-NTF-300-5. 113

Figure 129. Image showing the flexural strength results of the three samples evaluated for the admixture 02-LTF-300-5. 114

Figure 130. Image showing the flexural strength results of the three samples evaluated for the admixture 02-STF-300-5. 114

Figure 131. Image explaining the flexural strength/deformation behavior of admixture 02-STF-300-5. 115

Figure 132. Graph showing the average maximum flexural strength of the admixtures with a 300kg/m³ target density. 116

Figure 133. Graph showing the average maximum flexural strength of the admixtures with NTF and a 300kg/m³ target density. 117

Figure 134. Graph showing the average maximum flexural strength of the admixtures with LTF and a 300kg/m³ target density. 117

Figure 135. Graph showing the average maximum flexural strength of the admixtures with STF and a 300kg/m³ target density. 118

Figure 136. Image showing the flexural strength results of the three samples evaluated for the admixture 02-NF-500. 118

Figure 137. Image showing the flexural strength results of the three samples evaluated for the admixture 02-NTF-500-1,25. 119

Figure 138. Image showing the flexural strength results of the three samples evaluated for the admixture 02-LTF-500-1,25. 119

Figure 139. Image showing the flexural strength results of the three samples evaluated for the admixture 02-STF-500-1,25. 120

Figure 140. Image showing the flexural strength results of the three samples evaluated for the admixture 02-NTF-500-2,5. 120

Figure 141. Graph showing the average maximum flexural strength of the admixtures with a 500kg/m³ target density. 121

Figure 142. Dispersion graph of the average flexural strength of the NF admixtures compared to the average dry density. 122

Figure 143. Dispersion graph of the average flexural strength of the NTF admixtures with 4,5kg/m³ of fibers compared to the average dry density. 122

Figure 144. Dispersion graph of the average flexural strength of the LTF admixtures with 4,5kg/m³ of fibers compared to the average dry density. 123

Figure 145. Dispersion graph of the average flexural strength of the STF admixtures with 4,5kg/m³ of fibers compared to the average dry density. 123

Figure 146. Image showing the sample positioning on the machine for the compressive strength tests. 125

Figure 147. Image showing the compressive strength results of the three samples evaluated for the admixture without fibers (01-NF). 126

Figure 148. Image showing the compressive strength results of the three samples evaluated for the admixture with non-treated fibers (01-NTF). 126

Figure 149. Image showing the compressive strength results of the three samples evaluated for the admixture with salt-treated fibers (01-NaClTF). 127

Figure 150. Image showing the compressive strength results of the three samples evaluated for the admixture with lime-treated fibers (01-LTF). 127

Figure 151. Image showing the compressive strength results of the three samples evaluated for the admixture with sodium hydroxide-treated fibers (01-NaOHTF). 128

Figure 152. Image showing the compressive strength results of the three samples evaluated for the admixture with surfactant-treated fibers (01-STF)..... 128

Figure 153. Graph with the average maximum compressive strength of the admixtures analyzed for fiber selection. 129

Figure 154. Dispersion graph of the average compressive strength of the admixtures analyzed for fiber treatment selection compared to the average density measured after 28 days of maturation..... 130

Figure 155. Image showing the compressive strength results of the three samples evaluated for the admixture with 6mm fibers and 2,5% F/C ratio (01-6mm-2,5).. 131

Figure 156. Image showing the compressive strength results of the three samples evaluated for the admixture with 12mm fibers and 2,5% F/C ratio (01-12mm-2,5). 131

Figure 157. Image showing the compressive strength results of the three samples evaluated for the admixture with 20mm fibers and 2,5% F/C ratio (01-20mm-2,5). 132

Figure 158. Graph with the average maximum compressive strength of the admixtures analyzed for fiber length selection. 132

Figure 159. Dispersion graph of the average compressive strength of the admixtures analyzed for fiber length selection compared to the average density measured after 28 days of maturation..... 133

Figure 160. Image showing the compressive strength results of the three samples evaluated for the admixture with 12mm fibers and 2,5% F/C ratio (01-12mm-2,5). 134

Figure 161. Image showing the compressive strength results of the three samples evaluated for the admixture with 12mm fibers and 5% F/C ratio (01-12mm-5).... 134

Figure 162. Image showing the compressive strength results of the three samples evaluated for the admixture with 12mm fibers and 10% F/C ratio (01-12mm-10). 135

Figure 163. Graph with the average maximum compressive strength of the admixtures analyzed for fiber content selection..... 135

Figure 164. Dispersion graph of the average compressive strength of the admixtures analyzed for fiber content selection compared to the average density measured after 28 days of maturation..... 136

Figure 165. Image showing the compressive strength results of the three samples evaluated for the admixture 02-NF-100. 137

Figure 166. Image showing the compressive strength results of the three samples evaluated for the admixture 02-NTF-100-2,5..... 137

Figure 167. Image showing the compressive strength results of the three samples evaluated for the admixture 02-NTF-100-5..... 138

Figure 168. Image showing the compressive strength results of the three samples evaluated for the admixture 02-LTF-100-2,5..... 138

Figure 169. Image showing the compressive strength results of the three samples evaluated for the admixture 02-LTF-100-5. 139

Figure 170. Image showing the compressive strength results of the three samples evaluated for the admixture 02-STF-100-2,5. 139

Figure 171. Image showing the compressive strength results of the three samples evaluated for the admixture 02-STF-100-5. 140

Figure 172. Graph showing the average maximum compressive strength of the admixtures with a 100kg/m³ target density. 140

Figure 173. Graph showing the average maximum flexural strength of the admixtures with NTF and a 100kg/m³ target density. 141

Figure 174. Graph showing the average maximum flexural strength of the admixtures with LTF and a 100kg/m³ target density. 142

Figure 175. Graph showing the average maximum flexural strength of the admixtures with STF and a 100kg/m³ target density. 142

Figure 176. Image showing the compressive strength results of the three samples evaluated for the admixture 02-NF-300. 143

Figure 177. Image showing the compressive strength results of the three samples evaluated for the admixture 02-NTF-300-2,5. 143

Figure 178. Image showing the compressive strength results of the three samples evaluated for the admixture 02-NTF-300-5. 144

Figure 179. Image showing the compressive strength results of the three samples evaluated for the admixture 02-LTF-300-2,5. 144

Figure 180. Image showing the compressive strength results of the three samples evaluated for the admixture 02-LTF-300-5. 145

Figure 181. Image showing the compressive strength results of the three samples evaluated for the admixture 02-STF-300-2,5. 145

Figure 182. Image showing the compressive strength results of the three samples evaluated for the admixture 02-STF-300-5. 146

Figure 183. Graph showing the average maximum compressive strength of the admixtures with a 300kg/m³ target density. 146

Figure 184. Graph showing the average maximum compressive strength of the admixtures with NTF and a 300kg/m³ target density. 147

Figure 185. Graph showing the average maximum compressive strength of the admixtures with LTF and a 300kg/m³ target density. 148

Figure 186. Graph showing the average maximum compressive strength of the admixtures with STF and a 300kg/m³ target density. 148

Figure 187. Image showing the compressive strength results of the three samples evaluated for the admixture 02-NF-500. 149

Figure 188. Image showing the compressive strength results of the three samples evaluated for the admixture 02-NTF-500-1,25. 149

Figure 189. Image showing the compressive strength results of the three samples evaluated for the admixture 02-LTF-500-1,25. 150

Figure 190. Image showing the compressive strength results of the three samples evaluated for the admixture 02-STF-500-1,25. 150

Figure 191. Image showing the compressive strength results of the three samples evaluated for the admixture 02-NTF-500-2,5.....151

Figure 192. Graph showing the average maximum compressive strength of the admixtures with a 500kg/m³ target density. 151

Figure 193. Dispersion graph of the average compressive strength of the NF admixtures compared to the average dry density. 152

Figure 194. Dispersion graph of the average compressive strength of the NTF admixtures compared to the average dry density. 153

Figure 195. Dispersion graph of the average compressive strength of the LTF admixtures compared to the average dry density. 153

Figure 196. Dispersion graph of the average compressive strength of the STF admixtures compared to the average dry density. 154

Figure 197. Graphical representation of the exponential regression curve obtained from the values of thermal conductivity (X-axis) and wet density (Y-axis) in the experimental study carried out on extrudable foamed concrete samples with a humid density in the range 316-828 kg/m³. 155

List of tables

Table 1. Standard dosages for fiber-reinforced concrete [18]. 15

Table 2. Characteristics of the process and materials for each method of AM applicable in the construction sector. 33

Table 3. Characteristics of the mixes dedicated to selecting the fiber treatment... 59

Table 4. Characteristics of the mixes dedicated to selecting the fiber length and the fiber content. 60

Table 5. Characteristics of the mixes with a target density of 100 Kg/m^3 containing 12mm fibers with three treatment options and two fiber content ratios..... 61

Table 6. Characteristics of the mixes with a target density of 300 Kg/m^3 containing 12mm fibers with three treatment options and two fiber content ratios..... 62

Table 7. Characteristics of the mixes with a target density of 500 Kg/m^3 containing 12mm fibers with three treatment options and two fiber content ratios..... 62

Table 8. Results of the slump test for the first part of the experimental campaign dedicated to fiber treatment, length, and content choice 66

Table 9. Results of the slump test for the second part of the experimental campaign dedicated to the analysis of different target densities..... 67

Table 10. Summary of the results obtained from the microstructural analysis carried out on the image area selected for each evaluated admixture. 81

Table 11. Hypothesized thermal conductivity values for samples made with admixtures from the first part of the experimental campaign. 156

Table 12. Hypothesized thermal conductivity values for samples made with admixtures from the second part of the experimental campaign. 157

Bibliography

[1] M. Glavind, "5 - Sustainability of cement, concrete and cement replacement materials in construction," in *Woodhead Publishing Series in Civil and Structural Engineering*, J. M. B. T.-S. of C. M. Khatib, Ed. Woodhead Publishing, 2009, pp. 120–147.

[2] P. J. M. Monteiro, S. A. Miller, and A. Horvath, "Towards sustainable concrete," *Nat. Mater.*, vol. 16, no. 7, pp. 698–699, 2017.

[3] J. de Brito and R. Kurda, "The past and future of sustainable concrete: A critical review and new strategies on cement-based materials," *J. Clean. Prod.*, vol. 281, p. 123558, 2021.

[4] N. Lippiatt, T.-C. Ling, and S.-Y. Pan, "Towards carbon-neutral construction materials: Carbonation of cement-based materials and the future perspective," *J. Build. Eng.*, vol. 28, p. 101062, 2020.

[5] K. Parameswaran, "Sustainability Considerations in Innovative Process Development BT - Innovative Process Development in Metallurgical Industry: Concept to Commission," V. I. Lakshmanan, R. Roy, and V. Ramachandran, Eds. Cham: Springer International Publishing, 2016, pp. 257–280.

[6] M. Levesque, D. Millar, and J. Paraszczak, "Energy and mining – the home truths," *J. Clean. Prod.*, vol. 84, pp. 233–255, 2014.

[7] J. Luis Míguez, J. Porteiro, R. Pérez-Orozco, D. Patiño, and S. Rodríguez, "Evolution of CO2 capture technology between 2007 and 2017 through the study of patent activity," *Appl. Energy*, vol. 211, pp. 1282–1296, 2018.

[8] E. T. Asr, R. Kakaie, M. Ataei, and M. R. Tavakoli Mohammadi, "A review of studies on sustainable development in mining life cycle," *J. Clean. Prod.*, vol. 229, pp. 213–231, 2019.

[9] C. Maduabuchukwu Nwakaire, S. Poh Yap, C. Chuen Onn, C. Wah Yuen, and H. Adebayo Ibrahim, "Utilisation of recycled concrete aggregates for sustainable highway pavement applications; a review," *Constr. Build. Mater.*, vol. 235, p. 117444, 2020.

[10] C. E. de Normalisation, "Concrete-Part 1: Specification, performance, production and conformity," *EN206-1, 22 CEN*, vol. 69, p. 23, 2000.

[11] L. G. Li, Z. Y. Zhuo, J. Zhu, J. J. Chen, and A. K. H. Kwan, "Reutilizing ceramic polishing waste as powder filler in mortar to reduce cement content by 33%

and increase strength by 85%," *Powder Technol.*, vol. 355, pp. 119–126, 2019.

[12] Y. Cheng, F. Huang, G. Li, L. Xu, and J. Hou, "Test research on effects of ceramic polishing powder on carbonation and sulphate-corrosion resistance of concrete," *Constr. Build. Mater.*, vol. 55, pp. 440–446, 2014.

[13] C. F. Ferraris and J. M. Gaidis, "Connection between the rheology of concrete and rheology of cement paste," *Materials (Basel).*, vol. 89, pp. 388–393, 1992.

[14] P.-C. Aïtcin, "17 - The Influence of the Water/Cement Ratio on the Sustainability of Concrete," P. C. Hewlett and M. B. T.-L. C. of C. and C. (Fifth E. Liska, Eds. Butterworth-Heinemann, 2019, pp. 807–826.

[15] M. Silva and T. R. Naik, "Sustainable use of resources–recycling of sewage treatment plant water in concrete," in *Proceedings of the Second International Conference on Sustainable Construction Materials and Technologies, Ancona, Italy*, 2010, vol. 28.

[16] R. Kurad, J. D. Silvestre, J. de Brito, and H. Ahmed, "Effect of incorporation of high volume of recycled concrete aggregates and fly ash on the strength and global warming potential of concrete," *J. Clean. Prod.*, vol. 166, pp. 485–502, 2017.

[17] R. F. Zollo, "Fiber-reinforced concrete: an overview after 30 years of development," *Cem. Concr. Compos.*, vol. 19, no. 2, pp. 107–122, 1997.

[18] B. Wietek, "FC processing BT - Fiber Concrete: In Construction," B. Wietek, Ed. Wiesbaden: Springer Fachmedien Wiesbaden, 2021, pp. 59–76.

[19] N. Banthia, "Fiber reinforced concrete," *ACI SP-142ACI, Detroit, MI*, vol. 91, p. 119, 1994.

[20] V. Afroughsabet, L. Biolzi, and T. Ozbakkaloglu, "High-performance fiber-reinforced concrete: a review," *J. Mater. Sci.*, vol. 51, no. 14, pp. 6517–6551, 2016.

[21] M. Sriram and K. R. Aswin Sidhaarth, "Various properties of natural and artificial fibers with cementitious composites in hybrid form – A review," *Mater. Today Proc.*, vol. 60, pp. 2018–2025, 2022.

[22] S. V Klyuev, T. Khezhev, Y. V. Pukharenko, and A. V Klyuev, "Fiber Concrete on the Basis of Composite Binder and Technogenic Raw Materials," *Mater. Sci. Forum*, vol. 931, pp. 603–607, 2018.

[23] B. Chen, Z. Wu, and N. Liu, "Experimental Research on Properties of High-

Strength Foamed Concrete," *J. Mater. Civ. Eng.*, vol. 24, no. 1, pp. 113–118, Jan. 2012.

[24] O. Kayali, M. N. Haque, and B. Zhu, "Some characteristics of high strength fiber reinforced lightweight aggregate concrete," *Cem. Concr. Compos.*, vol. 25, no. 2, pp. 207–213, 2003.

[25] D. Falliano, D. De Domenico, G. Ricciardi, and E. Gugliandolo, "Compressive and flexural strength of fiber-reinforced foamed concrete: Effect of fiber content, curing conditions and dry density," *Constr. Build. Mater.*, vol. 198, pp. 479–493, 2019.

[26] E. Dawood and A. Hamad, "Toughness Behaviour of High Performance Lightweight Foamed Concrete Reinforced with Hybrid Fibres," *Struct. Concr.*, vol. 16, Mar. 2015.

[27] M. Amran *et al.*, "Fibre-Reinforced Foamed Concretes: A Review," *Materials (Basel).*, vol. 13, p. 4323, Sep. 2020.

[28] J. Castillo-Lara *et al.*, "Mechanical Properties of Natural Fiber Reinforced Foamed Concrete," *Materials (Basel).*, vol. 13, p. 3060, Jul. 2020.

[29] G. Araya-Letelier, F. C. Antico, M. Carrasco, P. Rojas, and C. M. García-Herrera, "Effectiveness of new natural fibers on damage-mechanical performance of mortar," *Constr. Build. Mater.*, vol. 152, pp. 672–682, 2017.

[30] K. W. Corscadden, J. N. Biggs, and D. K. Stiles, "Sheep's wool insulation: A sustainable alternative use for a renewable resource?," *Resour. Conserv. Recycl.*, vol. 86, pp. 9–15, 2014.

[31] C. Grădinaru, "SHEEP WOOL – A NATURAL MATERIAL USED IN CIVIL ENGINEERING," *Bul. INSTITUTULUI Politeh. DIN IAŞI*, vol. 63 (67), p. 21, Feb. 2017.

[32] I. Ahmad Wani and R. ul Rehman Kumar, "Experimental investigation on using sheep wool as fiber reinforcement in concrete giving increment in overall strength," *Mater. Today Proc.*, vol. 45, pp. 4405–4409, 2021.

[33] C. Maia Pederneiras, R. Veiga, and J. de Brito, "Rendering Mortars Reinforced with Natural Sheep's Wool Fibers," *Materials (Basel).*, vol. 12, no. 22, 2019.

[34] A. Fantilli, D. Jóźwiak-Niedźwiedzka, K. Gibas, and J. Dulnik, "THE COMPATIBILITY BETWEEN WOOL FIBERS AND CEMENTITIOUS MORTARS," 2017.

[35] V. Fiore, G. Di Bella, and A. Valenza, "Effect of Sheep Wool Fibers on Thermal Insulation and Mechanical Properties of Cement-Based Composites," *J. Nat. Fibers*, vol. 17, no. 10, pp. 1532–1543, 2020.

[36] V. Gadgihalli, M. Y.R, Chandana, and P. H. Dinakar, "ANALYSIS OF PROPERTIES OF CONCRETE USING SHEEP WOOL DIPPING IN SALT WATER AS FIBRE REINFORCEMENT ADMIXTURE," *Int. J. Res. -GRANTHAALAYAH*, vol. 5, no. 11, pp. 57–59, 2017.

[37] A. P. Fantilli, S. Sicardi, and F. Dotti, "The use of wool as fiber-reinforcement in cement-based mortar," *Acad. J. Civ. Eng.*, vol. 33, no. 2, pp. 341–346, 2015.

[38] A. P. Fantilli, S. Sicardi, and F. Dotti, "The use of wool as fiber-reinforcement in cement-based mortar," *Constr. Build. Mater.*, vol. 139, pp. 562–569, 2017.

[39] R. Alyousef *et al.*, "Effect of Sheep Wool Fiber on Fresh and Hardened Properties of Fiber Reinforced Concrete," *Int. J. Civ. Eng. Technol.*, vol. 10, pp. 190–199, 2019.

[40] R. Alyousef *et al.*, "Utilization of sheep wool as potential fibrous materials in the production of concrete composites," *J. Build. Eng.*, vol. 30, p. 101216, 2020.

[41] D. Jóźwiak-Niedźwiedzka and A. P. Fantilli, "Wool-Reinforced Cement Based Composites," *Materials (Basel).*, vol. 13, no. 16, 2020.

[42] A. P. Fantilli and D. Jóźwiak-Niedźwiedzka, "Influence of Portland cement alkalinity on wool-reinforced mortar," *Proc. Inst. Civ. Eng. - Constr. Mater.*, vol. 174, no. 3, pp. 172–181, 2021.

[43] Y. H. M. Amran, N. Farzadnia, and A. A. Abang Ali, "Properties and applications of foamed concrete; a review," *Constr. Build. Mater.*, vol. 101, pp. 990–1005, 2015.

[44] D. Aldridge, "INTRODUCTION TO FOAMED CONCRETE: WHAT, WHY, HOW?," in *Use of Foamed Concrete in Construction*, pp. 1–14.

[45] N. R. Iyer, "1 - An overview of cementitious construction materials," P. Samui, D. Kim, N. R. Iyer, and S. B. T.-N. M. in C. E. Chaudhary, Eds. Butterworth-Heinemann, 2020, pp. 1–64.

[46] L. Chica and A. Alzate, "Cellular concrete review: New trends for application in construction," *Constr. Build. Mater.*, vol. 200, pp. 637–647, 2019.

[47] K. Ramamurthy, E. K. Kunhanandan Nambiar, and G. Indu Siva Ranjani, "A

classification of studies on properties of foam concrete," *Cem. Concr. Compos.*, vol. 31, no. 6, pp. 388–396, 2009.

[48] M. R. Jones, K. Ozlutas, and L. Zheng, "Stability and instability of foamed concrete," *Mag. Concr. Res.*, vol. 68, no. 11, pp. 542–549, 2016.

[49] D. Asprone, F. Auricchio, C. Menna, and V. Mercuri, "3D printing of reinforced concrete elements: Technology and design approach," *Constr. Build. Mater.*, vol. 165, pp. 218–231, 2018.

[50] R. van Woensel, T. van Oirschot, M. J. H. Burgmans, P. D. Masi Mohammadi, and K. Hermans, "Printing Architecture: An Overview of Existing and Promising Additive Manufacturing Methods and Their Application in the Building Industry," *Int. J. Constr. Environ.*, vol. 9, no. 1, pp. 57–81, 2018.

[51] R. A. Buswell, W. R. Leal de Silva, S. Z. Jones, and J. Dirrenberger, "3D printing using concrete extrusion: A roadmap for research," *Cem. Concr. Res.*, vol. 112, pp. 37–49, 2018.

[52] T. T. Le, S. A. Austin, S. Lim, R. A. Buswell, A. G. F. Gibb, and T. Thorpe, "Mix design and fresh properties for high-performance printing concrete," *Mater. Struct.*, vol. 45, no. 8, pp. 1221–1232, 2012.

[53] G. De Schutter, K. Lesage, V. Mechtcherine, V. N. Nerella, G. Habert, and I. Agusti-Juan, "Vision of 3D printing with concrete — Technical, economic and environmental potentials," *Cem. Concr. Res.*, vol. 112, pp. 25–36, 2018.

[54] J. Buchli *et al.*, "Digital in situ fabrication - Challenges and opportunities for robotic in situ fabrication in architecture, construction, and beyond," *Cem. Concr. Res.*, vol. 112, pp. 66–75, 2018.

[55] D. Falliano, D. De Domenico, G. Ricciardi, and E. Gugliandolo, "Improving the flexural capacity of extrudable foamed concrete with glass-fiber bi-directional grid reinforcement: An experimental study," *Compos. Struct.*, vol. 209, pp. 45–59, 2019.

[56] A. du Plessis, A. J. Babafemi, S. C. Paul, B. Panda, J. P. Tran, and C. Broeckhoven, "Biomimicry for 3D concrete printing: A review and perspective," *Addit. Manuf.*, vol. 38, p. 101823, 2021.

[57] C. Gosselin, R. Duballet, P. Roux, N. Gaudillière, J. Dirrenberger, and P. Morel, "Large-scale 3D printing of ultra-high performance concrete – a new processing route for architects and builders," *Mater. Des.*, vol. 100, pp. 102–109, 2016.

[58] D. Falliano, D. De Domenico, G. Ricciardi, and E. Gugliandolo, "3D-printable lightweight foamed concrete and comparison with classical foamed concrete in terms of fresh state properties and mechanical strength," *Constr. Build. Mater.*, vol. 254, p. 119271, 2020.

[59] D. Falliano, E. Gugliandolo, D. De Domenico, and G. Ricciardi, "Experimental Investigation on the Mechanical Strength and Thermal Conductivity of Extrudable Foamed Concrete and Preliminary Views on Its Potential Application in 3D Printed Multilayer Insulating Panels BT - First RILEM International Conference on Concre," 2019, pp. 277–286.

[60] Y. W. D. Tay, Y. Qian, and M. J. Tan, "Printability region for 3D concrete printing using slump and slump flow test," *Compos. Part B Eng.*, vol. 174, p. 106968, 2019.

[61] S. Cho, A. van Rooyen, E. Kearsley, and G. van Zijl, "Foam stability of 3D printable foamed concrete," *J. Build. Eng.*, vol. 47, p. 103884, 2022.